

***In Vivo* Incorporation of Multiple
Unnatural Amino Acids**

Thesis by:

Erik Ali Rodriguez

In Partial Fulfillment of the Requirements
for the Degree of Doctor of Philosophy
in Chemistry



California Institute of Technology

Pasadena, CA 91125

2009

(Defended December 11, 2008)

©2009

Erik Ali Rodriguez

All Rights Reserved

*Dedicated to my Mother and family,
who have supported me throughout my life.*

Acknowledgements

I have been at Caltech for ten years and the experience has been amazing, starting as an undergraduate and leaving with a doctorate. I must thank Professor Dennis Dougherty, who has been an amazing advisor throughout my undergraduate and graduate research. Not many professors would give an undergraduate their own project that would eventually be published in PNAS. Professor Dougherty has always been helpful in my research, providing insight, new ideas, a different perspective, and being receptive to new ideas that may seem controversial. Throughout my research I have been allowed to develop new methods and molecules that many thought were unnecessary, but Professor Dougherty let me explore as long as the research wasn't too far fetched. Professor Dougherty is an expert of many scientific disciplines, an excellent writer, and an extremely imaginative research advisor and yet he is an amazing person to talk to, an incredible father, and treats everyone humanely and with respect. For all these reasons, it truly has been an honor and privilege to work in the Dougherty lab.

Professor Henry Lester has been like a second advisor with a hands-on attitude towards science. Professor Lester was always interested in discussing research, discussing implications of my work, and fostering new research ideas that combined chemistry and biology. Professor Lester showed me how to use an oscilloscope and calibrate a function generator. The collaboration between the Dougherty and Lester lab has been a great tool to learn different areas of biological research including transgenic mice, atomic force microscopy, fluorescence microscopy, and electrophysiology. I appreciate being able to use the Lester lab equipment and excellent help and suggestions from the Lester lab members. I would also like to thank my thesis committee consisting of Professor David Tirrell, Professor Nate Lewis, and Professor Judith Campbell for all their useful comments on my research and suggestions for my career.

Dr. Sarah May taught me all the basic molecular biology techniques when I began my research as undergraduate, even though my project was different from her research. Sarah also provided extremely large quantities of dCA-W, which was invaluable for all my tRNA screening experiments. I have enjoyed working with Dr. Rigo Pantoja and Dr. Mohammed Dibas on incorporating a fluorescent unnatural amino acid into the nicotinic

acetylcholine receptor. Dr. Joshua Maurer taught me techniques for working with bacterial ion channels, fluorescence microscopy, and electron microscopy. Dr. George Shapovalov performed electrophysiology recordings on MscL incorporated into giant unilamellar vesicles. Sean Gordon taught me how to create giant unilamellar vesicles and took confocal microscopy images of the vesicles. Purnima Deshpande has always been extremely useful for discussions on molecular biology, making biological stocks, and enjoyable conversations at safety meetings. Professor Linda Hsieh-Wilson has allowed me to use the lab's PCR thermal cycler, UV-visible spectrometer, and Li-Cor Odyssey. Heather Murrey has been extremely helpful with training on the Hsieh-Wilson equipment, discussions on molecular biology, and Western blots.

Working in the Dougherty lab as an undergraduate allowed me to interact with many senior graduate students and gain insight into their various personalities. Dr. Sarah May was helpful with molecular biology, very kind, and never gave up on a difficult project. Dr. Gabriel Brandt was knowledgeable about many areas of science. Dr. James Petersson was tremendously hard working, enjoyed science, was willing to lend a hand, and threw a fun party. Dr. Niki Zacharias was persistent with difficult experiments. Dr. David Dahan was helpful with fluorescence microscopy and a great family man. Dr. Don Elmore mainly performed computer simulations, but still performed experimental research and was ready to provide help. Dr. Joshua Maurer was helpful with experiments, very sure of himself, and adventurous in performing research in new areas. Dr. Darren Beene was fun to talk with, a great father, and accepted that I liked molecular biology more than chemistry. Dr. Tingwei Mu was hard working, knowledgeable, and helpful with experiments. Dr. Steve Spronk was always willing to be of assistance and well informed about areas outside of science. From all of them, I would try to assimilate their best attributes into my graduate career.

My graduate research has been enjoyable because of the great people in the Dougherty lab. Dr. Lori Lee was fun to talk to at work or at a party and a great cook. Dr. Amanda Cashin taught me oocyte injection and how to use the OpusXpress. Amanda was also kind and a social butterfly. Dr. Joanne Xiu worked very hard, was fun to work with, and was a great MC for Chinese New Year. Amy Eastwood shared dCA-Ala, is fun to talk to (if I remember or not), and is a great RA of Ricketts House. Michael Torrice is

helpful with experiments and always brings up interesting conversation topics. Katie McMenimen always lent me her laptop because I was too cheap to buy one, was familiar with fun attractions in the area, and good at getting free Bloody Marys. Ariele Hanek is a great opus captain and always gets the job done. Kristin Glietsman is interesting to talk to about her many endeavors including science, collaborations, travel, and dancing. Kiowa Bower is always entertaining and marches to the beat of a different drummer. Jinti Wang was very hard working, good at multi-tasking, amazingly talented at getting experiments done with brute force, and extremely respectful. Kay Limapichat is very talented, able to perform difficult experiments, and a great cameraman. Nyssa Puskar is hard working and was great dancer on Bourbon Street. Jai Shanata seems to always confound me with the single channel equations, but doesn't know what the French flag looks like at night. Angela Blum is a hard worker and hopefully will succeed at her new project. Sean Kedrowski is also hard working and with any luck will get the phosphorylated unnatural amino acid project into ion channels. Shawna Frazier takes on challenging projects, but seems to thrive and is fun to hang out with outside of the lab. The newest members of the lab, Noah Duffy and Darren Nakamura, are entertaining and I am sure they will do well in their research.

In the summer of 2000, I performed research with Professor Jacob Anglister at the Weizmann Institute, Israel. I am extremely grateful for the opportunity and enjoyed working in the Anglister lab. Professor Anglister was extremely kind and very helpful. Dr. Avraham Samson was my graduate mentor and taught me everything about structural biology using NMR. Jane Raymond was influential on my laboratory technique and writing everything in my notebook and I am thankful for the opportunity of being a teaching assistant during my undergraduate studies. Lauren Stolper is an amazing person and I am grateful for being chosen to study abroad at Cambridge University, England. Lauren was also extremely helpful with graduate fellowship applications. I am also thankful to the Minority Student Education office for all their support throughout my undergraduate career, organizing volunteer activities, their mentor program, and many other useful events. Anna Salazar and Patricio Vela were amazing friends that were undergraduates and graduates at Caltech who showed me around the Los Angeles area, took me clubbing, and were great neighbors.

I would also like to thank the Wednesday night crew consisting of Dr. Gavin Murphy, Heather Murrey, Chad Vecitis, David Ebner, Adam Dennis, Cristal Gama, Tammy Campbell, Adam Hartwick, Wally Bugg, Mary Devlin, Adrian Rice, Sarina Mohanty, and Julian Revie. They made graduate school entertaining and definitely more interesting. Gavin, Heather, Chad, Dave, Adam, Cristal, and Tammy were always up for darts, poker, bowling, and hanging out anywhere. We definitely have a lot of crazy stories to tell about graduate school.

Throughout undergraduate and graduate school at Caltech I have received funding from the National Science Foundation Graduate Fellowship, American Chemical Society Division of Biological Chemistry Travel Award, Mellon Minority Undergraduate Fellowship, American Chemical Society's Scholars Program, Benjamin A. Gilman International Scholarship, David and Lucile Packard Foundation Scholarship, Donald R. Beall Scholarship, Target All-Around Scholarship, Ford Salute to Education Scholarship, SEEK, Inc. Scholarship, and El Paso Ronald McDonald Restaurant Owner-Operators Hacer Scholarship. I am very appreciative for the scholarships because they allowed me to attend Caltech and travel abroad.

Finally, I would like to thank my Mom and family for supporting my education throughout all these years. My mom was always there to help me when I needed her, allowing me to dream and apply to the best colleges in the country, supportive of my decisions, and accepting that I wanted to go to school for so long. The rest of the family has always supported my education through gifts of books, donations for my orchestra trips, and applauding my accomplishments. I couldn't have finished without my family.

Abstract

Unnatural amino acid (UAA) incorporation is an invaluable technique that is seeing increased use. THG73 is an amber suppressor tRNA used to incorporate > 100 residues at the UAG, amber stop codon, in *Xenopus* oocytes. We have found that yeast Phe frameshift suppressors (YFFS) can incorporate UAAs at the CGGG and GGGU quadruplet codons *in vitro* and *in vivo*, allowing simultaneous incorporation of three UAAs in the nicotinic acetylcholine receptor (nAChR). The YFFS are more “orthogonal” than the amber suppressor tRNA, THG73, but the frameshift suppressors incorporate UAAs less efficiently than THG73. A library of tRNAs derived from THG73 has produced an amber suppressor that is “orthogonal” and suppresses similarly to THG73. An analogous opal suppressor tRNA allows incorporation of UAAs at the UGA, opal stop codon. The use of the amber, opal, CGGG, and GGGU codons should allow for the simultaneous incorporation of four UAAs *in vivo*. Bioorthogonal labeling of UAAs is useful for the addition of large fluorophores. We incorporated *p*-AcPhe at $\alpha 70$ of the nAChR and labeled with biotin and Cy5.5 hydrazide. Biotin and Cy5.5 hydrazide consistently labeled three proteins on oocytes not expressing $\alpha 70p$ -AcPhe and isn’t useful for site-specific labeling of ketone containing UAAs in oocytes. We explored the known subunit stoichiometry of the nAChR ($2\alpha:\beta:\gamma:\delta$) expressed in oocytes and detected each subunit with the HA tag by Western blot. The α -subunit is present in excess of the other subunits in a ratio of $\approx 3:1$, which is expected to be 2:1. UAAs are being sold commercially for detection of protein-protein interactions in eukaryotic cells. The UAAs are heterogeneously incorporated and little is known about the effect on protein function and stability. We heterogeneously incorporated UAAs into the nAChR and detected changes in function by shifts in EC_{50} . Many UAAs altered the function of the nAChR. Incorporation of photo-reactive UAAs allowed for detection of cross-linking by Western blot. Heterogeneously incorporated UAAs also altered the functional nAChR expression on the surface of oocytes. Site-specific and heterogeneous incorporation of multiple UAAs are useful techniques for novel experiments to explore protein function, FRET experiments, cross-linking, and protein expression.

Table of Contents

Acknowledgments	iv
Abstract	viii
Table of Contents	ix
List of Figures	xvi
List of Tables	xx
Chapter 1: Vesicle Reconstitution & Characterization of the Synthetic	
Mechanosensitive Channel of Large Conductance	1
1.1 Introduction	2
1.2 Results	5
1.2.1 Vesicle Reconstitution of Synthetic MscL	5
1.2.2 Electron Microscopy of B-Ec-MscL in MLVs	6
1.2.3 Oligomeric State of MscL Analyzed by Cross-Linking in MLVs .	7
1.2.4 Fluorescence Imaging	10
1.2.5 Electrophysiological Characterization of Pt Wire GUVs	15
1.3 Discussion	15
1.4 Experimental Methods	16
1.4.1 Synthetic B-Ec-MscL Samples	16
1.4.2 MLV Preparation and DDM-Mediated Reconstitution of B-Ec-MscL	17
1.4.3 GUV Preparation With Pt Wire Electrodes	17
1.4.4 GUV Preparation With ITO Coverslips	18
1.4.5 Electron Microscopy of B-Ec-MscL in MLVs	19
1.4.6 Cross-Linking of MscL in MLVs	20
1.4.7 Fluorescence Imaging	20
1.4.8 Electrophysiological Characterization of Pt Wire GUVs	21
1.5 References	21
Chapter 2: Evaluating Aminoacylation and Suppression Efficiency of Nonsense	
and Frameshift Suppressor tRNAs <i>In Vitro</i>	27
2.1 Introduction	28

2.2	Results	34
2.2.1	Experimental Design and Western Blot Analysis	34
2.2.2	HSAS Suppression on $\alpha_{\text{NHA}}154\text{UAG}$ and $\alpha_{\text{NHA}}154\text{UAG}374\text{UAG}$	35
2.2.3	HSAS and HSFS _{CCCG} Suppression on $\alpha_{\text{NHA}}154\text{UAG}374\text{CGGG}$	36
2.2.4	HSAS/HSFS and THG73/THG73FS-Ala Suppression on $\alpha_{\text{NHA}}154\text{XXX(X)}$	39
2.2.5	HSAS/HSFS and THG73/THG73FS-Ala Suppression on Single Constructs in Wheat Germ <i>In Vitro</i> Translation	41
2.2.6	HSAS/HSFS and THG73/THG73-W Suppression on the α_{NHA} .	44
2.2.7	Arg Mutations, Changing CGG Triplets to CGC Triplets	50
2.2.8	Optimization of the RRL <i>In Vitro</i> Reactions for Increased Suppression Efficiencies	53
2.2.9	Choosing a New Frameshift Suppressor tRNA, YFFS _{CCCG}	54
2.2.10	HSAS and HSFS Suppression at $\alpha_{\text{NHA}}149\text{XXX(X)}$	57
2.2.11	Suppression Efficiencies of Suppressor tRNAs Using Optimized Conditions	59
2.3	Discussion	60
2.4	Experimental Methods	64
2.4.1	Materials	64
2.4.2	α_{NHA} Mutations and mRNA Preparation	65
2.4.3	Frameshift Suppressor tRNA Gene Construction and tRNA Preparation	66
2.4.4	dCA-aa Synthesis and Ligation to Suppressor tRNAs	68
2.4.5	<i>In Vitro</i> Translation	68
2.4.6	Western Blotting and Densitometric Analysis	69
2.5	References	71
Chapter 3: <i>In Vivo</i> Incorporation of Multiple Unnatural Amino Acids through Nonsense and Frameshift Suppression		77
3.1	Introduction	78

3.2	Results	81
3.2.1	Testing Frameshift Suppression Viability <i>In Vivo</i>	81
3.2.2	UAA Incorporation By Frameshift Suppression	84
3.2.3	Masking Effects on Frameshift Suppression	88
3.2.4	Comparison of Frameshift and Nonsense Suppression Efficiencies	89
3.2.5	Comparison of Aminoacylation of Suppressor tRNA and Read-Through of Suppression Sites	91
3.2.6	The Effect of Discriminator and Acceptor Stem Mutations on YFFS _{CCCG}	92
3.2.7	Incorporation of Two UAAs	93
3.2.8	Incorporation of Three UAAs	95
3.3	Discussion	97
3.4	Experimental Methods	99
3.4.1	Materials	99
3.4.2	Gene Construction and RNA Preparation	101
3.4.3	dCA and dCA-UAA Ligation to Suppressor tRNA	102
3.4.4	<i>In Vivo</i> Suppression Experiments	103
3.4.5	Electrophysiology	104
3.5	References	104
Chapter 4:	Development of Improved Amber and Opal Suppressor tRNAs for Unnatural Amino Acid Incorporation <i>In Vivo</i>. Minimizing Misacylation of Suppressor tRNAs	110
4.1	Introduction	111
4.2	Results	113
4.2.1	Schematic for Site-Specific UAA Incorporation and Aminoacylation	113
4.2.2	Experimental Scheme for Evaluating Aminoacylation and Suppression by Electrophysiology	115
4.2.3	Identifying the Natural aa Placed on THG73 Using Electrophysiology	117

4.2.4	Testing Knob Mutations on THG73	118
4.2.5	Testing Aminoacylation of ENAS and ENAS A71 <i>In Vivo</i>	121
4.2.6	Testing Aminoacylation of THG73 Acceptor Stem Mutations .	122
4.2.7	Aminoacylation Tested at a Highly Promiscuous Site, β A70 ...	127
4.2.8	LysRS Does Not Aminoacylate THG73, TQAS', and TQAS ...	128
4.2.9	Analyzing THG73-W and TQAS-W Interactions with the Translational Machinery <i>In Vivo</i>	129
4.2.10	Comparing Aminoacylation of Amber, Opal, and Frameshift Suppressor tRNAs	132
4.3	Discussion	135
4.4	Experimental Methods	141
4.4.1	Materials	141
4.4.2	tRNA Gene Preparation and tRNA Transcription	141
4.4.3	nAChR Gene Preparation and mRNA Transcription	142
4.4.4	dCA and dCA-W Ligation to Suppressor tRNAs	143
4.4.5	<i>In Vivo</i> Aminoacylation and Suppression Experiments	143
4.4.6	Electrophysiology	144
4.5	References	145
Chapter 5:	Development of Improved Amber and Opal Suppressor tRNAs for Unnatural Amino Acid Incorporation <i>In Vivo</i>. Evaluating Suppression Efficiency of Suppressor tRNAs	152
5.1	Introduction	153
5.2	Results	155
5.2.1	Electrophysiology Assay	155
5.2.2	ENAS and ENAS A71 Suppression Efficiency	156
5.2.3	Testing Suppression Efficiency of THG73 Acceptor Stem Mutations	158
5.2.4	Combining Mutations Causes Averaging of the Suppression Efficiency	160
5.2.5	Suppression Efficiency of the Acceptor Stem Mutations Does Not Correlate With Stability of the Acceptor Stem	161

5.2.6	Testing Amber, Opal, and Frameshift Suppression Efficiency .	162
5.2.7	Natural aa and UAA Incorporation With Selected Suppressor tRNAs	164
5.3	Discussion	167
5.4	Experimental Methods	171
5.4.1	Materials	171
5.4.2	tRNA Gene Preparation and tRNA Transcription	172
5.4.3	nAChR Gene Preparation and mRNA Transcription	173
5.4.4	ΔG Calculations of Each tRNA Acceptor Stem	173
5.4.5	dCA-W and dCA-WF1 Ligation to Suppressor tRNAs	174
5.4.6	<i>In Vivo</i> Suppression Experiments	175
5.4.7	Electrophysiology	175
5.5	References	176
Chapter 6: Bioorthogonal Labeling of <i>p</i> -AcPhe Incorporated in the Nicotinic Acetylcholine Receptor in <i>Xenopus</i> Oocytes & Western Blot Determination of the Subunit Stoichiometry of the Nicotinic Acetylcholine Receptor in <i>Xenopus</i> Oocytes		
6.1	Introduction	181
6.2	Results	185
6.2.1	Screening Sites For Aminoacylation of tRNAs, Read-Through, and UAA Incorporation	185
6.2.2	Suppression of $\alpha 70$ UAG with TQAS-Biocytin	190
6.2.3	Analysis of ^{125}I -Streptavidin and ^{125}I - α -Bungarotoxin Binding to <i>Xenopus</i> Oocytes Expressing Wild-Type nAChR and UAA Incorporation of Biocytin	193
6.2.4	Bioorthogonal Labeling of $\alpha 70p$ -AcPhe With Biotin Hydrazide	195
6.2.5	Attempts to Block Nonspecific Biotin Hydrazide Labeling of Uninjected Oocytes	199
6.2.6	Bioorthogonal Labeling of $\alpha 70p$ -AcPhe with Cy5.5 Hydrazide	200

6.2.7	Analysis of ^{125}I -Streptavidin Binding to <i>Xenopus</i> Oocytes Labeled with Biotin Hydrazide	202
6.2.8	α -, β -, γ -, and δ -Subunit Detection By Western Blot	203
6.2.9	α_{HA} and β_{HA} Detection After Various Incubation Times	205
6.2.10	α_{HA} and β_{HA} Solubilization of Whole Cells or Insoluble Fraction	206
6.2.11	α -, β -, γ -, and δ -Subunit Stoichiometry Determined By Densitometric Analysis	207
6.3	Discussion	208
6.4	Experimental Methods	213
6.4.1	Materials	213
6.4.2	tRNA Transcription and dCA or dCA-UAA Ligation	213
6.4.3	nAChR Gene Preparation and mRNA Transcription	214
6.4.4	<i>In Vivo</i> nAChR Expression Experiments	214
6.4.5	Electrophysiology	215
6.4.6	Oocyte Labeling with Biotin Hydrazide and Cy5.5 Hydrazide ..	215
6.4.7	Oocyte Treatment with Carbohydrazide and NaBH_4	216
6.4.8	Whole Oocyte Homogenization and Membrane Preparation	216
6.4.9	Western Blotting of Proteins Expressed in <i>Xenopus</i> Oocytes ...	217
6.5	References	218
Chapter 7:	Unnatural Amino Acid Replacement Scanning in <i>Xenopus</i> oocytes	228
7.1	Introduction	229
7.2	Results	231
7.2.1	Unnatural Amino Acid Replacement Scanning	231
7.2.2	Met Derivatives	237
7.2.3	Pro Derivatives	238
7.2.4	Val Derivative	239
7.2.5	Leu Derivatives	239
7.2.6	Phe Derivatives	241
7.2.7	Trp Derivatives	243
7.2.8	Cross-Linking the nAChR with PLeu and PMet	245

7.2.9	Unnatural Amino Acid Replacement Scanning Expression	
	Determined by Electrophysiology and Western Blot	251
7.3	Discussion	253
7.4	Experimental Methods	260
7.4.1	Materials	260
7.4.2	nAChR Gene Preparation and mRNA Transcription	261
7.4.3	<i>In Vivo</i> nAChR Expression, UAARS, and Site-Specific UAA Incorporation	261
7.4.4	Electrophysiology	262
7.4.5	UV Irradiation	262
7.4.6	Whole Oocyte Homogenization	262
7.4.7	Western Blotting of Proteins Expressed in <i>Xenopus</i> Oocytes ...	263
7.5	References	263

List of Figures

Figure 1.1	Crystal structure of Tb-MscL	3
Figure 1.2	Diagram of a DOPC lipid and vesicle formation	4
Figure 1.3	Oligomeric analysis of MscL using DSS cross-linking in MLVs	9
Figure 1.4	Fluorescence imaging of B-Ec-MscL in MLVs	12
Figure 1.5	Fluorescence imaging of B-Ec-MscL GUVs prepared with Pt wire electrodes	13
Figure 1.6	GUVs prepared by ITO coverslips and fluorescence imaging	14
Figure 1.7	Diagram of Pt wire electrode chamber for GUV preparation	18
Figure 1.8	Diagram of ITO coverslip chamber for GUV preparation	19
Figure 2.1	UAA incorporation techniques	29
Figure 2.2	Mechanism of nonsense and frameshift suppression	32
Figure 2.3	Nucleotide sequences and cloverleaf structures of suppressor tRNAs tested <i>in vitro</i>	34
Figure 2.4	HSAS suppression on $\alpha_{\text{NHA}}154\text{UAG}$ and $\alpha_{\text{NHA}}154\text{UAG}374\text{UAG}$	36
Figure 2.5	HSAS and HSFS _{CCCG} suppression on $\alpha_{\text{NHA}}154\text{UAG}374\text{CGGG}$	38
Figure 2.6	HSAS/HSFS and THG73/THG73FS-Ala suppression at $\alpha_{\text{NHA}}154\text{XXX(X)}$	40
Figure 2.7	HSAS/HSFS and THG73/THG73FS-Ala suppression at $\alpha_{\text{NHA}}154\text{XXX(X)}$ in wheat germ <i>in vitro</i> translation	43
Figure 2.8	HSAS/HSFS suppression on α_{NHA} is dependent on the amount of tRNA added	46
Figure 2.9	HSAS/HSFS and THG73/THG73FS-W suppression on α_{NHA} or $\alpha_{\text{NHA}}154\text{XXX(X)}$	48
Figure 2.10	Densitometric analysis of HSAS/HSFS suppression on α_{NHA} and $\alpha_{\text{NHA}}154\text{XXX(X)}$	50
Figure 2.11	HSFS _{CCCG} suppression on $\alpha_{\text{NHA}}\text{R182}$ and $\alpha_{\text{NHA}}154\text{CGGGR182}$ mutants	52
Figure 2.12	YFFS _{CCCG-W} and HSFS _{CCCG} suppression at $\alpha_{\text{NHA}}154\text{XXX(X)}$	55

Figure 2.13	YFFS _{CCCG} , YFG73FS _{CCCG} , YFaFS _{CCCG} (-Trp), and HSFS _{CCCG} suppression and reaminoacylation (74 mer) tested at $\alpha_{\text{NHA}}154\text{CGGG}$...	57
Figure 2.14	HSFS _{CCCG} and HSAS suppression at $\alpha_{\text{NHA}}154\text{XXX(X)}$ and $\alpha_{\text{NHA}}149\text{XXX(X)}$	58
Figure 2.15	Average suppression efficiency and reaminoacylation of suppressor tRNAs using optimized Western blot conditions and $\alpha_{\text{NHA}}\text{R182}$	60
Figure 3.1	Multiple UAA incorporation in ion channels expressed in <i>Xenopus</i> oocytes	79
Figure 3.2	tRNAs and UAAs	82
Figure 3.3	nAChR suppression sites used in this research	83
Figure 3.4	THG73FS _{CCCG} anticodon loop mutations	86
Figure 3.5	Simultaneous incorporation of two UAAs, representative traces and fits to the Hill equation	95
Figure 3.6	Simultaneous incorporation of three UAAs	96
Figure 4.1	Site-specific UAA incorporation	115
Figure 4.2	Fits to the hill equation for $\beta 9'$ UAG + THG73 (74mer)/-dCA (76mer) and $\beta 9'$ Q	118
Figure 4.3	THG73 mutations and tRNAs studied	119
Figure 4.4	THG73 Knob mutations	120
Figure 4.5	ENAS and ENAS A71 aminoacylation tested at $\beta 9'$ UAG	122
Figure 4.6	THG73 acceptor stem mutations tested at $\beta 9'$ UAG	124
Figure 4.7	tRNA (74mer/-dCA) aminoacylation tested at a highly promiscuous site, βA70	127
Figure 4.8	tRNA aminoacylation tested at αK145	129
Figure 4.9	Amber, opal, and frameshift suppressor tRNAs tested at $\beta 9'$	135
Figure 5.1	THG73 mutations and tRNAs studied	157
Figure 5.2	ENAS-W and ENAS A71-W suppression at $\alpha 149\text{UAG}$	158
Figure 5.3	THG73 acceptor stem mutations suppressing at $\alpha 149\text{UAG}$	159
Figure 5.4	Amber, opal, and frameshift suppressor tRNAs suppression at $\alpha 149$...	164

Figure 5.5	Fits to the Hill equation for wild-type recovery and UAA incorporation at $\alpha 149$	166
Figure 6.1	$\alpha 70$ and aligned positions in the nAChR	186
Figure 6.2	Detection of $\alpha 70$ Biocytin by Western blot	192
Figure 6.3	Analysis of ^{125}I -Streptavidin or ^{125}I - α -Bungarotoxin labeling of <i>Xenopus</i> oocytes expressing wild-type nAChR and UAA incorporation of biocytin	195
Figure 6.4	Bioorthogonal labeling of <i>p</i> -AcPhe with biotin hydrazide	196
Figure 6.5	Detection of $\alpha 70$ <i>p</i> -AcPhe labeled with biotin hydrazide	197
Figure 6.6	Analysis of <i>p</i> -AcPhe labeled with biotin hydrazide	198
Figure 6.7	Uninjected oocytes labeled with biotin hydrazide after treatment with carbohydrazide or NaBH_4	200
Figure 6.8	Bioorthogonal labeling of $\alpha 70$ <i>p</i> -AcPhe with Cy5.5 hydrazide	202
Figure 6.9	Analysis of ^{125}I -Streptavidin binding to <i>Xenopus</i> oocytes treated with biotin hydrazide	203
Figure 6.10	Detection of the α_{HA} , β_{HA} , γ_{HA} , and δ_{HA} subunits of the nAChR	205
Figure 6.11	Detection of the α_{HA} and β_{HA} subunits at different incubation times	206
Figure 6.12	Increasing the yield of the α_{HA} and β_{HA} subunits	207
Figure 6.13	Average ratio of the β -, γ -, and δ -subunits relative to the α -subunit	208
Figure 7.1	Unnatural amino acids used in this research	230
Figure 7.2	Unnatural amino acid replacement scanning (UAARS)	234
Figure 7.3	Amino acid composition of the nAChR	236
Figure 7.4	Fits to the Hill equation for UAARS with PLeu, PMet, and F3Leu	240
Figure 7.5	Fits to the Hill equation for UAARS with <i>o</i> FPhe, <i>m</i> FPhe, <i>p</i> FPhe, 2Pyr, 3Pyr, and 4Pyr	242
Figure 7.6	Fits to the Hill equation for UAARS with FTrp and nonsense suppression experiments	244
Figure 7.7	Detecting cross-linking of $\alpha_{\text{HA His}}$ with the HA Ab	247
Figure 7.8	Detecting cross-linking of $\alpha_{\text{HA His}}$ with the His Ab and HA Ab	249

Figure 7.9	Detecting cross-linking of $\alpha_{\text{HA His}}$ with the HA Ab after extended UV irradiation	250
Figure 7.10	UAARS effect on functional nAChR expression detected by electrophysiology	252
Figure 7.11	UAARS effect on nAChR expression detected by Western blot	253

List of Tables

Table 3.1	HSAS and HSFS suppression experiments at the β 9' site	84
Table 3.2	THG73FS _{CCCG} and anticodon loop mutations suppression at α 149CGGG	86
Table 3.3	Wild-type recovery and UAA incorporation by frameshift suppression <i>in vivo</i>	87
Table 3.4	Masking experiments	89
Table 3.5	Comparison of suppression efficiency, aminoacylation, and read-through <i>in vivo</i>	90
Table 3.6	The effect of discriminator base and acceptor stem mutations on YFFS _{CCCG}	93
Table 3.7	Incorporation of two UAAs	95
Table 3.8	Oligos used in this research	100
Table 4.1	THG73 acceptor stem mutations	125
Table 5.1	THG73 acceptor stem mutations	161
Table 5.2	Natural aa and UAA incorporation with THG73, TQAS', TQAS, TQOpS', and TQOpS	166
Table 6.1	Expression tests at the α D70 aligned positions and β A19'	189
Table 7.1	UAARS EC ₅₀ determination	238

Chapter 1

Vesicle Reconstitution & Characterization

of the Synthetic

Mechanosensitive Channel of Large Conductance

1.1 Introduction

Mechanosensation is used in all three kingdoms of life for various functions. In bacteria, mechanosensation is necessary to regulate osmotic pressure and prevent lysis of the cell wall. Three distinct ion channels have been classified by their conductance in bacteria. The mechanosensitive channel of large conductance (MscL) has a conductance > 1 nS, the mechanosensitive channels of small conductance (MscS and MscK) have conductances between 0.3–0.5 nS, and the mechanosensitive channel of mini conductance (MscM) has a conductance between 0.1–0.15 nS (1–4). *E. coli* MscL was first cloned in 1994 and experiments explicitly showed that mechanosensation through the lipid bilayer could be performed by a single ion channel (5).

Rees and co-workers solved the crystal structure of MscL from *Mycobacterium tuberculosis* (Tb-MscL). The crystal structure revealed a channel formed by a homopentamer, where each subunit contained two transmembrane (TM) α helices and a third cytoplasmic α helix (Figure 1.1). The structure lacks the first 9 residues in the N-terminus and 33 residues in the C-terminus (6). Tb-MscL has sequence homology of 37% when compared to the *E. coli* MscL (Ec-MscL), with highest homology in the TM regions (7). MscL is thought to serve as a sensor for changes in osmolarity because the channel is gated by tension, through the lipid bilayer, that is near the lytic limit of most bacterial cells (1,8). Upon tension gating, MscL generates a large conductance of ≈ 3 nS, with multiple sub-conductance states (9,10). Synthetic MscL samples were prepared containing a N-terminal biotin moiety (B-Ec-MscL & B-Tb-MscL) (11) and this research was performed to reconstitute the channel into vesicles for characterization within the

lipid bilayer, analysis of the oligomeric state, and channel function through electrophysiology.

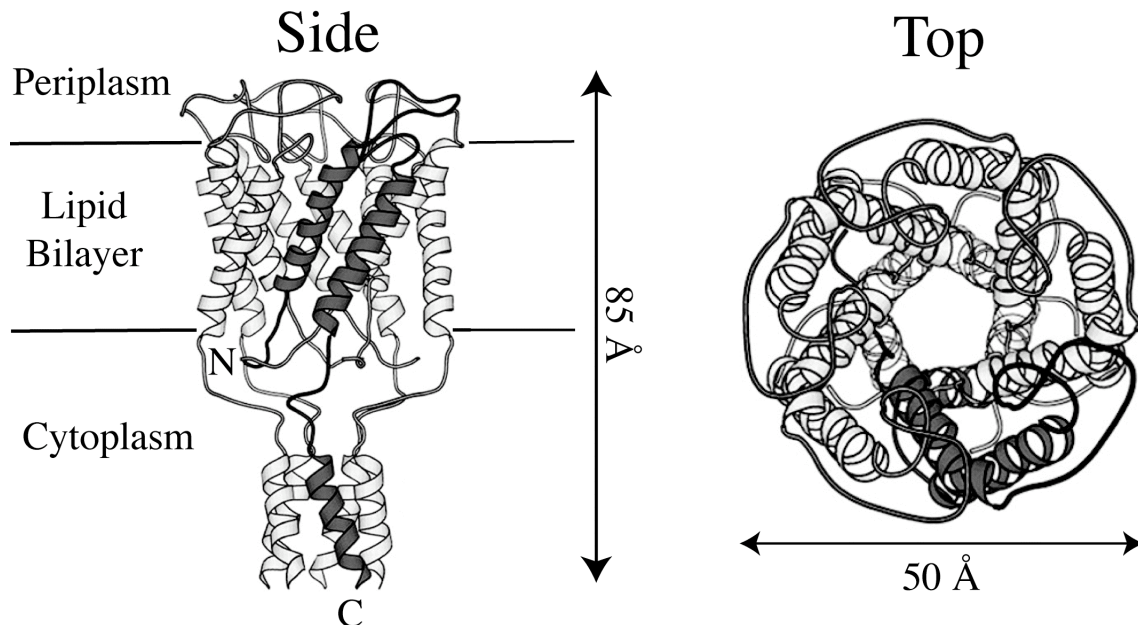


Figure 1.1: Crystal structure of Tb-MscL. Left, the structure shows a homopentameric arrangement perpendicular to the lipid bilayer with a single subunit highlighted. Each subunit contains two TM α helices and a cytoplasmic α helix. N is the N-terminus and C is the C-terminus of a single subunit. Right, a view from the periplasmic region. Figure adapted from (12).

Synthetic MscL samples initially are dissolved in trifluoroethanol (TFE) and therefore must be reconstituted into a lipid bilayer in order to form functional channels. Lipids used in this research include: 1,2-Dioleoyl-*sn*-Glycero-3-Phosphocholine (DOPC) (Figure 1.2 A) and azolectin, an extract from soybean containing 40% phosphocholine lipid derivatives. For vesicle formation, lipid is first dried in order to create a lipid film (Figure 1.2 B, 1). The addition of water causes this lipid layer to swell and form bilayers. With agitation multilamellar vesicles (MLVs) are formed (Figure 1.2 B, 2). MLVs can then be extruded through filters of specific diameters to form large unilamellar vesicles

(LUVs) or can be sonicated to form small unilamellar vesicles (SUVs) (Figure 1.2 B, 3 & 4) (13). Giant unilamellar vesicles (GUVs) are formed by the electroformation technique (14,15), which applies an oscillating electrical current with a geometric wave function (Figure 1.2 B, 5).

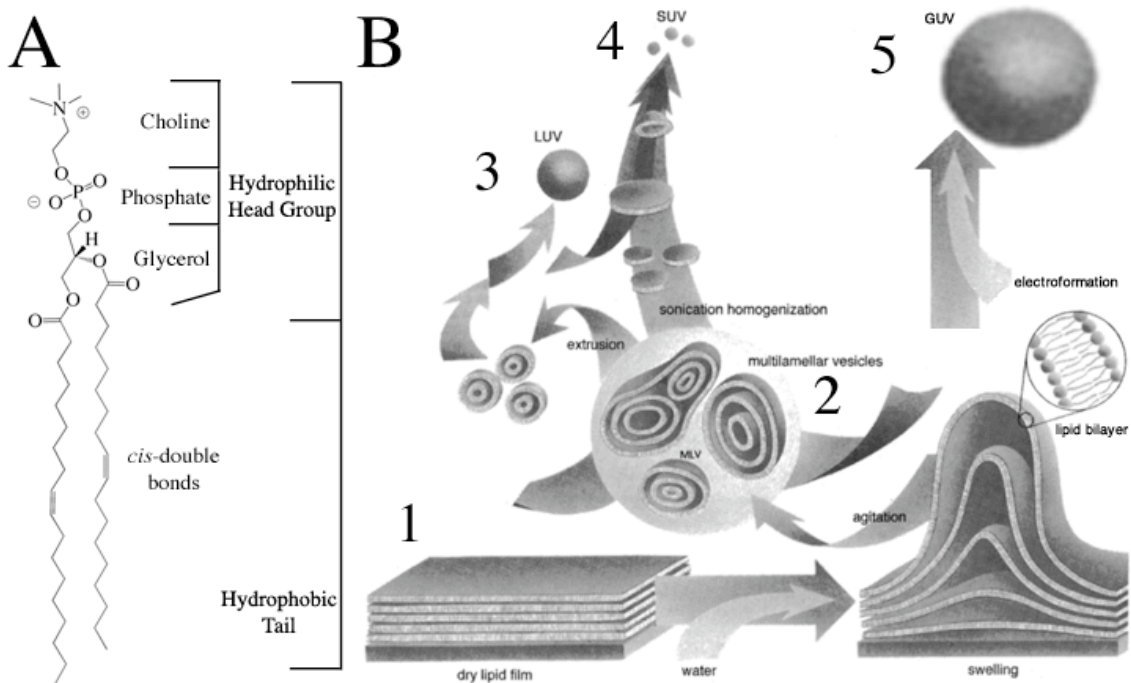


Figure 1.2: Diagram of a DOPC lipid and vesicle formation. (A) DOPC structure is shown with the hydrophilic head group and hydrophobic tail groups highlighted. (B) Vesicle formation. 1) The dried lipid film is shown and is the start of vesicle formation. 2) Upon addition of water the lipid swells and forms MLV upon agitation. 3) Extrusion of MLVs creates LUVs. 4) Sonication of MLVs creates a homogenous population of SUVs. 5) Electroformation of the dry lipid film when placed in water forms GUVs. Figure on right adapted from (13).

Many methods exist for incorporation of membrane proteins into vesicles, including organic solvent-mediated reconstitution, mechanical reconstitution, detergent-mediated reconstitution, and dried lipid-protein reconstitution. Organic solvent-mediated reconstitution has been used to incorporate rhodopsin into LUVs (16), but the organic solvents quickly degrade many membrane proteins (17). Mechanical reconstitution uses

force to fragment a bacterial cell and then fusion is allowed to occur with prepared MLVs. This method has been used for MscL preparations (18), but is not useable for a completely synthetic protein. Detergent-mediated reconstitution is the most successful and widely used procedure for reconstitution of membrane proteins into vesicles. Membrane proteins are purified, solubilized in an aqueous-detergent solution, and applied to a dry lipid film. MLVs containing lipid, protein, and detergent are then subjected to dialysis or polystyrene beads to selectively remove detergent (17,19). Detergent can alter the physical state of vesicles (20) and results in loss of reproducible gigaohm ($G\Omega$) seals necessary for electrophysiological characterization (18). Dried lipid-protein reconstitution involves the drying of both the lipid and protein and then forming vesicles. This method has been successfully used for the incorporation of gramicidin channels (21) and MscL (11).

1.2 Results

1.2.1 Vesicle Reconstitution of Synthetic MscL

Four different methods have been used for vesicle reconstitution of synthetic MscL, three of which will be discussed here. The fourth method was published recently and used a modified dried lipid-protein reconstitution technique (21) of drying MscL onto lipid and then forming unilamellar blisters by the addition of Mg^{2+} (11). The MLV preparation was developed by Dr. Joshua Maurer and found to have the pentameric oligomer state when cross-linked (Figure 1.3, A). Briefly, solubilized B-Tb-MscL in the detergent *n*-dodecyl β -D-maltoside (DDM) was used, and MLVs were formed by rehydration of dry DOPC (20). SUVs were formed upon selective removal of DDM

using polystyrene Bio-Beads and MLVs were then formed by the freeze-thaw technique (20,22). Removal of DDM is necessary to avoid thread-like micelles, open bilayer structures (19), and to obtain $G\Omega$ seals for patch clamp recording (18).

The electroformation technique initially developed by Angelova and Dimitrov was used to create GUVs (14,15). A Pt wire electrode chamber was hand made to create GUVs. The MLV preparation was dried on the Pt wires and a sine wave of 2 V at a frequency of 10 Hz was applied for one hour as previously described (23). A second indium tin oxide (ITO) coverslip chamber was also hand made, to create more uniform GUVs, in collaboration with Sean Gordon. Synthetic MscL was dried onto a previously dried lipid film (11) and a square wave voltage of 1.5 V at 10 Hz was applied for 1 h (24).

The MLV preparation was the easiest initial route for synthetic MscL characterization because the procedure was previously determined, and the observation of pentameric channels suggested functionally reconstituted MscL (Figure 1.3 A). The addition of concentrated Mg^{2+} to the MLVs was hoped to form blisters that could be used for electrophysiological recording (11,18). While SUVs and LUVs are unilamellar, they can't be used for electrophysiology because they are not large enough compared to the electrode opening and are not visible under a microscope (18). The electroformation technique was used to create GUVs that would be readily visualized under a microscope and amenable to patch-clamp analysis.

1.2.2 Electron Microscopy of B-Ec-MscL in MLVs

Electron microscopy (EM) on MLVs prepared with B-Ec-MscL was performed to visualize the membrane protein in the lipid bilayer through the binding of streptavidin-

coated gold beads to the N-terminal biotin moiety. MLVs were prepared containing B-Ec-MscL and without, as a control for non-specific labeling. Electron micrographs of MLVs showed many vesicles were ruptured and damaged when compared to light microscopy images (data not shown). Gold particles showed a random labeling pattern with no statistical difference between the control MLVs (data not shown). After two labeling trials, EM was abandoned because of a lack of uniform labeling required to demonstrate that B-Ec-MscL was reconstituted into the MLVs.

1.2.3 Oligomeric State of MscL Analyzed by Cross-Linking in MLVs

The crystal structure of Tb-MscL shows a homopentameric arrangement (6). Tb-MscL lacks any native cysteine residues for cross-linking and mutations would be necessary, which could alter channel organization. Lysines 99 and 100 form a cluster of charged residues in the cytoplasmic region of the structure and are $\sim 7 \text{ \AA}$ from the neighboring subunit counterparts. This proximity allows for the cross-linking of the primary amines using disuccinimidyl suberate (DSS), with a spacer arm of 11.4 \AA , as previously described (6).

The MLV and cross-linking method developed by Dr. Joshua Maurer showed a pentamer when DSS was added to B-Tb-MscL (Figure 1.3, A Lanes 2–4) similar to the cross-linking experiments performed by Rees and co-workers (6). Surprisingly, B-Tb-MscL shows some dimeric protein without DSS (Figure 1.3, A Lane 1). Achieving only a pentameric cross-linking was highly dependent on the amount of time the labeling was allowed to proceed (Dr. Joshua Maurer, personal communication). Figure 1.3, B Lanes 2–5 show cross-linking experiments using the same procedure with both B-Ec-MscL and Tb-MscL and show oligomer states higher than a pentamer. While B-Ec-MscL shows

nearly the same cross-linking with 1.5 and 3 μg B-Ec-MscL (Figure 1.3, B Lanes 2 & 3), the B-Tb-MscL samples show varying cross-linking with 1.5 and 3 μg of B-Tb-MscL (Figure 1.3, B Lanes 4 & 5). The variation in cross-linking shows the dependence on the amount of protein in the sample and shows the limitation in determining the number of subunits in an ion channels. Hexameric states have been previously reported in the literature based on cross-linking and EM (25,26). As a control, cross-linking was performed on proteins that were solubilized in DDM micelles, and no cross-linking was observed (Figure 1.3, B Lanes 6–9).

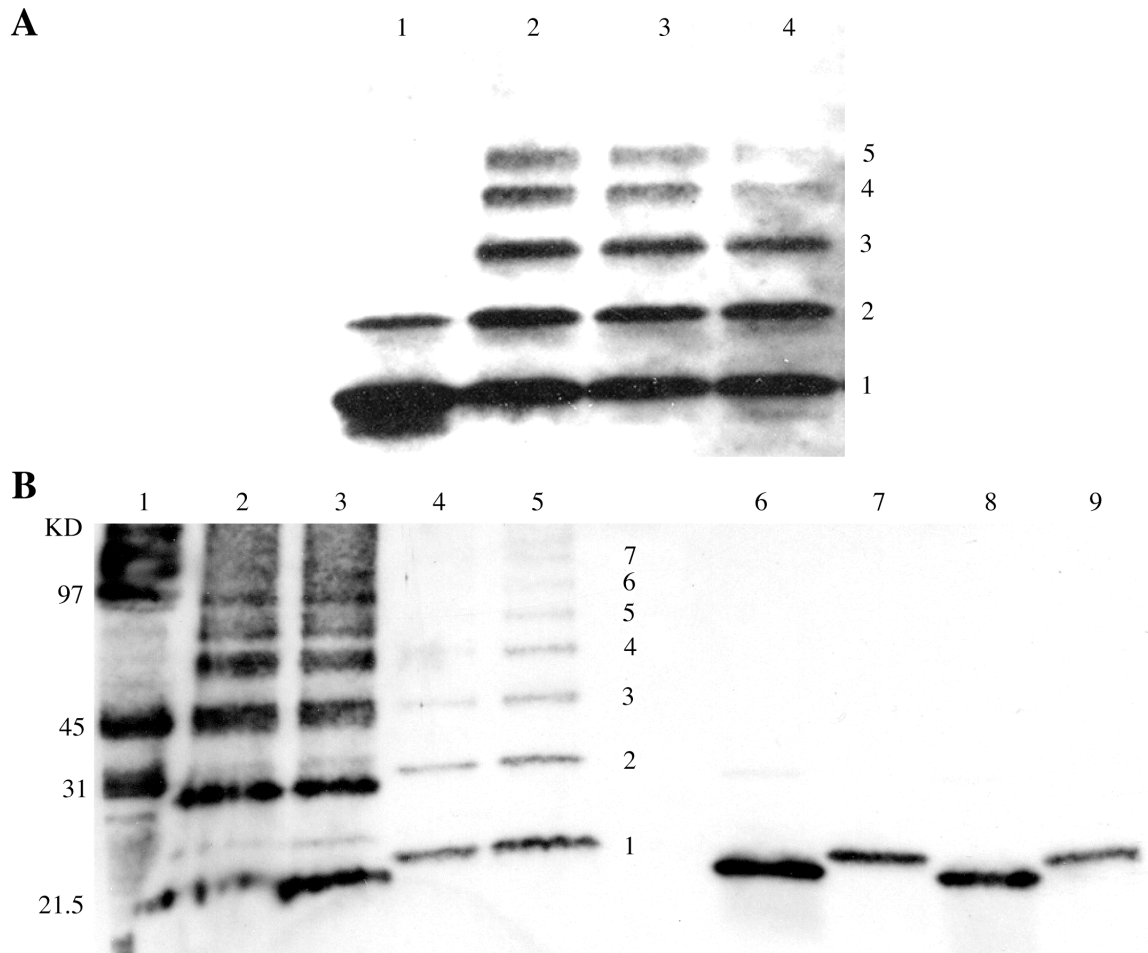


Figure 1.3: Oligomeric analysis of MscL using DSS cross-linking in MLVs. (A) Pentameric arrangement of B-Tb-MscL when incorporated into MLVs. Lane 1, B-Tb-MscL (2 μ g) without DSS. Lanes 2–4 are B-Tb-MscL (3 μ g) with DSS. Numbers to right represent number of subunits cross-linked. (B) Increased oligomers found when trying to replicate A. Lane 1, biotinylated molecular weight markers. Lane 2, B-Ec-MscL (1.5 μ g) with DSS. Lane 3, B-Ec-MscL (3 μ g) with DSS. Lane 4, B-Tb-MscL (1.5 μ g) with DSS. Lane 5, B-Tb-MscL (3 μ g) with DSS. Lanes 6 & 8, B-Ec-MscL (1 μ g) solubilized in DDM without and with DSS, respectively. Lanes 7 & 9, B-Tb-MscL (1 μ g) solubilized in DDM without and with DSS, respectively. Numbers in the center represent number of subunits cross-linked.

Reese and co-workers previously used the same technique for both Ec-MscL (3 μ g) and Tb-MscL (10 μ g), and the pentameric state was detected by staining with Coomassie brilliant blue (6). Coomassie brilliant blue has a detection limit of 0.1–0.5 μ g of protein (Amersham), while NeutrAvidin, HRP conjugated is at least 5 orders of

magnitude more sensitive with a detection limit of 0.05–1 pg of protein (Pierce). Therefore altering the detection may yield a similar pentameric oligomer state, but would give no definitive means for knowing the functional state of synthetic MscL within the MLVs.

1.2.4 Fluorescence Imaging

MLV preparations containing B-Ec-MscL, TFE (no protein), and biotinylated lipid (B-DHPE) were used for fluorescence labeling with streptavidin conjugated to AlexaFluor488 (streptavidin-AlexaFluor488). Initial fluorescence on MLV preparations with these three preparations failed to yield any differences between the three samples (data not shown). Labeling was performed using a sevenfold excess and caused a large degree of background labeling on the MLVs. The labeling procedure also involved removal of excess fluorophore by three freeze-thaw cycles, centrifugation, and resuspension, which causes the MLVs to aggregate and encapsulate non-specifically bound streptavidin-AlexaFluor488 (27).

B-Ec-MscL was then labeled with more biotin moieties using EZ-Link Sulfo-NHS-LC-Biotin (NHS-B), which reacts with the primary amine on lysine residues. The spacer arm is 22.4 Å, further than the N-terminal biotin, and would allow for multiple biotins on a single subunit. MLV preparations with B-Ec-MscL, TFE, and B-DHPE were treated with NHS-B and labeled with streptavidin-AlexaFluor488.

Figure 1.4 displays the results of this labeling trial and conditions are labeled above each column. Figure 1.4, row A shows vesicles formed with TFE and no protein. The fluorescence detected after exposure times of 200 ms and 1,000 ms shows no intensity change, and fluorescence is due to small amounts of fluorophore present in

solution and/or non-specifically bound to the vesicles. Figure 1.4, row B shows vesicles containing B-DHPE (same moles as B-Ec-MscL shown in Figure 1.4, C & D). The image at 200 ms exposure time shows high concentration of streptavidin-AlexaFluor488 bound to the vesicles (see Figure 1.4, B overlay) and exposure of 1,000 ms completely saturates the image. B-Ec-MscL MLVs are shown in Figure 1.4, and rows C & D exhibit very high fluorescing points along the surface of the vesicles. The lipid bilayer is not as uniformly labeled as in Clayton *et al.* (11), but illustrates a differential labeling among the controls and the vesicles containing B-Ec-MscL. Biotinylated lipid exhibits the highest fluorescent intensity and illustrates that the streptavidin-AlexaFluor488 is specifically labeling accessible biotin (Figure 1.4, row B), but B-Ec-MscL shows less fluorescence, suggesting the N-terminal biotin and lysine coupled biotin are less accessible to the streptavidin-AlexaFluor488 and/or the proteins are localizing to specific areas on the vesicles.

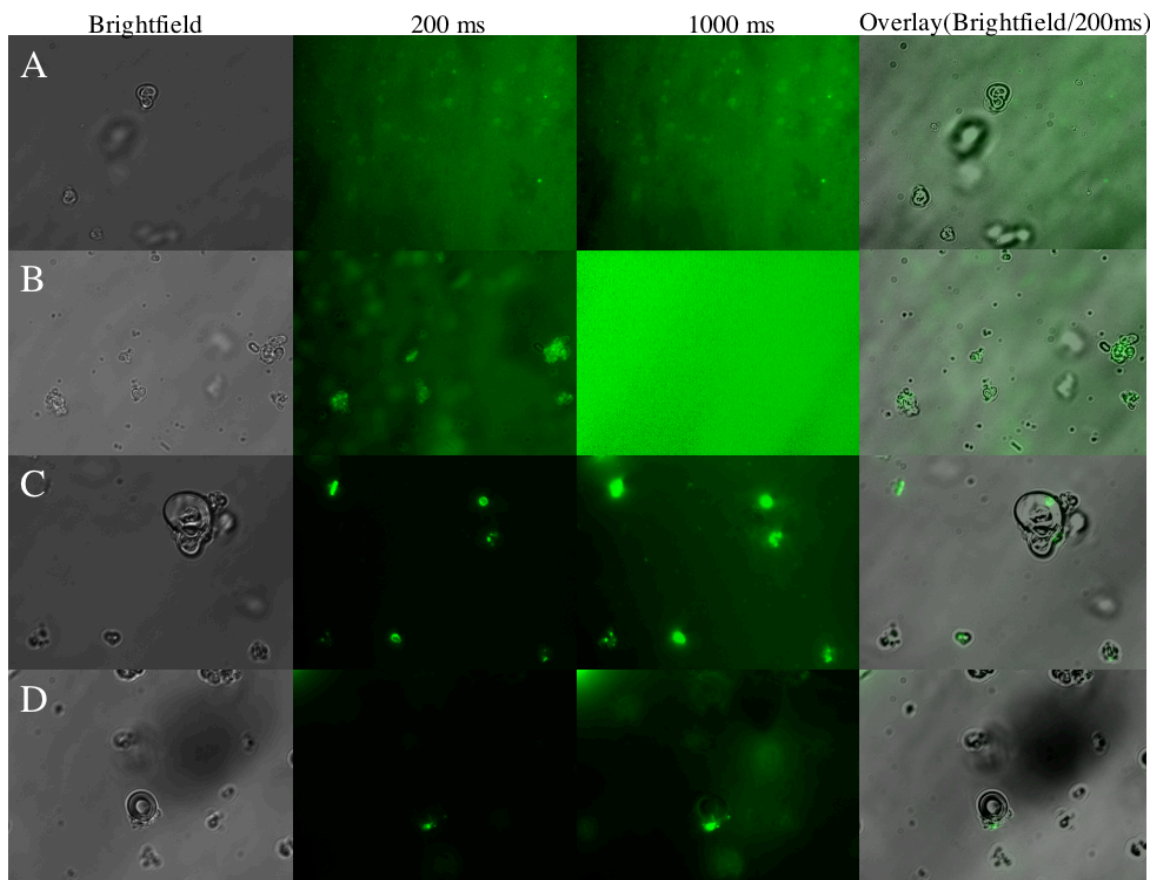


Figure 1.4: Fluorescence imaging of B-Ec-MscL in MLVs. All MLVs were subjected to the same procedure for additional labeling of biotin using NHS-B. Row A, Control MLVs lacking B-Ec-MscL (TFE only). Row B, MLVs containing biotinylated lipid (equivalent moles to B-Ec-MscL shown in C & D). Rows C & D, B-Ec-MscL containing MLVs. The far left column is imaging in brightfield. The two middle columns show fluorescence measurements with the exposure times listed above each column. The far right column is an overlay of the brightfield and fluorescence image (200 ms).

GUV fluorescence images were prepared using a lower concentration of streptavidin-AlexaFluor488 that was allowed to diffuse throughout the sample as described (11). Figure 1.5, A, D, and G–I show brightfield images of GUVs created using a 100 Hz frequency rather than 10 Hz. This frequency was chosen because the vesicles form in larger aggregates of GUVs, which are easier to locate. Note the unilamellar vesicles appear to have very thick bilayers due to the diffraction of light. Figure 1.5, B and C show a GUV fluorescing along the lipid bilayer and also show an

altered structure when compared to other brightfield GUVs. Many images showed large aggregates of streptavidin-AlexaFluor488 present along the vesicle surface (shown in Figure 1.5, E and F). However most GUVs showed no fluorescence (Figure 1.5, G–I) and were similar to the TFE control (data not shown).

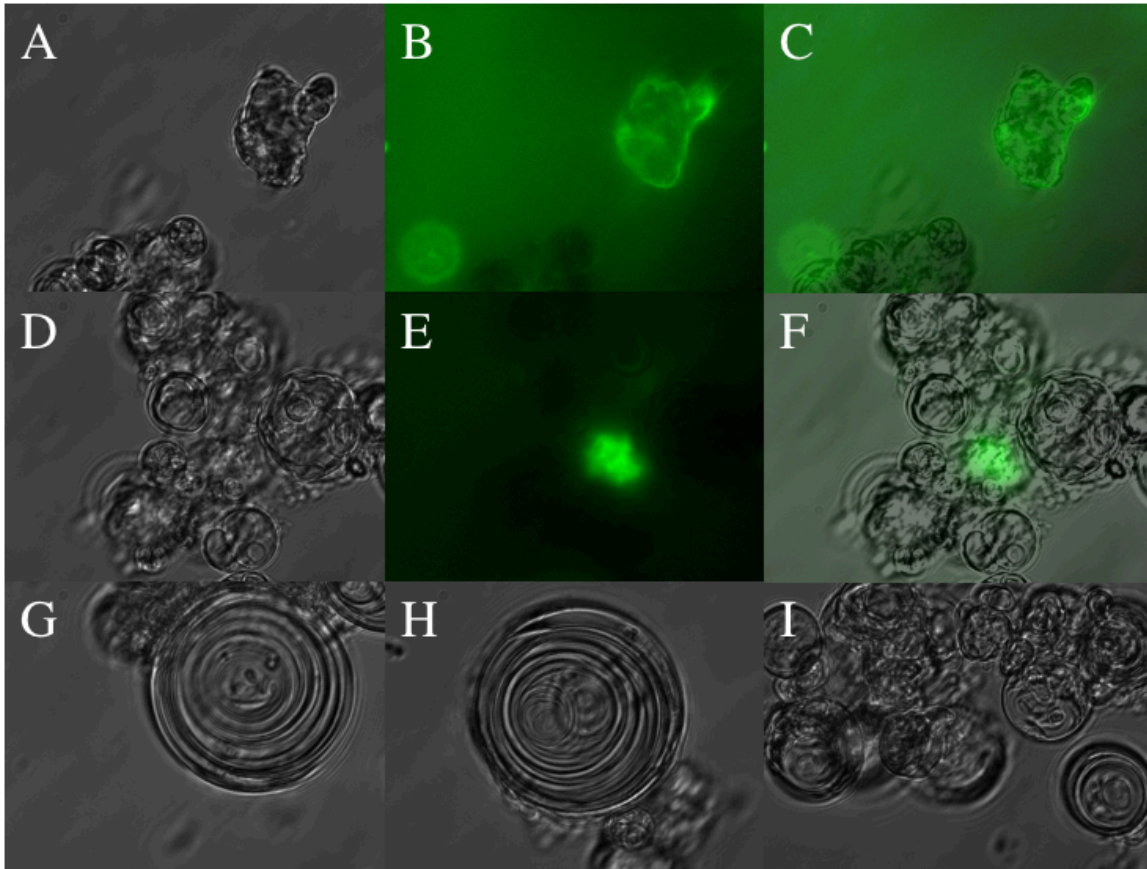


Figure 1.5: Fluorescence imaging of B-Ec-MscL GUVs prepared with Pt wire electrodes. (A & D) Brightfield images of B-Ec-MscL incorporated into GUVs. (B & E) Fluorescence images exposed for 100 ms. (C & F) Overlay of brightfield and fluorescence images. (G–I) Brightfield images of B-Ec-MscL incorporated in GUVs that showed no fluorescence.

The ITO coverslip GUV preparation was done in collaboration with Sean Gordon, who took all fluorescent images (Figure 1.6). DOPC GUVs were prepared by ITO coverslip electroformation and are shown in Figure 1.6, row A. The GUVs are labeled

with a hydrophobic fluorophore, DiI, which only fluoresces when incorporated into the lipid bilayer. Figure 1.6, B shows labeling of B-Ec-MscL incorporated into azolectin GUVs by perfusion of streptavidin-AlexaFluor488. The streptavidin-AlexaFluor488 is maintained outside of the vesicles throughout the labeling process, which is similar to vesicles perfused with AlexaFluor488 dye alone (data not shown). Figure 1.6, C shows B-Ec-MscL incorporated in azolectin GUVs washed with 1 mL of 1 X PBS. Fluorescent labeling is seen across all the lipid membranes, suggesting that the protein is distributed uniformly in the GUVs.

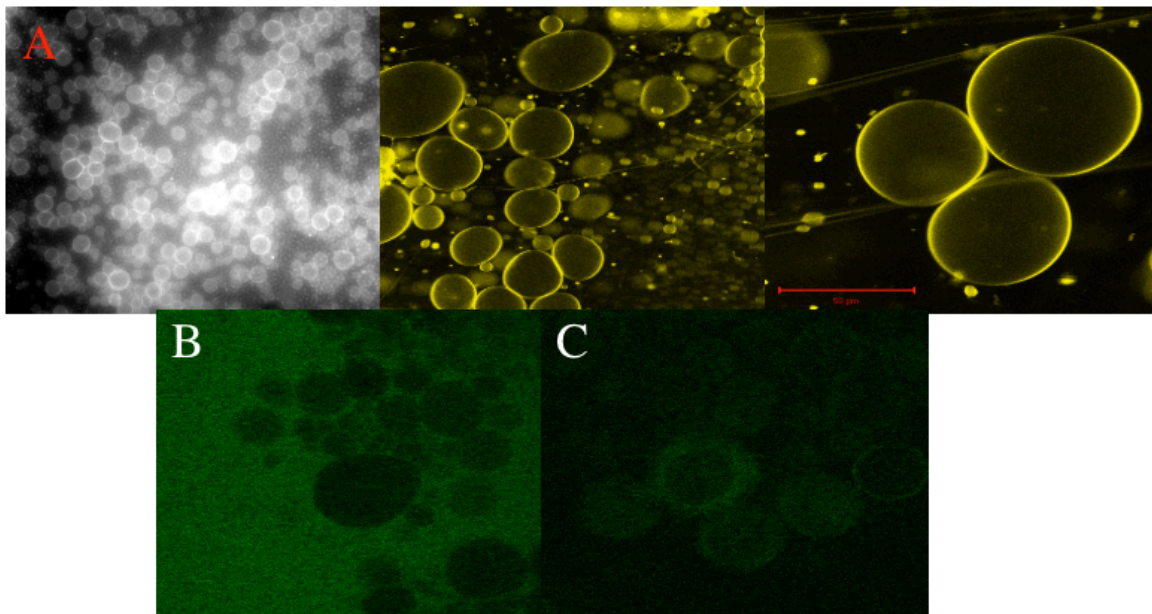


Figure 1.6: GUVs prepared by ITO coverslips and fluorescence imaging. (Row A) From left to right, DOPC GUVs under brightfield, fluorescence from DiI excitation, and fluorescence from DiI excitation zoomed in. Scale bar is 50 μm . Lower row is B-Ec-MscL incorporated in azolectin GUVs. (B) Perfusion with streptavidin-AlexaFluor488. (C) B-Ec-MscL incorporated in azolectin GUVs after wash with 1 X PBS to remove excess streptavidin-AlexaFluor488.

1.2.5 Electrophysiological Characterization of Pt Wire GUVs

Samples were prepared using DOPC and azolectin by the MLV preparation method, which reconstitutes B-Ec-MscL using DDM. After removal of the detergent using Bio-Beads, the samples were spread across the Pt wire and allowed to dry. Samples were given to Dr. George Shapovalov for single-channel patch-clamp recording. DOPC GUVs could not be studied because of failure to attain giga-ohm ($G\Omega$) seals. Azolectin GUVs containing B-Ec-MscL were able to attain $G\Omega$ seals and had similar channel activity to that reported for synthetic MscL (11). This clearly shows that B-Ec-MscL is incorporated in a functional state within the MLVs and subsequently into GUVs during electroformation with Pt wire electrodes. Interestingly the DOPC GUVs could not be recorded on, which is most likely due to the lipid composition of the membrane.

1.3 Discussion

The functional reconstitution of synthetic MscL was achieved through the use of the DDM-mediated reconstitution in MLVs and subsequent electroformation to create GUVs, which was shown by single-channel patch-clamp study. GUVs prepared by ITO coverslips show greater uniformity in spherical shape than GUVs prepared by a Pt wire. The ITO GUVs also have a higher yield, remain fixed to the translucent coverslip, and recording can easily be analyzed by electrophysiology performed on the giant vesicles. Overall, the GUV methods offer a means for reconstitution of functional MscL protein for electrophysiological characterization and should be amenable for the incorporation of other ion channels and membrane proteins.

GUV preparations are an optimal method for characterization of proteins *in vitro* through single-channel recordings in the absence of other proteins present within cells. KcsA, a tetrameric K⁺ channel, translated *in vitro* in the presence of LUVs was found to incorporate selectively within the lipid bilayer of LUVs (28). MscL and other simple homomeric prokaryotic ion channels may also spontaneously assemble into LUVs. Using this system along with nonsense suppression (29), unnatural amino acids could be selectively incorporated in MscL without the need for purification and GUVs could be made from LUVs. Many loss of function and gain of function MscL mutants were identified using a high throughput assay for channel function (30), but many of these mutations had drastic alterations in sterics or electrostatics when compared to the native amino acids. Unnatural amino acids could be incorporated at identified positions that are important for channel function and allowing analysis of specific interactions in more detail by electrophysiological characterization. Incorporation of fluorescent unnatural amino acids could also be utilized for fluorescence resonance energy transfer to gain dynamic information of ion channel function during gating.

1.4 Experimental Methods

1.4.1 Synthetic B-Ec-MscL Samples

B-Ec-MscL samples were chemically synthesized as described (11). Briefly, a modified native-chemical ligation technique was utilized to synthesize the full-length Ec-MscL with a biotin moiety placed at the N-terminus of the protein. Cysteine was substituted for glutamine 56 and asparagine 103 for the native-chemical ligation and selectively modified with bromoacetamide to produce side chains similar to native amino

acids in sterics and containing a terminal amide group. B-Tb-MscL was synthesized in a similar manner, substituting cysteine residues at glutamate 102 and serine 52 and masking with appropriate reagents. All samples were synthesized at Gryphon Therapeutics.

1.4.2 MLV Preparation and DDM-Mediated Reconstitution of B-Ec-MscL

10 X Rehydration Buffer (RB) (2.5 mM KCl, 1 mM EDTA, 50 mM HEPES, pH 7.2) was prepared and diluted as necessary. 79.8 μ l DOPC in chloroform (Avanti Polar Lipids) was placed in a glass vial and rotoevaporated to dryness for 10 min. 5.4 mg of DDM (Anatrace) was added to 1 mL 1 X RB (.5% DDM solution). 20.7 μ l of B-Ec-MscL in TFE (2 mg / mL) was placed into 220 μ l of .5% DDM solution and was directly added to the vial containing dried DOPC. The B-Ec-MscL / .5% DDM / TFE solution was agitated at room temperature for 5 h to allow for MLV formation. 16 mg of degassed Bio-Beads SM Adsorbents (Bio-Rad) was added to the MscL / .5% DDM / TFE solution, to selectively remove DDM as described in (19,22), and agitated at room temperature for 7 h. This preparation gave a protein-to-lipid ratio of 1:300.

1.4.3 GUV Preparation With Pt Wire Electrodes

GUVs were prepared by the electroformation technique as previously described (14,15,23). The chamber (shown in Figure 1.7) was hand made by attaching two 5 cm X 2 mm Pt wires (Alfa Aesar) 2 mm apart from each other with epoxy glue on a glass slide. Epoxy glue was placed 1 mm around the length of the Pt wires to create a reservoir. 4 μ l of the MLV preparation (described above) was spread across the Pt wires and dried under vacuum for 15 min. ~ 800 μ l of 1 X RB was added to the chamber and a sine wave of 2 V at 10 Hz frequency was applied for 1 h through the Pt wires.

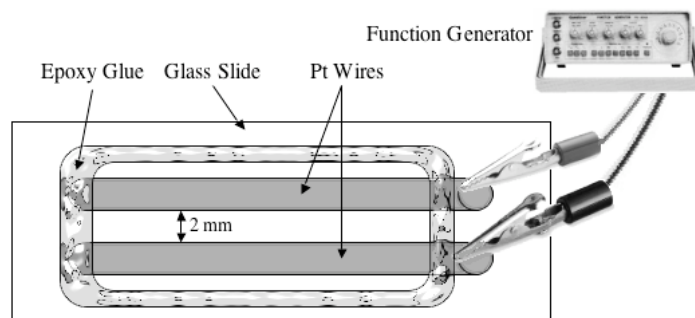


Figure 1.7: Diagram of Pt wire electrode chamber for GUV preparation.

1.4.4 GUV Preparation With ITO Coverslips

GUVs were prepared by the electroformation technique as previously described (14,15,24). GUVs are produced in varying diameter from 10 to 100 μm , with a mean diameter of 50 μm . The chamber (shown in Figure 1.8) was hand made by cutting a circle of 1.5 cm in a 35 X 10 mm plastic tissue culture dish (BD Biosciences). Coverslips were covered in a 75 \AA layer of ITO (gift from Jerry Pine). 4 X .5 cm copper electrical conducting tape was attached to the ITO layer of two coverslips. The first coverslip was attached to the bottom of the tissue culture dish, centered under the circle to fully cover, with epoxy glue. Vacuum grease (Dow Corning) was spread around the circle to form a liquid barrier and to create a spacer for the second coverslip. 4 μl of 1 μg / ml DOPC in chloroform (Avanti Polar Lipids) or 1 μg / ml azolectin in chloroform (Sigma-Aldrich) was spread across the attached coverslip and air-dried for 20 min. For B-Ec-MscL reconstitution, 24 ng (1:5000 protein to lipid ratio) or 121 ng (1:1000 protein to lipid ratio) of B-Ec-MscL in TFE was smeared across the dried lipid on the coverslip and dried for 30 min under vacuum as previously described (11,21). \sim 300 μl millipore water was added to the chamber (to fill) and the second coverslip placed on top (making sure full

water contact is made throughout the area). A square wave voltage of 1.5 V at 10 Hz frequency was applied for 1 h through the copper electrical conducting tape.

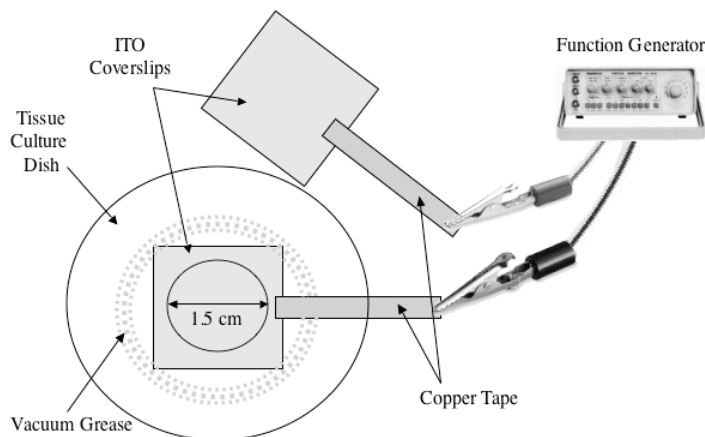


Figure 1.8: Diagram of ITO coverslip chamber for GUV preparation. (Top coverslip is placed on vacuum grease when square wave is applied.)

1.4.5 Electron Microscopy of B-Ec-MscL in MLVs

Samples were prepared as previously described (31). Copper grids were coated with collodion/carbon and evaporated under vacuum to be made hydrophobic (prepared by Pat Koen, Caltech Electron Microscope Facility). 10 μl of the MLV preparation (described above), with and without B-Ec-MscL, was labeled with 10 μl of AuroProbe EM Streptavidin G10 (Amersham Biosciences) with agitation for 12 h. The total sample (20 μl) was placed on the copper grid and allowed to dry for 1 min. #5 Whatman filter paper was used to dry remaining solution by touching the edge of the copper grid. 30 μl of a 1% phosphotungstic acid (Sigma-Aldrich) was added to the grid, left for 30 sec, and dried with filter paper. 30 μl of a 2% uranyl acetate (Sigma-Aldrich) solution was added to the grid, left for 30 sec, and dried with filter paper. Grids were examined in a

transmission electron microscope (Philips 420) in the Caltech Electron Microscope Facility.

1.4.6 Cross-Linking of MscL in MLVs

8.7 μl (1.5 μg B-Ec/Tb-MscL) or 17.4 μl (3 μg B-Ec/Tb-MscL) of the MLV vesicle preparation (described above) was mixed with 2.5 or 5 μl of 8 mM DSS (Pierce), respectively. Samples were sonicated for 5 min at room temperature and quenched with 10 μl of urea gel loading buffer (50 mM TrisCl, pH 6.8, 2% SDS, 10% glycerol, 10 M urea, and .1% bromophenol blue). Samples were boiled for 3 min and subjected to SDS-polyacrylamide gel electrophoresis and transferred to nitrocellulose. Biotinylated SDS-PAGE standards (Bio-Rad) were run as a molecular weight marker. Standard Western blot procedures were used and protein was visualized using 45 μl NeutrAvidin, HRP conjugated (Pierce).

1.4.7 Fluorescence Imaging

30 μl of MLV preparations (B-Ec-MscL, TFE, & *N*-(biotinoyl)-1,2-dihexadecanoyl-*sn*-glycero-3-phosphoethanolamine (B-DHPE) (Molecular Probes) were prepared to pH = 8 with KOH. 0.83 μl of 10 mM EZ-Link Sulfo-NHS-LC-Biotin (Pierce) was added and incubated at room temperature for 3 h. 6 μl of 0.1 mg / ml streptavidin-AlexaFluor488 (Molecular Probes) in 1 X PBS was added and agitated for 12 h. Samples were sequentially freeze-thawed 3 times, centrifuged 5 min, supernatant was removed, and MLVs were resuspended in 35 μl of 1 X RB. 2 μl of 0.1 mg / ml streptavidin-AlexaFluor488 (Molecular Probes) in 1 X PBS was added to 400 μl of Pt wire GUV preparation containing B-Ec-MscL (made at 100 Hz) and labeling was allowed to proceed for 1 h. Fluorescence was observed on an Olympus IX71 inverted

microscope equipped with a shuttered 175 W xenon arc lamp, 488 nm excitation filter, a 515 nm fluorescence cube, and an Olympus Plan Apo 60X /1.4 numerical aperture oil immersion objective. Images were recorded using a Photometrix CCD camera.

ITO coverslip prepared GUVs were made with 15.7 μg of DOPC and 0.19 μg DiI (Molecular Probes), from 5 mM stock solution in chloroform, and B-Ec-MscL as described above with 1:5000 or 1:1000 protein-to-lipid ratio. B-Ec-MscL GUVs were labeled by perfusion of 500 μl of 10 ng / μl streptavidin-AlexaFluor488. Fluorescence images were taken at this point (Figure 1.6, B) and then vesicles were washed with 1 mL of 1 X PBS. Fluorescence was observed on a Zeiss LSM Pascal Inverted confocal microscope equipped with an Ar Laser (488 nm, 25 mW), two-channel fluorescence/reflection, and motorized XY scanning stage. Images were acquired at 12 bit per channel and processed using Zeiss LSM v.3.0sp2. (Caltech Biological Imaging Center).

1.4.8 Electrophysiological Characterization of Pt Wire GUVs

GUVs were prepared with the Pt wire chamber (described above). B-Ec-MscL GUVs were prepared with either DOPC or azolectin lipids. Single-channel recordings were made by Dr. George Shapovalov as described in Clayton *et al.* (11).

1.5 References

1. Perozo, E., and Rees, D.C. (2003) Structure and mechanism in prokaryotic mechanosensitive channels. *Curr. Opin. Struct. Biol.*, **13**, 432–442.

2. Sukharev, S.I., Blount, P., Martinac, B., and Kung, C. (1997) Mechanosensitive channels of *Escherichia coli*: the MscL gene, protein, and activities. *Annu. Rev. Physiol.*, **59**, 633–657.
3. Wood, J.M. (1999) Osmosensing by bacteria: Signals and membrane-based sensors. *Microbiol. Mol. Biol. Rev.*, **63**, 230–262.
4. Morbach, S., and Kramer, R. (2002) Body shaping under water stress: Osmosensing and osmoregulation of solute transport in bacteria. *Chembiochem.*, **3**, 384–397.
5. Sukharev, S.I., Blount, P., Martinac, B., Blattner, F.R., and Kung, C. (1994) A large-conductance mechanosensitive channel in *E. coli* encoded by *mscL* alone. *Nature*, **368**, 265–268.
6. Chang, G., Spencer, R.H., Lee, A.T., Barclay, M.T., and Rees, D.C. (1998) Structure of the MscL homolog from *Mycobacterium tuberculosis*: A gated mechanosensitive ion channel. *Science*, **282**, 2220–2226.
7. Maurer, J.A., Elmore, D.E., Lester, H.A., and Dougherty, D.A. (2000) Comparing and contrasting *Escherichia coli* and *Mycobacterium tuberculosis* mechanosensitive channels (MscL). New gain of function mutations in the loop region. *J. Biol. Chem.*, **275**, 22238–22244.
8. Sukharev, S.I., Sigurdson, W.J., Kung, C., and Sachs, F. (1999) Energetic and spatial parameters for gating of the bacterial large conductance mechanosensitive channel, MscL. *J. Gen. Physiol.*, **113**, 525–540.

9. Anishkin, A., Gendel, V., Sharifi, N.A., Chiang, C.S., Shirinian, L., Guy, H.R., and Sukharev, S. (2003) On the conformation of the COOH-terminal domain of the large mechanosensitive channel MscL. *J. Gen. Physiol.*, **121**, 227–244.
10. Shapovalov, G., Bass, R., Rees, D.C., and Lester, H.A. (2003) Open-state disulfide crosslinking between *Mycobacterium tuberculosis* mechanosensitive channel subunits. *Biophys. J.*, **84**, 2357–2365.
11. Clayton, D., Shapovalov, G., Maurer, J.A., Dougherty, D.A., Lester, H.A., and Kochendoerfer, G.G. (2004) Total chemical synthesis and electrophysiological characterization of mechanosensitive channels from *Escherichia coli* and *Mycobacterium tuberculosis*. *Proc. Natl. Acad. Sci. USA*, **101**, 1764–4769.
12. Spencer, R.H., and Rees, D.C. (2002) The alpha-helix and the organization and gating of channels. *Annu. Rev. Biophys. Biomol. Struct.*, **31**, 207–233.
13. Lasic, D.D. (1997) *Liposomes in Gene Delivery*. CRC Press LLC, Boca Raton, FL.
14. Angelova, M., and Dimitrov, D. (1986) Liposome electroformation. *Faraday Discuss. Chem. Soc.*, **81**, 303–308.
15. Dimitrov, D., and Angelova, M. (1988) Lipid swelling and liposome electroformation mediated by electric fields. *Bioelectrochem. Bioenerg.*, **19**, 323–333.
16. Szoka, F., Jr., and Papahadjopoulos, D. (1978) Procedure for preparation of liposomes with large internal aqueous space and high capture by reverse-phase evaporation. *Proc. Natl. Acad. Sci. USA*, **75**, 4194–4198.

17. Rigaud, J.L., Pitard, B., and Levy, D. (1995) Reconstitution of membrane proteins into liposomes: Application to energy-transducing membrane proteins. *Biochim. Biophys. Acta.*, **1231**, 223–246.
18. Delcour, A.H., Martinac, B., Adler, J., and Kung, C. (1989) Modified reconstitution method used in patch-clamp studies of *Escherichia coli* ion channels. *Biophys. J.*, **56**, 631–636.
19. Knol, J., Sjollem, K., and Poolman, B. (1998) Detergent-mediated reconstitution of membrane proteins. *Biochemistry*, **37**, 16410–16415.
20. Lambert, O., Levy, D., Ranck, J.L., Leblanc, G., and Rigaud, J.L. (1998) A new "gel-like" phase in dodecyl maltoside-lipid mixtures: Implications in solubilization and reconstitution studies. *Biophys. J.*, **74**, 918–930.
21. Lougheed, T., Borisenko, V., Hand, C.E., and Woolley, G.A. (2001) Fluorescent gramicidin derivatives for single-molecule fluorescence and ion channel measurements. *Bioconjug. Chem.*, **12**, 594–602.
22. Chami, M., Steinfels, E., Orelle, C., Jault, J.M., Di Pietro, A., Rigaud, J.L., and Marco, S. (2002) Three-dimensional structure by cryo-electron microscopy of YvcC, an homodimeric ATP-binding cassette transporter from *Bacillus subtilis*. *J. Mol. Biol.*, **315**, 1075–1085.
23. Sanchez, S.A., Bagatolli, L.A., Gratton, E., and Hazlett, T.L. (2002) A two-photon view of an enzyme at work: *Crotalus atrox* venom PLA2 interaction with single-lipid and mixed-lipid giant unilamellar vesicles. *Biophys. J.*, **82**, 2232–2243.

24. Kahya, N., Pecheur, E.I., de Boeij, W.P., Wiersma, D.A., and Hoekstra, D. (2001) Reconstitution of membrane proteins into giant unilamellar vesicles via peptide-induced fusion. *Biophys. J.*, **81**, 1464–1474.
25. Blount, P., Sukharev, S.I., Moe, P.C., Schroeder, M.J., Guy, H.R., and Kung, C. (1996) Membrane topology and multimeric structure of a mechanosensitive channel protein of *Escherichia coli*. *Embo. J.*, **15**, 4798–4805.
26. Saint, N., Lacapere, J.J., Gu, L.Q., Ghazi, A., Martinac, B., and Rigaud, J.L. (1998) A hexameric transmembrane pore revealed by two-dimensional crystallization of the large mechanosensitive ion channel (MscL) of *Escherichia coli*. *J. Biol. Chem.*, **273**, 14667–14670.
27. Sou, K., Naito, Y., Endo, T., Takeoka, S., and Tsuchida, E. (2003) Effective encapsulation of proteins into size-controlled phospholipid vesicles using freeze-thawing and extrusion. *Biotechnol. Prog.*, **19**, 1547–1552.
28. van Dalen, A., van der Laan, M., Driessen, A.J., Killian, J.A., and de Kruijff, B. (2002) Components required for membrane assembly of newly synthesized K⁺ channel KcsA. *FEBS Lett.*, **511**, 51–58.
29. Dougherty, D.A. (2000) Unnatural amino acids as probes of protein structure and function. *Curr. Opin. Chem. Biol.*, **4**, 645–652.
30. Maurer, J.A., and Dougherty, D.A. (2003) Generation and evaluation of a large mutational library from the *Escherichia coli* mechanosensitive channel of large conductance, MscL: Implications for channel gating and evolutionary design. *J. Biol. Chem.*, **278**, 21076–21082.

31. Barnakov, A.N. (1994) Sequential treatment by phosphotungstic acid and uranyl acetate enhances the adherence of lipid membranes and membrane proteins to hydrophobic EM grids. *J. Microsc.*, **175**, 171–174.

Chapter 2

Evaluating Aminoacylation and Suppression

Efficiency of Nonsense and Frameshift

Suppressor tRNAs *In Vitro*

2.1 Introduction

Site-specific incorporation of unnatural amino acids (UAAs) into proteins biosynthetically is a valuable technique that is seeing increased use (1–4). UAAs are site-specifically incorporated into proteins translated *in vitro* and *in vivo* either by nonsense suppression or frameshift suppression (Figure 2.1). The primary site-specific incorporation technique is known as stop codon (nonsense) suppression and requires a suppressor tRNA, with a modified anticodon, that recognizes the stop codon. The amber stop codon (UAG) is primarily utilized for UAA incorporation (Figure 2.1 A), but the opal stop codon (UGA) has been utilized in eukaryotic cells to incorporate a single UAA (5,6). The suppressor tRNA can be chemically aminoacylated with an UAA (2,3,7–9) or enzymatically aminoacylated with an UAA using tRNA/aminoacyl-synthetase pairs (4,5,10,11). Currently over 100 UAAs or residues (five times greater than the 20 naturally occurring amino acids (aas)) have been incorporated by chemically aminoacylated tRNAs (12), but at the onset of this research only a single UAA could be incorporated into a protein.

The Dougherty group uses nonsense suppression of the amber codon (UAG) to incorporate a single UAA to probe a wide array of structural and functional properties of the mouse muscle nicotinic acetylcholine receptor (nAChR) *in vivo* (2,13–15). A modified *Tetrahymena thermophila* tRNA^{Gln}, containing the mutation U73G and the CUA anticodon, (THG73) (16) is chemically aminoacylated *in vitro* with an UAA and injected into *Xenopus* oocytes with ion channel mRNA (with the stop codon, UAG, at the suppression site). To obtain full-length protein, the UAA must be incorporated at the

amber codon or the protein is truncated (Figure 2.1 A) (16). This technique has also been extended to incorporate UAAs in mammalian cells using THG73 (13).

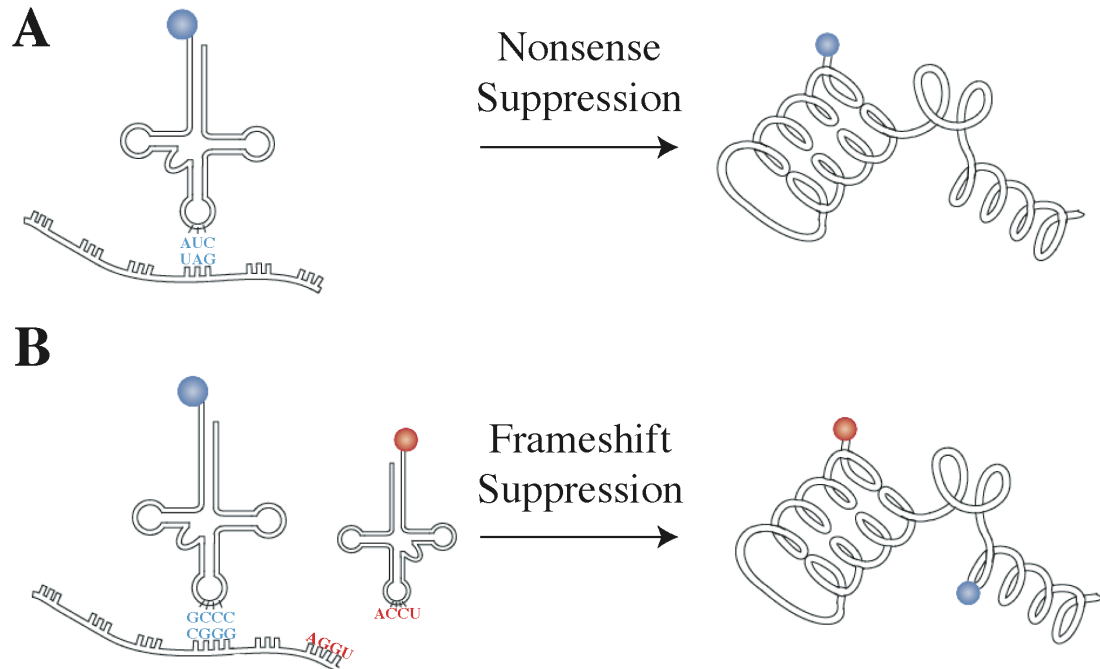


Figure 2.1: UAA incorporation techniques. (A) Nonsense suppression: a stop codon recognizing tRNA suppresses a stop codon and incorporates an UAA. (B) Frameshift suppression: a frameshift suppressor tRNA recognizes a quadruplet codon and incorporates an UAA. Initially this was the only technique that could incorporate multiple UAAs *in vitro* (17). Figure adapted from (1).

Pioneering work developed by Sisido and coworkers used quadruplet codons to incorporate UAAs, which is a technique known as frameshift suppression (18). Using two unique quadruplet codons allowed for the simultaneous incorporation of two UAAs into a single protein translated *in vitro* (17) (Figure 2.1 B). The technique was viable in prokaryotic (18,19) and eukaryotic (20,21) *in vitro* translation systems. Intriguingly, five-base codons could also be utilized to incorporate UAAs, but the suppression efficiency was much less than with four-base codons (22). However, frameshift

suppression was limited to *in vitro* translation systems and *in vivo* UAA incorporation by frameshift suppression had not been shown at the start of this project.

While a single UAA incorporation allows for many useful structure-function studies, incorporation of multiple UAAs would allow for a more diverse experiments; including FRET pairs (23), fluorescence quenching (24), unnatural sulfur derivatives for disulfide cross-linking, and alteration of the sterics and electrostatic properties of more than one amino acid within a protein. Frameshift suppression allows for the incorporation of multiple UAAs *in vitro*, either through the use of two four-base codons (17,24) (Figure 2.1 B) or through the use of one quadruplet codon and the amber codon (UAG) (23,25). These UAA incorporation experiments are typically performed on small, cytoplasmic proteins, such as streptavidin, and it was therefore unknown if large, multi-subunit proteins, such as ion channels, would be feasible for multiple UAA incorporation *in vivo*.

The mechanism of nonsense and frameshift suppression is shown in Figure 2.2. UAA incorporation by nonsense suppression is performed by a tRNA aminoacylated with an UAA that recognizes the stop codon placed at the suppression site (Figure 2.2 A). Competition for UAA incorporation arises from the protein release factor (RF1 and/or RF2, depending on the stop codon, in prokaryotes and eRF1 in eukaryotes) and recognition of the stop codon results in truncation of the protein, which is typically non-functional, unfolded, and degraded *in vivo* (Figure 2.2 B). Frameshift suppression requires a modified frameshift suppressor tRNA, containing a four-base anticodon, and incorporation of the UAA occurs by suppression at the quadruplet codon (18,25) (Figure 2.2 C). Competition for recognition of the suppression site arises from an endogenous

triplet recognizing tRNA, which causes a -1 frameshift and results in the presentation of an altered amino acid sequence and multiple stop codons (Figure 2.2 D). Another undesired suppression can result when the frameshift suppressor tRNA recognizes a triplet and the adjacent nucleotide (same sequence as the suppression site), resulting in a +1 frameshift. This undesired suppression results in loss of the UAA and results in truncation of the protein (Figure 2.2 E). Due to this undesirable suppression event, mutation of quadruplet codons that are recognized by the frameshift suppressor tRNA can be performed using the degeneracy of the genetic code to increase incorporation efficiency, this is known as “masking” and mutated genes are named the masked constructs (25).

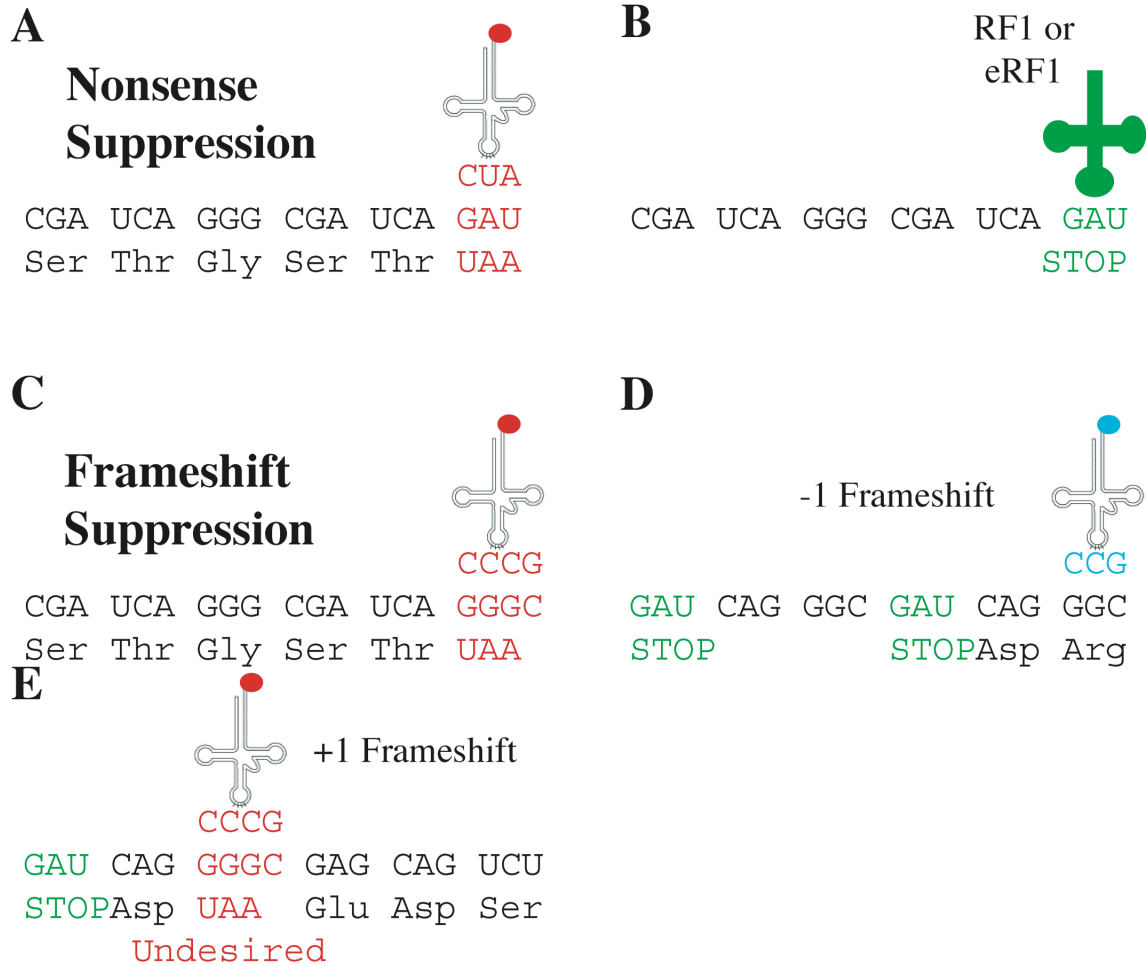


Figure 2.2: Mechanism of nonsense and frameshift suppression. (A) Nonsense suppression, an amber suppressor tRNA recognizes the desired UAG stop codon and incorporates an UAA. (B) Competition for nonsense suppression arises from a protein release factor (RF1, for UAG, in prokaryotes and eRF1 in eukaryotes) and causes termination of the protein sequence. (C) Frameshift suppression, a frameshift suppressor tRNA recognizes the desired four-base codon and incorporates an UAA. The CGGG codon is shown, but any four- or five-base codon is considered frameshift suppression. (D) Competition arises from endogenous tRNA that recognizes the first three bases of the quadruplet codon, which results in a -1 frameshift (at the same position shown in C) and results in truncation by stop codons (shown in green) presented after the -1 frameshift. (E) An undesired suppression event can occur where the frameshift suppressor tRNA recognizes another cognate four-base codon in the mRNA sequence, which results in the incorporation of an UAA and a +1 frameshift. The +1 frameshift causes truncation by stop codons (shown in green) presented after the +1 frameshift. mRNAs are written from 5' to 3' going from right to left. tRNAs are adapted from (1).

The development of frameshift suppression for the *in vivo* incorporation of multiple UAAs was initially analyzed *in vitro* to ensure that the eukaryotic ribosome would tolerate the extended anticodon of the frameshift suppressor tRNAs and/or four-base codons at the suppression site, which was unknown at the start of this research. Initial suppression experiments were performed on the mouse muscle nAChR α -subunit containing an N-terminal hemagglutinin epitope (α_{NHA}), which allows for analysis of truncated and full-length protein by Western blotting (14). The four-base codons analyzed in this study were CGGG (shown to suppress efficiently in previous studies (17,26)), CGUG, and CGUU. CGUG and CGUU were chosen because CGU is the least-used Arg triplet in rabbit (27), which should have less competition with endogenous triplet-recognizing tRNA^{Arg} during translation (Figure 2.2 D) and may increase the suppression efficiency (17,26,28). The human Ser amber suppressor (HSAS) (29), *Tetrahymena thermophila* Gln amber suppressor (THG73) (16), and yeast Phe amber suppressor (YFAS) (18) were used to prepare the frameshift suppressor tRNAs (shown in Figure 2.3). HSAS is aminoacylated by the seryl-tRNA synthetase (SerRS) in mammalian cells (13,29) and was chosen to create frameshift suppressor tRNAs because the *E. coli* SerRS crystal structure reveals no recognition of the anticodon loop (30) and mammalian cells also don't recognize the anticodon (31). THG73 is an orthogonal amber suppressor in *Xenopus* oocytes, in that it is not extensively aminoacylated by the endogenous aminoacyl-tRNA synthetases (aaRSs). THG73 has been used extensively for the incorporation of UAAs (18). YFAS has been modified by the Sisido group and shown to incorporate UAAs by suppressing quadruplet codons (17–19). To create the frameshift suppressor tRNAs, the appropriate anticodons (CCCG, CACG, AACG;

written 5'-3') were placed on HSAS, THG73, and YFAS (Figure 2.3). The frameshift suppressor tRNAs were analyzed *in vitro* by suppressing quadruplet codons in the α_{NHA} and suppression efficiency was evaluated by Western blots and densitometric analysis.

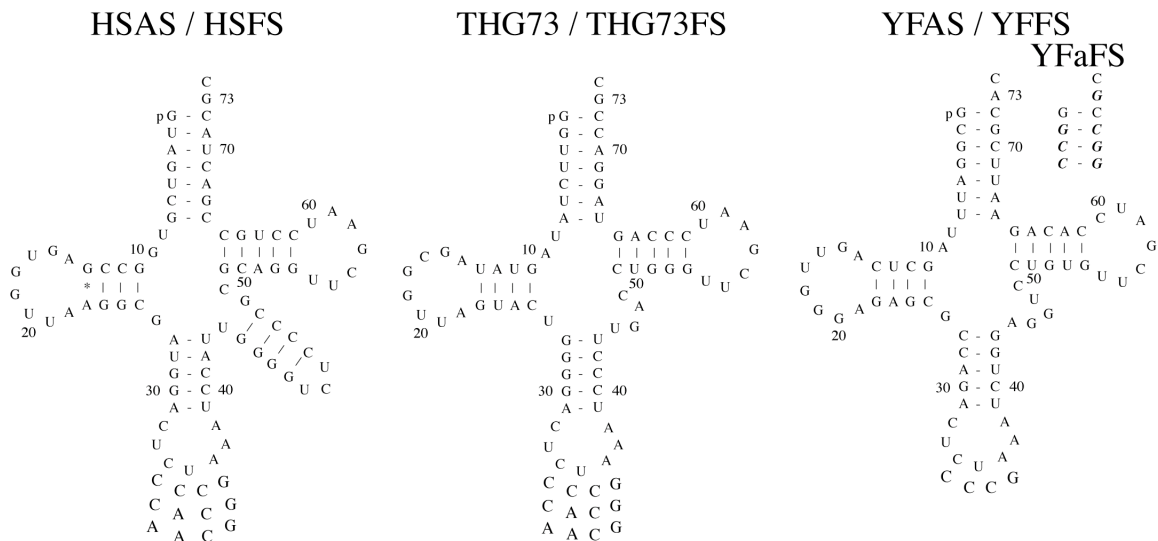


Figure 2.3: Nucleotide sequences and cloverleaf structures of suppressor tRNAs tested *in vitro*. On the left, the human Ser amber suppressor (HSAS) tRNA is shown and is aminoacylated *in vitro* by the SerRS (29). In the middle, *Tetrahymena thermophila* Gln amber suppressor U73G (THG73) is an orthogonal tRNA (not aminoacylated by aaRSs) used for the incorporation of UAAs primarily in *Xenopus* oocytes (16). On the right, the yeast Phe amber suppressor (YFAS) is shown and was the first tRNA used to incorporate UAAs *in vitro* (7). Mutations to the acceptor stem (shown in italics) of the YFAS are shown in the upper right and used by the Sisido group to reduce recognition of frameshift suppressor tRNAs by the GlyRS (19). Below the tRNAs are the four-base anticodons placed on each tRNA to create frameshift suppressor (FS) tRNAs tested *in vitro*.

2.2 Results & Discussion

2.2.1 Experimental Design and Western Blot Analysis

The nAChR α -subunit with the N-terminal HA tag (α_{NHA}) was the initial construct for all mutations because the N-terminal HA tag allows for detection by Western blot (14), all truncations could be visualized, and this was prior to any Arg amino acids that could cause a +1 frameshift (Figure 2.2 E). Initially, constructs were

created at Ser sites because HSAS and HSFS were predicted to be aminoacylated with Ser by the SerRS *in vitro*. Ser154 was chosen as the first suppression site because it was $\approx 1/3$ of the protein sequence. Ser374 was chosen as the second suppression site because it was $\approx 2/3$ of the protein sequence. These initial suppression sites were thought to be useful for *in vivo* studies later in *Xenopus* oocytes.

The α_{NHA} was translated using rabbit reticulocyte lysate (RRL), nuclease treated *in vitro* reactions unless otherwise noted. Standard Western blotting procedures were followed and done as published (14), unless otherwise noted. The full-length α subunit is predicted to run at 53 KD, but the α -subunit runs on gel as ≈ 45 KD (14). Densitometric analysis was performed using NIH Image, which imports scanned exposures and analyzes the pixel intensity. Bands are manually selected and the average pixel intensity for each band was taken. Suppression efficiency was calculated as written in the Experimental Methods.

2.2.2 HSAS Suppression on $\alpha_{\text{NHA}}154\text{UAG}$ and $\alpha_{\text{NHA}}154\text{UAG}374\text{UAG}$

Figure 2.4 shows $\alpha_{\text{NHA}}154\text{UAG}$ and $\alpha_{\text{NHA}}154\text{UAG}374\text{UAG}$ suppressed with HSAS. The Western blot illustrates that HSAS is aminoacylated in the RRL *in vitro* translation system by an endogenous aaRS, which was previously unknown. The $\alpha_{\text{NHA}}154\text{UAG}$ construct is suppressed 59% relative to α_{NHA} by 1 μg of HSAS (Figure 2.4, Lane 3), but increased suppression (94%) is seen with 2 μg of HSAS (Figure 2.4, Lane 5). The $\alpha_{\text{NHA}}154\text{UAG}374\text{UAG}$ construct contains two stop codons and requires two suppression events for full-length (FL) protein, and with 2 μg of HSAS the translation efficiency is 33% (Figure 2.4, Lane 7). This illustrates that suppression at two positions is not a concerted event (where suppression of the first UAG facilitates the suppression of

the second UAG), but rather that each suppression is an individual event and the translation efficiency of two sites is equal to the probability of a single suppression event (17). The single suppression efficiency is 59% with 1 μg HSAS and the double translation efficiency is 33% with 2 μg HSAS. The theoretical yield of full-length protein for two suppression events would be equal to $59\% \times 59\% = 35\%$, which is close to the actual value of 33%. The Western blot in Figure 2.4 is overexposed and the translation efficiencies listed here are actually overestimated.

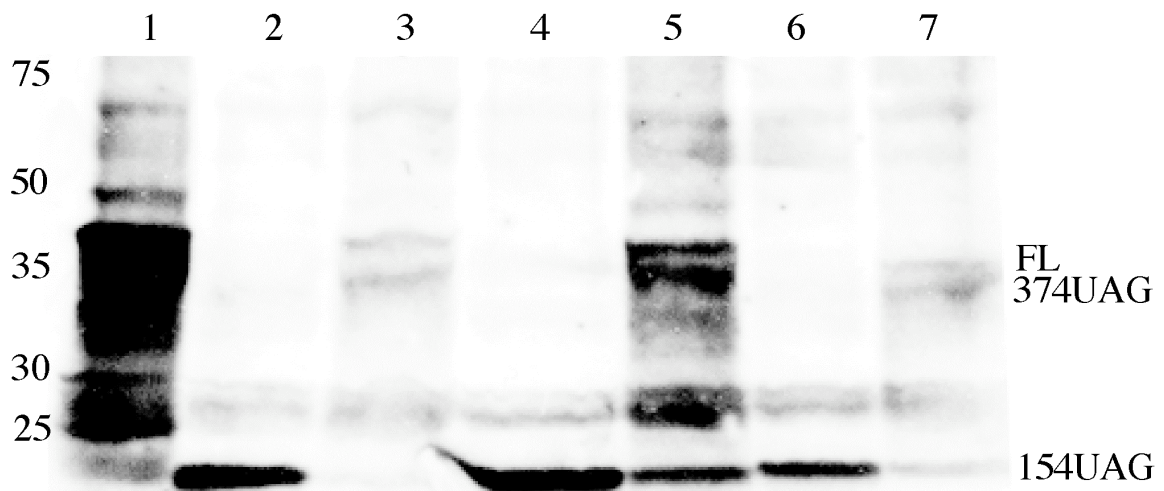


Figure 2.4: HSAS suppression on $\alpha_{\text{NHA}}154\text{UAG}$ and $\alpha_{\text{NHA}}154\text{UAG}374\text{UAG}$ (2 μg mRNA). Lane 1 shows α_{NHA} and has the highest translation *in vitro*. Lanes 2 and 4, $\alpha_{\text{NHA}}154\text{UAG}$ mRNA only. Lanes 3 and 5, HSAS suppression on $\alpha_{\text{NHA}}154\text{UAG}$ with 1 μg and 2 μg of HSAS, respectively. Lane 6, $\alpha_{\text{NHA}}154\text{UAG}374\text{UAG}$ mRNA only. Lane 7, $\alpha_{\text{NHA}}154\text{UAG}374\text{UAG}$ + 2 μg HSAS. Numbers on the left are molecular weight markers (KD). On the right, 154UAG is the first truncation not suppressed by HSAS, 374UAG is the second truncation after suppression of 154UAG (Lanes 6 and 7 only), and FL is full-length protein band.

2.2.3 HSAS and HSFS_{CCCG} Suppression on $\alpha_{\text{NHA}}154\text{UAG}374\text{CGGG}$

Figure 2.5 A shows that FL protein with $\alpha_{\text{NHA}}154\text{UAG}374\text{CGGG}$ is dependent on the addition of both HSAS and HSFS_{CCCG}, which has a 35% yield of full-length protein

relative to α_{NHA} (Figure 2.5 A, Lane 5). Figure 2.5 B was performed using a RRL coupled *in vitro* translation, where DNA is added and mRNA is transcribed in the system. This Western blot allows for a comparison of two suppression events on $\alpha_{\text{NHA}}154\text{UAG}374\text{CGGG}$ versus one suppression event on $\alpha_{\text{NHA}}154\text{UAG}$ (Figure 2.5 B). 55% translational efficiency is seen for $\alpha_{\text{NHA}}154\text{UAG}374\text{CGGG}$ with 2 μg of each HSAS and HSFS_{CCCG} (Figure 2.5 B, Lane 4), while $\alpha_{\text{NHA}}154\text{UAG}$ has a suppression efficiency of 44% with 2 μg of HSAS (Figure 2.5 B, Lane 7). Note efficiencies are exaggerated because the α_{NHA} band is saturated. The $\alpha_{\text{NHA}}154\text{UAG}374\text{CGGG}$ full-length protein yield is also exaggerated due to difficulty in separating the truncation band at 374CGGG and the FL band (Figure 2.5 A, Lane 5, and Figure 2.5 B, Lane 4).

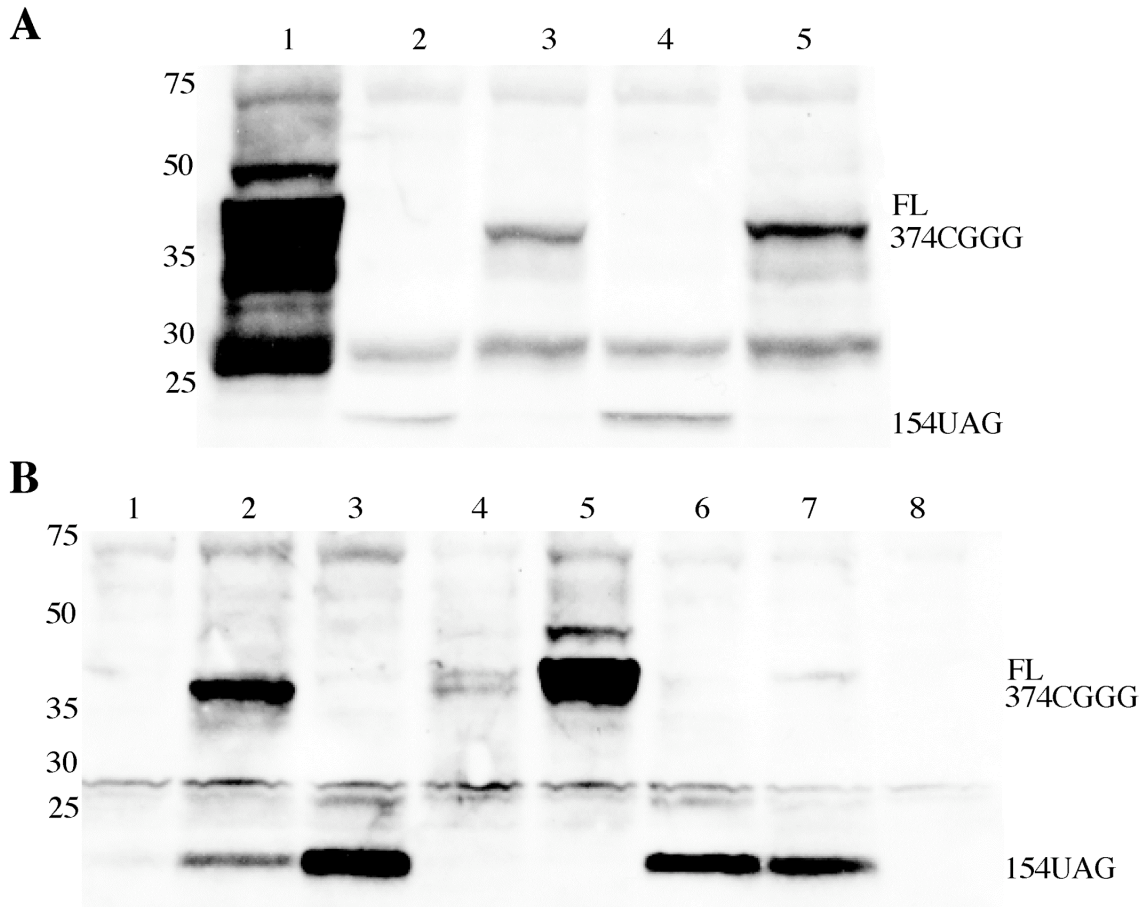


Figure 2.5: HSAS and HSFS_{CCCG} suppression on α_{NHA} 154UAG374CGGG. (A) Suppression in RRL with 2 μg mRNA. Lane 1, α_{NHA} mRNA only. Lane 2 is α_{NHA} 154UAG374CGGG mRNA only. Lane 3 is α_{NHA} 154UAG374CGGG + 2 μg HSAS, which truncates due to the 374CGGG frameshift. Lane 4 is α_{NHA} 154UAG374CGGG + 2 μg HSFS_{CCCG} and truncates at 154UAG. Lane 5 is α_{NHA} 154UAG374CGGG with 2 μg of HSAS and HSFS_{CCCG}. (B) Suppression in TNT RRL with 1 μg DNA. Lanes 1–4 are the same as Lanes 2–5 in part A. Lane 5 is α_{NHA} . Lane 6 is α_{NHA} 154UAG mRNA only. Lane 7 is α_{NHA} 154UAG + 2 μg of HSAS. Lane 8 is without mRNA and tRNA. Numbers on the left are molecular weight markers (KD). On the right, 154UAG is the first truncation not suppressed by HSAS, 374CGGG is the second truncation after suppression of 154UAG (not seen for part B Lanes 6–8), and FL is full-length protein band.

At this point in the research, it was determined that frameshift suppression efficiency was too low to proceed with UAAs. Even though HSAS and HSFS_{CCCG} are aminoacylated *in vitro* and should act similarly to endogenous tRNAs, there was not a significant amount of FL protein (Figure 2.5 A, Lane 5, and Figure 2.5 B, Lanes 4 & 7)

compared to the wild-type, α_{NHA} (Figure 2.5 A, Lane 1, and Figure 2.5 B, Lane 5). Also, the 374CGGG truncation was difficult to distinguish from the FL protein (Figure 2.5 A, Lanes 3 & 5, and Figure 2.5 B, Lanes 2 & 4) and an accurate translation efficiency could not be determined. Therefore, single quadruplet codon constructs were created to analyze frameshift suppression accurately and without the dependence of having 154UAG being suppressed prior to the 374CGGG site.

2.2.4 HSAS/HSFS and THG73/THG73FS-Ala Suppression on α_{NHA} 154XXX(X)

Figure 2.6 A shows HSAS and HSFS experiments on single suppression constructs at α_{NHA} Ser154XXX(X). α_{NHA} 154UAG suppression by HSAS showed suppression efficiency of 49% (Figure 2.6 A, Lane 3), while α_{NHA} 154CGGG suppression efficiency by HSFS_{CCCG} was 36% (Figure 2.6 A, Lane 5). The other two quadruplet codons, CGUG and CGUU, show negligible suppression and are within background intensity (Figure 2.6 A, Lanes 6–9). These efficiencies are exaggerated because the α_{NHA} band is saturated (Figure 2.6 A, Lane 1). Figure 2.6 B shows the same experiments as in Figure 2.6 A, but using THG73 and the THG73 frameshift suppressors, which were chemically aminoacylated with Ala. In Figure 2.6 B, no noticeable FL protein is seen for any of the THG73 suppressor tRNAs. Intriguingly the truncated protein band (UAG and four-base codons) was significantly reduced with the addition of tRNA (Figure 2.6 B, Lanes 3, 5, 7 & 9) (reproducible many times). Therefore it is possible that a contaminant may be present within the tRNA samples, even though similar results were continuously seen using newly transcribed tRNA, multiple precipitations with ethanol to remove salt and excess dCA-Ala, and using variable amounts of suppressor tRNA.

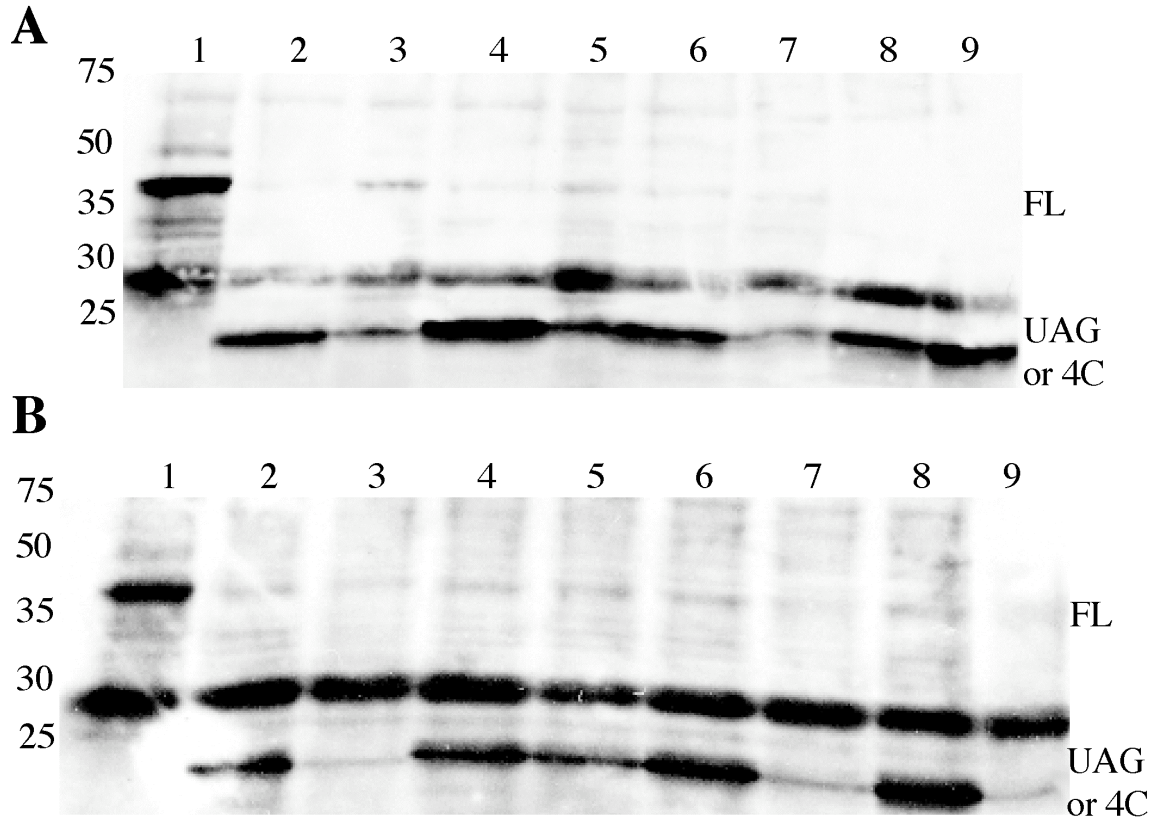


Figure 2.6: HSAS/HSFS and THG73/THG73FS-Ala suppression at $\alpha_{\text{NHA}}154\text{XXX}(X)$. 1 μg mRNA and 2 μg tRNA were used for both gels. (A) HSAS and HSFS suppression at $\alpha_{\text{NHA}}154\text{XXX}(X)$. Lane 1 is α_{NHA} . Lane 2 is $\alpha_{\text{NHA}}154\text{UAG}$. Lane 3 is $\alpha_{\text{NHA}}154\text{UAG} + \text{HSAS}$. Lane 4 is $\alpha_{\text{NHA}}154\text{CGGG}$. Lane 5 is $\alpha_{\text{NHA}}154\text{CGGG} + \text{HSFS}_{\text{CCCG}}$. Lane 6 is $\alpha_{\text{NHA}}154\text{CGUG}$. Lane 7 is $\alpha_{\text{NHA}}154\text{CGUG} + \text{HSFS}_{\text{CACG}}$. Lane 8 is $\alpha_{\text{NHA}}154\text{CGUU}$. Lane 9 is $\alpha_{\text{NHA}}154\text{CGUU} + \text{HSFS}_{\text{AACG}}$. (B) THG73-Ala and THG73FS-Ala suppression at $\alpha_{\text{NHA}}154\text{XXX}(X)$. Lane 1 shows α_{NHA} . Lane 2 is $\alpha_{\text{NHA}}154\text{UAG}$. Lane 3 is $\alpha_{\text{NHA}}154\text{UAG} + \text{THG73-Ala}$. Lane 4 is $\alpha_{\text{NHA}}154\text{CGGG}$. Lane 5 is $\alpha_{\text{NHA}}154\text{CGGG} + \text{THG73FS}_{\text{CCCG}}\text{-Ala}$. Lane 6 is $\alpha_{\text{NHA}}154\text{CGUG}$. Lane 7 is $\alpha_{\text{NHA}}154\text{CGUG} + \text{THG73FS}_{\text{CACG}}\text{-Ala}$. Lane 8 is $\alpha_{\text{NHA}}154\text{CGUU}$. Lane 9 is $\alpha_{\text{NHA}}154\text{CGUU} + \text{THG73FS}_{\text{AACG}}\text{-Ala}$. Numbers on the left are molecular weight markers (KD). On the right, UAG or 4C is the truncation at the stop codon or four-base codon, respectively, and FL is full-length protein band.

The HSFS and THG73FS suppressor tRNAs have not been tested in the literature and are possibly misfolding. Secondary structure of all the tRNAs were predicted using the program mfold to predict nucleic acid folding using standard ionic conditions (32). For HSAS and HSFS_{CCCG} the tRNAs had a similar fold, but were not the native structure shown in Figure 2.3. Interestingly the HSFS_{CACG} and HSFS_{AACG} had the same fold as

HSAS, but in the experiments they were shown to be worse suppressors (Figure 2.6 A). The number of structures for HSFS_{CACG} and HSFS_{AACG} (4 and 5, respectively) is greater than the two structures predicted for HSAS and HSFS_{CCCG}. HSFS_{CACG} and HSFS_{AACG} may therefore exist in multiple tertiary structures. THG73 structures were inconclusive because the G-U pair at the base of the anticodon stem (Figure 2.3) is not recognized by mfold. Therefore, the D-loop and the anticodon loop had to be constrained in order to obtain a similar THG73 structure shown in Figure 2.3. THG73FS_{CCCG} and THG73FS_{CACG} showed a similar fold to THG73 with the constraints. THG73FS_{AACG} did not fold properly even with constraints. Structure predictions using mfold are not highly accurate because the overall folding lacks fundamental interactions in a tertiary fold that stabilize the tRNA structure and therefore the folding was inconclusive at determining whether the tRNAs were misfolded by the extended anticodon.

2.2.5 HSAS/HSFS and THG73/THG73FS-Ala Suppression on Single Constructs in Wheat Germ *In Vitro* Translation

Another possibility for loss of protein bands was RNAi, which can occur due to small percentage of antisense tRNA present within a sample (T7 mMessage Machine Transcription kit Ambion manual) or by hybridization of tRNA to the mRNA transcript (RRL Promega manual). Wheat germ extract (WG) for *in vitro* translation of protein is recommended for RNA preparations that may contain low concentrations of dsRNA, which can inhibit the RRL protein translation (WG Promega manual). Figure 2.7 shows the HSAS/HSFS and THG73/THG73FS-Ala suppression experiments (same as Figure 2.6) run in WG reactions. Low translation efficiency of the full-length α_{NHA} protein is seen in both blots. Surprisingly, HSAS suppression on the $\alpha_{\text{NHA}}154\text{UAG}$ construct shows

more full-length protein than α_{NHA} (Figure 2.7 A, Lane 2). Only small amounts of full-length protein can be seen upon adding HSFS tRNAs (Figure 2.7 A, Lanes 4–9). No full-length protein was seen with THG73/THG73FS-Ala (Figure 2.7 B, Lanes 4–9). Intriguingly, both HSFS_{CCCG} and THG73FS_{CCCG}-Ala show a decrease in the truncated product when tRNA is added (Figure 2.7 A & B, Lane 5). $\alpha_{\text{NHA}}154\text{CGUG}$ also shows a decrease in truncation product when HSFS_{CACG} is added (Figure 2.7 A, Lane 7). This result suggests that RNAi may not be a problematic for the *in vitro* reactions. Therefore, there may be problems with tRNA samples containing a contamination, tRNAs suppressing other sites, and/or tRNAs inhibiting translation. Overall, translation in WG is significantly impaired and yields are not as high as in RRL, which has previously been seen in our lab (Dr. James Petersson and Dr. Niki Zacharias, personal communication).

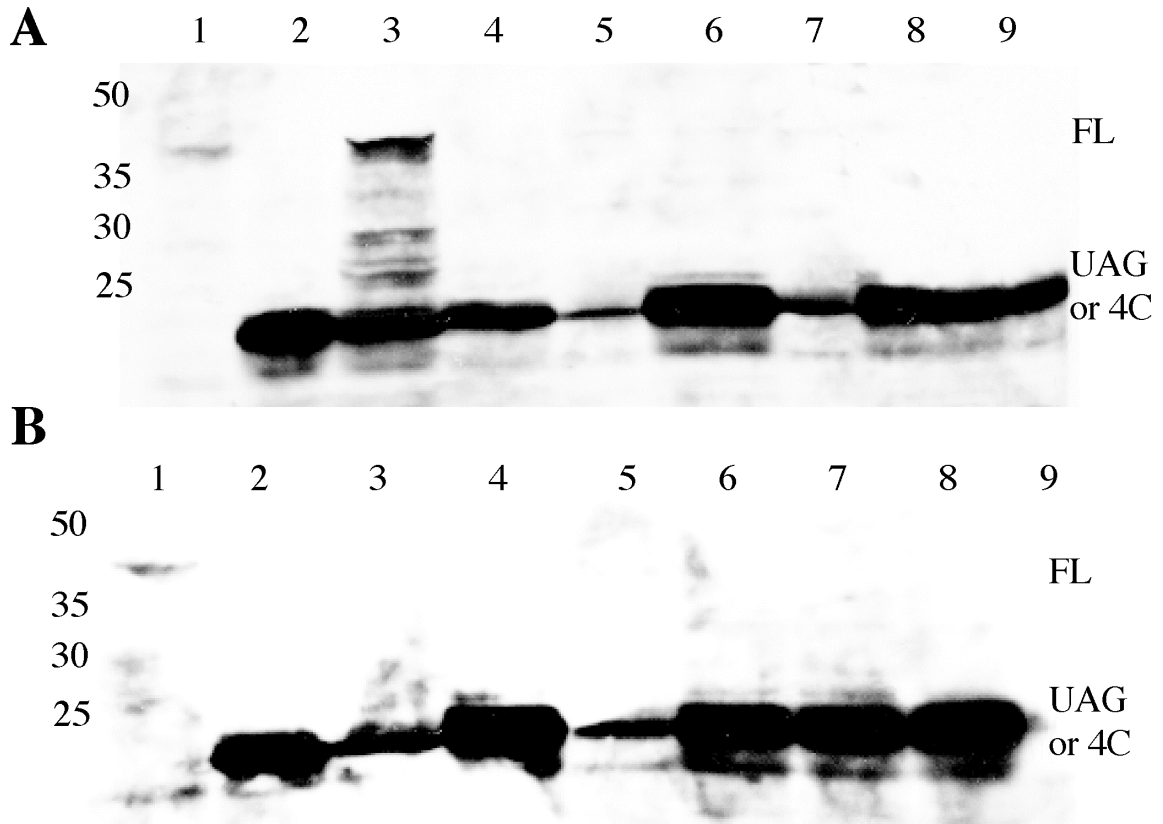


Figure 2.7: HSAS/HSFS and THG73/THG73FS-Ala suppression at $\alpha_{\text{NHA}}154\text{XXX(X)}$ in wheat germ *in vitro* translation. 1 μg mRNA and 2 μg tRNA (when added) were used for each lane. (A) Lane 1 is α_{NHA} . Lane 2 is $\alpha_{\text{NHA}}154\text{UAG}$. Lane 3 is $\alpha_{\text{NHA}}154\text{UAG} + \text{HSAS}$, which suppresses more efficiently than the translation of α_{NHA} (Lane 1). Lane 4 is $\alpha_{\text{NHA}}154\text{CGGG}$ and Lane 5 is $\alpha_{\text{NHA}}154\text{CGGG} + \text{HSFS}_{\text{CCCG}}$. Lane 6 is $\alpha_{\text{NHA}}154\text{CGUG}$ and Lane 7 is $\alpha_{\text{NHA}}154\text{CGUG} + \text{HSFS}_{\text{CACG}}$. Lane 8 is $\alpha_{\text{NHA}}15\text{CGUU}$ and Lane 9 is $\alpha_{\text{NHA}}154\text{CGUU} + \text{HSFS}_{\text{AACG}}$. (B) Lane 1 is α_{NHA} . Lane 2 is $\alpha_{\text{NHA}}154\text{UAG}$. Lane 3 is $\alpha_{\text{NHA}}154\text{UAG} + \text{THG73-Ala}$. Lane 4 is $\alpha_{\text{NHA}}154\text{CGGG}$ and Lane 5 is $\alpha_{\text{NHA}}154\text{CGGG} + \text{THG73FS}_{\text{CCCG}}\text{-Ala}$. Lane 6 is $\alpha_{\text{NHA}}154\text{CGUG}$ and Lane 7 is $\alpha_{\text{NHA}}154\text{CGUG} + \text{THG73FS}_{\text{CACG}}\text{-Ala}$. Lane 8 is $\alpha_{\text{NHA}}15\text{CGUU}$ and Lane 9 is $\alpha_{\text{NHA}}154\text{CGUU} + \text{THG73FS}_{\text{AACG}}\text{-Ala}$. Both Western blots show little full-length protein for α_{NHA} and translation appears impaired in the wheat germ system. Numbers on the left are molecular weight markers (KD). On the right, UAG or 4C is the truncation at the stop codon or four-base codon, respectively, and FL is full-length protein band.

Another hypothesis was that other sites were being recognized by the FS tRNAs and the reduction in truncated protein was caused by a premature +1 frameshift (Figure 2.2 E). Attempts to detect low molecular weight proteins by Western blot using nitrocellulose and PVDF membranes showed no bands below the 21.3 KD band (data not

shown). This means that there was no truncation present before the $\alpha_{\text{NHA}}154\text{XXXXX}$ suppression site, there is very little truncation of $\alpha_{\text{NHA}}154\text{XXXXX}$ in the sample (undetectable by Coomassie brilliant blue stain; detection limit of 0.1–0.5 μg or Ponceau S staining of the nitrocellulose membrane; detection limit of 1 μg), or the low molecular weight truncations are lost from the membrane during washes for the Western blot procedure.

2.2.6 HSAS/HSFS and THG73/THG73-W Suppression on the α_{NHA}

A new control was then used, which added the FS tRNAs to α_{NHA} . If the FS tRNAs were recognizing different codons, then these would be present on the wild-type α_{NHA} construct and would cause a reduction in the full-length protein band by a +1 frameshift (shown in Figure 2.2 E). Figure 2.8 shows HSFS suppression occurs on α_{NHA} and varies based on the amount of suppressor tRNA added. Figure 2.8 A was an internal control and further testing of the RNAi hypothesis, which should have inhibition of translation with very small amounts of dsRNA. The Western blot (Figure 2.8 A, Lanes 1–4) shows no significant change (< 3%) in full-length protein when 0.1 μg of HSFS_{CCCG}, HSFS_{CACG}, or HSFS_{AACG} is added, suggesting no inhibition by the RNAi mechanism. However, when 2 μg of FS tRNA is added to α_{NHA} there is a decrease in full-length protein (Figure 2.8 B, Lanes 2–4). HSFS_{CCCG} has a decrease of 38%, HSFS_{CACG} has a decrease of 12%, and HSFS_{AACG} has a decrease of 46% (Figure 2.8 B, Lanes 2–4) relative to α_{NHA} without tRNA (Figure 2.8 B, Lane 1). The difference in reduction in the α_{NHA} suggests that the reduction is not caused by simply the addition of tRNA or by a contaminant (which would be the same for all tRNAs prepared at the same time), but rather suggests a suppression event or events are occurring. Suppression for HSAS on

$\alpha_{\text{NHA}}154\text{UAG}$ was 60%, $\text{HSFS}_{\text{CCCG}}$ on $\alpha_{\text{NHA}}154\text{CGGG}$ was 56%, $\text{HSFS}_{\text{CACG}}$ on $\alpha_{\text{NHA}}\text{CGUG}$ was 33%, and $\text{HSFS}_{\text{AACG}}$ on $\alpha_{\text{NHA}}\text{CGUU}$ was 43.7% (when compared to α_{NHA}) (Figure 2.8 B, Lanes 5–8). HSAS was only 4.3% more efficient at suppression than $\text{HSFS}_{\text{CCCG}}$ in this trial. When only 0.1 μg of tRNA was added, suppression efficiency was much higher for HSAS than the HSFS tRNAs, this shows the importance of adding the appropriate amount of tRNA for increased suppression efficiency, which is most likely necessary to out compete endogenous triplet recognizing tRNA (shown in Figure 2.2 D).

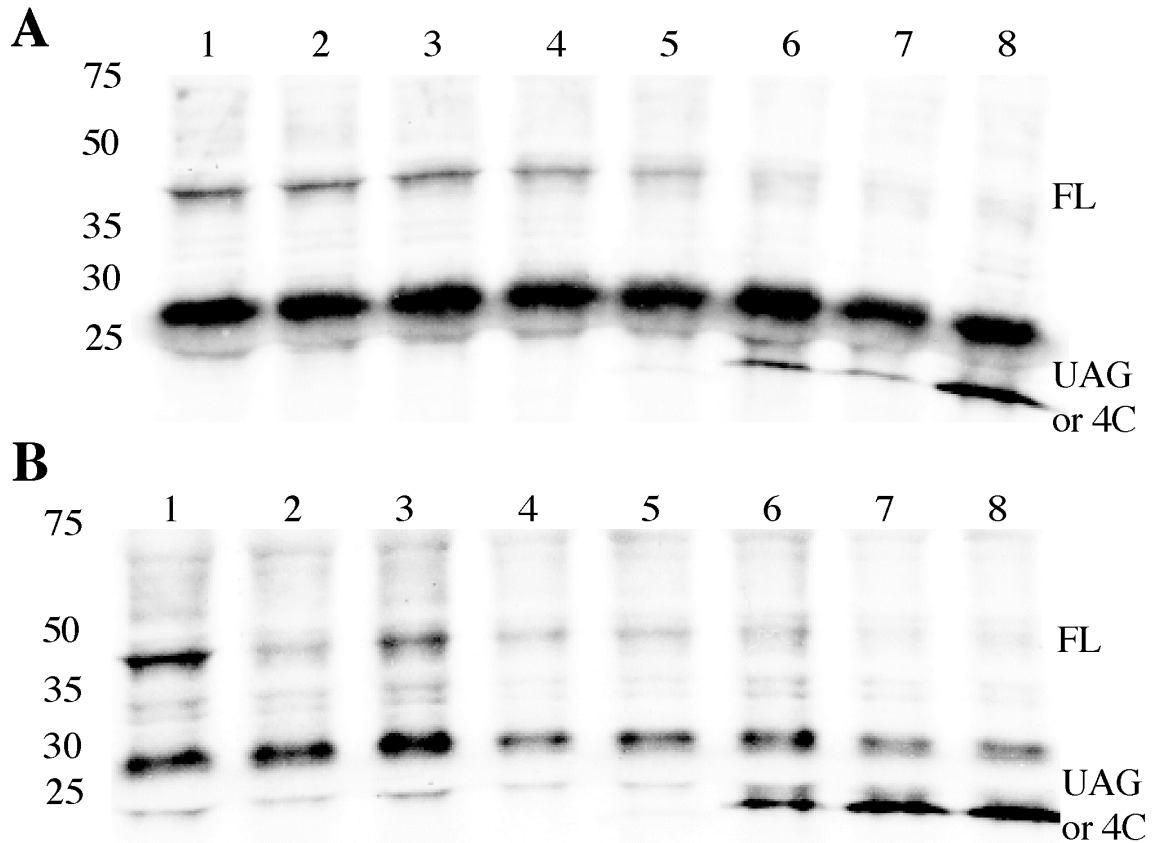


Figure 2.8: HSAS/HSFS suppression on α_{NHA} is dependent on the amount of tRNA added. 2 μg mRNA was used in each reaction. (A) 0.1 μg of HSAS or HSFS tRNA is added in the listed lanes. Lane 1 is α_{NHA} . Lane 2 is α_{NHA} + HSFS_{CCCG}. Lane 3 is α_{NHA} + HSFS_{CACG}. Lane 4 is α_{NHA} + HSFS_{AACG}. Change in full-length protein for α_{NHA} + HSFS tRNAs is < 3% (Lanes 2–4). Lane 5 is α_{NHA} 154UAG + HSAS. Lane 6 is α_{NHA} 154CGGG + HSFS_{CCCG}. Lane 7 is α_{NHA} 154CGUG + HSFS_{CACG}. Lane 8 is α_{NHA} 154CGUU + HSFS_{AACG}. (B) 2 μg HSAS or HSFS tRNA was used. Lanes are identical to part A, but with increased amount of tRNA. Full-length α_{NHA} protein is variable when HSFS tRNAs are added (Lanes 2–4) and is different for each tRNA. α_{NHA} 154CGGG suppression by HSFS_{CCCG} is comparable to α_{NHA} UAG suppression by HSAS (Lanes 5 & 6). Numbers on the left are molecular weight markers (KD). On the right, UAG or 4C is the truncation at the stop codon or four-base codon, respectively, and FL is full-length protein band.

Figure 2.9 shows representative experiments with HSAS/HSFS and THG73/THG73FS-W tRNAs. HSFS showed similar patterns of reduction on α_{NHA} and suppression on α_{NHA} 154XXX(X) as seen in Figure 2.8. However, Figure 2.9 A shows two unknown bands appearing at 29 KD with addition of HSFS_{CCCG} (Figure 2.9 A, Lanes

2 & 6, *) and 22.5 KD for HSFS_{CACG} with α_{NHA} CGUG (Figure 2.9 A, Lane 7). The band at 22.5KD can't be identified based on the Arg triplets in the α_{NHA} and the cause is unknown. The band at 29 KD could possibly be recognition of the Arg182CGG G and the result of a +1 frameshift (Figure 2.2 E). THG73FS_{CCCG}-W showed a significant decrease of full-length protein when added to α_{NHA} (Figure 2.9 B, Lane 2), but little full-length protein is seen when added to α_{NHA} 154CGGG (Figure 2.9 B, Lane 6). Very little suppression is seen with any of the THG73FS-W tRNAs (Figure 2.9 B, Lanes 6–8).

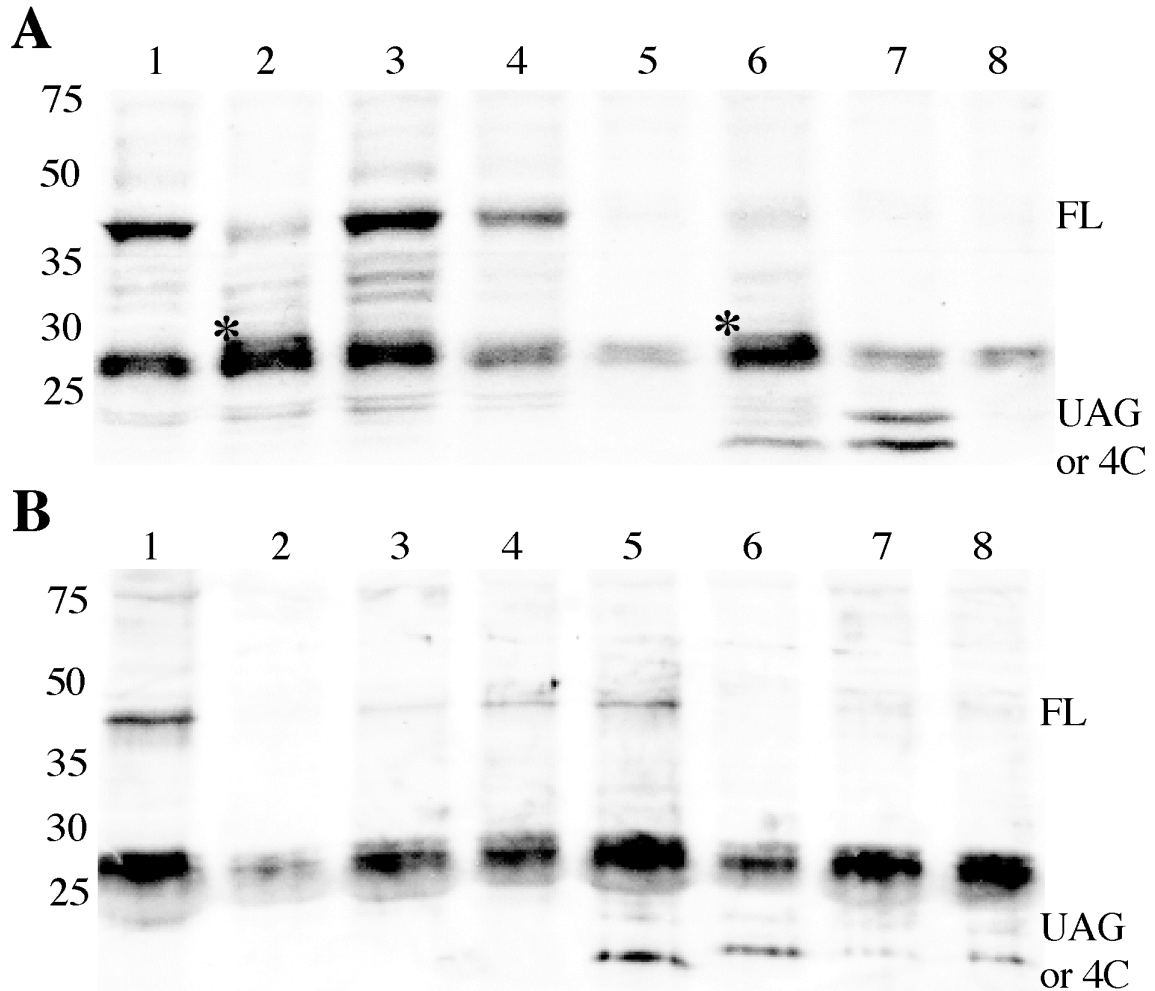


Figure 2.9: HSAS/HSFS and THG73/THG73FS-W suppression on α_{NHA} or $\alpha_{\text{NHA}}154\text{XXX(X)}$. 4 μg mRNA and 2 μg tRNA are used in both gels. (A) HSAS/HSFS suppression on α_{NHA} (Lanes 2-4) and on $\alpha_{\text{NHA}}154\text{XXX(X)}$ (Lanes 5-8). Lane 1 is α_{NHA} . Lane 2 is $\alpha_{\text{NHA}} + \text{HSFS}_{\text{CCCG}}$. Lane 3 is $\alpha_{\text{NHA}} + \text{HSFS}_{\text{CACG}}$. Lane 4 is $\alpha_{\text{NHA}} + \text{HSFS}_{\text{AACG}}$. Lane 5 is $\alpha_{\text{NHA}}154\text{UAG} + \text{HSAS}$. Lane 6 is $\alpha_{\text{NHA}}154\text{CGGG} + \text{HSFS}_{\text{CCCG}}$. Lane 7 is $\alpha_{\text{NHA}}154\text{CGUG} + \text{HSFS}_{\text{CACG}}$. Lane 8 is $\alpha_{\text{NHA}}154\text{CGUU} + \text{HSFS}_{\text{AACG}}$. The * represents a novel band only seen with $\text{HSFS}_{\text{CCCG}}$ and thought to be caused by a +1 frameshift at R182CGGG (Figure 2.2 E) (Lanes 2 & 6). (B) THG73/THG73FS-W suppression on α_{NHA} (Lanes 2-4) and on $\alpha_{\text{NHA}}154\text{XXX(X)}$ (Lanes 5-8). Lane 1 is α_{NHA} . Lane 2 is $\alpha_{\text{NHA}} + \text{THG73FS}_{\text{CCCG}}\text{-W}$. Lane 3 is $\alpha_{\text{NHA}} + \text{THG73FS}_{\text{CACG}}\text{-W}$. Lane 4 is $\alpha_{\text{NHA}} + \text{THG73FS}_{\text{AACG}}\text{-W}$. Lane 5 is $\alpha_{\text{NHA}}154\text{UAG} + \text{THG73-W}$. Lane 6 is $\alpha_{\text{NHA}}154\text{CGGG} + \text{THG73FS}_{\text{CCCG}}\text{-W}$. Lane 7 is $\alpha_{\text{NHA}}154\text{CGUG} + \text{THG73FS}_{\text{CACG}}\text{-W}$. Lane 8 is $\alpha_{\text{NHA}}154\text{CGUU} + \text{THG73FS}_{\text{AACG}}\text{-W}$. Note the novel band seen (* A, Lanes 2 & 6) was not seen in the $\text{THG73FS}_{\text{CCCG}}\text{-W}$ reactions. Numbers on the left are molecular weight markers (KD). On the right, UAG or 4C is the truncation at the stop codon or four-base codon, respectively, and FL is full-length protein band.

When looking at the average densitometric analysis of the HSAS/HSFS reduction or suppression trials, a clear pattern arises (Figure 2.10). The reduction in intensity of HSFS_{CCCG} added to α_{NHA} is similar to the increase in intensity of HSFS_{CCCG} added to the α_{NHA} 154CGGG, suggesting a single suppression event is occurring on α_{NHA} (Figure 2.10). Addition of HSFS_{CCCG} to α_{NHA} causes a reduction of 32% relative to α_{NHA} intensity without tRNA, or suppression efficiency of 32% for HSFS_{CCCG} on the α_{NHA} construct. When HSFS_{CCCG} is added to the α_{NHA} 154CGGG construct, full-length protein can only be attained by one suppression event at the desired suppression site (suppression at two sites would result in a +1 frameshift and lack of full-length protein) and the suppression efficiency is 45%. The truncation bands have about the same average intensity and there is no correlation for suppression efficiency and the intensity of the truncation band (Figure 2.10). Looking at the 28 KD and 70 KD (protein bands from the RRL), the intensity is approximately the same for all the lanes and shows that there is no global change in protein concentration (Figure 2.10). HSAS and HSFS_{CCCG} show the highest suppression efficiency in RRL and amber suppression appears to be better than frameshift suppression with these two tRNAs.

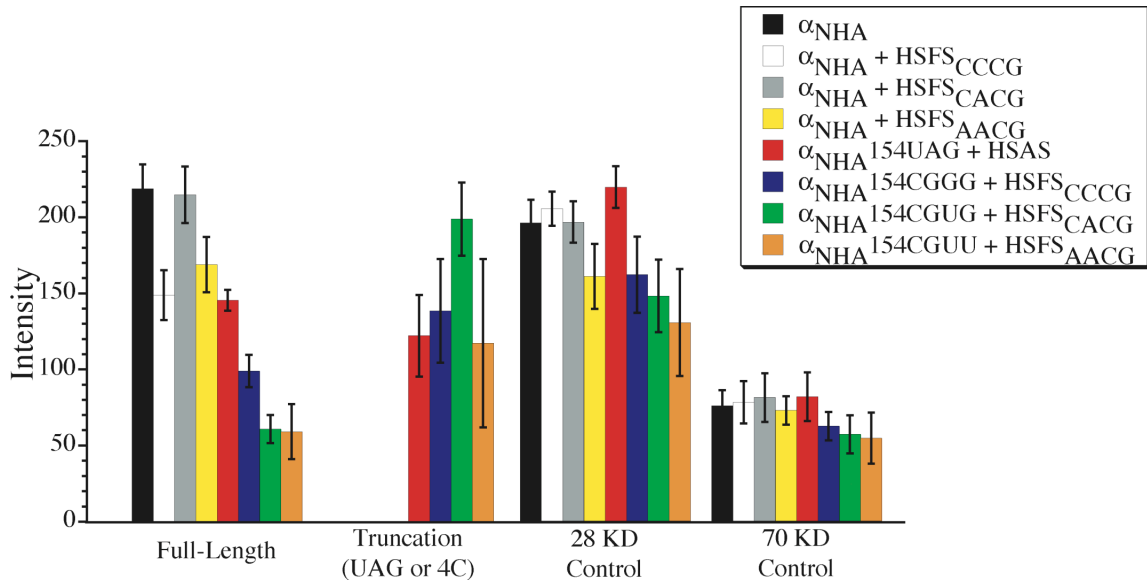


Figure 2.10: Densitometric analysis of HSAS/HSFS suppression on α_{NHA} and $\alpha_{\text{NHA}}154\text{XXX(X)}$ (average of 6 trials). The α_{NHA} shows the highest intensity of full-length protein, but close to the $\alpha_{\text{NHA}} + \text{HSFS}_{\text{CACG}}$ and suggesting $\text{HSFS}_{\text{CACG}}$ does not suppress α_{NHA} . α_{NHA} is decreased upon the addition of $\text{HSFS}_{\text{CCCG}}$ and $\text{HSFS}_{\text{AACG}}$. The intensity of $\alpha_{\text{NHA}} + \text{HSFS}_{\text{CCCG}}$ is nearly the same as $\alpha_{\text{NHA}}154\text{UAG} + \text{HSAS}$, suggesting one suppression event is occurring in both cases. $\alpha_{\text{NHA}}154\text{CGGG} + \text{HSFS}_{\text{CCCG}}$ shows highest amount of full-length protein for the FS tRNAs. The truncation bands are approximately the same for all tRNAs and show no significant decrease in intensity with increased FL protein. Looking at the 28 KD and 70 KD protein intensities (proteins present in the RRL), there is little difference in these bands between samples and there is no global change in protein concentration.

2.2.7 Arg Mutations, Changing CGG Triplets to CGC Triplets

The previous Western blots (Figure 2.9 A) suggest that the α_{NHA} construct contains a site that is suppressed by $\text{HSFS}_{\text{CCCG}}$. CGX triplets code for the amino acid Arg and are possible sites for suppression by $\text{HSFS}_{\text{CCCG}}$. Based on the 29 KD band (Figure 2.9 A, Lanes 2 & 6) and cognate sequence for $\text{HSFS}_{\text{CCCG}}$ being CGGG, Arg182 was first mutated from CGG to CGC. CGC was chosen to place the same nucleotide in the mRNA that would be used for recognition by the $\text{HSFS}_{\text{CCCG}}$ anticodon (5'-CCCG-3') and avoid recognition. The Arg mutants were placed in the α_{NHA} and $\alpha_{\text{NHA}}154\text{CGGG}$ constructs.

These are named by the construct with Arg mutation and the appropriate number following.

Figure 2.11 shows the Western blot of the Arg182 mutants. It was hoped the mutation would lead to a significant increase in the amount of full-length protein in both the $\alpha_{\text{NHA}}\text{R182}$ mutant (Figure 2.11, Lane 6) and $\alpha_{\text{NHA}}154\text{CGGGR182}$ mutant (Figure 2.11, Lane 4) upon addition of $\text{HSFS}_{\text{CCCG}}$. $\alpha_{\text{NHA}}\text{R182}$ shows higher full-length protein (Figure 2.11, Lane 5) than α_{NHA} (Figure 2.11, Lane 1), most likely because the $\alpha_{\text{NHA}}\text{R182}$ mRNA was prepared after the α_{NHA} mRNA. Upon addition of $\text{HSFS}_{\text{CCCG}}$ to the α_{NHA} and $\alpha_{\text{NHA}}\text{R182}$ (Figure 2.11, Lanes 2 & 6) a reduction of 41% and 35%, respectively, was seen when compared to the same mRNA without $\text{HSFS}_{\text{CCCG}}$. $\alpha_{\text{NHA}}154\text{UAG}$ suppression by HSAS is either 76% relative to α_{NHA} or 68% relative to $\alpha_{\text{NHA}}\text{R182}$ (Figure 2.11, Lane 8). $\text{HSFS}_{\text{CCCG}}$ suppression of $\alpha_{\text{NHA}}154\text{CGGGR182}$ and $\alpha_{\text{NHA}}154\text{CGGG}$ (Figure 2.11, Lanes 4 & 7, respectively) showed efficiency of 41% and 30%, respectively. The mutation at R182 shows an improvement of 7% at protecting the $\alpha_{\text{NHA}}\text{R182}$ from $\text{HSFS}_{\text{CCCG}}$ suppression (Figure 2.11, Lane 6) and an increase of 11% on the full-length protein for $\alpha_{\text{NHA}}154\text{CGGGR182}$ suppressed by $\text{HSFS}_{\text{CCCG}}$ (Figure 2.11, Lane 4). While this is an improvement, the suppression wasn't increased as much as was hoped and there may be other triplets that are recognized on α_{NHA} .

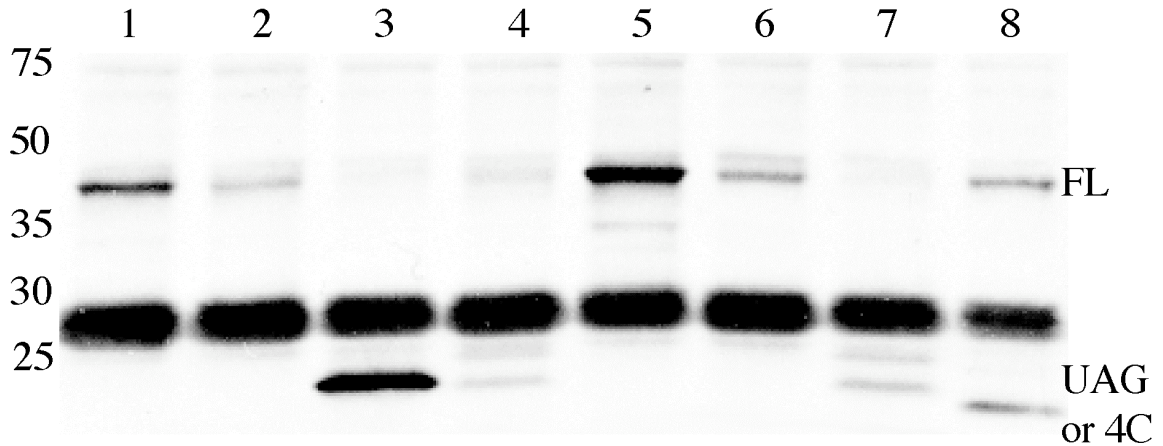


Figure 2.11: HSFS_{CCCG} suppression on α_{NHA} R182 and α_{NHA} 154CGGGR182 mutants. 2 μg mRNA and 2 μg tRNA were used for the experiments. Lane 1 is α_{NHA} and Lane 2 is α_{NHA} + HSFS_{CCCG}. Lane 3 is α_{NHA} 154CGGGR182 and Lane 4 is α_{NHA} 154CGGGR182 + HSFS_{CCCG}. Lane 5 is α_{NHA} R182 and Lane 6 is α_{NHA} R182 + HSFS_{CCCG}. Lane 7 is α_{NHA} 154CGGG + HSFS_{CCCG}. Lane 8 is α_{NHA} 154UAG + HSAS. Numbers on the left are molecular weight markers (KD). On the right, UAG or 4C is the truncation at the stop codon or four-base codon, respectively, and FL is full-length protein band.

Further Arg CGG triplets were mutated to CGC. Arg19 and Arg116 were chosen because they were closer to the N-terminus of the protein and these mutations should cause greater full-length protein or possibly new bands that could be detected on the Western blot. The α_{NHA} 154CGGGR19R116 mutation showed a slight increase in suppression when HSFS_{CCCG} was added when compared to α_{NHA} R182 + HSFS_{CCCG}. Overall, the α_{NHA} 154CGGG constructs with the Arg mutants showed little change in suppression efficiency. Therefore, it appears that only the in-frame CGGG codons need to be removed, such as R182. The R182 is present on the α_{NHA} in all experiments and is known as the “masked” construct (33).

2.2.8 Optimization of the RRL *In Vitro* Reactions for Increased Suppression

Efficiencies

In vitro translation reactions are sensitive to organic molecules and salt that is added with the tRNA and mRNA (RRL Promega manual). In order to add more mRNA and tRNA, desalting columns were used. The removal of excess salt and dCA-W from the mRNA transcription and tRNA ligations allowed for greater concentrations of mRNA and tRNA-W in the reactions, which caused increased protein production. The tRNAs are stored at -80 °C and this can cause aggregation and unfolding of the tRNA. tRNA was refolded at 65 °C for two minutes, as was done for UAA incorporation in *Xenopus* oocytes (8,16). Translation reactions were also allowed to proceed for 3–4 h, rather than 1.5 h. This allowed for increased protein, which was also seen by Dr. James Petersson (personal communication). These changes all helped to increase protein production and were easy to implement.

The most important factor was reducing competition with endogenous triplet recognizing tRNA in order to increase the suppression efficiency of the FS tRNA. The Sisido group performed UAA incorporation in *E. coli in vitro* translation system using 10-fold less Arg in the reaction (34). Removing Arg decreases the competition of the FS tRNAs with endogenous triplet recognizing tRNAs. Therefore, the Arg concentration was reduced 10-fold and this greatly increased the suppression efficiency, as discussed below. Finally, the concentration of tRNA is important for the suppression efficiency. The Sisido group used $\approx 6.8 \mu\text{g}$ of tRNA-dCA-UAA per 10 μl *E. coli* translation reaction (18). Addition of more tRNA-dCA-UAA also decreases competition with endogenous triplet recognizing tRNA and increased the overall amount of protein. After making

these optimizations, it was very easy to observe and quantify suppression in the RRL *in vitro* reactions.

2.2.9 Choosing a New Frameshift Suppressor tRNA, YFFS_{CCCG}

All three of THG73FS showed no suppression in the *in vitro* reactions (Figures 2.6 & 2.9), even though THG73 could suppress the amber codon. At the time, only the yeast Phe frameshift suppressor (YFFS) had been used to incorporate UAAs *in vitro* (18,19,26). YFFS_{CCCG} (sequence shown in Figure 2.3) was chosen as the next suppressor tRNA to be tested because HSFS_{CCCG} worked well in RRL and had been used extensively by the Sisido group.

YFFS_{CCCG}-W shows suppression in RRL and is dependent on the amount of tRNA added (Figure 2.12). Figure 2.12, Lanes 2 and 3 show $\alpha_{\text{NHA}}154\text{CGGG} + \text{YFFS}_{\text{CCCG}}\text{-W}$ with 3.4 μg and 6.8 μg , respectively, and show a suppression efficiency of 37% and 46%, respectively. This efficiency exceeded any of the THG73FS-A/W experiments. $\alpha_{\text{NHA}}154\text{CGGG} + \text{HSFS}_{\text{CCCG}}$ showed a suppression efficiency of 100% (Figure 2.12, Lane 4) using the optimized conditions. $\alpha_{\text{NHA}}154\text{UAG} + \text{HSAS}$ also had a suppression efficiency of 100% (Figure 2.12, Lane 6), showing that both nonsense and frameshift suppression could be comparable *in vitro* under optimized conditions.

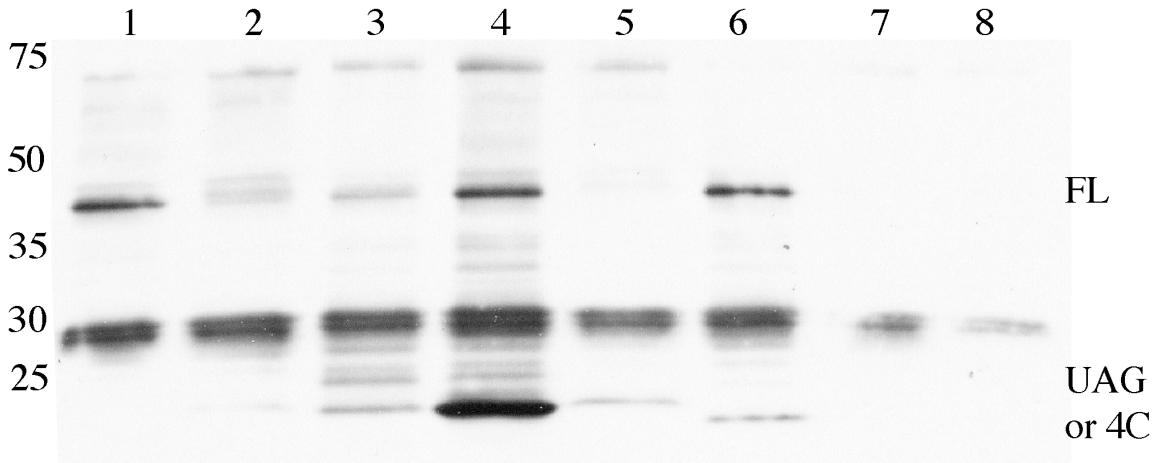


Figure 2.12: YFFS_{CCCG}-W and HSFS_{CCCG} suppression at $\alpha_{\text{NHA}}154\text{XXX}(X)$. 4 μg mRNA were used in each lane. Lane 1 is α_{NHA} . Lane 2 is $\alpha_{\text{NHA}}154\text{CGGG} + 3.4 \mu\text{g}$ YFFS_{CCCG}-W. Lane 3 is $\alpha_{\text{NHA}}154\text{CGGG} + 6.8 \mu\text{g}$ YFFS_{CCCG}-W. Lane 4 is $\alpha_{\text{NHA}}154\text{CGGG} + 5.5 \mu\text{g}$ HSFS_{CCCG}. Lane 5 is $\alpha_{\text{NHA}}154\text{CGGG}$. Lane 6 is $\alpha_{\text{NHA}}154\text{UAG} + 5.5 \mu\text{g}$ HSAS. Lane 7 is $\alpha_{\text{NHA}}154\text{UAG}$. Lane 8 is RRL without mRNA and tRNA. Note all constructs contain the R182 mutation and reactions were performed using optimized conditions. Numbers on the left are molecular weight markers (KD). On the right, UAG or 4C is the truncation at the stop codon or four-base codon, respectively, and FL is full-length protein band.

Previously, the Sisido group had shown that the YFFS_{CCCG} can be aminoacylated by endogenous aaRSs in *E. coli in vitro* reactions (19,35). In *E. coli in vitro* reactions, YFFS_{CCCG} is predominately aminoacylated by the ArgRS (35). However, YFFS_{ACCC} is recognized in *E. coli in vitro* reactions by the GlyRS and mutations were made to the acceptor stem (shown in Figure 2.3) to decrease recognition (19). These acceptor stem mutations were made to create YFaFS_{CCCG} (shown in Figure 2.3). The discriminator base (N73) is also an important recognition by many aaRSs in prokaryotic and eukaryotic cells (36,37). Work in *Xenopus* oocytes established that mutation of the discriminator base drastically decreased aminoacylation of THG73 (16). Therefore, A73 of YFFS_{CCCG} was mutated to G73 to create YFG73FS_{CCCG} (shown in Figure 2.3).

Figure 2.13 shows suppression (-Trp) and reaminoacylation experiments with YFFS_{CCCG}, YFG73FS_{CCCG}, and YFaFS_{CCCG}. YFFS_{CCCG}-W had a suppression efficiency of

16% (Figure 2.13, Lane 2) and YFFS_{CCCG} (74 mer) had 22% full-length protein of α_{NHA} (Figure 2.13, Lane 3). The suppression efficiency of YFFS_{CCCG}-W was not typical. YFG73FS_{CCCG}-W showed a suppression efficiency of 60% (Figure 2.13, Lane 4) and YFG73FS_{CCCG} (74 mer) had 24% full-length protein of α_{NHA} (Figure 2.13, Lane 5). YFFS_{CCCG} and YFG73FS_{CCCG} (74 mer) show approximately the same amount of reaminoacylation product (Figure 2.13, Lanes 3 & 5). YFaFS_{CCCG}-W had a suppression efficiency of 26% (Figure 2.13, Lane 6), but YFaFS_{CCCG} (74 mer) had 10% full-length protein of α_{NHA} (Figure 2.13, Lane 7). This reaminoacylation is very close to the α_{NHA} 154CGGG mRNA only, which had 9% of α_{NHA} (Figure 2.13, Lane 8). HSFS_{CCCG} showed a suppression efficiency of 33% (Figure 2.13, Lane 9). This Western blot shows that reaminoacylation of YFFS_{CCCG} and YFG73FS_{CCCG} can be problematic in the RRL using the optimized conditions.

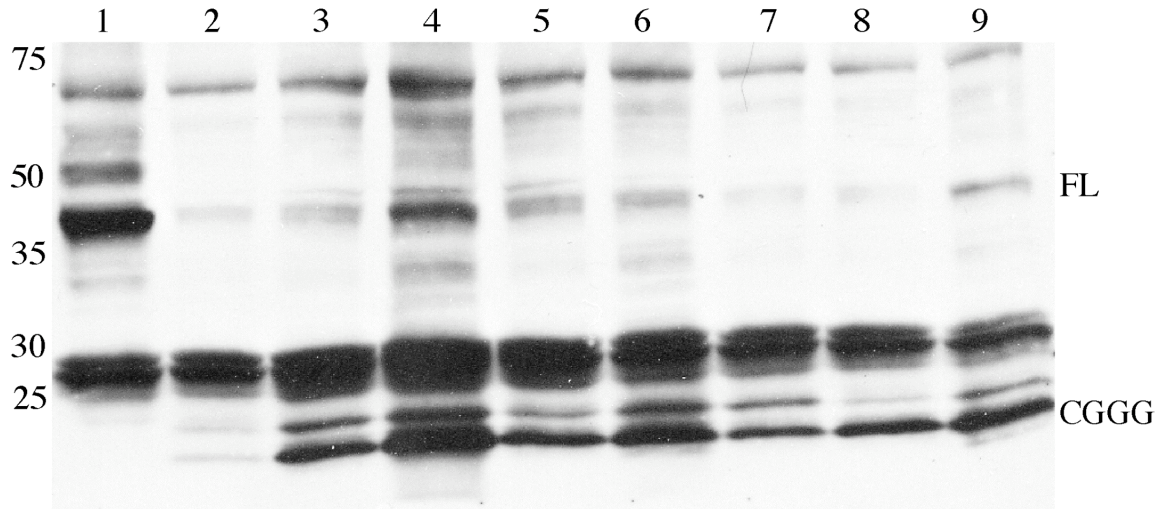


Figure 2.13: YFFS_{CCCG}, YFG73FS_{CCCG}, YFaFS_{CCCG} (-Trp), and HSFS_{CCCG} suppression and reaminoacylation (74 mer) tested at $\alpha_{\text{NHA}}154\text{CGGG}$. 4 μg of mRNA, 6.8 μg of YFFS_{CCCG}, YFG73FS_{CCCG}, YFaFS_{CCCG} (-W or 74 mer), and 5.5 μg of HSFS_{CCCG} were used in each lane. Lane 1 is α_{NHA} . Lane 2 is $\alpha_{\text{NHA}}154\text{CGGG} + \text{YFFS}_{\text{CCCG}}\text{-W}$. Lane 3 is $\alpha_{\text{NHA}}154\text{CGGG} + \text{YFFS}_{\text{CCCG}}$ (74 mer). Lane 4 is $\alpha_{\text{NHA}}154\text{CGGG} + \text{YFG73FS}_{\text{CCCG}}\text{-W}$. Lane 5 is $\alpha_{\text{NHA}}154\text{CGGG} + \text{YFG73FS}_{\text{CCCG}}$ (74 mer). Lane 6 is $\alpha_{\text{NHA}}154\text{CGGG} + \text{YFaFS}_{\text{CCCG}}\text{-W}$. Lane 7 is $\alpha_{\text{NHA}}154\text{CGGG} + \text{YFaFS}_{\text{CCCG}}$ (74 mer). Lane 8 is $\alpha_{\text{NHA}}154\text{CGGG}$. Lane 9 is $\alpha_{\text{NHA}}154\text{CGGG} + \text{HSFS}_{\text{CCCG}}$. All constructs contain the R182 mutation and reactions performed using optimized conditions. Numbers on the left are molecular weight markers (KD). On the right, CGGG is the truncation at the four-base codon and FL is full-length protein band.

2.2.10 HSAS and HSFS Suppression at $\alpha_{\text{NHA}}149\text{XXX(X)}$

All previous work had been done suppressing at $\alpha_{\text{NHA}}154\text{XXX(X)}$ and therefore we wanted to look at a second suppression site that would be in a similar location, but also useful for *in vivo* studies. We chose to study $\alpha_{149\text{W}}$ of the nAChR because this residue makes a cation- π interaction with acetylcholine and causes a noticeable shift in EC_{50} when fluorinated Trp (UAAs) are incorporated at the site (15). Figure 2.14 shows suppression experiments with HSAS and HSFS_{CCCG} at $\alpha_{\text{NHA}}154\text{XXX(X)}$ and $\alpha_{\text{NHA}}149\text{XXX(X)}$ for comparison. HSFS_{CCCG} suppresses comparably at both $\alpha_{\text{NHA}}154\text{CGGG}$ (Figure 2.14, Lane 2) and $\alpha_{\text{NHA}}149\text{CGGG}$ (Figure 2.14, Lane 5). HSAS also shows comparable suppression at both sites (Figure 2.14, Lanes 7 & 9). All

suppression was $> 100\%$ of α_{NHA} , which appears to not have translated well (Figure 2.14, Lane 1). Most intriguing is that you can see the difference in molecular weight of the truncation bands. The frameshift at $\alpha_{\text{NHA}}154\text{CGGG}$ is predicted to have a mass of 21.3 KD, $\alpha_{\text{NHA}}149\text{CGGG}$ is predicted to have a mass of 20.6 KD, $\alpha_{\text{NHA}}154\text{UAG}$ is predicted to have a mass of 20.4 KD, and $\alpha_{\text{NHA}}149\text{UAG}$ is predicted to have a mass of 20.2 KD. These were arranged on the Western blot from highest molecular weight (Figure 2.14, Lanes 2 & 3) to lowest molecular weight (Figure 2.14, Lanes 8 & 9). The correlation in migration and predicted mass shows that the frameshift suppression has the correct truncation pattern and is properly truncating in RRL.

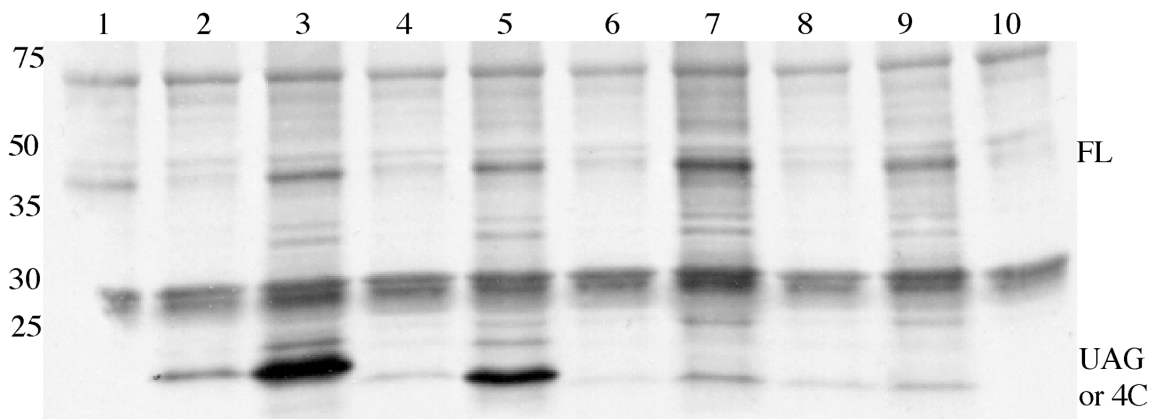


Figure 2.14: HSFS_{CCCG} and HSAS suppression at $\alpha_{\text{NHA}}154\text{XXX(X)}$ and $\alpha_{\text{NHA}}149\text{XXX(X)}$. 4 μg of mRNA and 5.5 μg of tRNA were used in each lane. Lane 1 is α_{NHA} . Lane 2 is $\alpha_{\text{NHA}}154\text{CGGG}$. Lane 3 is $\alpha_{\text{NHA}}154\text{CGGG} + \text{HSFS}_{\text{CCCG}}$. Lane 4 is $\alpha_{\text{NHA}}149\text{CGGG}$. Lane 5 is $\alpha_{\text{NHA}}149\text{CGGG} + \text{HSFS}_{\text{CCCG}}$. Lane 6 is $\alpha_{\text{NHA}}154\text{UAG}$. Lane 7 is $\alpha_{\text{NHA}}154\text{UAG} + \text{HSAS}$. Lane 8 is $\alpha_{\text{NHA}}149\text{UAG}$. Lane 9 is $\alpha_{\text{NHA}}149\text{UAG} + \text{HSAS}$. Lane 10 is RRL without mRNA and tRNA. All constructs contain the R182 mutation and reactions performed using optimized conditions. Numbers on the left are molecular weight markers (KD). On the right, UAG or 4C is the truncation at the stop codon or four-base codon, respectively, and FL is full-length protein band.

2.2.11 Suppression Efficiencies of Suppressor tRNAs Using Optimized Conditions

After performing Western blots with the optimized conditions and various suppressor tRNAs, the average suppression efficiency relative to $\alpha_{\text{NHA}}\text{R182}$ was calculated to allow comparison between different batches of RRL. Figure 2.15 shows the overall suppression efficiency. mRNA only for $\alpha_{\text{NHA}}\text{154CGGG}$ is 15% and $\alpha_{\text{NHA}}\text{154UAG}$ is 12% (Figure 2.15, gray bars) and represents the read-through of the suppression site *in vitro* and endogenous protein at the same molecular weight. HSFS_{CCCG} and HSAS suppress almost equivalently with the same amount of tRNA (Figure 2.15, blue bars). Suppression efficiency of the HSFS_{CCCG} is most likely increased because of the decreased concentration of Arg in the *in vitro* reactions, which causes less competition with endogenous triplet recognizing tRNA (Figure 2.2 D). Reaminoacylation of YFFS_{CCCG} (74 mer) occurs in the RRL *in vitro* translation and appears to be increased by the amount of tRNA added and the extended reaction times used under the optimized conditions (Figure 2.15, green bars). Suppression of YFFS_{CCCG}-W is also dependent on the amount of tRNA added and increases from 30% to 67% with 3.4 μg to 6.8 μg of YFFS_{CCCG}-W, respectively (Figure 2.15, red bars). THG73-W shows an average suppression efficiency of 66%, but only 2 μg of tRNA was used. Overall, frameshift is viable in the RRL *in vitro* system and should work in *Xenopus* oocytes.

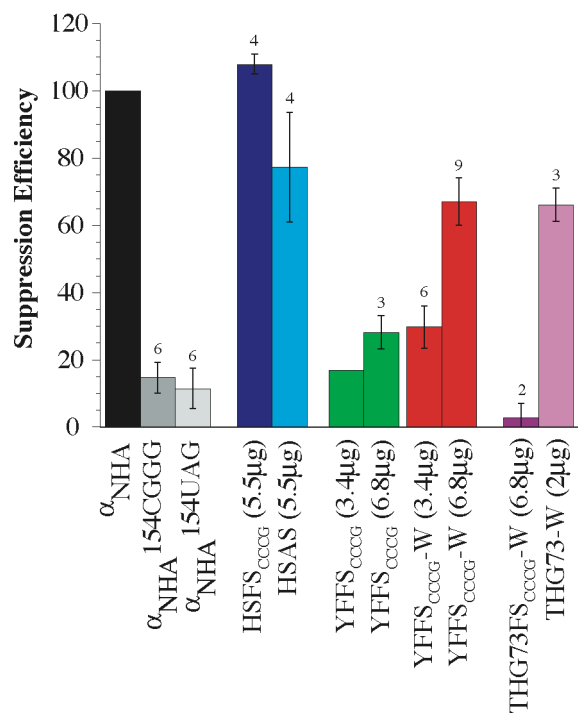


Figure 2.15: Average suppression efficiency and reaminoacylation of suppressor tRNAs using optimized Western blot conditions and α_{NHA} R182. All tRNA were added to their cognate suppression site at α_{NHA} 154. α_{NHA} 154XXX(X) alone is shown in gray and represents read-through of the protein and endogenous protein at the same molecular weight as the FL protein (background) *in vitro*. The suppression efficiency was expressed relative to α_{NHA} . HSFS_{CCCG} and HSAS show nearly the same suppression efficiency *in vitro* with this amount of tRNA. YFFS_{CCCG} (74 mer) is a reaminoacylation experiment to test if an endogenous aaRS recognizes the tRNA. YFFS_{CCCG}-W shows that expression varies with the amount of tRNA added to the RRL. THG73FS_{CCCG}-W shows no suppression and the intensity of the full-length band is actually less than the background of α_{NHA} 154CGGG alone, which was consistently seen. THG73-W shows approximately the same suppression efficiency as YFFS_{CCCG}-W, but there is much less tRNA used for the amber suppressor. Number of Western blot lanes used is listed above each bar, except for α_{NHA} R182, which was always used for normalization, and YFFS_{CCCG} (3.4 μ g), which was only performed once.

2.3 Discussion

The eukaryotic *in vitro* translation system described here was invaluable for gaining knowledge about the translational machinery and how the suppressor tRNAs suppress mRNA. RRL appears to be much more efficient in the translation of the nAChR α_{NHA} -subunit than the WG system (Figures 2.6 & 2.7, for direct comparison), which has

been seen by other members of our group (Dr. James Petersson and Dr. Niki Zacharias, personal communication). In order to achieve reproducible protein translation that was much greater than background, it was essential to optimize many components of the mRNA and tRNA handling and purification, reduction of competition for the frameshift suppressors by increasing the amount of tRNA added and decreasing the concentration of Arg, and extending the translation reaction time to 3–4 h. Under these conditions, suppression experiments gave consistent full-length protein intensities that were much stronger than bands with mRNA only (Figures 2.12–2.14). This is necessary to evaluate the suppression efficiency and determine if a suppression event has occurred.

The suppression sites studied here were CGGG, CGUG, and CGUU with both the HSFS and THG73FS tRNAs. CGUG and CGUU were untested at the time the research was performed and show little or no suppression with the HSFS tRNAs in the RRL system. CGGG had been previously used by the Sisido group to incorporate UAAs in *E. coli in vitro* reactions (17,34) and this work showed that CGGG also works in the RRL *in vitro* reactions. After this research was performed, the Sisido group tested multiple quadruplet codons in the RRL system. While CGUG and CGUU were not tested, CGAU showed no suppression efficiency and CGCU showed $\approx 26\%$ suppression efficiency in RRL (21). Therefore it is difficult to predict what quadruplet codons will be suppressible, but the Sisido group has performed many experiments now in *E. coli* and RRL *in vitro* systems to identify functional quadruplet codons (19,21).

HSAS and HSFS tRNAs are exceedingly useful tools for suppression experiments. Both the amber and frameshift suppressor tRNAs are aminoacylated *in vitro* (Figures 2.4–2.9 & 2.11–2.14) and therefore they are useful tools to test suppression

sites without the need to ligate aas or UAAs to the tRNA. Intriguingly, under the optimized conditions there is $\approx 100\%$ suppression efficiency for both HSAS and HSFS_{CCCG} with the same amount of tRNA (Figure 2.15). This suggests that even with the 10-fold reduction in concentration of Arg, competition with endogenous triplet recognizing tRNA with HSFS_{CCCG} (Figure 2.2 D) is comparable to the competition of HSAS with the protein release factor, eRF1 (Figure 2.2 B). The HSAS and HSFS tRNAs can also be compared to tRNA/aminoacyl-tRNA synthetase pairs that have been developed for the incorporation of UAAs *in vivo* (4,11,38). In both cases, the aa or UAA is placed on the tRNA by a protein in the translation reaction and is catalytic. This work establishes that both HSAS and HSFS_{CCCG} are accepted by the translational machinery equally (under the optimum conditions, Figure 2.15) and tRNA/aminoacyl-tRNA synthetase pairs (amber and frameshift) should be extremely useful for *in vitro* translation systems to produce high yields of protein containing multiple UAAs.

THG73 has been used extensively for incorporating UAAs in *Xenopus* oocytes using nonsense suppression at the amber codon (2,3,8,16). However, THG73FS_{CCCG} does not suppress in the *in vitro* translation reactions. Figure 2.9 B, Lane 2 shows a representative reaction where the addition of THG73FS_{CCCG} is added to α_{NHA} (wild-type) and there is virtually no full-length protein produced. When THG73FS_{CCCG} is added to $\alpha_{\text{NHA}}154\text{CGGG}$, there is no full-length protein (Figure 2.9 B, Lane 6) and the full-length band shows less intensity than read-through of the mRNA only (Figure 2.15). THG73FS_{CCCG} was not only non-functional, but has a unique phenotype of nearly abolishing translation and/or degrading protein (as determined by the Western blot analysis). Therefore, it is very unlikely that the THG73FS_{CCCG} is simply misfolding or

not accepted by the translational machinery. Rather it is more likely that the tRNA is stalling the ribosome, causing an RNAi response, or some other mechanism that could either stall translation or cause mRNA and/or protein degradation. THG73FS_{CCCG} is unique among the tested suppressor tRNAs for this reason and this information would be unattainable without the use of the *in vitro* system and Western blotting.

The YFFS_{CCCG} was not the original choice for a frameshift suppressor tRNA for the incorporation of UAAs. Previous work had shown that a modified yeast Phe amber suppressor (named MN3) was much less efficient than THG73 at suppressing the amber codon in *Xenopus* oocytes (16). MN3 was also shown to be aminoacylated in the *Xenopus* oocyte greater than THG73 (16). These reaminoacylation experiments were performed at aromatic amino acid sites, which would be the most logical aaRSs that would recognize MN3. YFFS_{CCCG}-W was able to suppress in the RRL system (Figures 2.12 & 2.13). After this research was performed, the Sisido group performed research in the RRL system with YFFS_{CCCG}-NitroPhe and obtained a suppression efficiency of 64% with 6.8 µg of tRNA suppressing at position 83CGGG of streptavidin (21). This is very close to the suppression efficiency of 68% with YFFS_{CCCG}-W (6.8 µg) suppressing at α_{NHA} 154CGGG (Figure 2.15). This work therefore agrees with the Sisido group and YFFS_{CCCG} should be useful for the incorporation of UAAs in *Xenopus* oocytes.

Frameshift suppression appears to be unrealistic for use in mammalian cells and other cells that are dividing, because the FS tRNAs would recognize sites on endogenous mRNA, which is suggested by identifying FS tRNAs *in vivo* (28). The recognition of other sites would cause a loss of the UAA and could be toxic to the cell. The *Xenopus* oocyte system is ideal for the use of frameshift suppression because the added mRNA is

predominately translated *in vivo*. Another advantage for the oocyte system is that the most used Arg triplets (AGG and AGA) (27) would not be recognized by the modified FS tRNAs used in this study. Therefore all possible Arg sites could be mutated to either AGG or AGA in the nAChR sequence. This would allow for only competition between the FS tRNAs and endogenous triplet recognizing tRNA at the suppression site. This should increase the total suppression efficiency of the FS tRNAs and may also increase the overall translation efficiency of the nAChR. However, the amount of mutagenesis required to mutate all Arg sites would be time consuming and the Western blots suggest that full-length protein is being produced, which should be detectable by the sensitive assay of electrophysiology.

2.4 Experimental Methods

2.4.1 Materials

Oligonucleotides were synthesized by the California Institute of Technology Biopolymer Synthesis facility. NotI was purchased from Roche Applied Science (Indianapolis). BamHI, EcoRI, FokI, DpnI, MluI, Bsu36I, BstXI, T4 DNA ligase, and T4 RNA ligase were purchased from New England Biolabs (Beverly, MA). Kinase Max, T7 MEGashortscript, and T7 mMessage mMachine kits were purchased from Ambion (Austin, TX). HA.11 monoclonal antibody from mouse was from Covance (Berkeley, CA). Peroxidase-conjugated affinipure goat anti-mouse IgG was from Jackson Immuno Research (Westgrove, PA).

2.4.2 α_{NHA} Mutations and mRNA Preparation

The α_{NHA} in the pAMV vector was a gift from Dr. Gabriel Brandt. UAG mutations (S154 & S374) and Arg point mutations (CGG to CGC) were made using the QuikChange Site-Directed Mutagenesis (Stratagene). Plasmids were purified using the QIAprep Spin Miniprep Kit (Qiagen), restriction enzyme screened (if possible), and sequenced at the Caltech DNA Sequencing facility.

Four-base codons were mutated by overlap-extension PCR as described (39). Mutagenic PCR primers were ordered with at least 20 base pairs after the mutation region, which consisted of 3 mismatched and 1 insertion for S154 and 5 mismatches and 1 insertion for S374 (extra 2 mismatches to place stop codons). The initial PCR reactions contained 100 ng of DNA template, 1 μg of appropriate outer primer and mutagenic primer, 1 μl 25 mM dNTPs, 5 μl 10X buffer, millipore water to 49 μl , and 1 μl PfuTurbo Hotstart DNA Polymerase (Stratagene). The reaction was run with 30 cycles of 95 °C 1 min, 55 °C 1 min, and 72 °C for 7 min. The reaction mixture was run on a 1% agarose gel and the appropriate length band was purified using QiaQuick Gel Extraction kit (Qiagen). 4 μl of the first two PCR reactions were subjected to another round of PCR using 1 μg of each outer primer. The reaction was run with 30 cycles of 95 °C 1 min, 55 °C 1 min, and 72 °C for 7 min, and the appropriate size band was purified by gel extraction. 25 μl of the PCR product was then digested with MluI and Bsu36I for S154 or Bsu36I and BstXI for S374. Trimmed DNA was gel purified. The trimmed product was subcloned into the trimmed α_{NHA} in the pAMV vector that was dephosphorylated by shrimp alkaline phosphatase (Boehringer Mannheim Biochemicals) with T4 DNA ligase overnight at 16 °C. The ligation reaction was electroporated into bacteria and plasmids

were purified using QIAprep Spin Miniprep Kit (Qiagen), restriction enzyme screened (if possible), and sequenced at the Caltech DNA Sequencing facility.

25–50 μ g of mutated DNA was linearized with NotI for 12 h. Linearization was gel screened for completion before extracting with 25:24:1 phenol:chloroform:isoamyl alcohol and precipitated with ethanol for 12 h. DNA was dissolved in 52 μ l DEPC water and concentration determined by UV. mRNA was transcribed *in vitro* using T7 mMessage Machine kit for 3–4 h. mRNA was purified using RNeasy kit (Qiagen) and quantified by UV absorption at 260 nm. mRNA was aliquoted and stored at -80 °C until used.

2.4.3 Frameshift Suppressor tRNA Gene Construction and tRNA Preparation

HSAS and THG73 tRNA genes in the pUC19 plasmid were a gift from Dr. Sarah Monahan. HSFS tRNAs were made by the following oligonucleotides: 5'-AATTCGTAATACGATCACTATAGTAGTCGTGGCCGAGTGGTTAAGGCGATGGACT(XXXX)AATCCATTGGGGTCTCCCCGCGCAGGTTCGAATCCTGCCGACTACGCCATGAGACCCATCCG-3'. THG73FS tRNAs were made by the following oligonucleotides: 5'-AATTCGTAATACGACTCACTATAGGTTCTATAGTATAGCGGTTAGTACTGGGGACT(XXXX)AATCCCTTGACCTGGGTTGAATCCCAGTAGGACCGCCAGAGACCCATCCG-3'. XXXX is CCCG, CACG, and AACG (written 5'-3') for both THG73 and HSAS tRNAs. YFFS_{CCCG} was prepared with the following oligonucleotides: 5'-AATTCGTAATACGACTCACTATAGCGGATTTAGCTCAGTTGGGAGAGCGCCAGACT(CCCG)AATCTGGAGGTCCTGTGTTCGATCCACAGAA TTCGCACCATGAGACCCATCCG-3'. Note, oligonucleotides contain overlapping ends for ligation into pUC19 with EcoRI and BamHI.

The oligonucleotides were phosphorylated using Kinase Max kit, annealed, ligated to pUC19 plasmid (linearized with EcoRI and BamHI, dephosphorylated with shrimp alkaline phosphatase, purified by gel, and extracted using QiaQuick Gel Extraction kit (Qiagen)) with T4 DNA ligase at 16 °C for 12 h. Bacteria were electroporated, plasmids were purified using QIAprep Spin Miniprep Kit (Qiagen), restriction enzyme screened for insert with EcoRI and BamHI, and sequenced at the Caltech DNA Sequencing facility. tRNA were prepared similarly to procedures previously described (16,40).

25–50 µg DNA was linearized with Fok1 for 12 h. The linearization was gel screened for completion before extracting with 25:24:1 phenol:chloroform:isoamyl alcohol and precipitation with ethanol for 12 h. DNA was dissolved in 52 µl DEPC water and concentration determined by UV absorption at 260 nm. tRNA was transcribed *in vitro* using T7-MEGAshortscript kit for 3–4 h, which creates a 74mer tRNA lacking the last two nucleotides. The tRNA was extracted with 25:24:1 phenol:chloroform:isoamyl alcohol and precipitated with isopropanol for 12 h. tRNA was dissolved in DEPC water, run on gel with a previously prepared tRNA sample, quantified by UV absorption at 260 nm, and verified as the correct mass using MALDI-TOF mass spectrometry as described for THG73 (41). Using optimized conditions, the tRNA was dissolved in RNase free water and desalted using CHROMA SPIN™-30 DEPC-H₂O columns (BD Biosciences, San Jose, CA). tRNA was aliquoted and stored at –80 °C until used.

2.4.4 dCA-aa Synthesis and Ligation to Suppressor tRNAs

The synthesis of dCA and the coupling of UAAs has been described previously (40,42). dCA-Ala was a gift from Amy Eastwood and dCA-Trp was a gift from Dr. Sarah Monahan. Ligation to THG73, THG73FS, and YFFS tRNAs was performed as previously described (40,41). Briefly, the tRNA is denatured by placing in boiling water and allowed to cool in an ice bath to ≈ 37 °C to refold the tRNA. The tRNA is ligated to the dCA-aa using T4 RNA ligase for 30 min (longer times result in increased hydrolysis of the aa). The reaction is then extracted using 25:24:1 phenol:chloroform:isoamyl alcohol at pH = 5.2 and precipitated with ethanol for 12 h (longer precipitation times can result in hydrolysis of the aa). The tRNA was resuspended in DEPC ≈ 1 μ g / μ l. Using optimized conditions, the tRNA was resuspended in RNase-free water and desalted using CHROMA SPIN™-30 DEPC-H₂O columns (BD Biosciences, San Jose, CA). The tRNA-dCA-aa was aliquoted and placed at -80 °C until used. Ligation efficiency was qualitatively determined by MALDI-TOF as previously described (41).

2.4.5 *In Vitro* Translation

The tRNA was normalized and more concentrated samples were diluted with DEPC water so the same amount of tRNA was added to each *in vitro* reaction. The same was done for the mRNA samples.

Rabbit reticulocyte lysate (RRL), nuclease treated (Promega), was thawed slowly on ice. All reactions on a gel were run with the same tube of RRL. For eight samples, 3/5 reactions were run as follows: 22 μ l RRL, 0.9 μ l 1 mM aa mix, 0.6 μ l RNase Inhibitor (Roche), various amounts of mRNA and/or tRNA (noted with each figure), and filled to 30 μ l with DEPC water. The NVOC protecting group was removed immediately

before use in *in vitro* reactions by irradiation of the tRNA-dCA-aa-NVOC for 5 min with a 1,000 W Hg(Xe) arc lamp as described (40). Translation was run at 30 °C for 1.5 h and placed at –80 °C. TNT Coupled Reticulocyte Lysate (Promega) was employed the same as RRL with DNA, following manufacturers protocol. The reaction was run for 1.5 h and placed at –80 °C.

Wheat germ extract (WG) (Promega) was thawed on ice and all reactions were performed with the same WG tube. 3/5 reactions were performed as follows: 15 µl WG, 1.33 µl 1 mM aa mix, 3.6 µl 1 M KOAc, 1 µl RNase Inhibitor (Roche), various amounts of mRNA and/or tRNA, and filled to 30 µl with DEPC water. Translation was run at 25 °C for 1.5 h and placed at –80 °C.

Under optimized conditions, the RRL reaction was performed as follows. For eight samples, 3/5 reactions were run as follows: 22 µl RRL, 1 µl 1 mM 19 aa mix (- Arg), 1 µl 0.1 mM Arg, 0.6 µl RNase Inhibitor (Roche), various amounts of mRNA and/or tRNA (noted with each figure and greater than un-optimized conditions), and filled to 30 µl with RNase free water. The tRNA was refolding at 65 °C for 2 min and the NVOC protecting group was removed immediately before use in *in vitro* reactions by irradiation of the tRNA-dCA-aa-NVOC for 5 min with a 1,000 W Hg(Xe) arc lamp as described (40). Translation was run at 30 °C for 3–4 h and placed at –80 °C.

2.4.6 Western Blotting and Densitometric Analysis

Western blotting was performed as previously described (14). Briefly 5 µl of crude *in vitro* translation was added to 5 µl of 2X SDS loading buffer. Samples were loaded on a 4–15% linear gradient ready gel Tris-HCl (Bio-Rad) and run at 150 V for 1.25 h or until the hemoglobin (red band from RRL) had run off the gel. Protein was

transferred to nitrocellulose (Bio-Rad) at 30 V for 30 min and 100 V for 1.5 h. Nitrocellulose was blocked for 1 h or overnight using non-fat dairy milk (NFDM) in 1X PBS / 0.1% Tween, placed in 62.5–87.5 μg 1° Ab anti-hemagglutinin (Covance) in 15 ml NFDM / 1X PBS / 0.1% Tween for 1 h, washed 4X with 30 ml 1X PBS / 0.1% Tween for 5 min each, placed in 4 μg Peroxidase-conjugated AffiniPure Goat Anti-Mouse IgG (Jackson ImmunoResearch) in 30 mL NFDM / 1X PBS / 0.1% Tween for 1 h, and washed 4X with 30 ml 1X PBS / 0.1% Tween for 5 min each. Nitrocellulose was visualized using ECL Detection Kit and Hyperfilm ECL (Amersham Biosciences). ECL reagents were left on nitrocellulose for 1 min and quickly exposed for 30 sec, 15 sec, 10 sec, and 5 sec during the highest intensity light emission (1–5 min after exposure to ECL reagents, *Amersham Biosciences manual*).

Densitometric analysis was performed using the NIH Image program (National Institute of Health). Calculation of band intensity was performed similar to the manner of Sisido and coworkers (34). A calibration curve could not be generated because the protein is present in a very small amount, so numbers are qualitative rather than quantitative. Background intensity was determined by various endogenous protein bands in the RRL. Intensities of protein bands reported here are average values across the entire lane. Translation (for two suppression site constructs) or suppression efficiency is calculated by $[(\text{Suppressed FL Protein Intensity})/(\text{Wild-type FL Protein Intensity}(\text{or similar control}))]*100$ or for suppression of the wild-type constructs; $[1-(\text{Wild-type} + \text{tRNA FL Intensity})/(\text{Wild-type FL Intensity})]*100$.

2.5 References

1. Link, A.J., Mock, M.L., and Tirrell, D.A. (2003) Non-canonical amino acids in protein engineering. *Curr. Opin. Biotechnol.*, **14**, 603–609.
2. Dougherty, D.A. (2000) Unnatural amino acids as probes of protein structure and function. *Curr. Opin. Biotechnol.*, **4**, 645–652.
3. Beene, D.L., Dougherty, D.A., and Lester, H.A. (2003) Unnatural amino acid mutagenesis in mapping ion channel function. *Curr. Opin. Neurobiol.*, **13**, 264–270.
4. Xie, J., and Schultz, P.G. (2005) An expanding genetic code. *Methods*, **36**, 227–238.
5. Zhang, Z., Alfonta, L., Tian, F., Bursulaya, B., Uryu, S., King, D.S., and Schultz, P.G. (2004) Selective incorporation of 5-hydroxytryptophan into proteins in mammalian cells. *Proc. Natl. Acad. Sci. USA*, **101**, 8882–8887.
6. Rodriguez, E.A., Lester, H.A., and Dougherty, D.A. (2007) Improved amber and opal suppressor tRNAs for incorporation of unnatural amino acids *in vivo*. Part 2: Evaluating suppression efficiency. *RNA*, **13**, 1715–1722.
7. Noren, C.J., Anthonycahill, S.J., Griffith, M.C., and Schultz, P.G. (1989) A general method for site-specific incorporation of unnatural amino acids into proteins. *Science*, **244**, 182–188.
8. Nowak, M.W., Kearney, P.C., Sampson, J.R., Saks, M.E., Labarca, C.G., Silverman, S.K., Zhong, W., Thorson, J., Abelson, J.N., Davidson, N. *et al.* (1995) Nicotinic receptor binding site probed with unnatural amino acid incorporation in intact cells. *Science*, **268**, 439–442.

9. Heckler, T.G., Chang, L.H., Zama, Y., Naka, T., Chorghade, M.S., and Hecht, S.M. (1984) T4 RNA ligase mediated preparation of novel "chemically misacylated" tRNA^{Phe}s. *Biochemistry*, **23**, 1468–1473.
10. Wang, L., Magliery, T.J., Liu, D.R., and Schultz, P.G. (2000) A new functional suppressor tRNA/aminoacyl-tRNA synthetase pair for the *in vivo* incorporation of unnatural amino acids into proteins. *J. Am. Chem. Soc.*, **122**, 5010–5011.
11. Chin, J.W., Cropp, T.A., Anderson, J.C., Mukherji, M., Zhang, Z., and Schultz, P.G. (2003) An expanded eukaryotic genetic code. *Science*, **301**, 964–967.
12. England, P.M. (2004) Unnatural amino acid mutagenesis: a precise tool for probing protein structure and function. *Biochemistry*, **43**, 11623–11629.
13. Monahan, S.L., Lester, H.A., and Dougherty, D.A. (2003) Site-specific incorporation of unnatural amino acids into receptors expressed in mammalian cells. *Chem. Biol.*, **10**, 573–580.
14. England, P.M., Zhang, Y.N., Dougherty, D.A., and Lester, H.A. (1999) Backbone mutations in transmembrane domains of a ligand-gated ion channel: Implications for the mechanism of gating. *Cell*, **96**, 89–98.
15. Zhong, W., Gallivan, J.P., Zhang, Y., Li, L., Lester, H.A., and Dougherty, D.A. (1998) From ab initio quantum mechanics to molecular neurobiology: A cation- π binding site in the nicotinic receptor. *Proc. Natl. Acad. Sci. USA*, **95**, 12088–12093.
16. Saks, M.E., Sampson, J.R., Nowak, M.W., Kearney, P.C., Du, F.Y., Abelson, J.N., Lester, H.A., and Dougherty, D.A. (1996) An engineered *Tetrahymena*

- tRNA^{Gln} for *in vivo* incorporation of unnatural amino acids into proteins by nonsense suppression. *J. Biol. Chem.*, **271**, 23169–23175.
17. Hohsaka, T., Ashizuka, Y., Sasaki, H., Murakami, H., and Sisido, M. (1999) Incorporation of two different nonnatural amino acids independently into a single protein through extension of the genetic code. *J. Am. Chem. Soc.*, **121**, 12194–12195.
 18. Hohsaka, T., Ashizuka, Y., Murakami, H., and Sisido, M. (1996) Incorporation of nonnatural amino acids into streptavidin through *in vitro* frame-shift suppression. *J. Am. Chem. Soc.*, **118**, 9778–9779.
 19. Hohsaka, T., Ashizuka, Y., Taira, H., Murakami, H., and Sisido, M. (2001) Incorporation of nonnatural amino acids into proteins by using various four-base codons in an *Escherichia coli in vitro* translation system. *Biochemistry*, **40**, 11060–11064.
 20. Hohsaka, T., Fukushima, M., and Sisido, M. (2002) Nonnatural mutagenesis in *E. coli* and rabbit reticulocyte lysates by using four-base codons. *Nucleic Acids Res. Suppl.*, 201–202.
 21. Taira, H., Fukushima, M., Hohsaka, T., and Sisido, M. (2005) Four-base codon-mediated incorporation of non-natural amino acids into proteins in a eukaryotic cell-free translation system. *J. Biosci. Bioeng.*, **99**, 473–476.
 22. Hohsaka, T., Ashizuka, Y., Murakami, H., and Sisido, M. (2001) Five-base codons for incorporation of nonnatural amino acids into proteins. *Nucleic Acids Res.*, **29**, 3646–3651.

23. Anderson, R.D., 3rd, Zhou, J., and Hecht, S.M. (2002) Fluorescence resonance energy transfer between unnatural amino acids in a structurally modified dihydrofolate reductase. *J. Am. Chem. Soc.*, **124**, 9674–9675.
24. Taki, M., Hohsaka, T., Murakami, H., Taira, K., and Sisido, M. (2002) Position-specific incorporation of a fluorophore-quencher pair into a single streptavidin through orthogonal four-base codon/anticodon pairs. *J. Am. Chem. Soc.*, **124**, 14586–14590.
25. Murakami, H., Kourouklis, D., and Suga, H. (2003) Using a solid-phase ribozyme aminoacylation system to reprogram the genetic code. *Chem. Biol.*, **10**, 1077–1084.
26. Murakami, H., Hohsaka, T., Ashizuka, Y., and Sisido, M. (1998) Site-directed incorporation of *p*-nitrophenylalanine into streptavidin and site-to-site photoinduced electron transfer from a pyrenyl group to a nitrophenyl group on the protein framework. *J. Am. Chem. Soc.*, **120**, 7520–7529.
27. Nakamura, Y., Gojobori, T., and Ikemura, T. (2000) Codon usage tabulated from international DNA sequence databases: Status for the year 2000. *Nucleic Acids Res.*, **28**, 292.
28. Magliery, T.J., Anderson, J.C., and Schultz, P.G. (2001) Expanding the genetic code: Selection of efficient suppressors of four-base codons and identification of "shifty" four-base codons with a library approach in *Escherichia coli*. *J. Mol. Biol.*, **307**, 755–769.

29. Capone, J.P., Sharp, P.A., and RajBhandary, U.L. (1985) Amber, ochre and opal suppressor tRNA genes derived from a human serine tRNA gene. *Embo. J.*, **4**, 213–221.
30. Price, S., Cusack, S., Borel, F., Berthet-Colominas, C., and Leberman, R. (1993) Crystallization of the seryl-tRNA synthetase:tRNA^{ser} complex of *Escherichia coli*. *FEBS Lett.*, **324**, 167–170.
31. Shimada, N., Suzuki, T., and Watanabe, K. (2001) Dual mode recognition of two isoacceptor tRNAs by mammalian mitochondrial seryl-tRNA synthetase. *J. Biol. Chem.*, **276**, 46770–46778.
32. Zuker, M. (2003) Mfold web server for nucleic acid folding and hybridization prediction. *Nucleic Acids Res.*, **31**, 3406–3415.
33. Rodriguez, E.A., Lester, H.A., and Dougherty, D.A. (2006) *In vivo* incorporation of multiple unnatural amino acids through nonsense and frameshift suppression. *Proc. Natl. Acad. Sci. USA*, **103**, 8650–8655.
34. Hohsaka, T., Kajihara, D., Ashizuka, Y., Murakami, H., and Sisido, M. (1999) Efficient incorporation of nonnatural amino acids with large aromatic groups into streptavidin in *in vitro* protein synthesizing systems. *J. Am. Chem. Soc.*, **121**, 34–40.
35. Nakata, H., Ohtsuki, T., Abe, R., Hohsaka, T., and Sisido, M. (2006) Binding efficiency of elongation factor Tu to tRNAs charged with nonnatural fluorescent amino acids. *Anal. Biochem.*, **348**, 321–323.
36. Giege, R., Sissler, M., and Florentz, C. (1998) Universal rules and idiosyncratic features in tRNA identity. *Nucleic Acids Res.*, **26**, 5017–5035.

37. Saks, M.E., Sampson, J.R., and Abelson, J.N. (1994) The transfer RNA identity problem: A search for rules. *Science*, **263**, 191–197.
38. Deiters, A., Cropp, T.A., Mukherji, M., Chin, J.W., Anderson, J.C., and Schultz, P.G. (2003) Adding amino acids with novel reactivity to the genetic code of *Saccharomyces cerevisiae*. *J. Am. Chem. Soc.*, **125**, 11782–11783.
39. Ling, M.M., and Robinson, B.H. (1997) Approaches to DNA mutagenesis: an overview. *Anal. Biochem.*, **254**, 157–178.
40. Nowak, M.W., Gallivan, J.P., Silverman, S.K., Labarca, C.G., Dougherty, D.A., and Lester, H.A. (1998) *In vivo* incorporation of unnatural amino acids into ion channels in *Xenopus* oocyte expression system. *Meth. Enzymol.*, **293**, 504–529.
41. Petersson, E.J., Shahgholi, M., Lester, H.A., and Dougherty, D.A. (2002) MALDI-TOF mass spectrometry methods for evaluation of *in vitro* aminoacyl tRNA production. *RNA*, **8**, 542–547.
42. Robertson, S.A., Noren, C.J., Anthony-Cahill, S.J., Griffith, M.C., and Schultz, P.G. (1989) The use of 5'-phospho-2 deoxyribocytidylylriboadenosine as a facile route to chemical aminoacylation of tRNA. *Nucleic Acids Res.*, **17**, 9649–9660.

Chapter 3

In Vivo Incorporation of Multiple
Unnatural Amino Acids Through
Nonsense and Frameshift Suppression

This chapter is reproduced, with modification, from *In vivo incorporation of multiple unnatural amino acids through nonsense and frameshift suppression*, by E. A. Rodriguez, H. A. Lester, and D. A. Dougherty, (2006) *Proc. Natl. Acad. Sci. USA*, **103**(23), 8650–8655. Copyright 2006 by the National Academy of Sciences USA.

3.1 Introduction

The site-specific incorporation of unnatural amino acids (UAAs) into proteins biosynthetically is a powerful methodology that is seeing increasing use. The primary approach has been stop codon (nonsense) suppression using a specially designed tRNA with an anticodon recognizing the stop codon. A wide range of *in vitro* translation systems has been employed, along with expression in *E. coli* and, to a lesser extent, yeast. Nonsense suppression in higher eukaryotes has for the most part been limited to the *Xenopus* oocyte (1,2). The incorporation of UAA(s) in *Xenopus* oocytes is shown in Figure 3.1. The mRNA with the suppression site(s) (stop and/or quadruplet codons) (Figure 3.1, 1) (for the mechanism of stop codon and quadruplet codon suppression see Figure 2.2) and the tRNA(s) chemically aminoacylated with the UAA(s) (Figure 3.1, 2) are injected into a *Xenopus* oocyte (Figure 3.1, 3). The oocyte is allowed to incubate for 1–2 days to allow for UAA(s) incorporation by the endogenous translational machinery, protein folding and processing, ion channel assembly, and export to the surface of the cell (Figure 3.1, 4). UAA(s) incorporation is then assayed using the sensitivity of electrophysiology (Figure 3.1, 5). Other experiments in higher eukaryotes have relied on the evolution of a unique tRNA and a complementary aminoacyl-tRNA synthetase (aaRS) to insert an UAA in response to the UAG or UGA stop codon, but currently only 3-iodo-tyrosine (3), p-benzoyl-phenylalanine (4), and 5-hydroxy-tryptophan (5) have been incorporated.

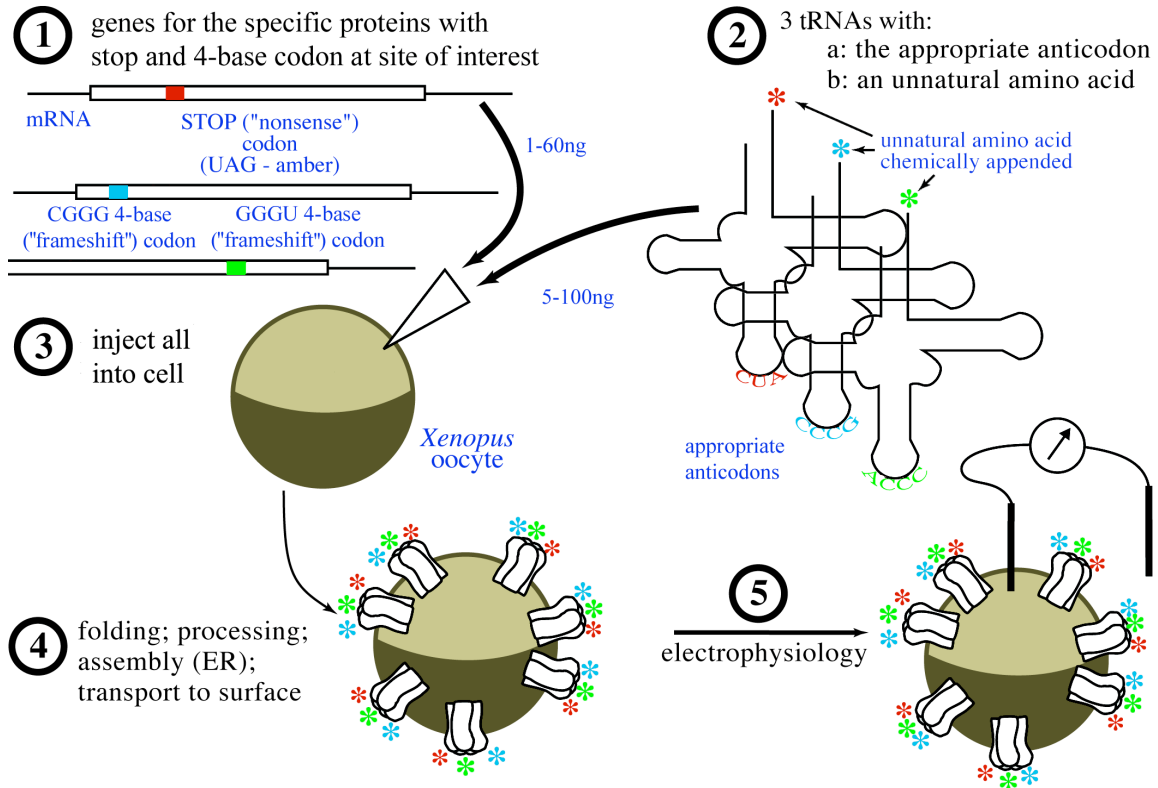


Figure 3.1: Multiple UAA incorporation in ion channels expressed in *Xenopus* oocytes. (1) mRNAs with the appropriate suppression sites are transcribed *in vitro*. (2) Suppressor tRNAs are transcribed *in vitro*. An UAA is synthesized and chemically aminoacylated onto the suppressor tRNAs. (3) mRNAs and tRNAs are micro-injected into the *Xenopus* oocyte. (4) Oocytes are incubated to allow for protein translation with UAAs site-specifically incorporated. The ion channels are folded, processed (signal sequence removal, glycosylation, etc.), assembled into multi-subunit channels, and transported to the plasma membrane. (5) UAA incorporation is detected using the sensitive assay of electrophysiology. Figure adapted from (2).

A remarkable variant of this approach is the use of quadruplet codons, a process termed frameshift suppression, that was pioneered by Sisido and coworkers (6,7). The success of this approach opens up the possibility of developing multiple new codons, and thus incorporating several different UAAs into a protein. This in turn would enable novel biophysical approaches such as incorporating fluorescence resonance energy transfer (FRET) pairs, new structural probes such as novel cross-linking approaches, and more detailed structure-function studies.

To date frameshift suppression *in vivo* has been performed only in *E. coli* by using a unique tRNA/aaRS pair, and homoglutamine is the only UAA incorporated by this method (8). It has yet to be established whether frameshift suppression by chemically aminoacylated tRNA can be effective *in vivo* in general, and in eukaryotic cells such as the *Xenopus* oocyte in particular. In fact, a previous attempt to perform frameshift suppression in *Xenopus* oocytes showed very poor suppression efficiency (9). Here we show that with appropriately designed frameshift suppressor (FS) tRNAs, frameshift suppression is a viable approach to UAA incorporation in eukaryotic cells. Also, the efficiency of frameshift suppression can be substantially improved by “masking” the mRNA of all in-frame quadruplet sequences that match the frameshift suppression site. In particular, we describe two tRNAs with 4-base anticodons that can deliver UAAs in response to the quadruplet codons CGGG and GGGU. When directly compared to an amber suppressor (AS) tRNA (THG73) that has been used extensively in *Xenopus* oocytes, the FS tRNAs are less efficient at delivering UAAs. However, both FS tRNAs are more “orthogonal” than THG73, producing much less incorporation of undesired natural amino acids at promiscuous sites. We also show that suppression by FS tRNAs increases nonlinearly with the amount of injected tRNA. To illustrate the potential of this methodology, we have successfully incorporated two and three different UAAs, simultaneously, into a neuroreceptor expressed in a *Xenopus* oocyte.

3.2 Results

3.2.1 Testing Frameshift Suppression Viability *In Vivo*

To determine whether frameshift suppression is viable in *Xenopus* oocytes, we chose to use a tRNA that can be aminoacylated *in vivo*. We selected the human serine amber suppressor (HSAS), because it is aminoacylated (with serine) in eukaryotic cells, and the seryl-tRNA synthetase does not recognize the anticodon (10–12). The CUA anticodon of HSAS was replaced with CCCG and ACCC to create the human serine frameshift suppressors (HSFS_{CCCG} and HSFS_{ACCC}) (cloverleaf structures shown in Figure 3.2, A), which recognize the quadruplet codons CGGG and GGGU, respectively. Prior research showed that these 4-base codons are efficient *in vitro* (7). Injection of wild-type muscle nicotinic acetylcholine receptor (nAChR) mRNA and either HSFS_{CCCG} or HSFS_{ACCC} (2.5 or 10 ng per oocyte; no amino acid ligated to the tRNA) into *Xenopus* oocytes resulted in no detectable channel expression. The addition of the original amber suppressor HSAS with wild type nAChR mRNA did show channel expression with 2.5 ng tRNA per oocyte, but not with 10 ng. These results suggested that the HSFS tRNAs were causing +1 frameshifts, resulting in undesirable truncation of wild-type protein and thus a lack of detectable current. Analysis of the four nAChR subunits revealed four CGGG and one GGGU in-frame quadruplet codons. These were mutated to degenerate codons (see methods) to avoid suppression, and we refer to the resulting mRNAs as the “masked” constructs. Other groups have similarly removed undesired in-frame quadruplets (7,9,13). Injection of 2.5 ng per oocyte of either unligated HSFS plus the masked nAChR mRNAs resulted in functional channels with the same EC₅₀ as channels

expressed without tRNA (data not shown). Unless otherwise noted, all subsequent experiments used such masked constructs.

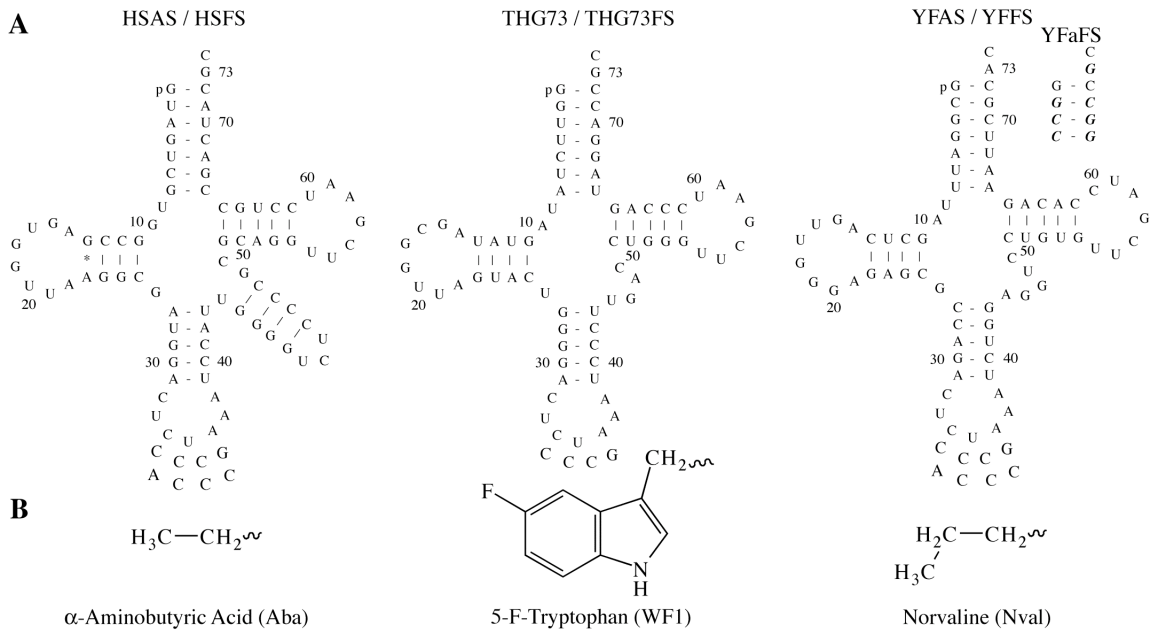


Figure 3.2: tRNAs and UAAs. (A) The AS tRNAs are shown with the CUA anticodon and the FS anticodons used in this study. YFaFS tRNA acceptor stem mutations are shown next to the YFFS tRNA body (italicized). (B) The three UAAs used in this study.

To test whether a naturally occurring amino acid (serine) could be incorporated in response to a quadruplet codon, we probed a highly conserved leucine of the nAChR M2 domain, a site designated Leu9' (shown in Figure 3.3). This is a promiscuous site in the nicotinic receptor, and replacement of the native leucine with essentially any natural amino acid produces a functional receptor, usually with a quite noticeable shift in EC_{50} . In particular, prior research showed that a leucine-to-serine mutation in the β subunit ($\beta 9'$) resulted in a ≈ 33 -fold increased sensitivity to acetylcholine (ACh) (14).

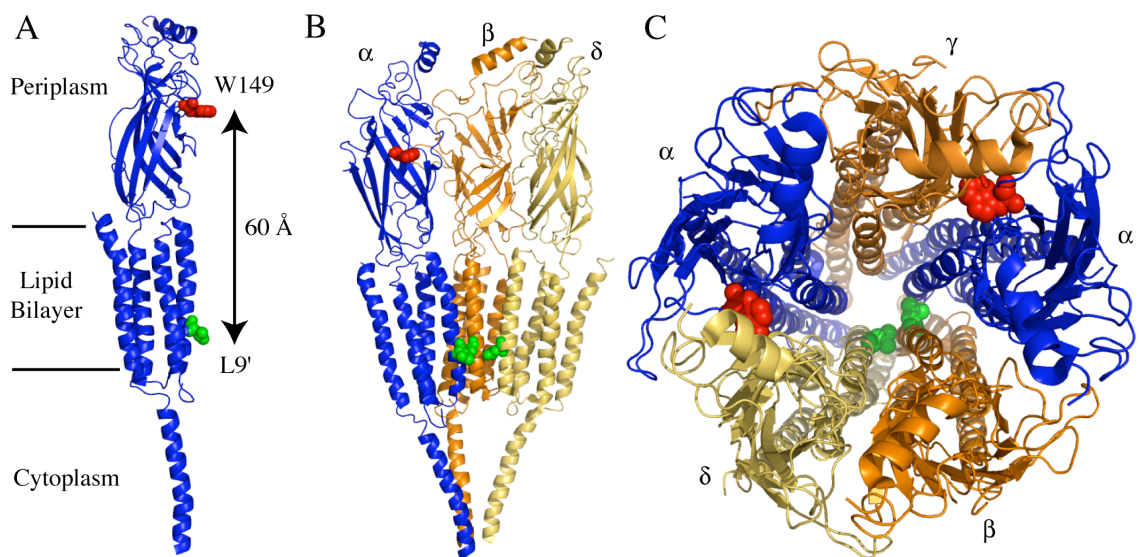


Figure 3.3: nAChR suppression sites used in this research. (A) The α -subunit of the nAChR. α W149 and α L9' are shown in red and green, respectively. (B) The α -, β -, and δ -subunits of the nAChR are shown. α W149 and α L9' are shown in red and green, respectively. These were the three subunits used to simultaneously incorporate three UAAs. (C) Top view of the nAChR with α W149 and α L9' shown in red and green, respectively. Due to the stoichiometry ($2\alpha:\beta:\gamma:\delta$), the simultaneous incorporation of three different UAAs at α 149UAG, β 9'CGGG, and δ 9'GGGU results in four UAAs per ion channel. Figure created from 2BG9.pdb (15).

The β 9' site was mutated to UAG, CGGG, or GGGU. When mutant mRNA was injected into *Xenopus* oocytes along with 2.5 ng of unligated HSAS or HSFS tRNA, which should be aminoacylated with serine by the endogenous seryl-tRNA synthetase, significant channel expression was seen. However, the EC_{50} values varied depending on the incubation time (Table 3.1, A). This suggested that natural amino acids other than serine were being placed at the β 9' site with two-day incubations, because the conventional mutant, β 9'Ser, shows no change in EC_{50} (Table 3.1, A). The variability in EC_{50} between one and two day incubations suggests that the tRNAs are being modified to accept other amino acids. Modification of yeast phenylalanine tRNA in *Xenopus* oocytes has been shown to increase greatly from one-to-two day incubation times (16). Thus, we avoid this complication by incubation for one day. Amber suppression is highly efficient

when the average maximal peak current (I_{\max}) is measured at 1.25 ng of tRNA per oocyte and decreases slightly when 2.5 ng is added (Table 3.1, B). CGGG shows lower suppression than GGGU, in agreement with previous *in vitro* studies (7,17). CGGG suppression is highly nonlinear, with a 330% increase in current when twice as much tRNA is injected (Table 3.1, B). GGGU however shows an almost linear relationship, with an increase of 86% in response to doubling (Table 3.1, B). These data suggest that HSFS_{ACCC} is a more efficient tRNA at recognizing its cognate quadruplet codon and/or has less competition with endogenous triplet tRNA in *Xenopus* oocytes than HSFS_{CCCG}. These experiments establish that frameshift suppression is viable in *Xenopus* oocytes, and that UAA incorporation should be feasible using the appropriate FS tRNA.

Table 3.1: HSAS and HSFS suppression experiments at the $\beta 9'$ site.

A

$\beta 9'$ X	tRNA (2.5 ng)	EC ₅₀ (1 day)*	n_H	n	EC ₅₀ (2 day)*	n_H	n
AGC (Serine)	none	1.5±.04	1.7±.07	5	1.5±.2	1.9±.3	3
UAG	HSAS	1.7±.06	1.7±.09	6	.70±.008	1.9±.07	14
CGGG	HSFS _{CCCG}	2.1±.09	1.7±.1	8	1.3±.1	1.9±.3	13
GGGU	HSFS _{ACCC}	1.9±.08	1.5±.08	9	.68±.1	1.7±.04	5

B

$\beta 9'$ X	tRNA	$I_{\max} \pm SE$ (1.25) [‡]	n	$I_{\max} \pm SE$ (2.5) [‡]	n	% HSAS (1.25) [‡]	% HSAS (2.5) [‡]	% Change [§]
UAG	HSAS	-19±2	12	-14±3	11	100%	100%	-26%
CGGG	HSFS _{CCCG}	-1.3±.3	10	-5.6±1	12	6.8%	40%	330%
GGGU	HSFS _{ACCC}	-8.6±3	10	-16±3	12	45%	110%	86%

* Incubation time. † Avg. I_{\max} (μA) recorded at 50 μM ACh. ‡ ng of tRNA. § 1.25 to 2.5 ng of tRNA.

3.2.2 UAA Incorporation By Frameshift Suppression

THG73 is an AS tRNA (cloverleaf structure shown in Figure 3.2, A) (18) used extensively for incorporating UAAs into various ion channels expressed in *Xenopus*

oocytes (2). Initially a FS derived from THG73 recognizing the quadruplet codon CGGG (THG73FS_{CCCG}) was tested for UAA incorporation. Attempts to suppress β⁹CGGG with THG73FS_{CCCG}-L, where Leu was chemically aminoacylated onto the tRNA, showed no current *in vivo*. This is consistent with data from Voss and coworkers, who saw very little UAA incorporation with THG73FS_{ACCC} in *Xenopus* oocytes (9).

Western blots of THG73FS_{CCCG}-W suggested that the tRNA may be stuck on the ribosome and stopping translation (Chapter 2). Uhlenbeck and coworkers have shown that nucleotides in the anticodon loop at position 32 and 38 effect ribosome binding of tRNAs (19). THG73FS_{CCCG} and most amber suppressors have C32 and A38 (Figures 3.2 & 3.4), which is the consensus sequence for optimal suppression by amber suppressor tRNAs and is thought to cause tighter binding to the ribosome. Mutations to tRNA^{Ala}_{GCC} at positions 32 and 38 alter ribosome binding where A32-A38 causes tighter binding to the ribosome, while C32-G38 and A32-U38 weaken binding to the ribosome (19). These mutations were placed on THG73FS_{CCCG} and shown in Figure 3.4. Another possibility is that THG73FS_{CCCG} could be recognizing multiple codons or even doublet codons, which would cause frameshifts and truncation of the gene. tRNA^{Gly}_(UCC & CCC) uses the 32nd position to discriminate the 3rd nucleotide of the triplet codon (20). tRNA^{Gly}_{CCC} (similar anticodon to THG73FS_{CCCG}) with C32, which is the same as THG73FS_{CCCG} (Figure 3.4), promotes doublet decoding of GG over the full triplet codon GGG (21). Therefore, mutations at the 32nd position could alter ribosomal binding and/or decoding of THG73FS_{CCCG} to allow for the incorporation of UAAs. THG73FS_{CCCG} was mutated to create the constructs THA32G73FS_{CCCG}, THG38G73FS_{CCCG}, and THA32U38G73FS_{CCCG} (shown in Figure 3.4). Suppression experiments were performed at α149CGGG with the

frameshift suppressor tRNAs ligated with Trp and compared to suppression at $\alpha 149\text{UAG}$ by the amber suppressor, THG73-W (Table 3.2). All mutations resulted in little expression and therefore none of the THG73-based frameshift suppressors are viable for UAA incorporation.

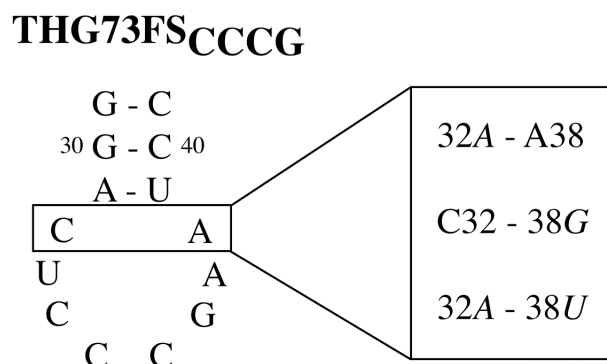


Figure 3.4: THG73FS_{CCCG} anticodon loop mutations. The last three base pairs of the anticodon stem and the anticodon loop are shown. The boxed region corresponds to C32-A38, where mutations were made. The box on the right shows mutations made (*italics*). On tRNA^{Ala}_{GGC}, A32-A38 increases ribosome binding, while C32-38G and A32-U38 decrease ribosome binding (19). C32 on tRNA^{Gly}_{CCC} promotes doublet decoding of GG and therefore mutations at the 32nd position may also promote quadruplet decoding (21).

Table 3.2: THG73FS_{CCCG} and anticodon loop mutations suppression at $\alpha 149\text{CGGG}$.

mRNA	tRNA	ng tRNA	n	$I_{\max}^* \pm \text{SE}$
$\alpha 149\text{UAG}$	THG73-W	9.4	12	$-2.8 \pm .6$
$\alpha 149\text{CGGG}$	THG73FS _{CCCG} -W	9.4	12	$-.019 \pm .002$
$\alpha 149\text{CGGG}$	THA32G73FS _{CCCG} -W	9.4	12	$-.013 \pm .002$
$\alpha 149\text{CGGG}$	THG38G73 _{CCCG} -W	9.4	12	$-.014 \pm .003$
$\alpha 149\text{CGGG}$	THA32U38G73FS _{CCCG} -W	9.4	12	$-.024 \pm .002$

* Avg. I_{\max} (μA) recorded at 1 mM ACh.

We then chose to screen yeast phenylalanine FS (YFFS) tRNAs, which were employed successfully by the Sisido group *in vitro* (7,17). We studied both YFFS_{CCCG} and YFaFS_{ACCC}; Figure 3.2, A, shows cloverleaf structures. The latter contains acceptor

stem mutations (denoted by the “a”) incorporated to reduce glycyI-tRNA synthetase recognition (7). We first evaluated a non-promiscuous position of the nAChR, α 149W, an agonist binding site tryptophan that makes a cation- π interaction with ACh (22) (shown in Figure 3.3). Wild-type recovery, i.e., suppressing the α 149 quadruplet codons with YFFS_{CCCG}-W or YFaFS_{ACCC}-W, resulted in functional, wild-type channels (Table 3.3). To demonstrate UAA incorporation we relied on previous work using the AS THG73 that established that 5-fluoro-tryptophan, WF1 (structure in Figure 3.2, B), incorporated at α 149 decreased the cation- π interaction and caused a \approx 4-fold increase in EC₅₀ (22). YFFS_{CCCG}-WF1 suppression at α 149CGGG resulted in a comparable increase in EC₅₀ (Table 3.3), establishing the successful incorporation of the UAA WF1.

Table 3.3: Wild-type recovery and UAA incorporation by frameshift suppression *in vivo*.

mRNA	tRNA	EC ₅₀ (theo) ^{(ref)†}	n _H	n
α 149CGGG	YFFS _{CCCG} -W*	56 \pm 2 (50) ⁽¹⁴⁾	1.8 \pm .07	8
α 149GGGU	YFaFS _{ACCC} -W*	53 \pm 2 (50) ⁽¹⁴⁾	1.6 \pm .03	8
β 9’GGGU	YFaFS _{ACCC} -Aba	16 \pm .9 (16) ⁽¹⁴⁾	1.3 \pm .08	7
δ 9’GGGU	YFaFS _{ACCC} -Nval	31 \pm 2 (36) ⁽¹⁴⁾	1.6 \pm .1	6
α 149CGGG	YFFS _{CCCG} -WF1	190 \pm 3 (200) ⁽²²⁾	1.6 \pm .03	10

* Rescue of wild type recovery by frameshift suppression.

† EC₅₀ values from THG73-UAA incorporation by nonsense suppression.

We next considered the previously mentioned Leu9’ residue (shown in Figure 3.3). Suppression at β 9’GGGU and δ 9’GGGU with YFaFS_{ACCC}-Aba and YFaFS_{ACCC}-Nval (UAA structures shown in Figure 3.2, B), respectively, resulted in reductions in EC₅₀ (Table 3.3) that were consistent with previous studies using the same UAAs and the AS THG73 (14). All frameshift suppression experiments had an I_{max} between -1.6 and

-4.4 μA , which is more than adequate for UAA studies *in vivo* and should allow for the incorporation of multiple UAAs. In all cases, injection of full-length tRNA that had no amino acid attached to the 3' end resulted in no detectable currents in response to added ACh, directly showing a lack of aminoacylation by endogenous, *Xenopus* aaRSs.

3.2.3 Masking Effects on Frameshift Suppression

Experiments with HSFS required the masking of the nAChR subunits in order to avoid protein truncation caused by +1 frameshifts. To demonstrate the effect on UAA incorporation, suppression experiments were performed with wild-type and masked constructs. The quadruplet codon GGGU was chosen because there was only one in-frame quadruplet in the signaling sequence of the nAChR β subunit and none in the α , γ , or δ subunits. Wild-type recovery was performed by suppressing at α 149GGGU with YFaFS_{ACCC}-W and adding either wild-type or masked β mRNA to the injection mixture. Table 3.4 shows the dramatic effect of masking one position on frameshift suppression. With a 1:1:1:1 ratio of α : β : γ : δ , the masked construct gives a 2.7-fold increase in I_{max} relative to wild type. As the amount of α subunit (which contains the suppression site) is increased, the masking effect decreases to 1.5-fold and 1.2-fold with subunit ratios of 5:1:1:1 and 10:1:1:1, respectively. Calculations that assume two, equally efficient quadruplet codons reproduce this trend (Table 3.4), suggesting that the α 149GGGU and the GGGU present in the β subunit have similar suppression efficiencies.

Table 3.4: Masking experiments.

$\alpha 149$ GGGU	:	β	$I_{\max}^* \pm \text{SE}$	n	% Difference (theo) [†]
1	:	1 wild type	$-.14 \pm .02$	11	63%
1	:	1 masked	$-.38 \pm .1$	11	(75%)
5	:	1 wild type	$-.35 \pm .1$	10	32%
5	:	1 masked	$-.52 \pm .2$	12	(31%)
10	:	1 wild type	$-.71 \pm .3$	11	15%
10	:	1 masked	$-.83 \pm .3$	12	(17%)

* Avg. I_{\max} (μA) recorded at 1 mM ACh.

[†] () are theoretical values = $1 - (P \text{ of } \alpha \text{ suppression})^2$, where both sites are assumed to have the same probability (P) and squared because of 2 α subunits per channel.

3.2.4 Comparison of Frameshift and Nonsense Suppression Efficiencies

To compare frameshift and nonsense suppression, the $\alpha 149$ and $\beta 9'$ sites were studied in more detail (shown in Figure 3.3). Suppression of $\alpha 149$ CGGG or GGGU with 10 ng of YFFS_{CCCG}-W or YFaFS_{ACCC}-W resulted in 38% and 48%, respectively, of the current from 10 ng of THG73-W suppression at $\alpha 149$ UAG (Table 3.5). Suppression of $\beta 9'$ UAG with 2 ng of THG73-L resulted in the largest I_{\max} (Table 3.5). Suppression at $\beta 9'$ CGGG or GGGU with 2 ng of YFFS_{CCCG}-L or YFaFS_{ACCC}-L resulted in 14% and 36%, respectively, of the current from THG73-L (Table 3.5). We conclude that amber suppression is more efficient than frameshift suppression, in agreement with a trend previously seen in a eukaryotic cell-free translation system (17). In particular, the suppression efficiency observed here follows the order: THG73 > YFaFS_{ACCC} > YFFS_{CCCG}.

Table 3.5: Comparison of suppression efficiency, aminoacylation, and read-through *in vivo*.

mRNA	tRNA	ng tRNA	n	$I_{\max} \pm SE$	% THG73
α 149UAG	THG73-W	10	18	-4.8 \pm 2	100%
α 149CGGG	YFFS _{CCCG} -W	10	20	-1.8 \pm .3	38%
α 149GGGU	YFaFS _{ACCC} -W	10	13	-2.3 \pm .9	48%
β 9'UAG	THG73-L [†]	2	15	-6.1 \pm 2	100%
β 9'CGGG	YFFS _{CCCG} -L [†]	2	12	-.84 \pm .2	14%
β 9'GGGU	YFaFS _{ACCC} -L [†]	2	9	-2.2 \pm .5	36%
β 9'CGGG	YFFS _{CCCG} -L [†]	6	13	-8.8 \pm .9	NA
β 9'GGGU	YFaFS _{ACCC} -L [†]	6	13	-16 \pm 2	NA
β 9'UAG	THG73-dCA	2	13	-4.8 \pm 1	100%
β 9'CGGG	YFFS _{CCCG} -dCA	2	13	-.42 \pm .8	8.8%
β 9'GGGU	YFaFS _{ACCC} -dCA	2	13	-.092 \pm .02	1.9%
β 9'UAG	THG73-dCA	6	13	-8.2 \pm 1	100%
β 9'CGGG	YFFS _{CCCG} -dCA	6	12	-1.2 \pm .3	15%
β 9'GGGU	YFaFS _{ACCC} -dCA	6	11	-.27 \pm .09	3.3%
					% UAG
β 9'UAG	-	-	13	-.37 \pm .1	100%
β 9'CGGG	-	-	13	-.085 \pm .03	23%
β 9'GGGU	-	-	13	-.078 \pm .02	21%

* Avg. I_{\max} (μ A) recorded at 1 mM ACh.

[†] Currents in response to 10 μ M and 1 mM ACh displayed a ratio of 0.1, as anticipated from the Hill equation fit for one, wild-type receptor.

Interestingly, the yield of receptors from frameshift suppression at the β 9' site was substantially improved by increasing the amount of tRNA injected. Suppression with 6 ng of YFFS_{CCCG}-L or YFaFS_{ACCC}-L gave dramatic increases in I_{\max} , with a % change of 950% and 630%, respectively (Table 3.5). This large change in I_{\max} in response to a modest increase in tRNA concentration implicates a competition with endogenous triplet tRNA that responds nonlinearly to the amount of injected FS tRNA. A comparable increase in the amount of injected THG73-L led to complications due to reacylation of the tRNA by endogenous aaRSs (undesired) and incorporation of natural

amino acids other than leucine, an issue that is addressed in detail in the following section, in the Discussion, and in Chapters 4 and 5.

3.2.5 Comparison of Aminoacylation of Suppressor tRNA and Read-Through of Suppression Sites

To evaluate aminoacylation *in vivo*, which is undesirable for any tRNA used to incorporate UAAs, the $\beta 9'$ site was again studied, because most amino acids produce functional receptors when substituted at this position (14). In all experiments, tRNAs that had been ligated to dCA but did not contain an amino acid at the 3' end were injected, in order to more closely mimic the biologically active, full-length tRNA. In order to maximize the potential for aminoacylation by endogenous aaRSs, two-day incubations and relatively large mRNA quantities (16.5 ng) were employed. Surprisingly, THG73-dCA, which has been used extensively for UAA incorporation in *Xenopus* oocytes, showed significant aminoacylation *in vivo*, with I_{\max} of -4.8 and -8.2 μA for 2 and 6 ng tRNA, respectively (Table 3.5). Note that under other conditions (less mRNA; shorter incubations) previous work has found no complications from aminoacylation using THG73-dCA in *Xenopus* oocytes (9,14,18). Still, the present results establish that THG73 is susceptible to aminoacylation by aaRSs, which is undesired. No aminoacylation was seen with 2 ng of THG73-L, suggesting that aminoacylation by endogenous aaRSs is more likely when non-aminoacylated THG73 is injected, as noted previously (18). Both FS tRNAs show much lower amounts of aminoacylation by aaRSs, as evidenced by the decrease in I_{\max} (Table 3.5). YFFS_{CCCG}-dCA shows only 8.8% and 15% of the I_{\max} of THG73-dCA at 2 and 6 ng, respectively. The most orthogonal suppressor is YFaFS_{ACCC}-dCA with 1.9% and 3.3% of the I_{\max} of

THG73-dCA at 2 and 6 ng, respectively. The orthogonality trend thus follows the order: YFaFS_{ACCC}-dCA>YFFS_{CCCG}-dCA>THG73-dCA. YFaFS_{ACCC} is the most orthogonal and efficient FS tRNA, and it therefore offers a viable replacement for THG73, especially when aminoacylation by aaRSs poses a problem *in vivo*.

Read-through at the $\beta 9'$ site was also assessed by injection of mRNA only (Table 3.5). $\beta 9'$ UAG showed the most read-through, presumably because there is only one in-frame stop codon before desired termination. $\beta 9'$ CGGG and $\beta 9'$ GGGU show 23% and 21% read-through relative to the UAG stop codon. This is consistent with the idea that an endogenous triplet tRNA recognizing the first three bases of a quadruplet codon causes a -1 frameshift, which then presents multiple stop codons (frameshift suppression and competition shown in Figure 2.2). Again, we designed this experiment to enhance signals from read-through by injecting large amounts of mRNA (50 ng). No current was detectable after injection of mRNA containing UAG, CGGG, or GGGU at position $\alpha 149$, confirming that this site is much less promiscuous than $\beta 9'$.

3.2.6 The Effect of Discriminator and Acceptor Stem Mutations on YFFS_{CCCG}

Table 3.5 shows that YFFS_{CCCG} is less orthogonal than YFaFS_{ACCC}, which contains mutations at the discriminator base (N73) and in the acceptor stem. In previous work the YFaFS_{ACCC} mutations were made to avoid glycyl-tRNA synthetase recognition for *in vitro* reactions, and they significantly reduced aminoacylation (7). In *S. cerevisiae* and *H. sapiens* the glycyl-tRNA synthetase recognizes the discriminator base (A73) and acceptor stem recognition includes C2-G71 (23,24). Both are present in YFFS_{CCCG}. Therefore, we mutated A73 to create YFG73FS_{CCCG}, and we mutated the acceptor stem to create YFaFS_{CCCG}. Aminoacylation was determined by injecting 16.5 ng tRNA, not

ligated to dCA, and β 9'CGGG. The single A73G mutation resulted in increased aminoacylation *in vivo* as indicated by the increase in I_{\max} relative to YFFS_{CCCG}, but incorporating the acceptor stem mutations and A73G resulted in slightly less aminoacylation than YFFS_{CCCG} when comparing I_{\max} (Table 3.6). The orthogonality trend was as follows: YFaFS_{CCCG} \approx YFFS_{CCCG} > YFG73FS_{CCCG} > THG73. These results suggest that glycyl-tRNA synthetase or another aminoacyl-tRNA synthetase is aminoacylating YFFS_{CCCG}, and if the glycyl-tRNA synthetase is aminoacylating the YFFS_{CCCG}, the recognition of the discriminator base in *Xenopus* oocytes differs from the other eukaryotes studied. There was no significant difference between YFaFS_{CCCG} and YFFS_{CCCG} by a one-way ANOVA, and we continued to use YFFS_{CCCG}. However, leaving A73 and only incorporating the acceptor stem mutations may create more orthogonal variants of YFFS_{CCCG} and YFaFS_{ACCC} for the *Xenopus* oocyte system.

Table 3.6: The effect of discriminator base and acceptor stem mutations on YFFS_{CCCG}.

mRNA	tRNA	$I_{\max}^* \pm SE$	n	% THG73
β 9'UAG	-	0.026 \pm 0.002	5	2.9%
β 9'UAG	THG73	0.89 \pm 0.4	11	100%
β 9'CGGG	-	0.021 \pm 0.005	6	2.4%
β 9'CGGG	YFFS _{CCCG}	0.29 \pm 0.1	14	33%
β 9'CGGG	YFG73FS _{CCCG}	0.71 \pm 0.2	12	80%
β 9'CGGG	YFaFS _{CCCG}	0.23 \pm 0.07	10	26%

* Avg. I_{\max} (μ A) recorded at 400 μ M ACh.

3.2.7 Incorporation of Two UAAs

To investigate the simultaneous incorporation of two UAAs, we again built on previous work using THG73 to incorporate UAAs into the nAChR at positions α 149, β 9' and δ 9' (shown in Figure 3.3). Importantly, EC_{50} changes associated with mutations at

these sites are independent of one another (22,25). This allows one to qualitatively anticipate the consequences of multiple mutations. In particular, both $\beta 9'$ Aba and $\delta 9'$ Nval produce predictable reductions in EC_{50} that should be reproduced when combined with mutations at $\alpha 149$ (14). That is, the previously noted 4-fold increase in EC_{50} seen when the native tryptophan at $\alpha 149$ is replaced by WF1 should persist when in combination with $\beta 9'$ Aba or $\delta 9'$ Nval.

Successful incorporation of two UAAs to produce large ACh-induced currents could be seen when a 5-fold excess of mutant-to-wild-type mRNA was used. Suppression with $\alpha 149$ UAG/THG73-W and $\beta 9'$ CGGG/YFFS_{CCCG}-L is a wild-type recovery experiment that gave the expected EC_{50} for ACh of 50 μ M (Table 3.7). Maintaining $\beta 9'$ CGGG/YFFS_{CCCG}-L, but substituting $\alpha 149$ UAG/THG73-WF1 resulted in the anticipated 4-fold increase in EC_{50} (Table 3.7) (22). For incorporation of two UAAs, $\alpha 149$ UAG/THG73-W or WF1 was combined with either $\beta 9'$ CGGG/YFFS_{CCCG}-Aba or $\delta 9'$ GGGU/YFaFS_{ACCC}-Nval (Table 3.7 and Figure 3.5 show representative traces and fits to the Hill equation). The $\alpha 149$ WF1:W EC_{50} ratios are 4.4 for the both β and $\delta 9'$ mutants. These experiments establish that frameshift suppression can be combined with nonsense suppression to incorporate two UAAs in a eukaryotic system.

Table 3.7: Incorporation of two UAAs.

Row	$\alpha 149$	tRNA	β or δ	tRNA	EC_{50} (theo) ^{(ref)*}	n_H	n
1	UAG	THG73-W	$\beta 9'$ CGGG	YFFS _{CCCG} -Aba	14 ± 4 (16) ⁽¹⁴⁾	1.7 ± 0.06	9
2	UAG	THG73-W	$\delta 9'$ GGGU	YFaFS _{ACCC} -Nval	41 ± 2 (36) ⁽¹⁴⁾	1.9 ± 1	9
3	UAG	THG73-W	$\beta 9'$ CGGG	YFFS _{CCCG} -L	50 ± 3 (50) ⁽²²⁾	1.4 ± 0.08	20
4	UAG	THG73-WF1	$\beta 9'$ CGGG	YFFS _{CCCG} -Aba	61 ± 3	1.5 ± 0.08	7
5	UAG	THG73-WF1	$\delta 9'$ GGGU	YFaFS _{ACCC} -Nval	180 ± 7	1.8 ± 1	6
6	UAG	THG73-WF1	$\beta 9'$ CGGG	YFFS _{CCCG} -L	200 ± 7 (200) ⁽²²⁾	1.3 ± 0.04	9

* EC_{50} values from THG73-UAA incorporation by nonsense suppression.

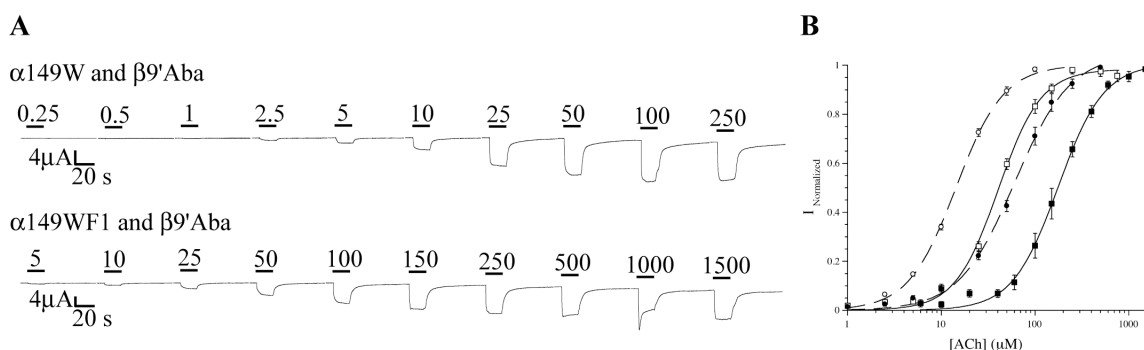


Figure 3.5: Simultaneous incorporation of two UAAs, representative traces and fits to the Hill equation. (A) Representative voltage-clamp current traces from oocytes expressing ion channels with two UAAs simultaneously incorporated. On the top $\alpha 149$ UAG/THG73-W and $\beta 9'$ CGGG/YFFS_{CCCG}-Aba is shown, which has an EC_{50} of 14 μ M ACh. The bottom shows $\alpha 149$ UAG/THG73-WF1 and $\beta 9'$ CGGG/YFFS_{CCCG}-Aba suppression and represents the incorporation of two UAAs. The EC_{50} is 61 μ M ACh and the ratio of the EC_{50} s (WF1:W) is 4.4. (B) Fits to the Hill equation from (left to right) show Row 1 (\circ), 2 (\square), 4 (\bullet), and 5 (\blacksquare) (Table 3.7). Row 3 and 6 are left out for clarity and have previously been reported (Table 3.3 & (22)).

3.2.8 Incorporation of Three UAAs

To demonstrate the incorporation of three UAAs, we combined the two-UAA incorporation experiments described above, taking advantage of the knowledge that EC_{50} is lowered monotonically by appropriate 9' mutations at multiple subunits (26). Thus one

expects a lower EC_{50} when $\beta 9'$ Aba and $\delta 9'$ Nval are incorporated simultaneously. Suppression of $\alpha 149$ UAG: $\beta 9'$ CGGG: γ : $\delta 9'$ GGGU using an mRNA ratio of 5:5:1:5 with THG73-W, YFFS_{CCCG}-Aba, and YFaFS_{ACCC}-Nval resulted in functional channel expression with an EC_{50} of 4.5 μ M ACh (Figure 3.6), which is lower than either of the two UAAs (Aba or Nval) incorporated separately. However, the same conditions with THG73-WF1 yielded only small currents. In order to obtain more expression, $\alpha 149$ UAG mRNA and THG73-WF1 were initially injected, and 24 hr later $\beta 9'$ CGGG: γ : $\delta 9'$ GGGU (5:1:5) was injected with YFFS_{CCCG}-Aba and YFaFS_{ACCC}-Nval (final mRNA ratio 5:5:1:5). This resulted in adequate expression and an EC_{50} of 19 μ M ACh (Figure 3.6). The ratio of the EC_{50} s ($\alpha 149$ WF1:W) is 4.2, confirming that three different UAAs were simultaneously incorporated *in vivo*, but this is actually four UAAs per ion channel because WF1 is incorporated in two α -subunits (Figure 3.3).

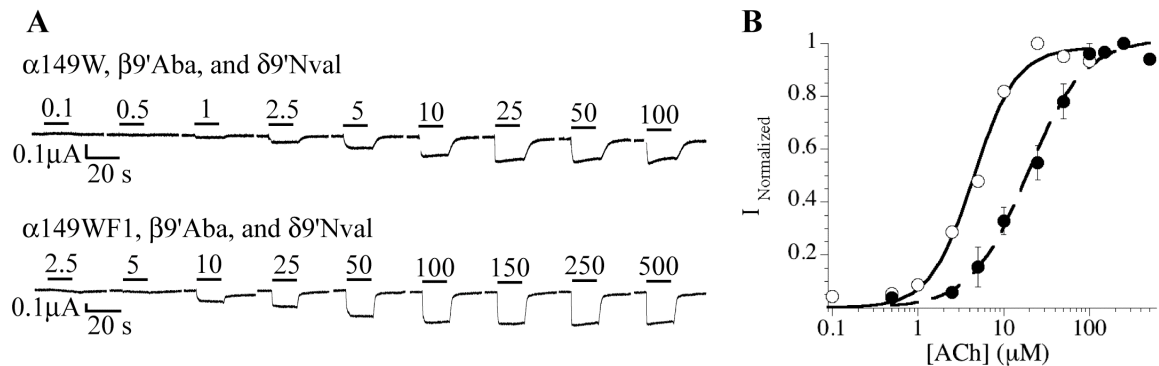


Figure 3.6: Simultaneous incorporation of three UAAs. (A) Representative current traces from oocytes incorporating three UAAs. (B) Dose-response curves showing: $\alpha 149$ W, $\beta 9'$ Aba, and $\delta 9'$ Nval (open circles) and $\alpha 149$ WF1, $\beta 9'$ Aba, and $\delta 9'$ Nval (closed circles). $EC_{50} = 4.5 \pm 4$, $n_H = 1.7 \pm 3$ and $EC_{50} = 19 \pm 2$, $n_H = 1.3 \pm 1$, respectively. The ratio of the EC_{50} s is 4.2.

3.3 Discussion

The present results establish that frameshift suppression is viable in a eukaryotic, vertebrate cell, and that it can be used to incorporate multiple unnatural amino acids (UAAs) in a single experiment. Previous work in *Xenopus* oocytes found that UAA incorporation using THG73FS_{ACCC} was inefficient, and it was proposed that either the *Xenopus* translational machinery was not compatible with frameshift suppression or that THG73FS_{ACCC} was a poor template for quadruplet recognition (9). Our results support the second rationalization, and a second FS derived from THG73, THG73FS_{CCCG}, is also not viable. Mutation of positions 32 and 38 on THG73FS_{CCCG} did not rescue the suppression efficiency (Table 3.2). It thus appears that THG73-derived FS tRNAs are either misfolded, not recognized by EF-Tu, or not accepted by other components of the translational machinery.

Frameshift suppression is viable in the *Xenopus* oocyte, however, using either HSFS or YFFS tRNAs. We find that in *Xenopus* oocytes, the quadruplet GGGU is suppressed more efficiently by both HSFS_{ACCC} and YFaFS_{ACCC} than the corresponding CGGG/tRNA pairs. This is seen despite the fact that in *Xenopus* the GGG triplet is used twice as frequently (12.9 per thousand) as the CGG triplet (27). Frameshift suppression must compete with endogenous triplet-recognizing tRNAs. Codon usage is apparently not a perfect predictor of frameshift suppression efficiency.

We have evaluated three different tRNAs: the amber suppressor THG73, and the frameshift suppressors YFFS_{CCCG} and YFaFS_{ACCC}. For UAA incorporation in the *Xenopus* oocyte, both YFFS tRNAs are less efficient than the AS THG73. This finding parallels results from earlier *in vitro* studies (17). Apparently, the competition between

release factors and the AS tRNA is less detrimental than the competition between FS tRNAs and endogenous, triplet-recognizing tRNA. This view is supported by the rapid, nonlinear rise in suppression efficiency when the amount of YFFS tRNA is increased (Table 3.5). CGGG-recognizing tRNAs are more sensitive to the amount injected than GGGU-recognizing tRNAs. Increasing the amount of FS tRNA for UAA incorporation is essential to maximize suppression efficiency.

The incorporation of UAAs site-specifically into proteins requires the suppressor tRNA to be orthogonal to the endogenous, aaRSs. Read-through of the suppression site or aminoacylation of the suppressor tRNA (once the chemically ligated UAA has been removed) can result in the undesired incorporation of natural amino acids at the suppression site. The two YFFS tRNAs studied here exhibit much more orthogonality than THG73 under the extreme conditions (extended incubation time and increased mRNA) used in Table 3.5. However, THG73 is an orthogonal suppressor tRNA to the *Xenopus* oocyte when used properly; THG73 has been used to successfully incorporate over 100 residues at scores of sites in 20 different proteins (1,2). Even promiscuous sites, such as the $\beta 9'$ UAG, can be efficiently suppressed by THG73-UAA when using less tRNA, mRNA, and incubation time (14). $\beta 9'$ UAG injected with THG73-dCA shows no greater current than mRNA alone with similar conditions. The small current is less than 1% of typical UAA incorporation experiments and is caused by read-through of the UAG codon (18). Voss and coworkers found that THG73 incorporated 3 UAAs and Phe with efficiencies of 93.5–99.5% (determined by THG73-UAA incorporation relative to natural amino acids placed by read-through or aminoacylation of THG73-dCA) using luciferase expressed in *Xenopus* oocytes (9). The current results show that the YFFS tRNAs are

even more orthogonal and so the efficiency of UAA incorporation (relative to natural amino acids) should be greater than THG73.

An important contributor to our ability to efficiently incorporate two and three UAAs is the masking of undesired quadruplets to prevent loss of UAA. In general, the requirement for masking of mRNA to remove undesirable quadruplet codons does complicate the frameshift suppression approach. The only previous examples of UAA incorporation in higher eukaryotes were performed by nonsense suppression (1–5,10). Frameshift suppression may be limited *in vivo* to cells that are dormant (such as *Xenopus* oocytes), that express large quantities of the target mRNA, or that come from genetically engineered organisms. Also, suppressor tRNAs may be limited to rare codons, because of possible toxicity arising from undesired suppression in other proteins (28).

The combination of nonsense and frameshift suppression allows one to incorporate multiple UAAs site-specifically into proteins expressed in *Xenopus* oocytes. These methods are compatible with our entire library of UAAs (2,29) and will allow for multiple UAAs to be incorporated into other ion channels for novel structure-function studies, cross-linking, and FRET experiments. In principle, further quadruplet codons could be utilized to simultaneously incorporate more than three UAAs.

3.4 Experimental Methods

3.4.1 Materials

All oligonucleotides were synthesized by Caltech Biopolymer Synthesis facility or Integrated DNA Technologies (IDT, Coralville, IA) (Listed in Table 3.8). NotI was purchased from Roche (Indianapolis, IN). BamHI, EcoRI, FokI, T4 DNA ligase, and T4

RNA ligase were purchased from NEB (Beverly, MA). Kinase Max, T7 MEGashortscript, and T7 mMessage mMachine kits were from Ambion (Austin, TX). dCA and NVOC-protected dCA-UAA were prepared as previously reported (14,22,30). ACh chloride was purchased from Sigma/Aldrich (St. Louis, MO).

Table 3.8: Oligos used in this research.

Masking	
α 182CGC-F	GGAAGCTCGCGGCTGGAAGCACTGGG
α 182CGC-R	CCCAGTGCTTCCAGCCGCGAGCTTCC
β 23AGG-F	CGGTGAGGCCGCGCAGGGAGGTGGGAGACCGCG
β 23AGG-R	CGCGGTCTCCACCTCCCTCGCCGGCCTCACCG
β 402AGG-F	CGATGGTCCAACCAGGGCTGTAGGTCTGCCTCAGG
β 402AGG-R	CCTGAGGCAGACCTACAGCCCTGGTTGGACCATCG
δ 195AGG-F	GGGAGATAGTGCATAGGGCAGCTAAGCTCAATGTGG
δ 195AGG-R	CCACATTGAGCTTAGCTGCCCTATGCACTATCTCCC
β 1AGC-F	CGCCCCAGGCGCCCGCGGGAGCGAAGCCGAAGGCC
β 1AGC-R	GGCCTTCGGCTTCGCICCCGCGGGCGCTGGGGCG
Suppression	
α 149TAG-F	GCAGCATGAAGCTGGGCACCTAGACCTATGACGGCTCTGTGG
α 149TAG-R	CCACAGAGCCGTCATAGGTCTAGGTGCCAGCTTCATGCTGC
α 149CGGG-F	GCAGCATGAAGCTGGGCACCCGGGACCTATGACGGCTCTGTGGTGGCC
α 149CGGG-R	GGCCACCACAGAGCCGTCATAGGTCCCGGGTGCCAGCTTCATGCTGC
α 149GGGT-F	GCAGCATGAAGCTGGGCACCCGGGTACCTATGACGGCTCTGTGGTGGCC
α 149GGGT-R	GGCCACCACAGAGCCGTCATAGGTACCCGGTGCCAGCTTCATGCTGC
β 9'TAG-F	GGGGCTCTCCATCTTTGCCCTGTAGACGCTCACTGTGTTCTTGCTGC
β 9'TAG-R	GCAGCAAGAACACAGTGAGCGTCTACAGGGCAAAGATGGAGAGCCCC
β 9'CGGG-F	GGGGCTCTCCATCTTTGCCCTGCGGGACGCTCACTGTGTTCTTGCTGCT GTTGGCCG
β 9'CGGG-R	CGGCCAACAGCAGCAAGAACACAGTGAGCGTCCCGCAGGGCAAAGAT GGAGAGCCCC
β 9'GGGT-F	GGGGCTCTCCATCTTTGCCCTGGGGTACGCTCACTGTGTTCTTGCTGCT GTTGGCCG
β 9'GGGT-R	CGGCCAACAGCAGCAAGAACACAGTGAGCGTACCCAGGGCAAAGAT GGAGAGCCCC
δ 9'GGGT-F	CCGTGGCCATCTCAGTGCTCGGGTGCCCAATCTGTCTTCTTGCTGCTTA TCTCCAAGAGGC
δ 9'GGGT-R	GCCTCTTGAGATAAGCAGCAGGAAGACAGATTGGGCACCCGAGCACT GAGATGGCCACGG
tRNA Genes	
HSFS _{CCCG} -F	AATTCGTAATACGACTCACTATAGTAGTCGTGGCCGAGTGGTTAAGGCCGA TGGACTCCCGAATCCATTGGGGTCTCCCCGCGCAGGTTCAATCCTGCC GACTACGCCATGAGACCCATCCG
HSFS _{CCCG} -R	GATCCGGATGGGTCTCATGGCGTAGTCGGCAGGATTCGAACCTGCGCGG GGAGACCCAATGGATTGCGGGAGTCCATCGCCTTAACCACTCGGCCACG

	<i>ACTACTATAGTGATGTATTACG</i>
THG73FS _{CCCG} -F	<i>AATTCGTAATACGACTCACTATAGGTTCTATAGTATAGCGGTTAGTACTGG GGACT<u>CCCG</u>AATCCCTTGACCTGGGTTCTGAATCCCAGTAGGACCGCCAT GAGACCCATCCG</i>
THG73FS _{CCCG} -R	<i>GATCCGGATGGGTCTCATGGCGGTCCTACTGGGATTCTGAACCCAGGTCA AGGGATT<u>CGGG</u>AGTCCCCAGTACTAACCGCTATACTATAGAACCTATAG TGAGTCGTATTACG</i>
YFFS _{CCCG} -F	<i>AATTCGTAATACGACTCACTATAGCGGATTTAGCTCAGTTGGGAGAGCGC CAGACT<u>CCCG</u>AATCTGGAGGTCCTGTGTTCGATCCACAGAATTCGCACC ATGAGACCCATCCG</i>
YFFS _{CCCG} -R	<i>GATCCGGATGGGTCTCATGGTGCGAATTCTGTGGATCGAACACAGGACC TCCAGATT<u>CGGG</u>AGTCTGGCGCCTCTCCCAACTGAGCTAAATCCGCTAT AGTGAGTCGTATTACG</i>
tRNA Primers	
YFG73FS _{CCCG} -F	<i>CGATCCACAGAATT<u>CGCG</u>CCATGAGACCCATCCG</i>
YFG73FS _{CCCG} -R	<i>CGGATGGGTCTCATGG<u>CG</u>CGAATTCTGTGGATCG</i>
YFa ₁ FS _{CCCG} -F	<i>CGTAATACGACTCACTATAGG<u>CC</u>ATTTAGCTCAGTTGGGAGAGCGCC</i>
YFa ₁ FS _{CCCG} -R	<i>GGCGCTCTCCCAACTGAGCTAAATGG<u>CC</u>TATAGTGAGTCGTATTACG</i>
YFaFS _{CCCG} -F	<i>CCTGTGTTCGATCCACAGAATGG<u>CC</u>CGCCATGAGACCCATCCGGATCC</i>
YFaFS _{CCCG} -R	<i>GGATCCGGATGGGTCTCATGGCG<u>GC</u>ATTCTGTGGATCGAACACAGG</i>
HSFS _{ACCC} -F	<i>GGCCGAGTGGTTAAGGCGATGGACT<u>ACCC</u>AATCCATTGGGGTCTCCCC GCGC</i>
HSFS _{ACCC} -R	<i>GCGCGGGGAGACCCCAATGGATTGGG<u>T</u>AGTCCATCGCCTTAACCACTC GGCC</i>
YFaFS _{ACCC} -F	<i>GCTCAGTTGGGAGAGCGCCAGACT<u>ACCC</u>AATCTGGAGGTCCTGTGTTC GATCC</i>
YFaFS _{ACCC} -R	<i>GGATCGAACACAGGACCTCCAGATTGGG<u>T</u>AGTCTGGCGCTCTCCCAAC TGAGC</i>

All mutated sites are underlined in the oligonucleotide sequence, except for tRNA genes where the underline is the anticodon and the flanking regions are italicized. F—Forward & R—Reverse (written 5' to 3').

3.4.2 Gene Construction and RNA Preparation

The α , β , γ , and δ subunits of the nicotinic acetylcholine receptor (nAChR) were previously subcloned in the pAMV vector (31). All four in-frame CGGG were mutated (underlined) to degenerate codons (α 182CGC, β 23AGG, β 402AGG, and δ 195AGG) and one GGGT was mutated at the fourth position (β 1AGC), these are known as “masked” constructs. α 149TAG, CGGG, GGGT; β 9'TAG, CGGG, GGGT; and δ 9'GGGT mutations were placed on masked constructs by QuikChange Site-Directed Mutagenesis (Stratagene, La Jolla, CA). Mutations were verified by DNA sequencing (Caltech

Sequencing/Structure Analysis Facility (SAF)). Template DNA was linearized with NotI and mRNA prepared by T7 mMessage mMachine kit. mRNA was purified using RNeasy Mini kit (Qiagen, Valencia, CA) and quantified by absorption at 260 nm.

THG73 and HSAS in pUC19 vector were previously made (10,18). Genes for HSFS_{CCCG}, THG73FS_{CCCG}, and YFFS_{CCCG} (sequence from (6)) with flanking EcoRI and BamHI overhangs were phosphorylated using Kinase Max kit, annealed, ligated with T4 DNA ligase into EcoRI and BamHI linearized pUC19 vectors, as previously described (30). A73G; C2G,G3C,G4C; and C69G,C70G,G71C mutations (from (7)) were sequentially placed by QuikChange mutagenesis on the YFFS_{CCCG} construct to obtain YFaFS_{CCCG} (“a” refers to acceptor stem mutations). HSFS_{ACCC} and YFaFS_{ACCC} (sequence from (7)) were prepared by replacing the anticodon of HSFS_{CCCG} and YFaFS_{CCCG} with ACCC using QuikChange. All mutations were verified by DNA sequencing (Caltech SAF). Template DNA for tRNA lacking the 3'CA was prepared by FokI digestion and tRNA was transcribed using T7 MEGashortscript kit. tRNA was desalted using CHROMA SPIN™-30 DEPC-H₂O columns (BD Biosciences, San Jose, CA) and concentration was determined by absorption at 260 nm.

3.4.3 dCA and dCA-UAA Ligation to Suppressor tRNA

dCA and NVOC-protected dCA-UAA were coupled to suppressor tRNA using T4 RNA ligase for 30 min, as previously described (30,32), desalted using CHROMA SPIN™-30 DEPC-H₂O columns, and quantified by absorption at 260 nm. tRNA ligation efficiency was determined by MALDI mass spectrometry (32) and all tRNA dCA or dCA-UAA ligations were greater than 75%.

3.4.4 *In Vivo* Suppression Experiments

Stage VI oocytes of *Xenopus laevis* were prepared as previously described (33). All tRNA were refolded at 65 °C for 2 min and tRNA-UAA were deprotected for 5 min by UV irradiation prior to injection (18). Injection volume for all experiments was 50 nl and incubation time was 44–52 hr, unless otherwise noted. Suppression of HSAS and either HSFS 1.25 or 2.5 ng tRNA, with 20 ng mRNA in a subunit ratio 2:5:1:1 α : β 9'(UAG, CGGG, or GGGU): γ : δ was recorded after 1 or 2 days. THG73-derived FS comparison was performed with 30 ng of mRNA in the subunit ratio 10:1:1:1 α 149(UAG or CGGG): β : γ : δ and 16.5 ng of THG73-W, THG73FS_{CCCG}-W, THA32G73FS_{CCCG}-W, THG38G73FS_{CCCG}-W, or THA32U38G73FS_{CCCG}-W. Single UAA incorporation was performed using 20–30 ng of mRNA in a subunit ratio of 10:1:1:1 α 149(CG GG or GGGU): β : γ : δ ; 2:5:1:1 α : β 9'GGGU: γ : δ ; or 2:1:1:5 α : β : γ : δ 9'GGGU with 4.8–16.5 ng of YFFS_{CCCG}/YFaFS_{ACCC}-UAA. Comparison of β masked and wild-type suppression contained 25 ng total mRNA injected in the subunit ratio listed in Table 3.4 with 1:1 γ : δ and 10 ng YFaFS_{ACCC}-W. For comparison of suppression efficiency and aminoacylation of tRNA *in vivo*, all mRNA was normalized to the same concentration and 16.5 ng of mRNA was injected in the subunit ratio 10:1:1:1 α 149(UAG, CGGG, or GGGU): β : γ : δ or 2:5:1:1 α : β 9'(UAG, CGGG, or GGGU): γ : δ with tRNA amounts listed in Table 3.5. For read-through experiments, 50 ng of mRNA in the ratio 2:5:1:1 α : β 9'(UAG, CGGG, or GGGU): γ : δ was injected. Comparison of acceptor stem mutations on YFFS_{CCCG} was performed with 20 ng of mRNA in the subunit ratio of α : β 9'(UAG or CGGG): γ : δ with 9.4 ng of THG73, YFFS_{CCCG}, YFG73FS_{CCCG}, and YFaFS_{CCCG} (not ligated to dCA). Two UAAs experiments were performed by injection of 20–30 ng mRNA in a subunit ratio

5:5:1:1 α 149UAG: β 9'CGGG: γ : δ or 5:1:1:5 α 149UAG: β : γ : δ 9'GGGU with 10–25 ng of each suppressor tRNA-UAA. For three UAAs— α 149W, β 9'Aba, δ 9'Nval—26 ng mRNA in a ratio of 5:5:1:5 α 149UAG: β 9'CGGG: γ : δ 9'GGGU was injected with 20 ng each suppressor tRNA-UAA, and a second injection of 33 ng each tRNA-UAA was done 24 h later. For α 149WF1, β 9'Aba, and δ 9'Nval, 8 ng α 149UAG mRNA with 50 ng of THG73-WF1 was injected, and a second injection of 18 ng mRNA with subunit ratio of 5:1:5 β 9'CGGG: γ : δ 9'GGGU with 25 ng of each YFFS_{CCCG}-Aba and YFaFS_{ACCC}-Nval was performed 24 h later. Oocytes were recorded three days after first injection.

3.4.5 Electrophysiology

Recordings used two-electrode voltage clamp on the OpusXpress 6000A (Axon Instruments, Union City, CA). ACh was stored at -20 °C as a 1 M stock, diluted in Ca²⁺-free ND96, and delivered to oocytes by computer-controlled perfusion system. For HSAS & HSFS experiments the holding potential was -60 mV, and all UAA experiments were done at either -60 mV or -80 mV. Dose-response data were obtained from at least 9 ACh concentrations and comparisons were tested at one drug concentration, except β 9'(UAG, CGGG, or GGGU) with tRNA-L used two concentrations, 10 μ M and 1 mM, to check for aminoacylation (Table 3.6). Dose-response relations were fit to the Hill equation to determine EC₅₀ and the Hill coefficient (η_H). All reported values are represented as a mean \pm SE of the tested oocytes (number (n) listed with each table).

3.5 References

1. Dougherty, D.A. (2000) Unnatural amino acids as probes of protein structure and function. *Curr. Opin. Biotechnol.*, **4**, 645–652.

2. Beene, D.L., Dougherty, D.A., and Lester, H.A. (2003) Unnatural amino acid mutagenesis in mapping ion channel function. *Curr. Opin. Neurobiol.*, **13**, 264–270.
3. Sakamoto, K., Hayashi, A., Sakamoto, A., Kiga, D., Nakayama, H., Soma, A., Kobayashi, T., Kitabatake, M., Takio, K., Saito, K. *et al.* (2002) Site-specific incorporation of an unnatural amino acid into proteins in mammalian cells. *Nucleic Acids Res.*, **30**, 4692–4699.
4. Hino, N., Okazaki, Y., Kobayashi, T., Hayashi, A., Sakamoto, K., and Yokoyama, S. (2005) Protein photo-cross-linking in mammalian cells by site-specific incorporation of a photoreactive amino acid. *Nat. Methods*, **2**, 201–206.
5. Zhang, Z., Alfonta, L., Tian, F., Bursulaya, B., Uryu, S., King, D.S., and Schultz, P.G. (2004) Selective incorporation of 5-hydroxytryptophan into proteins in mammalian cells. *Proc. Natl. Acad. Sci. USA*, **101**, 8882–8887.
6. Hohsaka, T., Ashizuka, Y., Murakami, H., and Sisido, M. (1996) Incorporation of nonnatural amino acids into streptavidin through *in vitro* frame-shift suppression. *J. Am. Chem. Soc.*, **118**, 9778–9779.
7. Hohsaka, T., Ashizuka, Y., Taira, H., Murakami, H., and Sisido, M. (2001) Incorporation of nonnatural amino acids into proteins by using various four-base codons in an *Escherichia coli in vitro* translation system. *Biochemistry*, **40**, 11060–11064.
8. Anderson, J.C., Wu, N., Santoro, S.W., Lakshman, V., King, D.S., and Schultz, P.G. (2004) An expanded genetic code with a functional quadruplet codon. *Proc. Natl. Acad. Sci. USA*, **101**, 7566–7571.

9. Shafer, A.M., Kalai, T., Bin Liu, S.Q., Hideg, K., and Voss, J.C. (2004) Site-specific insertion of spin-labeled L-amino acids in *Xenopus* oocytes. *Biochemistry*, **43**, 8470–8482.
10. Monahan, S.L., Lester, H.A., and Dougherty, D.A. (2003) Site-specific incorporation of unnatural amino acids into receptors expressed in mammalian cells. *Chem. Biol.*, **10**, 573–580.
11. Anderson, J.C., Magliery, T.J., and Schultz, P.G. (2002) Exploring the limits of codon and anticodon size. *Chem. Biol.*, **9**, 237–244.
12. Saks, M.E., Sampson, J.R., and Abelson, J.N. (1994) The transfer RNA identity problem: A search for rules. *Science*, **263**, 191–197.
13. Murakami, H., Kourouklis, D., and Suga, H. (2003) Using a solid-phase ribozyme aminoacylation system to reprogram the genetic code. *Chem. Biol.*, **10**, 1077–1084.
14. Kearney, P.C., Zhang, H., Zhong, W., Dougherty, D.A., and Lester, H.A. (1996) Determinants of nicotinic receptor gating in natural and unnatural side chain structures at the M2 9' position. *Neuron*, **17**, 1221–1229.
15. Miyazawa, A., Fujiyoshi, Y., and Unwin, N. (2003) Structure and gating mechanism of the acetylcholine receptor pore. *Nature*, **423**, 949–955.
16. Grosjean, H., Droogmans, L., Giege, R., and Uhlenbeck, O.C. (1990) Guanosine modifications in runoff transcripts of synthetic transfer RNA-Phe genes microinjected into *Xenopus* oocytes. *Biochim. Biophys. Acta.*, **1050**, 267–273.

17. Taira, H., Fukushima, M., Hohsaka, T., and Sisido, M. (2005) Four-base codon-mediated incorporation of non-natural amino acids into proteins in a eukaryotic cell-free translation system. *J. Biosci. Bioeng.*, **99**, 473–476.
18. Saks, M.E., Sampson, J.R., Nowak, M.W., Kearney, P.C., Du, F.Y., Abelson, J.N., Lester, H.A., and Dougherty, D.A. (1996) An engineered *Tetrahymena* tRNA^{Gln} for *in vivo* incorporation of unnatural amino acids into proteins by nonsense suppression. *J. Biol. Chem.*, **271**, 23169–23175.
19. Olejniczak, M., Dale, T., Fahlman, R.P., and Uhlenbeck, O.C. (2005) Idiosyncratic tuning of tRNAs to achieve uniform ribosome binding. *Nat. Struct. Mol. Biol.*, **12**, 788–793.
20. Claesson, C., Lustig, F., Boren, T., Simonsson, C., Barciszewska, M., and Lagerkvist, U. (1995) Glycine codon discrimination and the nucleotide in position 32 of the anticodon loop. *J. Mol. Biol.*, **247**, 191–196.
21. O'Connor, M. (1998) tRNA imbalance promotes -1 frameshifting via near-cognate decoding. *J. Mol. Biol.*, **279**, 727–736.
22. Zhong, W., Gallivan, J.P., Zhang, Y., Li, L., Lester, H.A., and Dougherty, D.A. (1998) From ab initio quantum mechanics to molecular neurobiology: A cation- π binding site in the nicotinic receptor. *Proc. Natl. Acad. Sci. USA*, **95**, 12088–12093.
23. Hipps, D., Shiba, K., Henderson, B., and Schimmel, P. (1995) Operational RNA code for amino acids: species-specific aminoacylation of minihelices switched by a single nucleotide. *Proc. Natl. Acad. Sci. USA*, **92**, 5550–5552.

24. Nameki, N., Tamura, K., Asahara, H., and Hasegawa, T. (1997) Recognition of tRNA^{Gly} by three widely diverged glycyl-tRNA synthetases. *J. Mol. Biol.*, **268**, 640–647.
25. Kearney, P.C., Nowak, M.W., Zhong, W., Silverman, S.K., Lester, H.A., and Dougherty, D.A. (1996) Dose-response relations for unnatural amino acids at the agonist binding site of the nicotinic acetylcholine receptor: Tests with novel side chains and with several agonists. *Mol. Pharmacol.*, **50**, 1401–1412.
26. Labarca, C., Nowak, M.W., Zhang, H., Tang, L., Deshpande, P., and Lester, H.A. (1995) Channel gating governed symmetrically by conserved leucine residues in the M2 domain of nicotinic receptors. *Nature*, **376**, 514–516.
27. Nakamura, Y., Gojobori, T., and Ikemura, T. (2000) Codon usage tabulated from international DNA sequence databases: Status for the year 2000. *Nucleic Acids Res.*, **28**, 292.
28. Magliery, T.J., Anderson, J.C., and Schultz, P.G. (2001) Expanding the genetic code: Selection of efficient suppressors of four-base codons and identification of "shifty" four-base codons with a library approach in *Escherichia coli*. *J. Mol. Biol.*, **307**, 755–769.
29. England, P.M. (2004) Unnatural amino acid mutagenesis: a precise tool for probing protein structure and function. *Biochemistry*, **43**, 11623–11629.
30. Nowak, M.W., Gallivan, J.P., Silverman, S.K., Labarca, C.G., Dougherty, D.A., and Lester, H.A. (1998) *In vivo* incorporation of unnatural amino acids into ion channels in *Xenopus* oocyte expression system. *Meth. Enzymol.*, **293**, 504–529.

31. Nowak, M.W., Kearney, P.C., Sampson, J.R., Saks, M.E., Labarca, C.G., Silverman, S.K., Zhong, W., Thorson, J., Abelson, J.N., Davidson, N. *et al.* (1995) Nicotinic receptor binding site probed with unnatural amino acid incorporation in intact cells. *Science*, **268**, 439–442.
32. Petersson, E.J., Shahgholi, M., Lester, H.A., and Dougherty, D.A. (2002) MALDI-TOF mass spectrometry methods for evaluation of *in vitro* aminoacyl tRNA production. *RNA*, **8**, 542–547.
33. Quick, M.W., and Lester, H.A. (1994) Methods for expression of excitability proteins in *Xenopus* oocytes. In Narahashi, T. (ed.), *Ion Channels of Excitable Cells*. Academic Press, San Diego, CA, Vol. 19, pp. 261–279.

Chapter 4

Improved Amber and Opal Suppressor tRNAs
for Incorporation of Unnatural Amino Acids

In Vivo, Part 1.

Minimizing Misacylation of Suppressor tRNAs.

This chapter is reproduced, with modification, from *Improved amber and opal suppressor tRNAs for incorporation of unnatural amino acids in vivo. Part 1: Minimizing misacylation*, by E. A. Rodriguez, H. A. Lester, and D. A. Dougherty, (2007) *RNA*, **13(10)**, 1703–1714. Copyright 2007 by the RNA Society.

4.1 Introduction

Incorporation of unnatural amino acids (UAAs) site-specifically in proteins biosynthetically is a powerful tool that is increasingly being used. The primary approach has been stop codon (nonsense) suppression using a designed tRNA with an anticodon recognizing the stop codon. In higher eukaryotes, nonsense suppression by a tRNA chemically aminoacylated with an UAA (tRNA-UAA) is primarily limited to *Xenopus* oocytes, where microinjection of the mutant mRNA and tRNA-UAA is straightforward, and electrophysiology allows for sensitive detection of UAA incorporation (shown in Figure 3.1) (1,2). Recently, site-specific UAA incorporation was performed in *Xenopus* oocytes using frameshift suppression of the quadruplet codons CGGG and GGGU, which allowed for the simultaneous incorporation of three UAAs (3).

THG73, an amber suppressor tRNA from *T. thermophila* with a G73 mutation, has been used extensively to incorporate over 100 residues in 20 different proteins (1,2). With THG73 and any other suppressor tRNAs, a key issue is orthogonality. An orthogonal tRNA is one that is not measurably aminoacylated with natural amino acids (aas) by endogenous aminoacyl-tRNA synthetases (aaRSs). Unlike its mathematical counterpart, there can be degrees of orthogonality when referring to tRNAs. While the orthogonality of THG73 has been evaluated using *in vitro* translation in *E. coli* (4), wheat germ (5), and rabbit reticulocyte lysate (6), the primary application of THG73 has been for *in vivo* translation in *Xenopus* oocytes, which is the focus of the present work. The orthogonality of THG73 is acceptable when injecting low quantities of mutant

mRNA and/or tRNA-UAA with incubation times less than 2 d (7,8). However, increasing the amount of mutant mRNA and/or tRNA-UAA, or incubation times of 2 d — which we will term “excessive” conditions — led to increased aminoacylation of THG73 *in vivo* with natural aa(s) (3). This is highly undesirable, because incorporation of natural aas at the suppression site leads to a heterogeneous mixture of proteins containing an UAA or natural aa(s) and limits the quantity of protein that can be produced by UAA incorporation.

Previous work from our labs showed that yeast Phe frameshift suppressor tRNAs (YFFS_{CCCG} and YFaFS_{ACCC}) were aminoacylated much less than THG73 *in vivo*, but suppression of the quadruplet codons was less efficient than with THG73 and varied greatly with the amount of frameshift suppressor tRNA injected (3). Previously, an *E. coli* Asn amber suppressor (ENAS) tRNA was shown to be highly orthogonal *in vivo* (9) and *in vitro* (4,10,11). Here we show that ENAS has similar amounts of aminoacylation to THG73, suggesting that other well-characterized amber suppressor tRNAs could be prone to aminoacylation under excessive conditions.

Therefore, we chose to determine the aa that was being placed on THG73 using the sensitivity of electrophysiology and a well-characterized mutation site of the nicotinic acetylcholine receptor (nAChR), and determined the aa to be Gln. Using this knowledge, we created “Knob” mutations on THG73 previously shown to reduce aminoacylation of *E. coli* tRNA₂^{Gln} by the *E. coli* glutaminyl-tRNA synthetase (GlnRS) (12). The Knob mutations on THG73 resulted in tRNAs that showed drastically reduced

suppression efficiency *in vivo*, making them not viable replacements. The *E. coli* GlnRS has been shown to interact with the acceptor stem of the tRNA in the crystal structure (13), which was subsequently shown to be sensitive to base pairs and/or backbone positioning of the tRNA acceptor stem (14–16). We created seven unique tRNAs with mutations in the 2nd to 4th positions of the acceptor stem, and analyzed their function *in vivo* relative to THG73. Mutations in the acceptor stem decreased aminoacylation significantly. This library of *T. thermophila* Gln amber suppressor (TQAS) tRNAs can be used to screen for orthogonality in other eukaryotic cells. To show the generality of the acceptor stem mutations, we also created *T. thermophila* Gln opal suppressor (TQOpS' and TQOpS) tRNAs that are also aminoacylated less than THG73. The acceptor stem mutations have general application for the creation of orthogonal suppressor tRNAs for UAA incorporation in higher eukaryotic cells, where random mutagenesis combined with high-throughput screens is not readily applicable.

4.2 Results

4.2.1 Schematic for Site-Specific UAA Incorporation and Aminoacylation

Figure 4.1 shows a schematic for the steps leading to UAA incorporation *in vivo*. Upon injection of the tRNA-dCA-UAA, the tRNA can bind to EF-1 α and/or other components of the translational machinery in a reversible fashion (Figure 4.1, A). It has been shown that the prokaryotic ortholog EF-Tu can protect tRNA-dCA-UAA from hydrolysis *in vitro* (17) (Figure 4.1, C), thus favoring incorporation of UAA by

recognition of the suppressor site on the mRNA (Figure 4.1, B). If tRNA lacking the terminal CA (74mer) is injected, it can be converted to the full-length tRNA by the addition of CA *in vivo* (Figure 4.1, D). The full-length tRNA, either tRNA-dCA or tRNA-CA (76mer), may then be aminoacylated with a natural aa by an endogenous aaRS (Figure 4.1, E). The tRNA-dCA-aa can then bind EF-1 α and/or other components of the translational machinery (Figure 4.1, F) and lead to the incorporation of a natural aa at the suppression site (Figure 4.1, G) in competition with the suppression by tRNA-dCA-UAA (Figure 4.1, B), a highly undesirable outcome. After translation, both UAA and natural aa incorporation causes the tRNA-dCA/CA to be released from the ribosome (Figure 4.1, H), which can further contribute to the undesired natural aa incorporation (Figure 4.1, E–G).

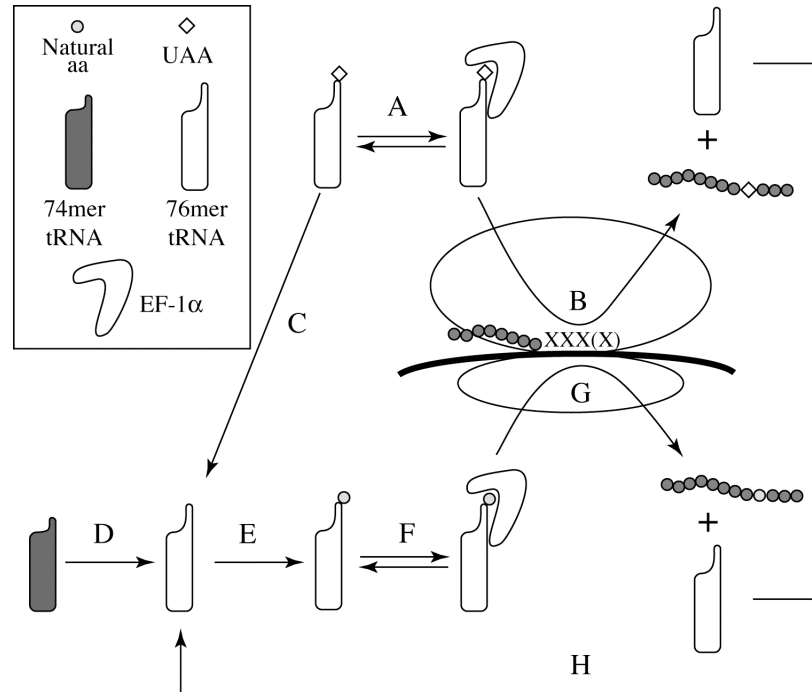


Figure 4.1: Site-specific UAA incorporation. (A) tRNA-dCA-UAA binds EF-1 α and/or other components of the translational machinery. (B) UAA is incorporated at the suppression site (XXX(X)), resulting in a protein with an UAA. (C) Undesired hydrolysis and/or aaRS editing results in irreversible loss of the UAA, resulting in tRNA-dCA (76mer). (D) Injection of the tRNA (lacking dCA, 74mer) is converted to a 76mer *in vivo* by the addition of CA (tRNA-CA). (E) Undesired recognition of the suppressor tRNA-dCA/CA by endogenous aaRS(s) can result in aminoacylation of the tRNA with a natural aa. (F) tRNA-dCA/CA-aa binds EF-1 α and/or other components of the translational machinery. (G) Undesired protein translation can occur by placing a natural aa at the suppression site (XXX(X)), rather than termination at the stop codon or a frameshift, and this competes with UAA incorporation. (H) After translation the tRNA-dCA/CA is released into the cytoplasm and can repeat steps E–H.

4.2.2 Experimental Scheme for Evaluating Aminoacylation and Suppression by

Electrophysiology

All experiments were performed on the nAChR, which has been extensively studied by the site-specific incorporation of UAAs. The muscle-type nAChR is a pentamer composed of α -, β -, γ -, and δ -subunits in the ratio of 2:1:1:1, respectively

(Figure 3.3). In order to compare experiments from different batches of oocytes, we normalized the average maximal current in response to 1 mM ACh for each suppressor tRNA to the corresponding average maximal current for THG73. Wild-type mRNA expression would be the most desirable normalization, but injection of 20–60 ng of mRNA (as in the aminoacylation experiments) would produce wild-type currents greater than 100 μ A, resulting in current saturation.

To evaluate aminoacylation, we chose a Leu site in the second transmembrane helix (M2) of the β subunit termed $\beta 9'$ (shown in Figure 3.3). This site has been shown to tolerate placement of many natural aas and UAAs (18–20), with most causing characteristic shifts in ACh EC_{50} . Previously, THG73 was shown to incorporate natural aa(s) at this site under excessive conditions (3). A possible complication for experiments designed to probe aminoacylation is read-through of the stop codon, which can be tested for by injecting mRNA only into the *Xenopus* oocyte. We find that at the $\beta 9'$ site, such read-through is insubstantial, producing currents that are \approx 3.5% of those seen when THG73 is included.

During the course of this research, we noticed variations in aminoacylation depending on whether the oocytes were acquired from Xenopus Express or Nasco. *Xenopus laevis* frogs from Xenopus Express are caught in Africa, while Nasco frogs are bred in a laboratory and are from a similar gene pool (Linda Northey, personal communication). For each experiment, the figure legends state the supplier(s) of the oocytes.

4.2.3 Identifying the Natural aa Placed on THG73 Using Electrophysiology

As noted above, we focus on the $\beta 9'$ site of the nAChR, which for the wild-type $\beta 9'L$ (shown in Figure 3.3) has an EC_{50} of 50 μM for ACh. For the well-characterized $\beta 9'S$ the EC_{50} is lowered ≈ 33 -fold to 1.5 μM ACh (18), and the lowering of EC_{50} has been shown to scale with the polarity of the residue introduced at the $\beta 9'$ position (18).

Injection of $\beta 9'UAG + THG73$ (74mer) under excessive conditions produces receptors with an EC_{50} of 0.24 μM ACh (Figure 4.2), which is lower than any substitution previously tested at the $\beta 9'$ position. When $\beta 9'UAG + THG73$ -dCA (76mer) was evaluated, an EC_{50} of 0.88 μM was obtained. We chose to screen $\beta 9'Q$ because THG73 evolved to suppress the amber codon with Gln in *T. thermophila* (21), and many amber suppressor tRNAs are aminoacylated with Gln *in vivo* (22). The conventional mutant $\beta 9'Q$ has an EC_{50} of 0.31 μM ACh (Figure 4.2). While the EC_{50} of $\beta 9'Q$ and $\beta 9'UAG + THG73$ (74mer) are comparable, there is ≈ 3 -fold increase in EC_{50} when $\beta 9'UAG + THG73$ -dCA (76mer) is injected (Figure 4.2). These results suggest that the full-length THG73-dCA (76mer) is aminoacylated with amino acids other than Gln. Apparently, this is less important for THG73 (74mer), which must have CA added *in vivo* to become a full-length tRNA (Figure 4.1, D). From these results, we conclude that the predominant natural aa placed on THG73 is Gln.

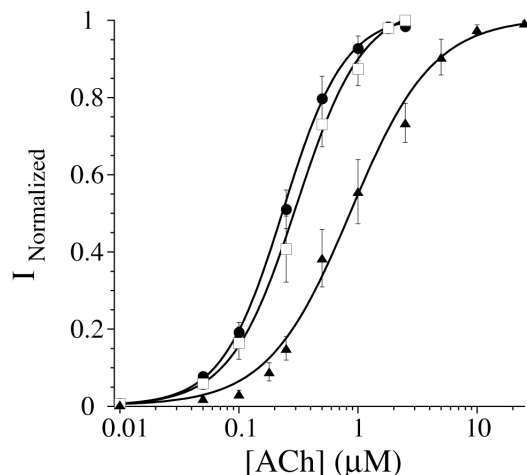


Figure 4.2: Fits to the hill equation for $\beta 9'$ UAG + THG73 (74mer)/-dCA (76mer) and $\beta 9'$ Q. Filled circles are $\beta 9'$ UAG + THG73 (74mer) [16 ng per oocyte], open squares are $\beta 9'$ Q, and filled triangles are $\beta 9'$ UAG + THG73-dCA (76mer) [5 ng per oocyte]. EC_{50} values are $.24 \pm .006$, $.31 \pm .02$, and $.88 \pm .08$ μM ACh, respectively. In each experiment $n > 3$ oocytes.

4.2.4 Testing Knob Mutations on THG73

Much is known about the recognition of tRNA by the GlnRS, and key interactions have been assigned to various “knobs” on the tRNA, termed K1, K2, and K3 (Figure 4.3). In a study of aminoacylation of *E. coli* tRNA₂^{Gln} by the *E. coli* GlnRS (12), the mutations that produced the greatest reduction in aminoacylation were K2, K2K3, and K1K2K3. We therefore incorporated these mutations into THG73, and tested for orthogonality at the $\beta 9'$ site.

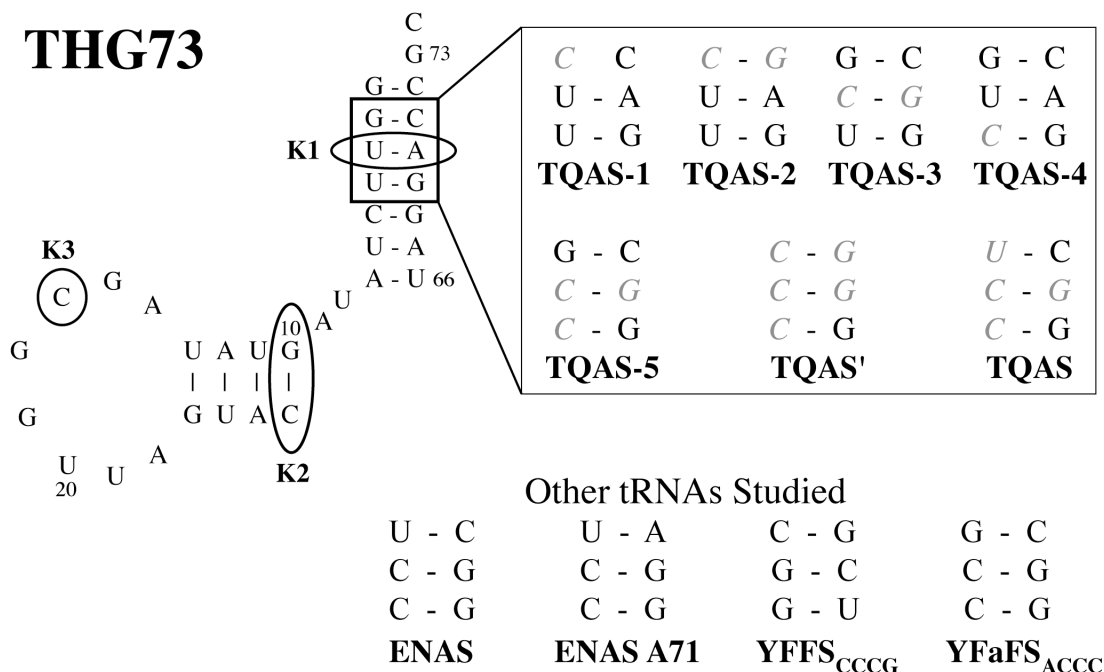


Figure 4.3: THG73 mutations and tRNAs studied. Circled positions on THG73 correspond to the Knob mutations from (12), where K1 is C3-G70, K2 is C10-G25, and K3 is G17. The boxed region on THG73 corresponds to the 2nd to 4th positions of the acceptor stem (mutations are shown in gray italics in the right box). Note THG73 K1 and TQAS-3 are the same mutation. Other tRNAs studied are shown at the bottom with only the 2nd to 4th positions of the acceptor stem shown. ENAS and TQAS contain the same nucleotides at these positions.

As shown in Figure 4.4, THG73 K2, THG73 K2K3, and THG73 K1K2K3 all show less than 20% aminoacylation *in vivo* when compared to THG73 at β^9 UAG (Figure 4.4). However, when each tRNA was chemically ligated with dCA-W and injected with α 149UAG (a non-permissive site), less than 3% of the current of THG73-W was seen (Figure 4.4). Therefore THG73 K2, THG73 K2K3, and THG73 K1K2K3 are nonfunctional in the *Xenopus* oocyte and are not viable alternatives for UAA incorporation *in vivo*.

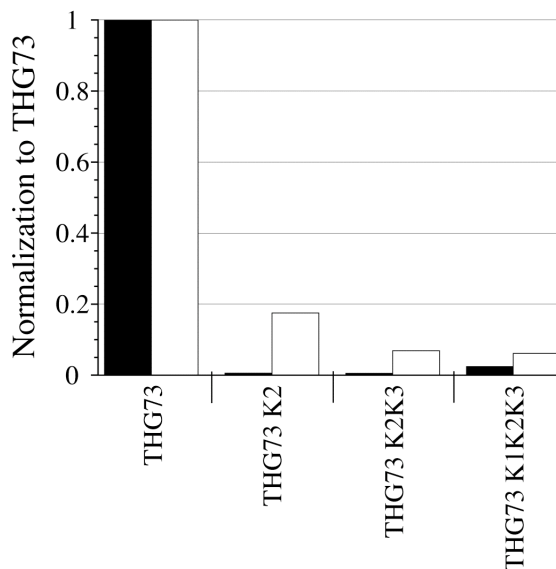


Figure 4.4: THG73 Knob mutations. Individual tRNA average current were normalized by appropriate THG73 average current and bars represent this average ratio. (Total number of oocytes tested is 91, where each bar is $15 > n > 5$ oocytes.) Black bars correspond to tRNA-W [21 ng per oocyte] suppressing at α 149UAG and white bars correspond to tRNA (74mer) [17 ng per oocyte] + β 9'UAG in *Xenopus Express* oocytes. THG73 Knob mutations are $< 20\%$ when suppressing at α 149UAG and show they are not functional alternatives for UAA incorporation.

We conclude that THG73 is very sensitive to the K2 and K3 mutations in the D-stem and D-loop, respectively, which make tertiary contacts with the variable loop to form the characteristic L-shape, tRNA structure. Previous replacement of the THG73 anticodon with ACCC (8) and CCCG (3) also resulted in nonfunctional frameshift suppressors *in vivo*. THG73 appears to be exceptionally sensitive to mutation within the D domain and the anticodon loop, which limits the regions where this tRNA can be mutated to create functional tRNAs.

4.2.5 Testing Aminoacylation of ENAS and ENAS A71 *In Vivo*

With the failure of the knob mutations to produce functional tRNAs for UAA incorporation, we chose to screen the *E. coli* Asn amber suppressor (ENAS), which was shown to be orthogonal *in vitro* (4) and *in vivo* (9). When analyzing the structure of ENAS, we noticed that the 2nd position of the acceptor stem contained the non-Watson-Crick base pair U2-C71. We created the variant ENAS C71A to form the canonical pair U2-A71 (Figure 4.3) present in the wild-type tRNA (9).

While injection of ENAS or ENAS A71 (74mer) with β 9'UAG resulted in less aminoacylation than THG73 in both *Xenopus* Express and Nasco oocytes, the effect was much more pronounced with Nasco oocytes (Figure 4.5). The EC₅₀s of ENAS (74mer) or ENAS A71 (74mer) with β 9'UAG were 2.0 ± 0.1 and 1.5 ± 0.1 μ M ACh, respectively, in Nasco oocytes. These EC₅₀s are larger than the 0.31 μ M ACh for β 9'Q (Figure 4.2), suggesting that ENAS and ENAS A71 are aminoacylated by another natural aa or a mixture of natural aas.

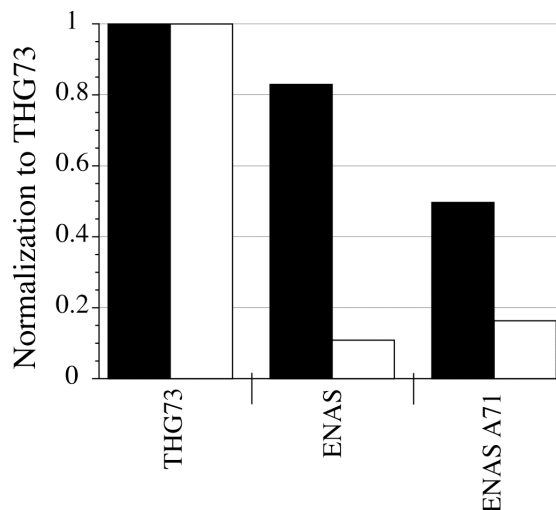


Figure 4.5: ENAS and ENAS A71 aminoacylation tested at β^9 UAG. Individual tRNA (74mer) [17 ng per oocyte] average current was normalized to THG73 (74mer) average current and bars represent this average ratio. (Total number of oocytes tested is 75, where each bar is $22 > n > 5$ oocytes.) Black and white bars correspond oocytes from Xenopus Express and Nasco, respectively. ENAS and ENAS A71 show a large amount of aminoacylation in Xenopus Express oocytes after a 2 d incubation, which has not been seen *in vitro* (4) or *in vivo* (9). Aminoacylation is drastically reduced when tested in Nasco oocytes.

While ENAS and ENAS A71 tRNAs do show improved orthogonality compared to THG73, the suppression efficiencies of ENAS-W and ENAS A71-W were less than 26% of THG73-W in both Xenopus Express and Nasco oocytes (Chapter 5 & (23)). As such, neither ENAS tRNA is a viable replacement for THG73 for UAA incorporation in *Xenopus* oocytes.

4.2.6 Testing Aminoacylation of THG73 Acceptor Stem Mutations

The *E. coli* GlnRS contacts the tRNA acceptor stem in the crystal structure (13), and biochemical experiments have shown specific base pairs and/or positioning of the backbone affect aminoacylation *in vivo* (14–16). As such, we decided to screen various

mutations in the 2nd to 4th positions of the acceptor stem (shown in Figure 4.3) to create a library of *T. thermophila* Gln amber suppressor (TQAS) tRNAs (note in this nomenclature THG73 would be known as TQAS-0). The mutation G2C on THG73 (TQAS-1) results in the 2nd position having C2 C71, which results in a non-functional tRNA and serves as a negative control. The single helix pair mutations C2-G71, C3-G70, and C4 are named TQAS-2, TQAS-3, and TQAS-4, respectively (Figure 4.3). We then created the double helix pair mutation C3-G70 & C4 (TQAS-5) and the triple helix pair mutation C2-G71, C3-G70, & C4 (TQAS'). Finally we placed the ENAS acceptor stem from the 2nd to 4th position, including the U2-C71, on THG73 to create TQAS (Figure 4.3).

All acceptor stem mutations reduced aminoacylation relative to THG73 in both *Xenopus* Express and Nasco oocytes when tested at β 9'UAG (Figure 4.6 & Table 4.1). TQAS-1 shows the same amount of current as β 9'UAG mRNA injection alone, but due to the C2 C71 in the acceptor stem TQAS-1-W is unable to suppress α 149UAG in both *Xenopus* Express and Nasco oocytes (Chapter 5 & (23)). In *Xenopus* Express oocytes, the single helix pair mutations on THG73 all lower aminoacylation, with orthogonality following the order TQAS-2 < TQAS-3 < TQAS-4 (Figure 4.6). Reduction is also seen for the single helix pair mutations in Nasco oocytes, but the orthogonality trend is TQAS-4 \approx TQAS-3 < TQAS-2. These results are consistent with previous biochemistry experiments that showed the 2nd and 3rd positions are GlnRS identity elements (14,15),

and that removing the wobble (U4-G69) at the 4th position reduces aminoacylation in *E. coli* (16).

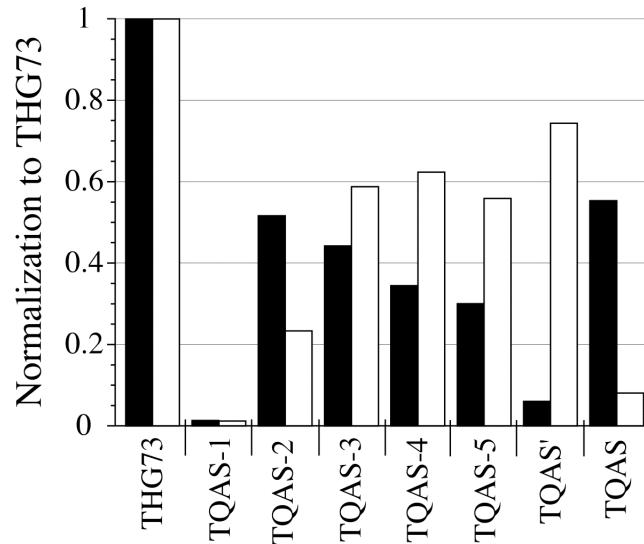


Figure 4.6: THG73 acceptor stem mutations tested at $\beta 9'$ UAG. Individual tRNA (74mer) [16 ng per oocyte] average current was normalized to THG73 (74mer) average current. Bar colors are the same as in Figure 4.5. Total number of oocytes tested is 189 and each bar is $26 > n > 8$ oocytes. All mutations in the acceptor stem lower aminoacylation *in vivo* relative to THG73. TQAS-1 shows lack of aminoacylation, but is not accepted by the translational machinery (Thesis Chapter 5 & (23)). TQAS' and TQAS are the most orthogonal tRNAs in Xenopus Express and Nasco oocytes, respectively.

Table 4.1: THG73 acceptor stem mutations

tRNA	Xenopus Express ^a	Nasco ^a	Average ^b
THG73	1.00	1.00	1.00
TQAS-1	0.01	0.01	0.01
TQAS-2	0.52	0.23	0.38
TQAS-3	0.44	0.59	0.52
TQAS-4	0.34	0.62	0.48
TQAS-5	0.30 (0.15) ^c	0.56	0.43
TQAS'	0.06 (0.08) ^c	0.74	0.40
TQAS	0.55	0.08	0.32
U2-C71 (TQAS)	[4.27] ^d	[0.24] ^d	[1.43] ^d

^a Values from Figure 4.6.

^b Average of Xenopus Express and Nasco aminoacylation from Figure 4.6.

^c Theoretical values calculated by the multiplication of the single mutations.

^d Theoretical value for U2-C71 calculated by TQAS/(TQAS-3 X TQAS-5).

We then combined mutations to reduce aminoacylation further in *Xenopus* oocytes. In *Xenopus* Express oocytes, combining the mutations results in a multiplicative reduction in aminoacylation for TQAS-5 and TQAS' (Table 4.1), while TQAS, which contains U2-C71, shows the largest amount of aminoacylation (Figure 4.6). The overall aminoacylation trend in *Xenopus* Express oocytes is THG73 >> TQAS ≈ TQAS-2 > TQAS-3 > TQAS-4 > TQAS-5 >> TQAS', making TQAS' the most orthogonal tRNA (Figure 4.6). The same tRNAs tested in Nasco oocytes show no logical trend in combining mutations (Table 4.1), and TQAS is the most orthogonal tRNA. Nasco oocytes display the overall aminoacylation trend THG73 >> TQAS' > TQAS-4 ≈ TQAS-3 ≈ TQAS-5 > TQAS-2 >> TQAS (Figure 4.6). Overall the mutations suggest C-G pairs in the acceptor stem reduce aminoacylation in *Xenopus* Express oocytes. Nasco oocytes prefer the C-G mutation at the 2nd position (TQAS-2, Figure

4.3) or the non-Watson-Crick U-C pair at the 2nd position, along with C-G pairs at the 3rd and 4th positions (TQAS, Figure 4.3). While differences in the *Xenopus* Express and Nasco oocytes were unanticipated, Figure 4.6 shows that the TQAS tRNA library contained an orthogonal tRNA for each genetic background.

4.2.7 Aminoacylation Tested at a Highly Promiscuous Site, β A70

The β 9' site can incorporate many natural aas and UAAs (18–20), but we chose to further test aminoacylation of the orthogonal tRNAs selected (TQAS' and TQAS) at another highly permissive nAChR site, β A70. Structural studies place this residue on a highly exposed loop of the receptor (24,25). Previous work on the aligned α D70UAG showed that it can incorporate the large UAA biocytin with little change in the EC_{50} (26). Other work has shown that biocytin is a challenging residue for nonsense suppression (11), supporting the notion that α D70 is a promiscuous site. Therefore we studied the α D70-aligned site in the β -subunit, β A70, considering only Nasco oocytes.

With the injection of β 70UAG mRNA only, large amounts of current were obtained, indicating that this read-through represents $\approx 30\%$ of the current observed in the aminoacylation experiments (Figure 4.7). This large amount of read-through is not typical of most sites studied (β 9'UAG discussed above and α 145UAG below), and is most likely caused by the high promiscuity for aa incorporation. Injection of THG73-dCA and TQAS'-dCA with β 70UAG in Nasco oocytes resulted in approximately the same amount of aminoacylation (Figure 4.7, white bars), which is consistent with increased TQAS' aminoacylation with Nasco oocytes (Figure 4.6). However, TQAS

shows very little aminoacylation compared to THG73 at this site (Figure 4.7), and subtracting the mRNA only results in 9% aminoacylation relative to THG73 (also background subtracted).

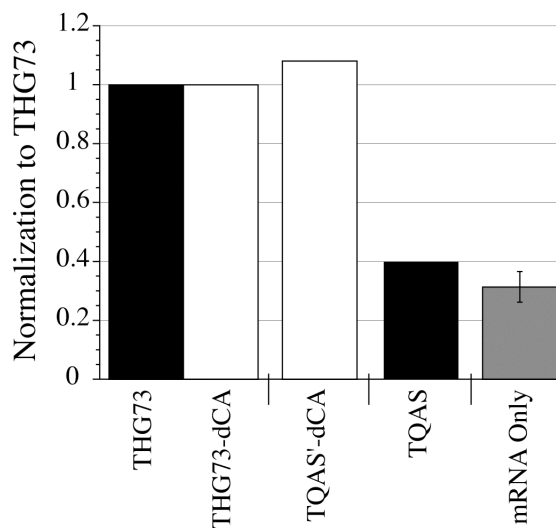


Figure 4.7: tRNA (74mer/-dCA) aminoacylation tested at a highly promiscuous site, β A70. All experiments were performed in Nasco oocytes. Black bars are tRNA (74mer), white bars are tRNA-dCA, and the gray bar is mRNA only. Average currents for TQAS'-dCA and TQAS were normalized to THG73-dCA and THG73, respectively. mRNA only was normalized to THG73. Total number of oocytes tested is 60, where each bar is $15 > n > 6$ oocytes with 9 ng of tRNA per oocyte. mRNA only shows significant read-through of the UAG stop codon. THG73, THG73-dCA, and TQAS'-dCA all show significant aminoacylation when assayed at β 70UAG. TQAS shows comparable currents to the injection of mRNA only, showing less aminoacylation of TQAS in Nasco oocytes.

The EC_{50} s for mRNA only, THG73, TQAS'-dCA, and TQAS were 71 ± 1 , 56 ± 3 , 58 ± 3 , and 46 ± 2 μ M ACh, respectively, and showed little change from the wild-type EC_{50} of 50 μ M ACh. These studies further show that TQAS is the most orthogonal tRNA and that TQAS' is aminoacylated extensively in Nasco oocytes.

4.2.8 LysRS Does Not Aminoacylate THG73, TQAS', and TQAS

THG73 was shown to be aminoacylated by Gln at the $\beta 9'$ site (Figure 4.2). However, the 9' position is a conserved Leu in all of the nAChR subunits and forms the hydrophobic gate to the channel (18). Therefore it is possible that anionic or cationic aas such as Asp, Glu, Lys, and Arg may not be incorporated at the $\beta 9'$ position or may produce nonfunctional receptors if they are. This is concerning because many amber suppressor tRNAs have been shown to be aminoacylated by LysRS and/or GlnRS *in vivo* (22), and mutations to the anticodon stem of an amber suppressor tRNA^{Tyr} have shifted the GlnRS or LysRS recognition *in vitro* (27). To evaluate this possibility, we studied a conserved Lys residue in the α -subunit of the nAChR, $\alpha K145$, to test if suppressor tRNAs were aminoacylated by LysRS and/or GlnRS. The conventional mutant $\alpha K145Q$ gave an EC₅₀ of $144 \pm 2 \mu\text{M}$ ACh (Figure 4.8), a ≈ 3 -fold increase relative to the wild-type EC₅₀ of $50 \mu\text{M}$ ACh.

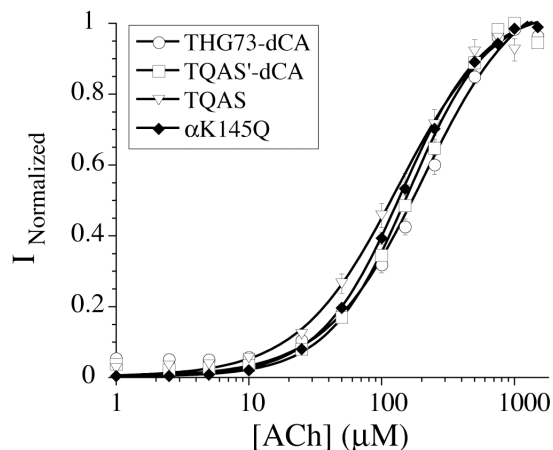


Figure 4.8: tRNA aminoacylation tested at α K145. Total number of oocytes tested is 36, where each dose-response is $17 > n > 5$ oocytes. EC_{50} values are 167 ± 14 , 165 ± 14 , 134 ± 15 , and 144 ± 2 μ M ACh in the order listed in the legend with 7.5 ng of tRNA per oocyte. All tRNAs are still aminoacylated by Gln and not Lys (wild-type $EC_{50} = 50$ μ M ACh).

Injection of α 145UAG mRNA alone resulted in very small currents, such that EC_{50} could not be determined. Injection of α 145UAG with THG73-dCA, TQAS'-dCA, and TQAS resulted in EC_{50} s of 167 ± 14 , 165 ± 14 , and 134 ± 15 μ M ACh, respectively (Figure 4.8). The EC_{50} s for all tRNAs are ≈ 3 -fold increased relative to the wild-type EC_{50} , and therefore all of the tRNAs are aminoacylated by GlnRS and not by LysRS in *Xenopus* oocytes.

4.2.9 Analyzing THG73-W and TQAS-W Interactions with the Translational Machinery *In Vivo*

In Figure 4.1, we outlined the desired events for the incorporation of UAA and the undesired possibility of incorporation of natural aas at the suppression site. THG73 was previously shown to be orthogonal to the translational machinery *in vitro* and *in vivo* when using less mRNA and/or tRNA along with incubations less than 2 d (4–8). We

have shown that with increasing all three of the aforementioned conditions, producing so-called excessive conditions, THG73 can be aminoacylated *in vivo*. Under these same conditions, TQAS' shows $\approx 90\%$ reduction in the aminoacylation product in *Xenopus* Express oocytes (Figure 4.6).

To analyze interactions with the translational machinery we used the temporal control of injection. By injecting tRNA-W first, we analyze the protection of the tRNA-W by EF-1 α and/or other components of the translational machinery (Figure 4.1, A) from the undesired, irreversible loss of the UAA by hydrolysis and/or aaRS editing (Figure 4.1, C). Subsequent injection of mRNA to assay protein production (Figure 4.1, B) allows for comparison to what is seen when tRNA-W and mRNA are injected simultaneously. The tRNA-aa bond is highly labile at physiological pH. In a recent study, a sample of dCA-Val at pH 7.8 without translational machinery components was 69% hydrolyzed after a 1 h incubation (28). The cytoplasm of a *Xenopus* oocyte is estimated to be between pH 7.3–7.7 (29,30), and therefore some hydrolysis of tRNA-dCA-W would be expected after 3.5 h, if not protected by other proteins. EF-Tu has been shown to protect YFFS_{CCCG}-UAA from hydrolysis *in vitro*, but significant loss was seen after 1 h (17).

Simultaneous injection of THG73-W/TQAS'-W (10 ng per oocyte) and α 149UAG mRNA gave average maximal currents of -3.9 ± 1 and -4.1 ± 1 μ A, respectively, in *Xenopus* Express oocytes. Surprisingly, we see no loss in current from either THG73-W or TQAS'-W when injecting mRNA 3.5 h after the tRNA-W, with -3.9

± 0.5 and $-3.9 \pm 1 \mu\text{A}$, respectively. Injection of twice as much THG73-W (20 ng per oocyte) resulted in $-6.3 \pm 2 \mu\text{A}$. This illustrates that the translation system is not saturated, but there is not a linear increase in current with twice as much tRNA-W in a single injection. Therefore, interactions with EF-1 α and/or other proteins specifically protect both suppressor tRNA-Ws from deacylation by aaRS(s) and hydrolysis, which is not problematic after 3.5 h in the *Xenopus* oocytes.

A double injection protocol, in which a second dose of aminoacyl tRNA is injected 24 h after the first, allows us to assay competition between the suppressor tRNA-W and tRNA-Q (generated by aminoacylation *in vivo*) after 24 h (Figure 4.1, B & G). Only aromatic aas can function at $\alpha 149\text{UAG}$, and suppressing with tRNA-W results in wild-type channels. If, however, there is competition with tRNA-Q, then, during the second 24 h there will be a decrease in the overall protein production, or less than double the current. In the event, a double injection with a 24 h interval of THG73-W/TQAS'-W with $\alpha 149\text{UAG}$ showed currents of -8.9 ± 2 and $-8.6 \pm 3 \mu\text{A}$, respectively, which is greater than twice the protein relative to the single injection. The higher protein production is mostly likely due to residual mRNA from the 1st injection, even though nonsense-mediated decay in *Xenopus* oocytes is expected to remove most mRNA with premature stop codons after 18 h (31).

The double injection studies establish that aminoacylation of the tRNA-dCA in *Xenopus* oocytes (Figure 4.1, E-H) is not problematic for the first 24+ h *in vivo* for either THG73 and TQAS', because there is no reduction in protein and therefore lack of

competition for the suppression site. This is surprising because THG73 is aminoacylated $\approx 90\%$ more than TQAS' in *Xenopus* Express oocytes after 2 d (Figure 4.6). This does, however, agree with previous investigations of THG73 orthogonality *in vivo* with incubations of 24 h or less (7).

4.2.10 Comparing Aminoacylation of Amber, Opal, and Frameshift Suppressor tRNAs

Increasing the number of UAAs to be simultaneously incorporated site-specifically requires the use of a unique stop or quadruplet codon for each UAA. Previously we screened two yeast Phe frameshift suppressor tRNAs, YFFS_{CCCG} and YFaFS_{ACCC}, in *Xenopus* oocytes and found that both tRNAs were aminoacylated much less than THG73 when tested at the $\beta 9'$ site. However, their suppression efficiency was decreased relative to THG73 *in vivo*, although still adequate for UAA incorporation (3). Previous work has established that the opal (UGA) and ochre (UAA) stop codons can be suppressed in mammalian cells when using suppressor tRNAs that are aminoacylated by endogenous aaRSs (32) or by the import of an exogenous *E. coli* aaRSs (33). The opal codon has also been used to incorporate an UAA in mammalian cells using a tRNA/synthetase pair (34). Also, an opal suppressor was previously created by replacing the anticodon of THG73 with UCA, but this opal suppressor tRNA (not chemically ligated to an UAA) is aminoacylated *in vitro* and results in protein translation, or aminoacylation product, $> 90\%$ when compared to wild-type translation. Under the same conditions as the opal suppressor tRNA, THG73 and ENAS showed $< 5\%$

aminoacylation product (4), suggesting that the opal suppressor derived from THG73 would be highly aminoacylated *in vivo* and not viable for nonsense suppression. In *T. thermophila*, the ochre suppressor has been shown to suppress both the ochre and amber codons (21), and so it would not be viable for the simultaneous incorporation of multiple UAAs.

To test the generality of the acceptor stem mutations at reducing aminoacylation *in vivo*, we created *T. thermophila* Gln opal suppressor tRNAs (TQOpS' and TQOpS) by replacing the anticodon of TQAS' and TQAS with UCA.

All four subunits of the nAChR terminated with the opal (UGA) stop codon, and these were all mutated to the ochre (UAA) stop codon to avoid suppression by TQOpS' or TQOpS. The masked construct had an EC_{50} of $53 \pm 3 \mu\text{M}$ ACh, comparable to the wild-type EC_{50} of $50 \mu\text{M}$. Injection of $\beta 9'$ UGA with no tRNA resulted in 2.8% of the current normalized to THG73 (74mer), vs. 1.7% with $\beta 9'$ UAG. The opal codon thus showed ≈ 1.6 -fold greater read-through than the amber codon, which has previously been noted in *E. coli* (35). Aminoacylation was tested under identical conditions with THG73, TQAS', TQAS, TQOpS', TQOpS, YFFS_{CCCG}, and YFaFS_{ACCC} at the $\beta 9'$ suppression site, stop codon or quadruplet codon, with tRNA (74mer) and tRNA-dCA (76mer). This was done to validate initial screens using only (74mer) and comparisons between (74mer) and (76mer) in Figures 4.4, 4.5, 4.6, and 4.7. Comparison of suppressor tRNAs (74mer) and tRNA-dCAs (76mer) show no significant difference for each individual suppressor tRNA in *Xenopus* Express or Nasco oocytes (Figure 4.9).

Once again TQAS' and TQAS showed much less aminoacylation in *Xenopus* Express and Nasco oocytes, respectively, relative to THG73. TQOpS' and TQOpS both show less than $\approx 40\%$ and $\approx 9\%$ aminoacylation, respectively, compared to THG73 (Figure 4.9). This shows that the acceptor stem mutations on THG73 are able to reduce aminoacylation for both amber and opal suppressor tRNAs. YFaFS_{ACCC} and YFFS_{CCCG} show a similar trend to that previously reported (Chapter 3 & (3)) with average aminoacylation product of 19% and 3%, respectively, of THG73. The orthogonality trend is as follows: YFaFS_{ACCC} > TQAS' (*Xenopus* Express) \approx TQOpS > YFFS_{CCCG} > TQAS (Nasco) \approx TQOpS' \gg THG73, which is aminoacylated the most.

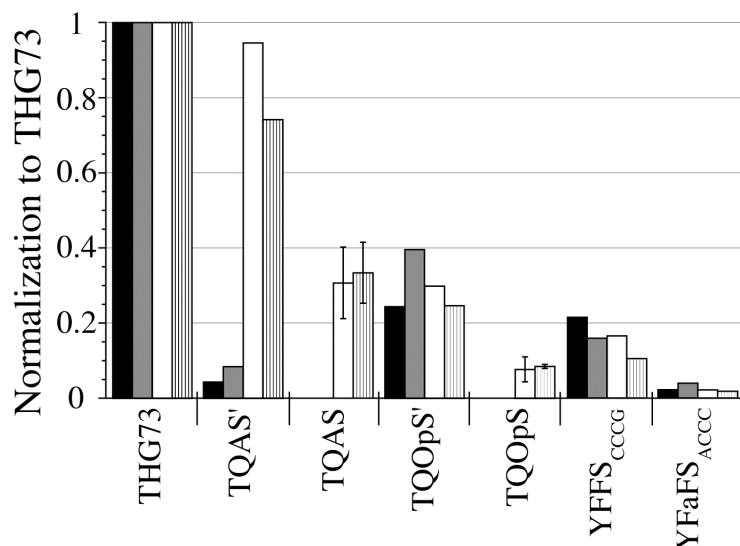


Figure 4.9: Amber, opal, and frameshift suppressor tRNAs tested at $\beta 9'$. All tRNA 74mer or -dCA [7.5 ng per oocyte] average currents were normalized to THG73 74mer or -dCA average currents, respectively. Black bars are tRNA 74mer + $\beta 9'$ (UAG, UGA, CGGG, or GGGU) and gray bars are tRNA-dCA (76mer) + $\beta 9'$ (UAG, UGA, CGGG, or GGGU) in Xenopus Express oocytes. White and Hatched bars are tRNA 74mer and 76mer, respectively, in Nasco oocytes. Total number of oocytes is 276, where $17 > n > 5$. TQAS' and TQAS show significantly reduced aminoacylation in Xenopus Express and Nasco oocytes, respectively, when compared to THG73. Both opal suppressor tRNAs (TQOpS' and TQOpS) show less aminoacylation than THG73. Overall, the frameshift suppressor YFaFS_{ACCC} is the most orthogonal tRNA in both Xenopus Express and Nasco oocytes.

4.3 Discussion

THG73 is an amber suppressor tRNA that has been used extensively for the incorporation of greater than 100 residues in 20 proteins (1,2). Using conditions such as low quantities of mRNA and/or tRNA with incubation times less than 2 d, THG73 has been shown to be orthogonal *in vitro* (4–6) and *in vivo* (7,8). However, increasing the amount of mRNA and tRNA with incubation of 2 d leads to the aminoacylation of THG73 by an endogenous aaRS *in vivo* (3). We show that the *E. coli* Asn amber

suppressor (ENAS) and ENAS A71 are both susceptible to aminoacylation by aaRSs of the *Xenopus* oocyte (Figure 4.5), even though aminoacylation has not been observed *in vitro* (4,10,11) or *in vivo* (9). This suggests that many well-characterized amber suppressor tRNAs may become aminoacylated *in vivo* when using increased amounts of mRNA and tRNA along with incubations of 2 d, which is desirable for increased amounts of protein.

By using the sensitivity of electrophysiology and the well-characterized $\beta 9'$ site, we have been able to show that the natural aa placed on THG73 is predominantly if not exclusively Gln (Figure 4.2). The THG73 (74mer) and $\beta 9'$ Q show comparable EC_{50} s, but THG73-dCA (76mer) shows \approx 3-fold increase in EC_{50} (Figure 4.2). These experiments suggest that THG73-dCA (76mer) is more readily aminoacylated by other endogenous aaRSs, perhaps due to the unnatural dCA at the 3' end, but the predominant aa is still Gln. Similar conditions with the THG73 (74mer) resulted in equivalent EC_{50} as $\beta 9'$ Q and therefore the active THG73-CA (Figure 4.1, D) appears to be more stringently recognized by the GlnRS.

Intriguingly, THG73 is very sensitive to the previously discussed “knob” mutations meant to disrupt recognition by GlnRS, and the derived tRNAs are not viable for UAA incorporation. The K2 mutation alone destroys activity, and combining it with other knob mutations provides little rescue. The K2 mutation resides within the D domain of THG73, which makes tertiary contacts with the variable loop to form the characteristic L-shape tRNA structure. This mutation may result in misfolding of the

THG73, but it apparently has little effect on *E. coli* tRNA₂^{Gln} (12). Interestingly, the K1, or TQAS-3, mutation was shown to be functional by itself on THG73 (Chapter 5 & (23)), but it is non-functional in combination with K2 and K3 (Figure 4.4). Replacement of the THG73 anticodon with ACCC (8) or CCCG (3) resulted in nonfunctional frameshift suppressors *in vivo*. THG73 appears to be sensitive to mutation within the D domain and the anticodon loop, but tolerates acceptor stem mutations.

ENAS and ENAS A71 aminoacylation in *Xenopus* Express oocytes is comparable to THG73, but there is a 40% decrease due to the U2-C71 vs. U2-A71, respectively, (Figure 4.5) at the 2nd position of the acceptor stem (Figure 4.3). ENAS A71 is more orthogonal, which suggests that the U-A is not recognized by endogenous aaRSs as readily as U-C. The opposite trend is seen in Nasco oocytes, but orthogonality is significantly improved for both ENAS and ENAS A71. Clearly, the identity of the 2nd pair has a strong effect on aminoacylation *in vivo*.

We hypothesized that similar mutations on THG73 could result in less aminoacylation by the GlnRS, because the identity set includes the 2nd to 4th positions of the acceptor stem (13–16). The acceptor stem mutations (shown in Figure 4.3) greatly reduced aminoacylation *in vivo* (Figure 4.6 & Table 4.1). In *Xenopus* Express oocytes, the single helix pair mutations could be combined to further reduce aminoacylation in a multiplicative manner (Table 4.1). In contrast, Nasco oocytes showed a strong dependence on specific sequences, and there was no logical trend based on the single helix pair mutations. This non-classical identity set has previously been identified on

yeast Phe tRNA, where combining mutations could compensate for deleterious single mutations to increase aminoacylation *in vitro* (36). While variation due to the Xenopus Express and Nasco oocytes was unanticipated, the library of six functional TQAS tRNAs was able to find an orthogonal suppressor tRNA for each genetic background. We can anticipate that as other workers move the UAA methodology into other cell types, different orthogonality issues could arise. The library of tRNAs created here contains diverse mutations in the acceptor stem that should allow for orthogonal tRNA selection in other eukaryotic cells, where high-throughput assays for tRNA screening are currently lacking.

Using the temporal control of injection, we were able to evaluate THG73-W and TQAS'-W interactions with the protein translation machinery and competition with the suppressor tRNAs aminoacylated with Gln after 1 d. Shockingly, there is no change in suppression efficiency when the mRNA and tRNA-W are injected simultaneously or when the mRNA was injected 3.5 h after tRNA-W. These experiments show that both suppressor tRNAs are equally protected by EF-1 α and/or other components of the translational machinery for at least 3.5 h, which has not been observed *in vitro* with or without EF-Tu (17,28). Most importantly, this shows that aaRS editing and/or hydrolysis (Figure 4.1, C) are not problematic with 10 ng of tRNA-W injected in oocytes. Injection of 20 ng of THG73-W resulted in a 60% increase in current with a single injection, establishing the lack of saturation at 10 ng, although the response is non-linear. By injecting mRNA and tRNA-W followed by a 2nd injection of the same after

24 h, we could see if there was competition for the suppression of α 149UAG by tRNA-Q (Figure 4.1, B & G). The double injection for both THG73-W/TQAS'-W showed a slightly greater than 2-fold increase in current, indicating a lack of competition with tRNA-Q slightly after 24 h. This agrees with previous experiments using less than 24 h incubation times (7,8). Aminoacylation of THG73 therefore takes place after 24 h and is not different from TQAS' in *Xenopus Express* oocytes in the first 24 h. However, TQAS' is aminoacylated \approx 90% less than THG73 after 2 d. Overall, both THG73 and TQAS' interact with the protein translational machinery similarly in *Xenopus Express* oocytes.

In order to simultaneously incorporate multiple UAAs, it is necessary to use a unique stop or quadruplet codon for each UAA. Previously, three UAAs could be simultaneously incorporated using amber and frameshift suppression with the UAG, CGGG, and GGGU suppression sites (3). A second nonsense site, either opal (UGA) or ochre (UAA), would be valuable for the incorporation of four UAAs. However, the *T. thermophila* ochre suppressor recognizes both the ochre (UAA) and amber (UAG) stop codons (21). The opal codon has been used to incorporate an UAA in mammalian cells using a tRNA/synthetase pair (34) and should be feasible for the UAA incorporation in *Xenopus* oocytes. Previous work with an opal suppressor created from THG73 by the replacement of the anticodon with UCA resulted in a large amount of aminoacylation *in vitro* and production of greater than 90% protein relative to wild-type protein (4). These results suggest that the THG73-derived opal suppressor would be aminoacylated much

more than the THG73 amber suppressor and would not be able to be evaluated under the conditions tested in this paper. To test the generality of the acceptor stem mutations at reducing aminoacylation, we replaced the anticodon of TQAS' and TQAS with UCA to create TQOpS' and TQOpS, respectively. Both TQOpS' and TQOpS show a great reduction in aminoacylation *in vivo* relative to THG73 (Figure 4.9) and are viable suppressor tRNAs for UAA incorporation at the opal codon (Chapter 5 & (23)). Intriguingly, there is no significant difference in aminoacylation of TQOpS' in *Xenopus Express* and *Nasco oocytes* (Figure 4.9), which suggests the opal suppressor is recognized by a different aaRS(s) and variation in aminoacylation is caused by the GlnRS, which we have shown recognizes THG73, TQAS', and TQAS (Figure 4.8); the tRNAs show different amounts of aminoacylation depending on the genetic background (Figures 4.6 & 4.9).

We have shown that acceptor stem mutations have wide applicability for the creation of orthogonal suppressor tRNAs for the incorporation of UAAs in higher eukaryotic cells. TQAS' and TQAS still retain slight aminoacylation by the GlnRS in *Xenopus Express* and *Nasco oocytes*, respectively. Mutations in the anticodon stem have been shown to decrease GlnRS recognition and may further reduce aminoacylation, but these mutations can also lead to increased LysRS recognition (27). The acceptor stem mutations have no adverse effect on the suppression efficiency and can increase the suppression efficiency by as much as 40% (Chapter 5 & (23)). While aminoacylation

was shown to be dependent on the genetic background of the oocytes, there is no effect on the suppression efficiencies of the TQAS tRNAs (Chapter 5 & (23)).

In summary, we have created a TQAS tRNA library that will aid in the identification of orthogonal tRNAs for use with higher eukaryotic cells. When combined with the evaluation of suppression efficiencies described in Chapter 5 and (23), these tRNAs should significantly expand the applicability of site-specific incorporation of UAAs by chemically aminoacylated tRNAs.

4.4 Experimental Methods

4.4.1 Materials

All oligonucleotides were synthesized by Integrated DNA Technologies (Coralville, IA). NotI was from Roche Applied Science (Indianapolis). BamHI, EcoRI, FokI, T4 DNA ligase, and T4 RNA ligase were from NEB (Beverly, MA). Kinase Max, T7 MEGAshortscript, and T7 mMessage mMachine kits were from Ambion (Austin, TX). ACh chloride and yeast inorganic pyrophosphatase were purchased from Sigma-Aldrich. dCA and 6-nitroveratryloxycarbonyl protected dCA-W was prepared as reported in (37,38).

4.4.2 tRNA Gene Preparation and tRNA Transcription

THG73, YFFS_{CCCG}, and YFaFS_{ACCC} subcloned in the pUC19 vector were previously made (3,7). Genes for ENAS (sequence from (4)) with flanking EcoRI and BamHI overhangs were phosphorylated using Kinase Max kit, annealed, and ligated with

T4 DNA ligase into EcoRI and BamHI linearized pUC19 vector as described (39). ENAS A71 (original sequence from (9) with G1-C72 insertion for T7 polymerase transcription) was created by QuikChange mutagenesis on ENAS in pUC19. Knob mutations from (12) (K2 is C10-G25; K2K3 is C10-G25 & G17; and K1K2K3 is C3-G70, C10-G25, & G17) on THG73 were created by QuikChange mutagenesis. Acceptor stem mutations on THG73 were created by QuikChange mutagenesis and shown in Figure 4.3. Replacing the anticodon of TQAS' and TQAS from CUA to UCA by QuikChange mutagenesis created TQOpS' and TQOpS, respectively. All mutations were verified by DNA sequencing (California Institute of Technology Sequencing / Structure Analysis Facility). Template DNA for tRNA lacking the 3'CA was prepared by FokI digestion, and tRNA was transcribed using the T7 MEGAshortscript kit with .5 μ l of yeast inorganic pyrophosphatase (40 U/ml in 75 mM Tris, 10 mM MgCl₂, and pH 7). tRNA was desalted using CHROMA SPIN-30 DEPC-H₂O columns (BD Biosciences), and concentration was determined by absorption at 260 nm.

4.4.3 nAChR Gene Preparation and mRNA Transcription

The masked α -, β -, γ -, and δ -subunits of the nAChR subcloned in the pAMV vector were previously prepared (3). All four subunits terminate with the opal (UGA) stop codon and each UGA was mutated to the ochre (UAA) stop codon to avoid possible suppression by TQOpS' and TQOpS. α 149UAG and β 9'(UAG, CGGG, and GGGU) were previously prepared on the masked constructs (3). β 70UAG, α 145Q, α 145UAG, and β 9'UGA were prepared by QuikChange mutagenesis. Mutations were verified by

DNA sequencing (California Institute of Technology Sequencing / Structure Analysis Facility). DNA was linearized with NotI and mRNA was prepared with the T7 mMessage mMachinE kit with .5 μ l of yeast inorganic pyrophosphatase. mRNA was purified by using the RNeasy Mini kit (Qiagen, Valencia, CA) and quantified by absorption at 260 nm.

4.4.4 dCA and dCA-W Ligation to Suppressor tRNAs

75 μ M (used instead of 300 μ M because there was no change in ligation efficiency) of dCA or 6-nitroveratryloxycarbonyl protected dCA-W were coupled to suppressor tRNAs by using T4 RNA ligase for 30 min as previously reported (39,40), desalted using CHROMA SPIN-30 DEPC-H₂O columns, and quantified by absorption at 260 nm. tRNA ligation efficiency was qualitatively determined by MALDI mass spectrometry (40), and all tRNA ligations were identical within each prepared group and greater than 80%.

4.4.5 *In Vivo* Aminoacylation and Suppression Experiments

Prior to *in vivo* aminoacylation and suppression experiments, all tRNAs and mRNAs were simultaneously made and normalized by UV and densitometric analysis using AlphaEaseFC Stand Alone (Alpha Innotech, San Leandro, CA). Stage VI oocytes of *Xenopus laevis* were prepared as described (41). All tRNAs were refolded at 65 °C for 2 min and 6-nitroveratryloxycarbonyl protected dCA-W was deprotected for 5 min by UV irradiation before injection (7). Oocytes were injected with 50 nl of mRNA alone or with tRNA and incubated at 18 °C for 44–52 h. For EC₅₀ determination of β 9^Q

(Figure 4.2), 3 ng of mRNA in the ratio of 2:1:1:1 for $\alpha:\beta^9\text{Q}:\gamma:\delta$ was injected. 20 ng of mRNA in a subunit ratio of 2:5:1:1 for $\alpha:\beta^9\text{UAG}:\gamma:\delta$ or 10:1:1:1 for $\alpha^{149}\text{UAG}:\beta:\gamma:\delta$ was injected in Figures 4.2, 4.4, and 4.5. Figures 4.6, 4.7, and 4.8 used the same ratio, but 40 ng to 60 ng of mRNA was injected per oocyte. In Figure 4.9, 40 ng of mRNA was injected in a subunit ratio of 2:5:1:1 for $\alpha:\beta^9(\text{UAG, UGA, CGGG, or GGGU}):\gamma:\delta$. The amount of tRNA injected is listed with each figure.

4.4.6 Electrophysiology

Recordings employed two-electrode voltage clamp on the OpusXpress 6000A (Molecular Devices). ACh was stored at $-20\text{ }^\circ\text{C}$ as a 1 M stock, diluted in Ca^{2+} -free ND96, and delivered to oocytes by computer-controlled perfusion system. For all experiments, the holding potential was -60 mV . Dose-response data was obtained from at least eight ACh concentrations and all tRNA aminoacylation or suppression comparisons were tested with a single 1 mM ACh dose. Dose-response relations were fit to the Hill equation to determine the EC_{50} and Hill coefficient (n_{H}). All reported values are represented as a mean \pm SE of the tested oocytes (number of oocytes (n) is listed with each figure).

4.5 References

1. Dougherty, D.A. (2000) Unnatural amino acids as probes of protein structure and function. *Curr. Opin. Biotechnol.*, **4**, 645–652.
2. Beene, D.L., Dougherty, D.A., and Lester, H.A. (2003) Unnatural amino acid mutagenesis in mapping ion channel function. *Curr. Opin. Neurobiol.*, **13**, 264–270.
3. Rodriguez, E.A., Lester, H.A., and Dougherty, D.A. (2006) *In vivo* incorporation of multiple unnatural amino acids through nonsense and frameshift suppression. *Proc. Natl. Acad. Sci. USA*, **103**, 8650–8655.
4. Cload, S.T., Liu, D.R., Froland, W.A., and Schultz, P.G. (1996) Development of improved tRNAs for *in vitro* biosynthesis of proteins containing unnatural amino acids. *Chem. Biol.*, **3**, 1033–1038.
5. England, P.M., Lester, H.A., and Dougherty, D.A. (1999) Mapping disulfide connectivity using backbone ester hydrolysis. *Biochemistry*, **38**, 14409–14415.
6. Rothman, D.M., Petersson, E.J., Vazquez, M.E., Brandt, G.S., Dougherty, D.A., and Imperiali, B. (2005) Caged phosphoproteins. *J. Am. Chem. Soc.*, **127**, 846–847.
7. Saks, M.E., Sampson, J.R., Nowak, M.W., Kearney, P.C., Du, F.Y., Abelson, J.N., Lester, H.A., and Dougherty, D.A. (1996) An engineered *Tetrahymena* tRNA^{Gln} for *in vivo* incorporation of unnatural amino acids into proteins by nonsense suppression. *J. Biol. Chem.*, **271**, 23169–23175.

8. Shafer, A.M., Kalai, T., Bin Liu, S.Q., Hideg, K., and Voss, J.C. (2004) Site-specific insertion of spin-labeled L-amino acids in *Xenopus* oocytes. *Biochemistry*, **43**, 8470–8482.
9. Kleina, L.G., Masson, J.M., Normanly, J., Abelson, J., and Miller, J.H. (1990) Construction of *Escherichia coli* amber suppressor tRNA genes. II. Synthesis of additional tRNA genes and improvement of suppressor efficiency. *J. Mol. Biol.*, **213**, 705–717.
10. Murakami, H., Kourouklis, D., and Suga, H. (2003) Using a solid-phase ribozyme aminoacylation system to reprogram the genetic code. *Chem. Biol.*, **10**, 1077–1084.
11. Murakami, H., Ohta, A., Ashigai, H., and Suga, H. (2006) A highly flexible tRNA acylation method for non-natural polypeptide synthesis. *Nat. Methods*, **3**, 357–359.
12. Liu, D.R., Magliery, T.J., and Schultz, P.G. (1997) Characterization of an 'orthogonal' suppressor tRNA derived from *E. coli* tRNA₂^{Gln}. *Chem. Biol.*, **4**, 685–691.
13. Perona, J.J., Swanson, R.N., Rould, M.A., Steitz, T.A., and Soll, D. (1989) Structural basis for misaminoacylation by mutant *E. coli* glutaminyl-tRNA synthetase enzymes. *Science*, **246**, 1152–1154.

14. Jahn, M., Rogers, M.J., and Soll, D. (1991) Anticodon and acceptor stem nucleotides in tRNA^{Gln} are major recognition elements for *E. coli* glutaminyl-tRNA synthetase. *Nature*, **352**, 258–260.
15. Ibba, M., Hong, K.W., Sherman, J.M., Sever, S., and Soll, D. (1996) Interactions between tRNA identity nucleotides and their recognition sites in glutaminyl-tRNA synthetase determine the cognate amino acid affinity of the enzyme. *Proc. Natl. Acad. Sci.*, **93**, 6953–6958.
16. McClain, W.H., Schneider, J., Bhattacharya, S., and Gabriel, K. (1998) The importance of tRNA backbone-mediated interactions with synthetase for aminoacylation. *Proc. Natl. Acad. Sci.*, **95**, 460–465.
17. Nakata, H., Ohtsuki, T., Abe, R., Hohsaka, T., and Sisido, M. (2006) Binding efficiency of elongation factor Tu to tRNAs charged with nonnatural fluorescent amino acids. *Anal. Biochem.*, **348**, 321–323.
18. Kearney, P.C., Zhang, H., Zhong, W., Dougherty, D.A., and Lester, H.A. (1996) Determinants of nicotinic receptor gating in natural and unnatural side chain structures at the M2 9' position. *Neuron*, **17**, 1221–1229.
19. Filatov, G.N., and White, M.M. (1995) The role of conserved leucines in the M2 domain of the acetylcholine receptor in channel gating. *Mol. Pharmacol.*, **48**, 379–384.

20. Kosolapov, A.V., Filatov, G.N., and White, M.M. (2000) Acetylcholine receptor gating is influenced by the polarity of amino acids at position 9' in the M2 domain. *J. Membr. Biol.*, **174**, 191–197.
21. Hanyu, N., Kuchino, Y., Nishimura, S., and Beier, H. (1986) Dramatic events in ciliate evolution: Alteration of UAA and UAG termination codons to glutamine codons due to anticodon mutations in two *Tetrahymena* tRNAs^{Gln}. *EMBO. J.*, **5**, 1307–1311.
22. Normanly, J., Kleina, L.G., Masson, J.M., Abelson, J., and Miller, J.H. (1990) Construction of *Escherichia coli* amber suppressor tRNA genes. III. Determination of tRNA specificity. *J. Mol. Biol.*, **213**, 719–726.
23. Rodriguez, E.A., Lester, H.A., and Dougherty, D.A. (2007) Improved amber and opal suppressor tRNAs for incorporation of unnatural amino acids *in vivo*. Part 2: Evaluating suppression efficiency. *RNA*, **13**, 1715–1722.
24. Unwin, N. (2005) Refined structure of the nicotinic acetylcholine receptor at 4Å resolution. *J. Mol. Biol.*, **346**, 967–989.
25. Brejc, K., van Dijk, W.J., Klaassen, R.V., Schuurmans, M., van Der Oost, J., Smit, A.B., and Sixma, T.K. (2001) Crystal structure of an ACh-binding protein reveals the ligand-binding domain of nicotinic receptors. *Nature*, **411**, 269–276.
26. Gallivan, J.P., Lester, H.A., and Dougherty, D.A. (1997) Site-specific incorporation of biotinylated amino acids to identify surface-exposed residues in integral membrane proteins. *Chem. Biol.*, **4**, 739–749.

27. Fukunaga, J., Ohno, S., Nishikawa, K., and Yokogawa, T. (2006) A base pair at the bottom of the anticodon stem is reciprocally preferred for discrimination of cognate tRNAs by *Escherichia coli* lysyl- and glutaminyl-tRNA synthetases. *Nucleic Acids Res.*, **34**, 3181–3188.
28. Wang, B., Zhou, J., Lodder, M., Anderson, R.D., 3rd, and Hecht, S.M. (2006) Tandemly activated tRNAs as participants in protein synthesis. *J. Biol. Chem.*, **281**, 13865–13868.
29. Webb, D.J., and Nuccitelli, R. (1981) Direct measurement of intracellular pH changes in *Xenopus* eggs at fertilization and cleavage. *J. Cell. Biol.*, **91**, 562–567.
30. Sasaki, S., Ishibashi, K., Nagai, T., and Marumo, F. (1992) Regulation mechanisms of intracellular pH of *Xenopus laevis* oocyte. *Biochim. Biophys. Acta.*, **1137**, 45–51.
31. Whitfield, T.T., Sharpe, C.R., and Wylie, C.C. (1994) Nonsense-mediated mRNA decay in *Xenopus* oocytes and embryos. *Dev. Biol.*, **165**, 731–734.
32. Capone, J.P., Sedivy, J.M., Sharp, P.A., and RajBhandary, U.L. (1986) Introduction of UAG, UAA, and UGA nonsense mutations at a specific site in the *Escherichia coli* chloramphenicol acetyltransferase gene: use in measurement of amber, ochre, and opal suppression in mammalian cells. *Mol. Cell. Biol.*, **6**, 3059–3067.
33. Kohrer, C., Sullivan, E.L., and RajBhandary, U.L. (2004) Complete set of orthogonal 21st aminoacyl-tRNA synthetase-amber, ochre and opal suppressor

- tRNA pairs: concomitant suppression of three different termination codons in an mRNA in mammalian cells. *Nucleic Acids Res.*, **32**, 6200–6211.
34. Zhang, Z., Alfonta, L., Tian, F., Bursulaya, B., Uryu, S., King, D.S., and Schultz, P.G. (2004) Selective incorporation of 5-hydroxytryptophan into proteins in mammalian cells. *Proc. Natl. Acad. Sci. USA*, **101**, 8882–8887.
35. Anderson, J.C., and Schultz, P.G. (2003) Adaptation of an orthogonal archaeal leucyl-tRNA and synthetase pair for four-base, amber, and opal suppression. *Biochemistry*, **42**, 9598–9608.
36. Frugier, M., Helm, M., Felden, B., Giege, R., and Florentz, C. (1998) Sequences outside recognition sets are not neutral for tRNA aminoacylation. Evidence for nonpermissive combinations of nucleotides in the acceptor stem of yeast tRNA^{Phe}. *J. Biol. Chem.*, **273**, 11605–11610.
37. Robertson, S.A., Noren, C.J., Anthony-Cahill, S.J., Griffith, M.C., and Schultz, P.G. (1989) The use of 5'-phospho-2 deoxyribocytidylylriboadenosine as a facile route to chemical aminoacylation of tRNA. *Nucleic Acids Res.*, **17**, 9649–9660.
38. Zhong, W., Gallivan, J.P., Zhang, Y., Li, L., Lester, H.A., and Dougherty, D.A. (1998) From ab initio quantum mechanics to molecular neurobiology: A cation- π binding site in the nicotinic receptor. *Proc. Natl. Acad. Sci. USA*, **95**, 12088–12093.

39. Nowak, M.W., Gallivan, J.P., Silverman, S.K., Labarca, C.G., Dougherty, D.A., and Lester, H.A. (1998) *In vivo* incorporation of unnatural amino acids into ion channels in *Xenopus* oocyte expression system. *Meth. Enzymol.*, **293**, 504–529.
40. Petersson, E.J., Shahgholi, M., Lester, H.A., and Dougherty, D.A. (2002) MALDI-TOF mass spectrometry methods for evaluation of *in vitro* aminoacyl tRNA production. *RNA*, **8**, 542–547.
41. Quick, M.W., and Lester, H.A. (1994) Methods for expression of excitability proteins in *Xenopus* oocytes. In Narahashi, T. (ed.), *Ion Channels of Excitable Cells*. Academic Press, San Diego, CA, Vol. 19, pp. 261–279.

Chapter 5

Improved Amber and Opal Suppressor tRNAs for Incorporation of Unnatural Amino Acids

In Vivo, Part 2.

Evaluating Suppression Efficiency of Suppressor tRNAs.

This chapter is reproduced, with modification, from *Improved amber and opal suppressor tRNAs for incorporation of unnatural amino acids in vivo. Part 2: Evaluating suppression efficiency*, by E. A. Rodriguez, H. A. Lester, and D. A. Dougherty, (2007) *RNA*, **13(10)**, 1715–1722. Copyright 2007 by the RNA Society.

5.1 Introduction

Incorporation of unnatural amino acids (UAAs) site-specifically into proteins is a powerful technique that is seeing increased use. Typically, the UAA is incorporated at a stop codon (nonsense suppression) using an orthogonal tRNA with an anticodon recognizing the stop codon. In higher eukaryotes, nonsense suppression by chemically aminoacylated tRNAs is mostly limited to the *Xenopus* oocyte, where injection of the mutant mRNA and suppressor tRNA chemically aminoacylated with the UAA is straightforward, and electrophysiology allows for sensitive detection of UAA incorporation (shown in Figure 3.1) (1,2). Previously only a single UAA could be incorporated into a given protein expressed in *Xenopus* oocytes, but frameshift suppression allows for the simultaneous incorporation of three UAAs, using the amber stop codon (UAG) and the quadruplet codons, CGGG and GGGU (3).

In developing optimal procedures for nonsense suppression, two key issues must be addressed. The first is “orthogonality”; the suppressor tRNA must not be recognized by any of the endogenous aminoacyl-tRNA synthetases (aaRSs) of the expression system, as this would lead to competitive incorporation of natural amino acids (aas) at the mutation site (Figure 4.1). In Chapter 4, we developed and evaluated the orthogonality of a library of suppressor tRNAs, establishing that several new mutations increase the orthogonality of amber suppressor tRNAs (Chapter 4 & (4)). The second issue is suppression efficiency. In order to produce adequate quantities of protein,

optimal use of the chemically aminoacylated tRNA is essential, as this stoichiometric reagent is often not available in large quantities. This is especially true when considering incorporation of biophysical probes for fluorescence or cross-linking strategies that often require more protein than the much-used electrophysiological approaches.

THG73, an amber suppressor tRNA from *T. thermophila* with a G73 mutation, has been used extensively to incorporate greater than 100 residues in 20 different proteins in *Xenopus* oocytes (1,2). In the present work, we evaluate a number of tRNAs for their suppression efficiency in *Xenopus* oocytes compared to THG73. We find that an *E. coli* Asn amber suppressor (ENAS) tRNA that was shown to incorporate UAAs better than THG73 *in vitro* (5) is in fact significantly less efficient than THG73 in *Xenopus* oocytes.

We also evaluate several other tRNAs that contain mutations in the 2nd to 4th positions of the acceptor stem on THG73. Our study of tRNA orthogonality showed such mutations can have interesting consequences on aminoacylation *in vivo* (Chapter 4 & (4)). A number of studies have shown that acceptor stem, anticodon stem, D stem, and T stem structure can influence suppression efficiency, often finding that replacement of non-Watson-Crick base pairs with canonical pairs increases efficiency (6–8). We therefore created a library of *T. thermophila* Gln amber suppressor (TQAS) mutants that strengthened the acceptor stem with C-G/G-C pairs and replaced the non-Watson-Crick

pair U4-G69 with C4-G69. Many of the mutant tRNAs had increased suppression efficiency over THG73, but there was a lack of correlation with the stability of the acceptor stem in *Xenopus* oocytes. Intriguingly, a mutant tRNA with U2-C71 and mutations in the 3rd and 4th positions was found to suppress UAG more efficiently than THG73 in *Xenopus* oocytes. In contrast, when creating *T. thermophila* Gln opal suppressor (TQOpS) tRNAs, the U2-C71 mutation had an adverse effect on suppression efficiency compared to C2-G71 tRNA (TQOpS'). Thus, *in vivo* nonsense suppression efficiencies of both UAG and UGA stop codons are affected by mutations in the acceptor stem of tRNAs. Overall, we have created a TQAS tRNA library that is functional in *Xenopus* oocytes and an opal suppressor tRNA for the incorporation of UAAs by chemical aminoacylation.

5.2 Results

5.2.1 Electrophysiology Assay

All experiments were performed by suppression in the nicotinic acetylcholine receptor (nAChR), which is a pentameric ion channel composed of α -, β -, γ -, and δ -subunits in the ratio of 2:1:1:1, respectively (Figure 3.3). For comparison of the suppression efficiency and the incorporation of UAAs, the well-characterized α W149 site was utilized (Figure 3.3). This site can only function with the incorporation of aromatic aas or aromatic UAAs, because it makes a cation- π interaction with ACh (9).

In order to compare suppression efficiencies across different batches of oocytes, we normalized the average maximal current for each tRNA to the average maximal current for THG73, obtained concurrently. This ratio allows for comparison of suppression efficiencies even if protein expression varies between batches of oocytes.

During the course of this research, we noticed variations in aminoacylation depending on whether the oocytes were obtained from frogs purchased from Xenopus Express or Nasco (Chapter 4 & (4)). *Xenopus laevis* frogs from Xenopus Express are caught in Africa, while Nasco frogs are bred in a laboratory and are from a similar gene pool (Linda Northey, personal communication). We therefore tested the suppression efficiency of tRNAs to see if there was any difference between Xenopus Express and Nasco oocytes. When different suppliers are used in experiments, they are explicitly labeled with each figure.

5.2.2 ENAS and ENAS A71 Suppression Efficiency

The *E. coli* Asn amber suppressor (ENAS) tRNA has been shown previously to have a greater suppression efficiency than THG73 in some instances in an *E. coli in vitro* translation system (5). ENAS has been used extensively to incorporate UAAs *in vitro* and can also tolerate substitution to the anticodon to suppress quadruplet codons for the incorporation of multiple UAAs (10,11). Therefore ENAS may be a valuable alternative to THG73 for the creation of amber and/or frameshift suppressor tRNAs *in vivo*. ENAS contains the insertion G1-C72 to allow for optimal T7 RNA polymerase transcription

and thus has an 8 base pair acceptor stem (5). THG73 and the yeast Phe frameshift suppressor tRNAs (YFFS_{CCCCG} and YFaFS_{ACCC}) are derived from eukaryotic cells and have a 7 base pair acceptor stem (3). When analyzing the structure of ENAS, we noticed that the 2nd position of the acceptor stem contains the non-Watson-Crick base pair U2-C71, and thus we created the variant ENAS A71 to form the canonical pair U2-A71 (Figure 5.1) that is present in the wild-type *E. coli* Asn tRNA (12). Suppression of α 149UAG with either ENAS-W or ENAS A71-W resulted in substantially diminished suppression efficiency (Figure 5.2), with the best case being only 26% relative to THG73-W. Overall, ENAS is not a viable alternative to THG73 for the incorporation of UAAs in *Xenopus* oocytes.

G - C	<i>C</i> C	<i>C</i> - G	G - C
U - A	U - A	U - A	<i>C</i> - G
U - G	U - G	U - G	U - G
THG73	TQAS-1	TQAS-2	TQAS-3
(-8.9)	(-2.6)	(-8.9)	(-10.9)
G - C	G - C	<i>C</i> - G	U - C
U - A	<i>C</i> - G	<i>C</i> - G	<i>C</i> - G
<i>C</i> - G	<i>C</i> - G	<i>C</i> - G	<i>C</i> - G
TQAS-4	TQAS-5	TQAS'	TQAS*
(-11.8)	(-13.9)	(-13.9)	(-10.3)
U - C	U - A	<i>C</i> - G	G - C
<i>C</i> - G	<i>C</i> - G	G - C	<i>C</i> - G
<i>C</i> - G	<i>C</i> - G	G - U	<i>C</i> - G
ENAS	ENAS A71	YFFS_{CCCCG}	YFaFS_{ACCC}
(-12.7)*	(-14.2)	(-7.5)	(-11.0)

Figure 5.1: THG73 mutations and tRNAs studied. The 2nd to 4th positions of the acceptor stem are shown for all tRNAs, with mutations in gray italics. ENAS and TQAS contain the same nucleotides at these positions. Below each tRNA is the Δ G (kcal/mol) of the entire acceptor stem calculated using mfold (13). TQOpS' and TQOpS have the same Δ G as TQAS' and TQAS, respectively. * Δ G calculated as described in Experimental Methods.

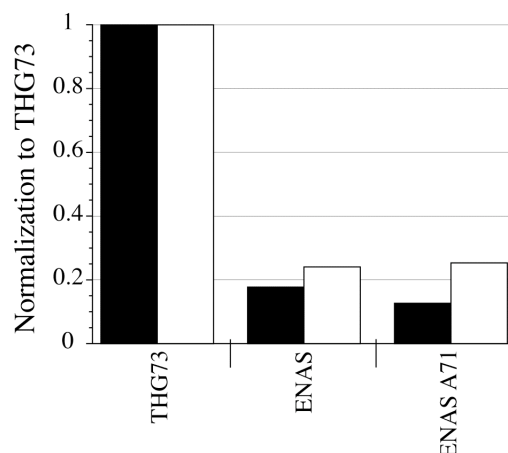


Figure 5.2: ENAS-W and ENAS A71-W suppression at α 149UAG. tRNA-W [21 ng per oocyte] average current was normalized by THG73-W average current and bars represent this average ratio (Total oocytes tested is 40, $17 > n > 11$). Black and white bars correspond to Xenopus Express and Nasco oocytes, respectively. ENAS-W and ENAS A71-W produce less than 26% of the THG73-W current when suppressing at α 149UAG. Therefore neither ENAS nor ENAS A71 offer improved suppression over THG73 in *Xenopus* oocytes.

Another option would be to create frameshift suppressors from ENAS. However, previous work has shown that frameshift suppressors derived from amber suppressor tRNAs are less efficient in rabbit reticulocyte lysate (14) and in *Xenopus* oocytes (3), so we did not screen frameshift suppressor tRNAs derived from ENAS.

5.2.3 Testing Suppression Efficiency of THG73 Acceptor Stem Mutations

We next tested the recently developed *T. thermophila* Gln amber suppressor (TQAS) tRNA library (shown in Figure 5.1) (Chapter 4 & (4)) for suppression efficiency at α 149UAG. The mutation G2C on THG73 (TQAS-1) results in the placement of C2 C71 at the 2nd position of the acceptor stem. According to a free energy calculation by

mfold (13), this causes a distortion in the acceptor stem whereby the base pairs C2-G73 and G1-C74 are formed, while the CA extension is reduced by two nucleotide lengths. Not surprisingly, TQAS-1-W shows only 1% of the suppression efficiency of THG73-W in both *Xenopus* Express and Nasco oocytes (Figure 5.3), a value only slightly greater than α 149UAG mRNA only.

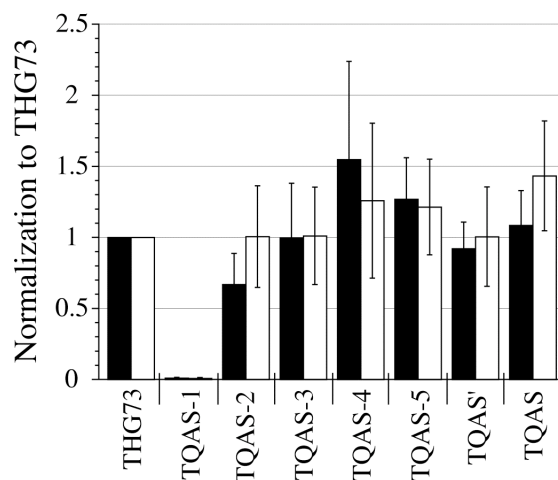


Figure 5.3: THG73 acceptor stem mutations suppressing at α 149UAG. tRNA-W [9 ng per oocyte] average currents were normalized to THG73-W average current, the ratios were averaged, and error bars represent the standard error of ≥ 3 normalization experiments ($17 > n > 8$ oocytes per experiment, for a total of 709 oocytes tested). Bar colors are the same as in Figure 5.2. TQAS-1 is nonfunctional because it represents less than 1% of THG73-W. All other tRNAs show significant current and acceptance by the translational machinery. TQAS-4-W, TQAS-5-W, and TQAS-W all have greater average suppression efficiency than THG73-W at α 149UAG.

The single helix pair mutations C2-G71 and C3-G70 (TQAS-2 and TQAS-3, respectively) show similar suppression efficiency to THG73-W in both *Xenopus* Express and Nasco oocytes (Figure 5.3). The single mutation U4C (TQAS-4) removes the non-

Watson-Crick pair at the 4th position and increases suppression efficiency by 55% and 26% in *Xenopus* Express and Nasco oocytes, respectively (Figure 5.3).

Combining the C3-G70 and C4 mutations (TQAS-5) shows an increase in suppression efficiency of 26% and 21% in *Xenopus* Express and Nasco oocytes, respectively (Figure 5.3). Combining all of the functional single helix pair mutations created TQAS', which suppresses equivalently to THG73-W even though there are five mutations in the acceptor stem (Figure 5.3). Placement of the ENAS 2nd to 4th helix pairs on THG73 created TQAS (Figure 5.1). TQAS-W is more efficient in Nasco oocytes with 43% increase in suppression efficiency, compared to 9% increase in suppression efficiency in *Xenopus* Express oocytes (Figure 5.3). The structures of Figure 5.1 constitute a library of amber suppressor tRNAs containing various acceptor stem mutations, which function *in vivo* comparably or superior to the parent tRNA, THG73.

5.2.4 Combining Mutations Causes Averaging of the Suppression Efficiency

While analyzing suppression efficiency, we noticed a trend where combining the acceptor stem mutations caused an averaging of the single mutations. Table 5.1 lists values from Figure 5.3 and also shows the average of the two normalization experiments for each tRNA-W. TQAS-5 contains the mutations from both TQAS-3 and TQAS-4 and has a suppression efficiency of 1.27 and 1.21, relative to THG73-W, in *Xenopus* Express and Nasco oocytes, respectively. The average of TQAS-3 and TQAS-4 is 1.28 and 1.14 in *Xenopus* Express and Nasco oocytes, respectively (Table 5.1). TQAS' contains the

mutations from TQAS-2, TQAS-3, and TQAS-4 and has a suppression efficiency of .92 and 1.00 in *Xenopus* Express and Nasco oocytes, respectively. The average of TQAS-2, TQAS-3, and TQAS-4 is 1.07 and 1.09 in *Xenopus* Express and Nasco oocytes, respectively (Table 5.1).

Table 5.1: THG73 acceptor stem mutations.

tRNA	ΔG	<i>Xenopus</i> Express ^a	Nasco ^a	Average ^b
THG73	-8.9	1.00	1.00	1.00
TQAS-1	-2.6	0.01	0.01	0.01
TQAS-2	-8.9	0.67	1.00	0.84
TQAS-3	-10.9	1.00	1.01	1.00
TQAS-4	-11.8	1.55	1.26	1.40
TQAS-5	-13.9	1.27 (1.28) ^c	1.21 (1.14) ^c	1.24 (1.20) ^c
TQAS'	-13.9	.92 ^d (1.07) ^c	1.00 (1.09) ^c	0.96 (1.08) ^c
TQAS	-10.3	1.09	1.43	1.26

^a Normalized values from Figure 5.3.

^b Average of *Xenopus* Express and Nasco suppression efficiency.

^c Theoretical values calculated by the average of the single mutations.

^d Normalized value is larger in Figure 5.4 with 1.15, Average 2 normalizations = 1.04 (Theoretical = 1.07).

5.2.5 Suppression Efficiency of the Acceptor Stem Mutations Does Not Correlate With Stability of the Acceptor Stem

Previous work has shown that non-Watson-Crick mutations within tRNAs have an adverse effect on suppression efficiency (6–8), but these mutations would also reduce the free energy (ΔG) of the stem regions. Therefore we calculated the ΔG of the acceptor stem using mfold (13). Mfold does not recognize the U-C pair, and therefore we calculated the ΔG as described in the Experimental Methods. Plotting the TQAS

library suppression efficiency as a function of ΔG showed no correlation in *Xenopus* Express or Nasco oocytes. TQAS-5 and TQAS' share the highest ΔG values of the library, but suppression efficiency is different due to averaging of single mutations (Table 5.1). Therefore, ΔG of the acceptor stem is not a reliable predictor for tRNA suppression efficiency under the conditions currently used.

5.2.6 Testing Amber, Opal, and Frameshift Suppression Efficiency

Incorporating multiple UAAs simultaneously requires the use of a unique stop or quadruplet codon for each UAA. Previously we have incorporated three UAAs simultaneously using THG73, YFFS_{CCCG}, and YFaFS_{ACCC} suppressor tRNAs at the corresponding suppression sites, UAG, CGGG, and GGGU (3). Suppression efficiency of the opal (UGA) codon has been shown to be comparable to the amber (UAG) codon in mammalian cells when using suppressor tRNAs that are aminoacylated by endogenous aaRSs or by the import of exogenous *E. coli* aaRSs (15,16). The opal codon has also been utilized to incorporate an UAA in mammalian cells using a tRNA/synthetase pair (17). However, when using a chemically aminoacylated tRNA, an opal suppressor that efficiently suppresses the opal codon and is adequately orthogonal is currently lacking. Sisido and coworkers tested a yeast Phe opal suppressor in rabbit reticulocyte lysate, but the suppression efficiency was only 15% (compared to 65% for the yeast Phe amber suppressor) (14). An opal suppressor created by changing the anticodon of THG73 to UCA resulted in large amounts of aminoacylation *in vitro* (5).

We replaced the anticodons of TQAS' and TQAS with UCA to create TQOpS' and TQOpS, respectively. Both TQOpS' and TQOpS show reduced aminoacylation when compared to THG73 in *Xenopus* oocytes (Chapter 4 & (4)).

Suppression efficiencies of THG73-W, TQAS'-W, TQAS-W, TQOpS'-W, TQOpS-W, YFFS_{CCCG}-W, and YFaFS_{ACCC}-W were evaluated at the α 149 suppression site (Figure 5.4). All mRNA and tRNAs were normalized to allow for identical conditions. Amber suppression is the most efficient, and the suppression efficiency follows the order of TQAS-W > TQAS'-W > THG73-W in Nasco oocytes (Figure 5.4). Opal suppression with TQOpS'-W and TQOpS-W has a suppression efficiency of 48% and 21%, respectively, relative THG73-W in Nasco oocytes (Figure 5.4). TQAS-W and TQOpS-W were not tested in *Xenopus* Express oocytes because TQAS was not originally selected as an orthogonal tRNA until screening in Nasco oocytes (Chapter 4 & (4)), but all other tRNAs show comparable suppression efficiency in both *Xenopus* Express and Nasco oocytes (Figures 5.3 & 5.4). Overall, TQOpS'-W shows the greatest opal suppression efficiency with 54% and 48% in *Xenopus* Express and Nasco oocytes, respectively, and it is a better suppressor tRNA than either frameshift suppressor (Figure 5.4). The suppression efficiency trend is thus TQAS-W > TQAS'-W > THG73-W > TQOpS'-W > YFaFS_{ACCC}-W \approx TQOpS'-W > YFFS_{CCCG}-W.

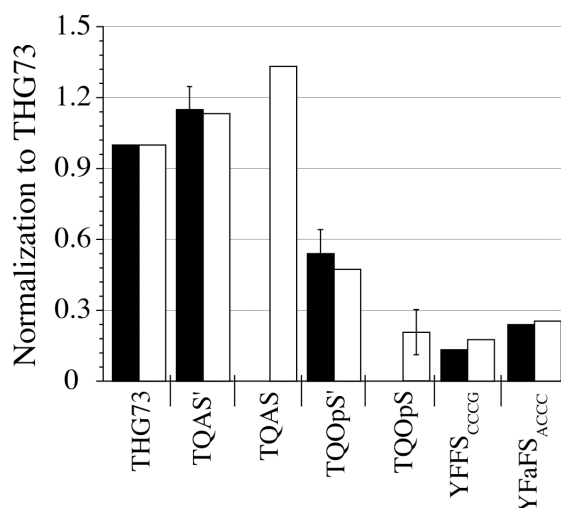


Figure 5.4: Amber, opal, and frameshift suppressor tRNAs suppression at $\alpha 149$. tRNA-W [7.5 ng per oocyte] average current was normalized to THG73-W average current. TQAS'-W, TQOpS'-W, and TQOpS-W were performed twice and error bars represent the standard error. Total oocytes tested is 161 oocytes, where $16 > n > 5$ for each experiment. Bar colors are the same as in Figure 5.2. Amber suppression (THG73-W, TQAS'-W, or TQAS-W) is the most efficient. Opal suppression is variable, with TQOpS'-W and TQOpS-W suppressing 48% and 21%, respectively, of THG73-W in Nasco oocytes. YFFS_{CCCG}-W suppresses less than YFaFS_{ACCC}-W, as previously seen in *Xenopus* oocytes (3). TQAS'-W and TQAS-W show increased suppression compared to THG73-W.

5.2.7 Natural aa and UAA Incorporation With Selected Suppressor tRNAs

To evaluate incorporation of a natural aa and an UAA using TQAS', TQAS, TQOpS', and TQOpS, we chose to suppress the well-characterized, non-promiscuous site $\alpha 149$. The Trp at $\alpha 149$ makes a cation- π interaction with ACh, and the incorporation of the UAA, 5-F-Tryptophan (WF1), results in ≈ 4 -fold increase in the EC_{50} for ACh. Incorporation of Trp at the $\alpha 149$ UAG/UGA site is a wild-type recovery experiment because it places the natural aa at the suppression site. All tRNA-W were

injected along with mRNA containing the appropriate codon at site $\alpha 149$, and the EC_{50} was determined by fits to the Hill equation (Figure 5.5). All tRNA-W showed the correct EC_{50} except for TQOpS-W, which showed a slightly higher EC_{50} than the wild-type nAChR (Figure 5.5 & Table 5.2). Injection of $\alpha 149$ UGA with TQOpS (74mer) resulted in only 3% of the current relative to the injection of $\alpha 149$ UGA with TQOpS-W and an EC_{50} for the aminoacylation product could not be determined. The natural aa must be aromatic for functional receptors when suppressing at the $\alpha 149$ site and cannot be Trp (EC_{50} would have been wild-type) and therefore is most likely either Tyr or Phe, which are expected to produce substantially higher EC_{50} values than Trp (9). However, TQOpS-W weakly suppresses the $\alpha 149$ UGA site relative to TQOpS' (Figure 5.4), which is the better suppressor tRNA in both Xenopus Express and Nasco oocytes.

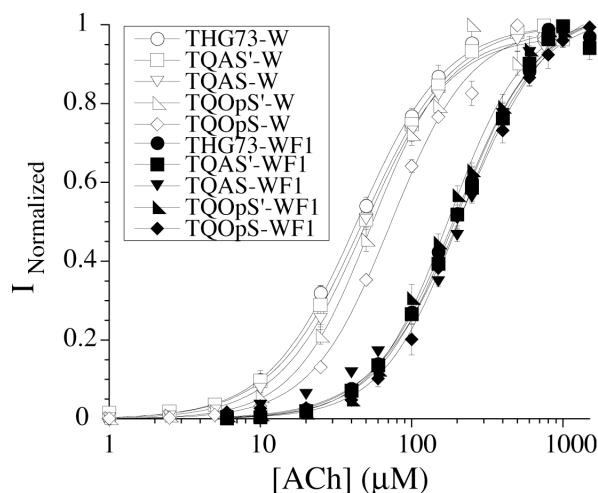


Figure 5.5: Fits to the Hill equation for wild-type recovery and UAA incorporation at $\alpha 149$. Suppression of tRNA-W [9 ng per oocyte] at $\alpha 149$ (UAG or UGA) places the natural aa and results in wild-type EC_{50} ($\approx 50 \mu\text{M}$ ACh) for all tRNAs tested except TQOpS-W (white diamond), which gave the same EC_{50} in two experiments (see Table 5.2). Incorporation of WF1 at $\alpha 149$ results in a 4-fold increase in EC_{50} ($200 \mu\text{M}$ ACh) (9). All tRNA-WF1 suppressing at $\alpha 149$ (UAG or UGA) give similar EC_{50} s and show that all tRNAs are able to incorporate an UAA. All experiments were done in Nasco oocytes and give the same EC_{50} s as W or WF1 incorporation in Xenopus Express oocytes (3). EC_{50} s, n_H , and n are listed in Table 5.2.

Table 5.2: Natural aa and UAA incorporation with THG73, TQAS', TQAS, TQOpS', and TQOpS

$\alpha 149$	tRNA	EC_{50} (theoretical) ^a	n_H	n ^b
UAG	THG73-W	44 ± 1 (50)	1.5 ± 0.05	4
UAG	TQAS'-W	48 ± 1 (50)	1.5 ± 0.05	7
UAG	TQAS-W	$49 \pm .9$ (50)	1.5 ± 0.04	8
UGA	TQOpS'-W	54 ± 5 (50)	1.7 ± 0.2	7
UGA	TQOpS-W	63 ± 2 (50)	1.7 ± 0.07	4
UAG	THG73-WF1	197 ± 9 (200)	1.6 ± 0.09	4
UAG	TQAS'-WF1	201 ± 10 (200)	1.6 ± 0.1	6
UAG	TQAS-WF1	201 ± 10 (200)	1.7 ± 0.2	8
UGA	TQOpS'-WF1	192 ± 12 (200)	1.6 ± 0.1	4
UGA	TQOpS-WF1	200 ± 4 (200)	1.8 ± 0.07	5

^a EC_{50} values from wild-type nAChR ($50 \mu\text{M}$ ACh) or THG73-WF1 ($200 \mu\text{M}$ ACh) incorporation from (9).

^b n is number of oocytes tested.

We then incorporated the UAA, WF1 at the $\alpha 149$ suppression site with the injection of tRNA-WF1 and determined the EC_{50s} (Figure 5.5 & Table 5.2). All tRNAs are able to incorporate WF1 at the $\alpha 149$ suppression and show the correct EC_{50s} (Figure 5.5 & Table 5.2). All experiments were performed in Nasco oocytes and give the same EC_{50s} as W or WF1 incorporation at $\alpha 149UAG$ in *Xenopus Express* oocytes (3). TQAS' and TQAS are both viable suppressor tRNAs for the incorporation of natural aas and UAAs, which suggests that the entire *T. thermophila* Gln amber suppressor (TQAS) tRNA library would also be able to incorporate natural aas and UAAs.

5.3 Discussion

THG73 is an amber suppressor previously shown to suppress UAAs better than a modified yeast Phe amber suppressor (MN3) in *Xenopus* oocytes (18). An *E. coli in vitro* translation has shown that ENAS suppresses better than THG73 in some instances (5). We show that in *Xenopus* oocytes ENAS and ENAS A71 both suppress less than 26% relative to THG73 (Figure 5.2). Reduced suppression efficiency may result from less acceptance of *E. coli* derived amber suppressor tRNAs and/or the extra base pair in the acceptor stem by the eukaryotic translational machinery. Therefore neither ENAS nor ENAS A71 offer an improvement over THG73. As a result, frameshift suppressor tRNAs derived from ENAS were not screened.

Interestingly, many acceptor stem mutations show no adverse effects on function, and there is no statistically significant difference in suppression efficiency in *Xenopus* Express and Nasco oocytes (Figure 5.3), which was seen for aminoacylation (Chapter 4 & (4)). Most *in vivo* assays employ suppressor tRNAs that are aminoacylated *in vivo* by endogenous or exogenous aaRS(s) (6,8,12,15,16,19,20). By chemically aminoacylating mutant suppressor tRNAs, we avoid any bias that may result from suppressor tRNAs being differentially aminoacylated. Therefore, we are able to look at mutant tRNA-W interactions with the translational machinery after aminoacylation by evaluating protein production, or suppression efficiency. All mutations to the acceptor stem of THG73, excluding the disruptive C2 C71 of TQAS-1, result in functional suppressor tRNAs, and many have improved suppression efficiency over THG73 (Figure 5.3). TQAS-4, TQAS-5, and TQAS all have increased suppression efficiency (Figure 5.3 & Table 5.1) and contain the U4C mutation, which removes a non-Watson-Crick U-G pair at the 4th position of the acceptor stem.

Previous work has established that removing non-Watson-Crick base pairs increases suppression efficiency *in vitro* and *in vivo* (6–8). Intriguingly, TQAS contains U2-C71 and results in a functional suppressor tRNA with increased suppression efficiency relative to THG73 (Figure 5.3 & Table 5.1). C-U/U-C pairs have been identified in the acceptor stems of eukaryotic tRNAs (21). However, selection schemes for orthogonal tRNA/synthetase pairs have not identified such mismatches in *E. coli*

tRNAs, even though $\approx 98.4\%$ of the randomized library would contain a mismatch (22). Therefore non-Watson-Crick base pairs are tolerated by the eukaryotic translational machinery and may serve some special function in higher eukaryotes, as previously suggested (21).

Combining the acceptor stem mutations resulted in an averaging of the suppression efficiency (Table 5.1). This result is intriguing because it reflects the interactions of the chemically aminoacylated mutant tRNA-W with proteins such as EF-1 α and the ribosome, but not with aaRSs. All mutations are in the acceptor stem (Figure 5.1) and maintain the rest of the tRNA body constant. TQAS-4 contains the single mutation U4C, which replaces the non-Watson-Crick base pair U-G, and shows the highest average suppression efficiency (Table 5.1). This mutation most likely increases interactions with EF-1 α , the ribosome, and/or another protein. However, this mutation combined with other mutations results in reduced suppression efficiency in TQAS-5, TQAS', and TQAS (Table 5.1). This clearly illustrates that the mutations are not additive and no single mutation dominates in influencing the suppression efficiency. This suggests there is no dominant protein interaction that strictly influences the suppression efficiency, but rather the ensemble of all protein interactions affects the overall suppression efficiency.

The acceptor stem ΔG does not correlate with suppression efficiency. Removal of non-Watson-Crick base pairs has been shown to increase suppression efficiency in

various regions of tRNAs (6–8), which would also increase the ΔG of the tRNA in helix forming regions. Using our TQAS library, we related suppression efficiency as a function of ΔG of the acceptor stem and found no overall trend. The replacement of the non-Watson-Crick base pair U4-G69 with C4-G69 (TQAS-4) resulted in increased average suppression efficiency, but was not significantly different from the TQAS library (Figure 5.3). TQAS-5 and TQAS' have the same ΔG (Figure 5.1), but different suppression efficiencies (Figure 5.3). This difference is caused by various combinations of single mutations that result in an averaging of suppression efficiency (Table 5.1) due to interactions with proteins in the translational machinery. Therefore, it is difficult to predict the tRNA with the best suppression efficiency just by ΔG of the acceptor stem under the conditions used in these experiments.

An efficient opal suppressor tRNA is highly desirable for the incorporation of multiple UAAs in eukaryotic cells. By replacing the anticodon of TQAS' and TQAS with UCA, we created the opal suppressors TQOpS' and TQOpS, respectively. TQOpS'-W shows suppression efficiency of $\approx 50\%$ relative to THG73-W, while TQOpS-W has a suppression efficiency of 21% (Figure 5.4). Intriguingly, the amber suppressor TQAS-W has greater suppression efficiency than TQAS'-W (Figures 5.3 & 5.4), but the opal suppressors show the reverse trend (Figure 5.4). Therefore UAG and UGA suppression shows differential preference for acceptor stem mutations. TQOpS-W suppresses better than either frameshift suppressor, YFFS_{CCCG}-W and YFaFS_{ACCC}-W

(Figure 5.4). TQOpS incorporates W and the UAA, WF1, at α 149UGA (Figure 5.5 & Table 5.2) and therefore is a viable suppressor tRNA for the incorporation of multiple UAAs *in vivo*.

TQAS' and TQAS can incorporate W and the UAA, WF1, at α 149UAG (Figure 5.5 & Table 5.2). This suggests that the entire TQAS tRNA library, excluding TQAS-1, will be able to incorporate UAAs *in vivo*. TQAS' and TQAS were specifically screened because they showed the least amount of aminoacylation in *Xenopus* Express and Nasco oocytes, respectively (Chapter 4 & (4)). Therefore both orthogonal tRNAs, in their respective genetic background, are able to incorporate UAAs. The TQAS tRNA library therefore offers a diverse range of acceptor stem mutations for the selection of orthogonal tRNAs (Chapter 4 & (4)). The TQAS library will be valuable for screening in other eukaryotic cells, where screening of randomized libraries may not be feasible.

5.4 Experimental Methods

5.4.1 Materials

All oligonucleotides were synthesized by Integrated DNA Technologies (Coralville, IA). NotI was from Roche Applied Science (Indianapolis). BamHI, EcoRI, FokI, T4 DNA ligase, and T4 RNA ligase were from NEB (Beverly, MA). Kinase Max, T7 MEGAshortscript, and T7 mMessage mMachine kits were from Ambion (Austin, TX). ACh chloride and yeast inorganic pyrophosphatase were purchased from Sigma-

Aldrich. 6-nitroveratryloxycarbonyl protected dCA-W and dCA-WF1 was prepared as reported in (9).

5.4.2 tRNA Gene Preparation and tRNA Transcription

THG73, YFFS_{CCCG}, and YFaFS_{ACCC} subcloned in the pUC19 vector were previously made (3,18). Genes for ENAS (sequence from (5)) with flanking EcoRI and BamHI overhangs were phosphorylated using Kinase Max kit, annealed, and ligated with T4 DNA ligase into EcoRI and BamHI linearized pUC19 vector as described (23). ENAS A71 (original sequence from (12) and containing the G1-C72 insertion for T7 polymerase transcription) was created by QuikChange mutagenesis on ENAS in pUC19. Acceptor stem mutations on THG73 were created by QuikChange mutagenesis and shown in Figure 5.1 (gray italics). Replacing the anticodon of TQAS' and TQAS from CUA to UCA by QuikChange mutagenesis created TQOpS' and TQOpS, respectively. All mutations were verified by DNA sequencing (California Institute of Technology Sequencing / Structure Analysis Facility). Template DNA for tRNA lacking the 3'CA was prepared by FokI digestion, and tRNA was transcribed using the T7 MEGashortscript kit with .5 μ l of yeast inorganic pyrophosphatase (40 U/ml in 75 mM Tris, 10 mM MgCl₂, and pH 7). tRNA was desalted using CHROMA SPIN-30 DEPC-H₂O columns (BD Biosciences), and concentration was determined by absorption at 260 nm.

5.4.3 nAChR Gene Preparation and mRNA Transcription

The masked α -, β -, γ -, and δ -subunits of the nAChR subcloned in the pAMV vector were previously prepared (3). All four subunits terminate with the opal (UGA) stop codon and each UGA was mutated to the ochre (UAA) codon to avoid possible suppression by TQOpS' and TQOpS. α 149(UAG, CGGG, and GGGU) were previously prepared on the masked constructs (3). α 149UGA was prepared by QuikChange mutagenesis. Mutations were verified by DNA sequencing (California Institute of Technology Sequencing / Structure Analysis Facility). DNA was linearized with NotI and mRNA was prepared with the T7 mMessage mMachine kit with .5 μ l of yeast inorganic pyrophosphatase. mRNA was purified by using the RNeasy Mini kit (Qiagen, Valencia, CA) and quantified by absorption at 260 nm.

5.4.4 ΔG Calculations of Each tRNA Acceptor Stem

The entire acceptor stem for each tRNA was used rather than the entire tRNA because only secondary interactions are determined by mfold (13) and the correct clover leaf structure was not obtained for each tRNA. The entire acceptor stem—seven helix pairs for THG73, TQAS library, YFFS_{CCCG}, and YFaFS_{ACCC}, and eight helix pairs for ENAS and ENAS A71 (due to the insertion of G1-C72 for T7 RNA polymerase transcription) with a U₈ linker—was utilized, and default parameters (37 °C) of mfold were used to calculate ΔG s (13) (values listed for each tRNA acceptor stem in Figure 5.1). For TQAS and ENAS, a U-C pair is present in the acceptor stem and this pair is

not recognized by mfold (13), even though the U-C pair can form hydrogen bonding interactions in RNA helices (24–26). Previously, non-Watson-Crick base pair thermodynamics (37 °C) were obtained by determining the stabilizing/destabilizing effect upon placement in a RNA helix (seven base pairs total with mismatch) and relating those parameters to a reference RNA helix (six base pairs) (26). The U-C pair was removed to create a reference RNA helix and the ΔG of TQAS($\Delta U2-C71$) and ENAS($\Delta U2-C71$) with a U_8 linker was determined using mfold. 0.26 kcal/mol was added to the determined ΔG value to obtain the number listed in Figure 5.1 for TQAS and ENAS. 0.26 kcal/mol is the average value of two separate measurements of CU/UC pairs in RNA helices and was used because the exact nucleotide sequence was not measured (26). The ΔG for TQOpS' and TQOpS are the same for TQAS' and TQAS, respectively.

5.4.5 dCA-W and dCA-WF1 Ligation to Suppressor tRNAs

75 μM (used instead of 300 μM because there was no change in ligation efficiency) of 6-nitroveratryloxycarbonyl protected dCA-W or dCA-WF1 were coupled to suppressor tRNAs by using T4 RNA ligase for 30 min as previously reported (23,27), desalted using CHROMA SPIN-30 DEPC-H₂O columns, and quantified by absorption at 260 nm. tRNA ligation efficiency was qualitatively determined by MALDI mass spectrometry (27), and all tRNA ligations were identical within each prepared group and greater than 80%.

5.4.6 *In Vivo* Suppression Experiments

Prior to *in vivo* suppression experiments, all tRNAs and mRNAs were simultaneously made and normalized by UV and densitometric analysis using AlphaEaseFC Stand Alone (Alpha Innotech, San Leandro, CA). Stage VI oocytes of *Xenopus laevis* were prepared as described (28). All tRNAs were refolded at 65 °C for 2 min and 6-nitroveratryloxycarbonyl protected dCA-W or dCA-WF1 was deprotected for 5 min by UV irradiation before injection (18). Oocytes were injected with 50 nl of mRNA alone or with tRNA and incubated at 18 °C for 44–52 h. 20 ng of mRNA in a subunit ratio of 10:1:1:1 for α 149UAG: β : γ : δ was injected in Figures 5.2, 5.3, and 5.5 using the same ratio, but 40 ng and 60 ng of mRNA, respectively, was injected per oocyte. In Figure 5.4, 40 ng of mRNA in a subunit ratio of 10:1:1:1 for α 149(UAG, UGA, CGGG, or GGGU): β : γ : δ . Amounts of tRNA injected are listed with the legend of each figure.

5.4.7 Electrophysiology

Recordings employed two-electrode voltage clamp on the OpusXpress 6000A (Molecular Devices). ACh was stored at -20 °C as a 1 M stock, diluted in Ca²⁺-free ND96, and delivered to oocytes by computer-controlled perfusion system. For all experiments, the holding potential was -60 mV. Dose-response data was obtained from at least eleven ACh concentrations and all tRNA suppression experiments were tested with a single 1 mM ACh dose. Dose-response relations were fit to the Hill equation to

determine the EC₅₀ and Hill coefficient (n_H). All reported values are represented as a mean \pm SE of the tested oocytes (number of oocytes (n) is listed with each figure).

5.5 References

1. Dougherty, D.A. (2000) Unnatural amino acids as probes of protein structure and function. *Curr. Opin. Biotechnol.*, **4**, 645–652.
2. Beene, D.L., Dougherty, D.A., and Lester, H.A. (2003) Unnatural amino acid mutagenesis in mapping ion channel function. *Curr. Opin. Neurobiol.*, **13**, 264–270.
3. Rodriguez, E.A., Lester, H.A., and Dougherty, D.A. (2006) *In vivo* incorporation of multiple unnatural amino acids through nonsense and frameshift suppression. *Proc. Natl. Acad. Sci. USA*, **103**, 8650–8655.
4. Rodriguez, E.A., Lester, H.A., and Dougherty, D.A. (2007) Improved amber and opal suppressor tRNAs for incorporation of unnatural amino acids *in vivo*. Part 1: Minimizing misacylation. *RNA*, **13**, 1703–1714.
5. Cload, S.T., Liu, D.R., Froland, W.A., and Schultz, P.G. (1996) Development of improved tRNAs for *in vitro* biosynthesis of proteins containing unnatural amino acids. *Chem. Biol.*, **3**, 1033–1038.
6. Hou, Y.M., and Schimmel, P. (1992) Novel transfer RNAs that are active in *Escherichia coli*. *Biochemistry*, **31**, 4157–4160.

7. Ohtsuki, T., Manabe, T., and Sisido, M. (2005) Multiple incorporation of non-natural amino acids into a single protein using tRNAs with non-standard structures. *FEBS Lett.*, **579**, 6769–6774.
8. Buttcher, V., Senger, B., Schumacher, S., Reinbolt, J., and Fasiolo, F. (1994) Modulation of the suppression efficiency and amino acid identity of an artificial yeast amber isoleucine transfer RNA in *Escherichia coli* by a G-U pair in the anticodon stem. *Biochem. Biophys. Res. Commun.*, **200**, 370–377.
9. Zhong, W., Gallivan, J.P., Zhang, Y., Li, L., Lester, H.A., and Dougherty, D.A. (1998) From ab initio quantum mechanics to molecular neurobiology: A cation- π binding site in the nicotinic receptor. *Proc. Natl. Acad. Sci. USA*, **95**, 12088–12093.
10. Murakami, H., Ohta, A., Ashigai, H., and Suga, H. (2006) A highly flexible tRNA acylation method for non-natural polypeptide synthesis. *Nat. Methods*, **3**, 357–359.
11. Murakami, H., Kourouklis, D., and Suga, H. (2003) Using a solid-phase ribozyme aminoacylation system to reprogram the genetic code. *Chem. Biol.*, **10**, 1077–1084.
12. Kleina, L.G., Masson, J.M., Normanly, J., Abelson, J., and Miller, J.H. (1990) Construction of *Escherichia coli* amber suppressor tRNA genes. II. Synthesis of additional tRNA genes and improvement of suppressor efficiency. *J. Mol. Biol.*, **213**, 705–717.

13. Zuker, M. (2003) Mfold web server for nucleic acid folding and hybridization prediction. *Nucleic Acids Res.*, **31**, 3406–3415.
14. Taira, H., Fukushima, M., Hohsaka, T., and Sisido, M. (2005) Four-base codon-mediated incorporation of non-natural amino acids into proteins in a eukaryotic cell-free translation system. *J. Biosci. Bioeng.*, **99**, 473–476.
15. Capone, J.P., Sedivy, J.M., Sharp, P.A., and RajBhandary, U.L. (1986) Introduction of UAG, UAA, and UGA nonsense mutations at a specific site in the *Escherichia coli* chloramphenicol acetyltransferase gene: use in measurement of amber, ochre, and opal suppression in mammalian cells. *Mol. Cell. Biol.*, **6**, 3059–3067.
16. Kohrer, C., Sullivan, E.L., and RajBhandary, U.L. (2004) Complete set of orthogonal 21st aminoacyl-tRNA synthetase-amber, ochre and opal suppressor tRNA pairs: concomitant suppression of three different termination codons in an mRNA in mammalian cells. *Nucleic Acids Res.*, **32**, 6200–6211.
17. Zhang, Z., Alfonta, L., Tian, F., Bursulaya, B., Uryu, S., King, D.S., and Schultz, P.G. (2004) Selective incorporation of 5-hydroxytryptophan into proteins in mammalian cells. *Proc. Natl. Acad. Sci. USA*, **101**, 8882–8887.
18. Saks, M.E., Sampson, J.R., Nowak, M.W., Kearney, P.C., Du, F.Y., Abelson, J.N., Lester, H.A., and Dougherty, D.A. (1996) An engineered *Tetrahymena* tRNA^{Gln} for *in vivo* incorporation of unnatural amino acids into proteins by nonsense suppression. *J. Biol. Chem.*, **271**, 23169–23175.

19. Jahn, M., Rogers, M.J., and Soll, D. (1991) Anticodon and acceptor stem nucleotides in tRNA^{Gln} are major recognition elements for *E. coli* glutaminyl-tRNA synthetase. *Nature*, **352**, 258–260.
20. McClain, W.H., Schneider, J., Bhattacharya, S., and Gabriel, K. (1998) The importance of tRNA backbone-mediated interactions with synthetase for aminoacylation. *Proc. Natl. Acad. Sci.*, **95**, 460–465.
21. Goodenbour, J.M., and Pan, T. (2006) Diversity of tRNA genes in eukaryotes. *Nucleic Acids Res.*, **34**, 6137–6146.
22. Anderson, J.C., and Schultz, P.G. (2003) Adaptation of an orthogonal archaeal leucyl-tRNA and synthetase pair for four-base, amber, and opal suppression. *Biochemistry*, **42**, 9598–9608.
23. Nowak, M.W., Gallivan, J.P., Silverman, S.K., Labarca, C.G., Dougherty, D.A., and Lester, H.A. (1998) *In vivo* incorporation of unnatural amino acids into ion channels in *Xenopus* oocyte expression system. *Meth. Enzymol.*, **293**, 504–529.
24. Tanaka, Y., Kojima, C., Yamazaki, T., Kodama, T.S., Yasuno, K., Miyashita, S., Ono, A., Ono, A., Kainosho, M., and Kyogoku, Y. (2000) Solution structure of an RNA duplex including a C-U base pair. *Biochemistry*, **39**, 7074–7080.
25. Holbrook, S.R., Cheong, C., Tinoco, I., Jr., and Kim, S.H. (1991) Crystal structure of an RNA double helix incorporating a track of non-Watson-Crick base pairs. *Nature*, **353**, 579–581.

26. Kierzek, R., Burkard, M.E., and Turner, D.H. (1999) Thermodynamics of single mismatches in RNA duplexes. *Biochemistry*, **38**, 14214–14223.
27. Petersson, E.J., Shahgholi, M., Lester, H.A., and Dougherty, D.A. (2002) MALDI-TOF mass spectrometry methods for evaluation of *in vitro* aminoacyl tRNA production. *RNA*, **8**, 542–547.
28. Quick, M.W., and Lester, H.A. (1994) Methods for expression of excitability proteins in *Xenopus* oocytes. In Narahashi, T. (ed.), *Ion Channels of Excitable Cells*. Academic Press, San Diego, CA, Vol. 19, pp. 261–279.

Chapter 6

Bioorthogonal Labeling of *p*-AcPhe Incorporated in

the Nicotinic Acetylcholine Receptor

in *Xenopus* Oocytes

&

Western Blot Determination of the

Subunit Stoichiometry of

the Nicotinic Acetylcholine Receptor

in *Xenopus* Oocytes

6.1 Introduction

Recent work has established new techniques to specifically label proteins *in vitro* and *in vivo* using genetically encoded sequences or small molecules with chemical functionalities unique from those found in living cells. These peptide sequences, unnatural sugar analogs, unnatural biotin moieties, and unnatural amino acids (UAAs) allow for specific labeling by a “bioorthogonal” small molecule reporter through enzymatic or chemical reaction (1). The tetracysteine motif has been utilized to selectively react with bisarsenical fluorescent dyes, such as FAsH and ReAsH (2,3). A 15 amino acid sequence has been utilized to attach a biotin or an unnatural biotin that contains a ketone moiety to a protein using the *E. coli* biotin ligase (4,5). Unnatural sugar analogs with ketones, aldehydes, and azides have been incorporated *in vivo* using endogenous enzymes and labeled with biotin for purification or fluorophores for imaging (1,6–12). UAAs have been incorporated *in vivo* using endogenous aminoacyl tRNA-synthetases, mutant aminoacyl tRNA-synthetases, or an orthogonal tRNA/synthetase pair to incorporate ketones, aldehydes, diketones, azides, and alkynes and labeled with biotin and fluorophores (13–22).

The ketone functionality has been used extensively to label glycosylated proteins containing unnatural sugar analogs and proteins containing UAAs. The ketone is biorestricted in that it is bioorthogonal only on the cell surface because the interior of the cell contains acetylated proteins and keto/aldehydic metabolites (1). The ketone has been used extensively to label proteins *in vitro* that are purified or in crude cell lysates from *E. coli*, HEK 293T cells, and rat neurons (4,6,19,20). The ketone has also been used to label proteins on the cell surface of *E. coli*, jurkat cells, HL-60 cells, and HeLa cells

(4,10,11,13,20). In this research, we incorporated the UAA *p*-Acetyl-L-phenylalanine (*p*-AcPhe) into the α -subunit of the mouse muscle nicotinic acetylcholine receptor (nAChR) expressed in *Xenopus* oocytes and attempted to site-specifically label with biotin hydrazide and cyanine5.5 (Cy5.5) hydrazide.

Many membrane proteins form multimeric complexes, and the stoichiometry is precisely regulated by the insertion into the endoplasmic reticulum, folding transitions, post-translational modification, interactions with other subunits and/or chaperones, forming the final oligomeric complex (for many membrane proteins), subsequent transport to the golgi (where further oligomerization can take place), and export to the cell membrane (where further oligomerization can also occur) (23–29). To add further complexity, many ion channels are heteromeric and contain different subunits. For example, for the nAChRs there are ten α -subunits (α_1 - α_{10}), four β -subunits (β_1 - β_4), a γ -subunit, a δ -subunit, and an ϵ -subunit. These subunits can form homomeric channels ($5\alpha_7$) and heteromeric channels ($2\alpha_1:\beta_1:\gamma:\delta$, $\alpha_1:\beta_1:\gamma:\delta:\epsilon$, $2\alpha_3:3\beta_4$, $3\alpha_4:2\beta_2$, and $2\alpha_4:3\beta_2$) (30). For seventeen genes there is a possibility of 283,985 combinations, but most are not biologically relevant.

Determining subunit stoichiometry in ion channels can be complicated. Classically, macroscopic or single-channel electrophysiology recordings have been used to predict the subunit composition when analyzing inactivation or expressing wild-type and mutant channels with altered conductances (31–33). However, electrophysiology can't always accurately predict the subunit stoichiometry of ion channels. For example, cyclic nucleotide-gated (CNG) channels were thought to have a stoichiometry of 2CNGB1:2CNGA2 (34), but recent FRET experiments (35) and biochemical analysis

(36) have shown that the channels have a stoichiometry of 3CNGA1:CNGA2. Recent experiments have attached GFP to ion channels and used time-resolved photobleaching to determine the stoichiometry of the NMDAR (2NR1:2NR3B); this was confirmed by verification of known stoichiometries of 2NR1:2NR2B and 3CNGA1:CNGA2 (37).

As the Dougherty and Lester labs have started studying neuronal nAChRs and γ -aminobutyric acid receptors (GABARs), subunit stoichiometry has become a concern. In this research, we hoped to use the known stoichiometry of the mouse muscle nAChR ($2\alpha:\beta:\gamma:\delta$) and try to attain this stoichiometry by densitometric analysis of Western blots. Using subunits containing the HA tag in the M3-M4 loop, it was hoped that the HA antibody would bind similarly to each subunit and insertion of nine amino acids (HA tag) would not perturb ion channel function as much as ≈ 240 amino acids for GFP. Previous work has shown that the nAChR subunits degrade rapidly when not assembled in ion channel complexes (27,28,38). We hoped that by using whole cells and looking at the total amount of each subunit protein, we would be able to determine the subunit ratio of the nAChR and apply this technology to the neuronal nAChRs and GABARs.

6.2 Results

6.2.1 Screening Sites For Aminoacylation of tRNAs, Read-Through, and UAA Incorporation

We chose to screen α D70 and aligned sites in the mouse muscle nAChR (Figure 6.1). These sites were chosen because the large UAA biocytin could be incorporated efficiently at α D70 and subsequently labeled with streptavidin without a significant shift in EC_{50} (39). α D70 is part of the main immunogenic region (MIR) of the nAChR, and this region binds many antibodies, including those associated with myasthenia gravis (a human autoimmune disease) (40,41). The α D70 site can therefore tolerate a large UAA, detection by streptavidin and antibodies shows the region is highly accessible, and should be accessible to small molecule, bioorthogonal reporters. The cryo-EM images of the *Torpedo* nAChR subsequently followed the biochemical work and clearly shows that MIR is highly exposed (Figure 6.1) (42). The α D70 aligned sites were chosen because it was hoped that these sites would incorporate UAAs efficiently and allow for multiple UAA incorporation for fluorescent resonance energy transfer (FRET) experiments. The β A19' site was also chosen because mutating this site to Cys allows for labeling when the nAChR is in the open state (43) and the site tolerates the incorporation of a large fluorescent UAA, Lys(BODIPYFL) (44).

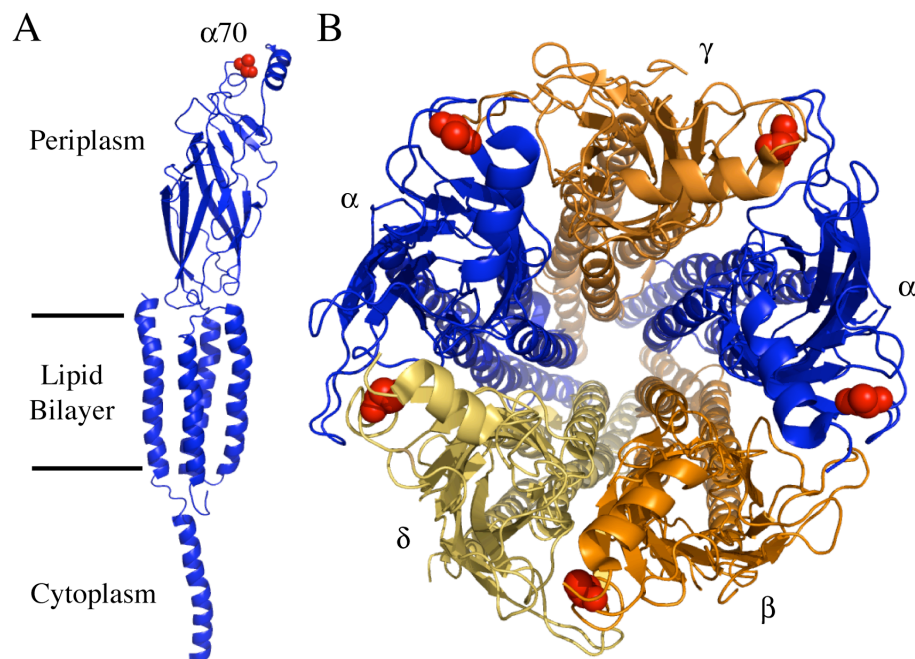


Figure 6.1: $\alpha 70$ and aligned positions in the nAChR. (A) The α -subunit of the nAChR is shown with the lipid bilayer as a reference. $\alpha D70$ is shown in the extracellular domain in red. Incorporation of the UAA biocytin allows for labeling with radioactive streptavidin (39). This residue is part of the MIR and accessible to antibodies. (B) A top view of the nAChR with the residues aligned with $\alpha D70$ shown in red. The amino acids at these positions are as follows: $\beta A70$, $\gamma K70$, and $\delta N70$ in the mouse muscle nAChR (residues shown are from the *Torpedo* nAChR). Image created from 2BG9.pdb (42).

In order to screen the selected sites, the amber (UAG), opal (UGA), and quadruplet (GGGU) codons were utilized to prepare for multiple UAA incorporation. THG73 is an amber suppressor tRNA used extensively to incorporate UAAs in *Xenopus* oocytes (45–47). THG73 is aminoacylated with Gln in *Xenopus* oocytes when incubated for > 1 day and large quantities of tRNA are used (48,49). TQAS is an amber suppressor tRNA created from THG73 by the placement of four mutations in the acceptor stem (shown in Figure 4.3), is aminoacylated much less than THG73, and shows similar suppression efficiency in *Xenopus* oocytes from Nasco (48,50). TQAS' is an amber suppressor tRNA created from THG73 by the placement of five mutations in the acceptor stem (shown in Figure 4.3), is aminoacylated comparably to THG73, and shows similar

suppression efficiency in *Xenopus* oocytes from Nasco (48,50). YFaFS_{ACCC} is a frameshift suppressor tRNA (shown in Figure 3.2) shown to be the most orthogonal suppressor tRNA tested in *Xenopus* oocytes, but has a suppression efficiency of $\approx 30\%$ when compared to the amber suppressor tRNAs (48–50). TQOpS' is an opal suppressor tRNA created from THG73 by the placement of five mutations in the acceptor stem and containing the anticodon UCA (shown in Figure 4.3), is aminoacylated much less than THG73, and is capable of incorporating an UAA (48,50).

Table 6.1 shows aminoacylation of tRNAs, read-through, and UAA incorporation experiments at the selected sites (experimental concept discussed in Chapter 4 and shown in Figure 4.1). In the experiments, THG73 was added in large quantities and incubated for 2 days in order to obtain aminoacylation with Gln *in vivo*. Any site that could incorporate a large UAA should also incorporate Gln. For UAA incorporation, 5-F-Tryptophan (WF1) (chemical structure in Figure 3.2) was chemically ligated to the suppressor tRNA.

$\alpha 70\text{UAG}$ shows large aminoacylation product when incubated with THG73, but this aminoacylation product is reduced when incubated with TQAS (Table 6.1). $\alpha 70\text{UAG}$ mRNA injected alone shows little read-through of the UAG stop codon (Table 6.1) and therefore this site is optimal for the incorporation of UAAs. $\beta 70\text{UAG}$ and $\beta 70\text{GGGU}$ show extremely large read-through when mRNA is injected alone, which is very rare, and therefore this site is not useful for UAA incorporation (Table 6.1). THG73 is aminoacylated similarly to TQAS' at $\beta 70\text{UAG}$ in Nasco oocytes (Table 6.1). TQAS and YFaFS_{ACCC} are aminoacylated much less and close to the $\beta 70\text{XXX(X)}$ mRNA alone (Table 6.1). Interestingly, TQAS'-WF1 shows a 180% increase in current compared to

THG73 (Table 6.1) and shows that UAA incorporation by the chemically aminoacylated tRNA is much more efficient at producing functional channels than THG73 being aminoacylated with Gln *in vivo*, which is in agreement with previous experiments (45,48). The β 19'XXX(X) position shows large amounts of read-through with large quantities of mRNA injected alone, but much less than the β 70 position (Table 6.1). THG73 also shows a reduction of $\approx 79\%$ in current when tested at β 19'UAG when compared to β 70UAG (Table 6.1). TQAS and YFaFS_{ACCC} also show larger amounts of aminoacylation, relative to THG73, at the β 19' position when compared to the β 9' position (see Chapter 4 and (48,49)). Therefore the β 19' position is not optimal for UAA and requires the use of less mRNA to avoid read-through and use of orthogonal tRNAs to avoid aminoacylation signals that can be comparable to suppression, which has been done experimentally for the incorporation of a fluorescent UAA (44).

δ 69 experiments show little current with suppressor tRNAs that are not chemically aminoacylated and with the injection of mRNA only (Table 6.1). THG73 injected with δ 69UAG is comparable to mRNA only, indicating that the site doesn't tolerate the incorporation of Gln (Table 6.1). The δ 69 position is not useful for the incorporation of UAAs. δ 70UGA also shows very little current with the injection of TQOpS', TQOpS'-WF1, and mRNA alone (Table 6.1). Intriguingly, there is an 80% reduction in current when TQOpS'-WF1 is injected relative to TQOpS', which is not chemically aminoacylated, (Table 6.1) and shows that WF1 is not tolerated at δ 70UGA. The δ 70UGA position is not optimal for incorporation of UAAs. The optimum site screened was α 70UAG because it showed very little read-through when mRNA alone

was injected and low aminoacylation currents were obtained with TQAS. α 70UAG was therefore chosen for further experiments.

Table 6.1: Expression tests at the α D70 aligned positions and β A19'.

mRNA	tRNA	Norm	n ^a
α 70UAG	THG73	1.0 ^b	16
α 70UAG	TQAS	0.27	15
α 70UAG		0.017	16
β 70UAG	THG73	1.0 ^c	16
β 70UAG	THG73-dCA	1.0 ^d	11
β 70UAG	TQAS'-dCA	1.1	12
β 70UAG	TQAS	0.40	12
β 70UAG	TQAS'-WF1	2.8	12
β 70UAG		0.31	14
β 70GGGU	YFaFS _{ACCC}	0.41	15
β 70GGGU		0.40	16
β 19'UAG	THG73	1.0 ^e	16
β 19'UAG	TQAS	0.36	15
β 19'UAG		0.23	16
β 19'GGGU	YFaFS _{ACCC}	0.24	16
β 19'GGGU		0.14	16
δ 69UAG	THG73	1.0 ^f	16
δ 69UAG	TQAS	0.82	16
δ 69UAG		0.92	16
δ 69GGGU	YFaFS _{ACCC}	0.64	15
δ 69GGGU		1.0	16
δ 70UGA	TQOpS'-dCA	1.0 ^g	7
δ 70UGA	TQOpS'-WF1	0.20	7
δ 70UGA		0.54	6

^a Number of oocytes tested.

^b Average $I_{\max} = -19 \mu\text{A}$

^c Average $I_{\max} = -15 \mu\text{A}$

^d Average $I_{\max} = -13 \mu\text{A}$

^e Average $I_{\max} = -2.9 \mu\text{A}$

^f Average $I_{\max} = -0.26 \mu\text{A}$

^g Average $I_{\max} = -0.31 \mu\text{A}$

6.2.2 Suppression of $\alpha 70$ UAG with TQAS-Biotin

In order to directly detect an UAA incorporated into the nAChR by Western blot, large amounts of protein are needed, which usually requires multiple injections, large amounts of tRNA-UAA, choosing only oocytes that are expressing $> 10 \mu\text{A}$, and removing membranes from 10–25 oocytes for each gel lane (51,52). Multiple injections are not optimal because oocyte death increases with the number of injections and requires large amounts of tRNA-UAA. Manually removing membranes from oocytes is also tedious and time consuming for a large number of samples and variability can arise from incomplete removal of the membrane. For the following Western blots, saturating amounts of TQAS-Biotin were prepared and only a single injection was performed with large amounts of mRNA. Biotin is a difficult UAA to incorporate *in vitro* and *in vivo* (39,53), but the average maximal current obtained from a single injection of $\alpha 70$ UAG + TQAS-Biotin was $-10.4 \mu\text{A}$ (23% relative to wild-type current with half the mRNA), which is more than sufficient for detection by Western blot. Whole-cell detection of an UAA was also explored because it requires fewer oocytes for each lane, is not as time consuming, and there is less variability.

Figure 6.2 shows detection of $\alpha 70$ Biotin using four whole oocytes (Figure 6.2, A & B) or twenty oocyte membranes (Figure 6.2, C & D). The Western blots show that many endogenous proteins are biotinylated in uninjected *Xenopus* oocytes (Figure 6.2, A, Lanes 2–4, and Figure 6.2, C, Lanes 2–4), but the endogenous proteins don't overlap with the α -subunit of the nAChR (Figure 6.2, B & D). Using four oocytes per lane, the UAA biotin can be detected in three separate samples (Figure 6.2, A, Lanes 5–7), and no band is observed at the same molecular weight for uninjected oocytes (Figure 6.2, A,

Lanes 2–4) or wild-type nAChR (Figure 6.2, A, Lanes 8–10). The α -subunit is clearly detected using the HA tag with four whole cells for α 70Biocytin and for the wild-type nAChR (Figure 6.2, B, Lanes 5–10). By the whole-cell Western blot, the suppression efficiency of TQAS-Biocytin at α 70UAG is 8.7% relative to the wild-type nAChR, which is not an ideal comparison because the wild-type nAChR has only half the mRNA of the suppression experiment.

Manually removing the oocyte membranes shows decreased amounts of endogenous biotinylated proteins (Figure 6.2, C, Lanes 2–10) and therefore most of the biotinylated proteins are not associated with the membrane surface. α 70Biocytin is clearly visualized only in the membrane preparation (Figure 6.2, C, Lane 7) and there is no α 70Biocytin detected in the supernatant (Figure 6.2, C, Lanes 5–6). The α -subunit is clearly visualized in the membrane preparation of both α 70Biocytin and the wild-type nAChR (Figure 6.2, D, Lanes 7 & 10), but the α -subunit is also visible in the supernatant of the wild-type nAChR (Figure 6.2, D, Lanes 8–9). This is most likely caused by the presence of 0.07% SDS in the hypotonic solution used to remove the oocyte membranes and may only be visible in the wild-type nAChR due to the large amount of α -subunit present. By manually removing the membrane of the oocytes, the suppression efficiency of TQAS-Biocytin at α 70UAG is 58% relative to wild-type nAChR, which has half the amount of mRNA. Overall the Western blots of the whole cell homogenization and manually removed membranes are comparable, but α 70Biocytin shows a stronger signal in the whole cell preparation with only four cells (Figure 6.2, A, Lanes 5–7) compared to the signal from biocytin from twenty manually removed membranes (Figure 6.2, C, Lane 7). Therefore, whole-cell homogenization was used for the remainder of the Western

blots because of stronger signal, ease of experiments, and to avoid loss of protein that can cause variability.

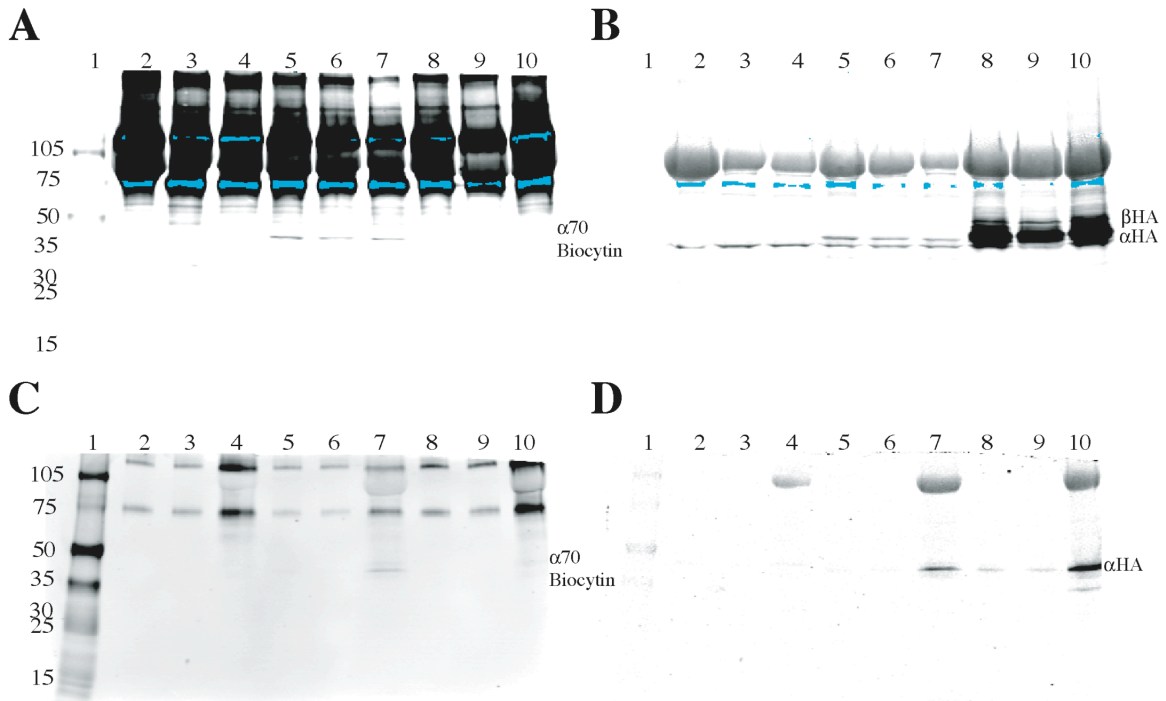


Figure 6.2: Detection of $\alpha 70$ Biocytin by Western blot. (A) Whole-cell detection of $\alpha 70$ Biocytin. (B) Whole-cell detection of HA tag. (A & B) Lane 1, molecular weight maker. Lanes 2–4, uninjected oocytes. Lanes 5–7, are $\alpha_{\text{NHA}} 70$ UAG + TQAS-Biocytin. Lanes 8–10 are α_{HA} and β_{HA} . Each lane contains four homogenized oocytes. Blue bands in A and B represent pixels saturated by detection with Streptavidin-680. (C) Membrane detection of $\alpha 70$ Biocytin. (D) Membrane detection of HA tag. (C & D) Lane 1, molecular weight marker. Lanes 2 and 3, supernatant of uninjected oocytes. Lane 4, membrane preparation of uninjected oocytes. Lanes 5 and 6, supernatant of $\alpha_{\text{NHA}} 70$ UAG + TQAS-Biocytin. Lane 7, membrane preparation of $\alpha_{\text{NHA}} 70$ UAG + TQAS-Biocytin. Lanes 8 and 9, supernatant of α_{HA} . Lane 10, membrane preparation of α_{HA} . Twenty oocyte membranes were manually stripped in a low detergent, hypotonic solution and placed in an eppendorf. Membranes were pelleted by centrifugation and the supernatant is the soluble fraction. Numbers on the left are molecular weight markers (KD).

6.2.3 Analysis of ^{125}I -Streptavidin and ^{125}I - α -Bungarotoxin Binding to *Xenopus* Oocytes Expressing Wild-Type nAChR and UAA Incorporation of Biocytin

Previous experiments identified significant binding of ^{125}I -Streptavidin to oocytes expressing $\alpha 70\text{UAG} + \text{THG73-Biocytin}$, but there was a lack of significant binding to $\alpha 76\text{UAG} + \text{THG73-Biocytin}$ (39). Using Dr. Justin Gallivan's lab notebook, I reanalyzed all of the experiments performed to gain further insights on the amount of endogenous biotinylated protein on the *Xenopus* oocyte surface and to obtain information on unpublished results. All experiments were performed previously by Dr. Gallivan and unfortunately the health of the oocytes and expression of nAChR with different batches of oocytes was not always available.

Figure 6.3 shows the analysis of ^{125}I -Streptavidin and ^{125}I - α -Bungarotoxin binding to oocytes expressing wild-type nAChR, mRNA with the amber (UAG) codon at the site of interest, incorporation of natural amino acids or UAAs by nonsense suppression, and biocytin incorporated at various positions. Data are given as a ratio of the average signal of the tested sample divided by the average signal of the blank. Figure 6.3 shows there is ≈ 2 -fold increase in signal when ^{125}I -Streptavidin is used to label uninjected oocytes, oocytes injected with mRNA only, and mRNA + THG73 (dCA or dCA-X, where X is Tyr, *p*-AcPhe, or ketoTyr). The suppression of THG73-Biocytin at all positions other than $\alpha 70\text{UAG}$ showed no significant increase in radioactive signal (Figure 6.3, orange bar, left), in agreement with published experiments (39). Only suppression of $\alpha 70\text{UAG} + \text{THG73-Biocytin}$ resulted in significant radioactive signal (Figure 6.3), which is also in agreement with published experiments (39). Therefore, endogenous biotinylated proteins may be present on the extracellular membrane of *Xenopus* oocytes, as shown by the

increase in radioactive signal, or this may be due to nonspecific binding of ^{125}I -Streptavidin to the membrane surface.

Two ^{125}I - α -Bungarotoxin molecules are expected to bind a single nAChR receptor because there are two α -subunits (54). The labeling of ^{125}I - α -Bungarotoxin and ^{125}I -Streptavidin is similar on uninjected oocytes (Figure 6.3, red bars) even though ≈ 3 times greater concentration was used for ^{125}I - α -Bungarotoxin labeling (39). Intriguingly, the ^{125}I - α -Bungarotoxin radioactive signal is increased for all injections and there is a greater difference over uninjected oocytes when compared to ^{125}I -Streptavidin labeling (Figure 6.3). mRNA only (for all sites tested in (39)) shows an increase in ^{125}I - α -Bungarotoxin binding and suggests that the read-through product is accessible on the surface and in agreement with electrophysiology data for $\alpha 70\text{UAG}$ shown in Table 6.1. mRNA + THG73-dCA also shows a significant increase in labeling and is in agreement with functional channels on the surface (Table 6.1). Incorporation of *p*-AcPhe, ketoTyr, or Tyr by THG73 results in the highest labeling and shows the average suppression efficiency at various sites is much greater than THG73-Biocytin at various sites (Figure 6.3, right, light-green bar compared to orange bar). $\alpha 70\text{UAG}$ + THG73-Biocytin shows robust binding of ^{125}I - α -Bungarotoxin, but suppression of THG73-Biocytin at other sites shows little channel expression by electrophysiology (39) and no statistical difference of ^{125}I - α -Bungarotoxin labeling over uninjected oocytes (Figure 6.3, right, orange bar compared to red bar).

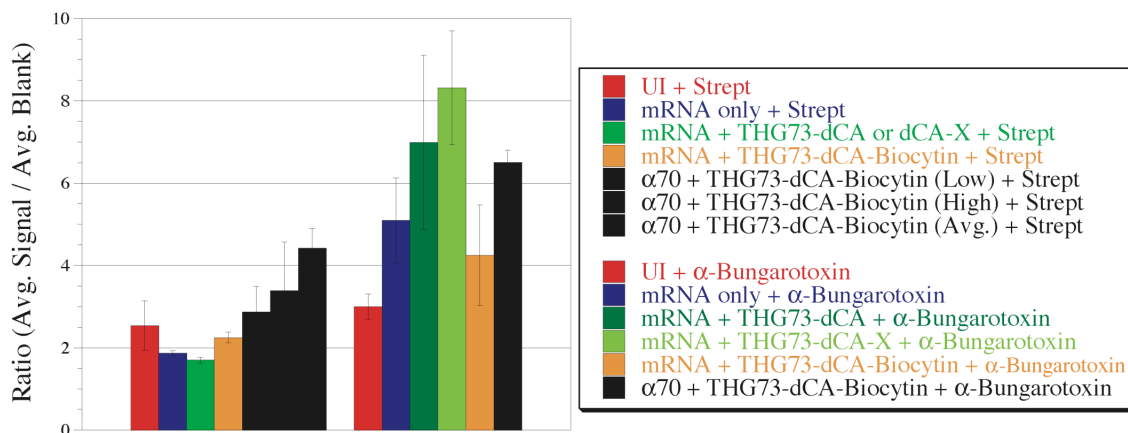


Figure 6.3: Analysis of ^{125}I -Streptavidin or ^{125}I - α -Bungarotoxin labeling of *Xenopus* oocytes expressing wild-type nAChR and UAA incorporation of biocytin. Abbreviations: UI is uninjected oocytes; Strept is ^{125}I -Streptavidin; mRNA refers to any other suppression site other than $\alpha 70\text{UAG}$; THG73-dCA is the 76mer tRNA; THG73-dCA-X is THG73 ligated with Tyr, *p*-AcPhe, or ketoTyr (shouldn't bind ^{125}I -Streptavidin); THG73-dCA-Biocytin is THG73-Biocytin; $\alpha 70$ is $\alpha 70\text{UAG}$, (Low) is the lowest avg. I_{max} in an oocyte batch; (High) is the highest avg. I_{max} in an oocyte batch; (Avg.) is when oocytes were labeled without determining the avg. I_{max} ; and α -Bungarotoxin is ^{125}I - α -Bungarotoxin.

6.2.4 Bioorthogonal Labeling of $\alpha 70p\text{-AcPhe}$ With Biotin Hydrazide

The incorporation of *p*-AcPhe at $\alpha 70$ introduces a ketone on the surface of *Xenopus* oocytes (Figure 6.1), which can be labeled with hydrazides. The ketone is bioorthogonal only on the cell surface because the interior of the cell contains acetylated proteins and keto/aldehydic metabolites (1). The desired bioorthogonal reaction of *p*-AcPhe with biotin hydrazide, which is membrane impermeant, is shown in Figure 6.4. *p*-AcPhe was incorporated at $\alpha 70\text{UAG}$ using TQAS and showed an average maximal current of $-27.3 \mu\text{A}$ (61% relative to wild-type current with half the mRNA), which is \approx 3-fold greater when compared to TQAS-Biocytin incorporation. To analyze the reaction of biotin hydrazide with *p*-AcPhe, we chose Western blot detection because $\alpha 70\text{Biocytin}$ and $\alpha 70\text{Biocytin}$ bound to streptavidin showed little shift in EC_{50} (39) and Western blot allows for visualization of all protein bands labeled with biotin hydrazide.

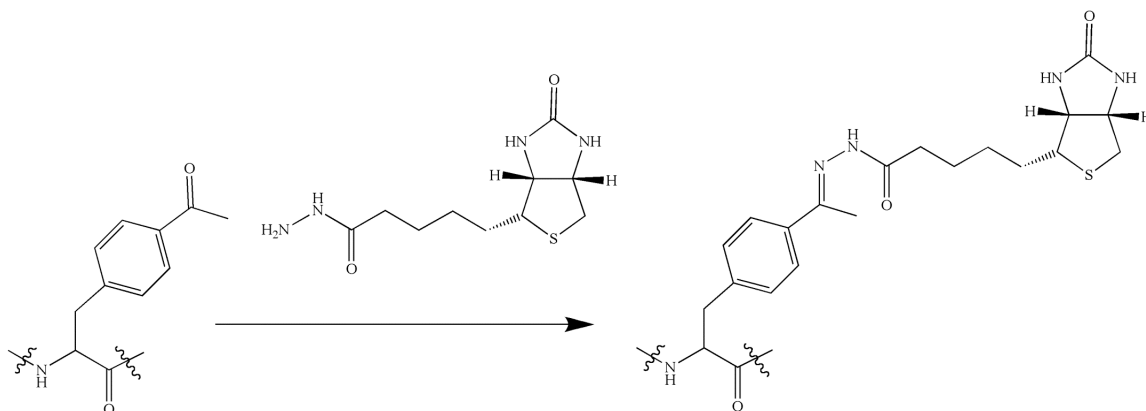


Figure 6.4: Bioorthogonal labeling of *p*-AcPhe with biotin hydrazide. *p*-AcPhe is incorporated at $\alpha 70$ and expressed on the extracellular surface of the *Xenopus* oocyte (Figure 6.1). The cells are labeled with biotin hydrazide, which can't cross the cell membrane unless it is permeabilized. The hydrazide reacts with the ketone to produce a hydrazone and covalently attaches biotin to *p*-AcPhe.

Labeling of $\alpha 70p$ -AcPhe with biotin hydrazide is shown in Figure 6.5. Labeling of permeabilized, uninjected oocytes and permeabilized, $\alpha 70$ UAG + TQAS-*p*-AcPhe with biotin hydrazide results in detection of many proteins with Streptavidin-680 (Figure 6.5, A, Lanes 4 & 7), which is more intense than non-permeabilized oocytes (Figure 6.5, A, Lanes 3 & 6). $\alpha 70p$ -AcPhe shows no labeling above the uninjected oocytes (Figure 6.5, A, Lanes 3 & 6). $\alpha 70p$ -AcPhe shows greater α -subunit signal (Figure 6.5, B, Lane 5) than $\alpha 70p$ -AcPhe labeled with biotin hydrazide (Figure 6.5, B, Lane 6). The reaction of ketones with hydrazides is pH sensitive and optimum in the range of pH = 4–6.5 (1,6,10,13,19). Therefore biotin hydrazide labeling of $\alpha 70p$ -AcPhe was tested from pH = 4–7.5 (Figure 6.5, C). Biotin hydrazide labeling of $\alpha 70p$ -AcPhe shows three distinct protein bands when the pH = 4–6.6 (Figure 6.5, C, Lanes 4–9). Intriguingly, varying pH also alters protein translation of the $\alpha 70p$ -AcPhe subunit, which is optimum at pH = 6.3–7.5 (Figure 6.5, D, Lanes 8–10) and is severely decreased at pH = 4 (Figure 6.5, D, Lanes 3–4).

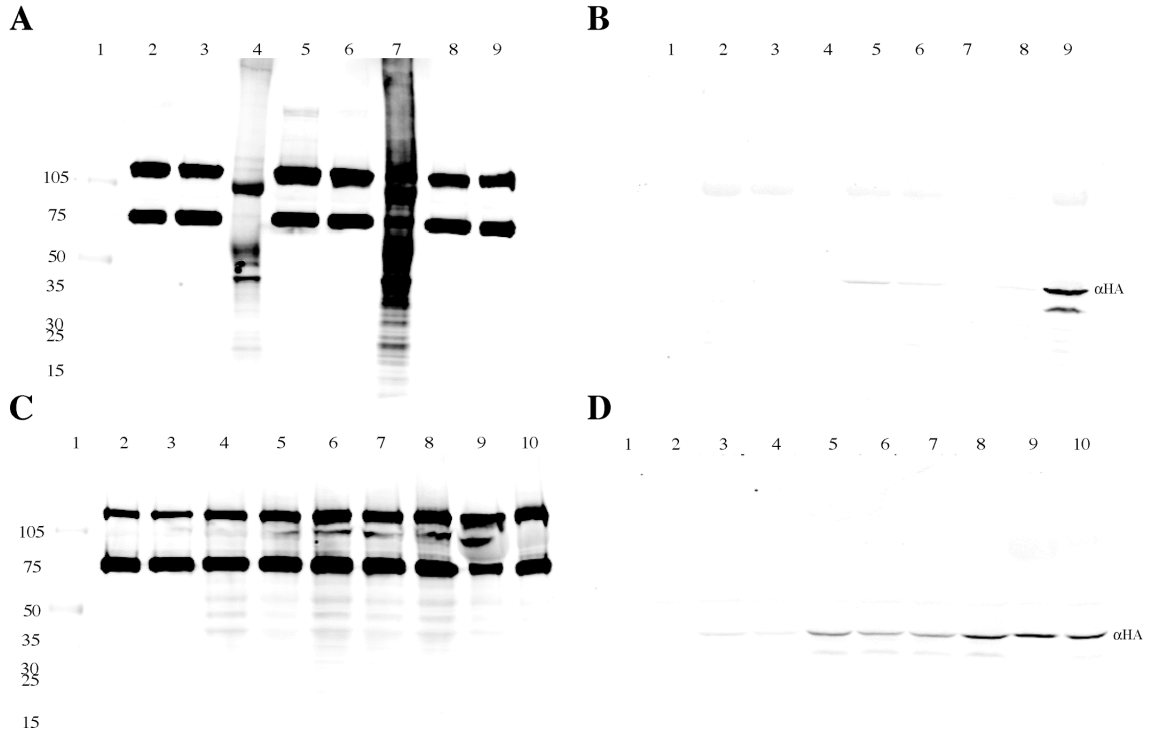


Figure 6.5: Detection of $\alpha 70p$ -AcPhe labeled with biotin hydrazide. (A) Whole-cell detection of biotin hydrazide labeling of intact and permeabilized oocytes. (B) Detection of the HA tag. (A & B) Lane 1, molecular weight marker. Lane 2, uninjected oocytes. Lane 3 is uninjected oocytes labeled with 1 mM biotin hydrazide, pH = 7.5. Lane 4 is uninjected oocytes permeabilized with detergent and labeled with 1 mM biotin hydrazide, pH = 7.5. Lane 5 is $\alpha_{NHA}70UAG + TQAS-p$ -AcPhe. Lane 6 is $\alpha_{NHA}70UAG + TQAS-p$ -AcPhe labeled with 1 mM biotin hydrazide, pH = 7.5. Lane 7 is $\alpha_{NHA}70UAG + TQAS-p$ -AcPhe permeabilized with detergent and labeled with 1 mM biotin hydrazide, pH = 7.5. Lane 8 is uninjected oocytes. Lane 9 is α_{HA} . (C) Whole-cell detection of biotin hydrazide labeling of intact oocytes with different pH. (D) Detection of α_{NHA} . (C & D) Lane 1, molecular weight marker. Lane 2 is uninjected oocytes labeled with 1 mM biotin hydrazide, pH = 4. Lane 3, $\alpha_{NHA}70UAG + TQAS-p$ -AcPhe, pH = 4. Lane 4, $\alpha_{NHA}70UAG + TQAS-p$ -AcPhe labeled with 1 mM biotin hydrazide, pH = 4. Lane 5, $\alpha_{NHA}70UAG + TQAS-p$ -AcPhe labeled with 1 mM biotin hydrazide, pH = 4.6. Lane 6, $\alpha_{NHA}70UAG + TQAS-p$ -AcPhe labeled with 1 mM biotin hydrazide, pH = 5.3. Lane 7, $\alpha_{NHA}70UAG + TQAS-p$ -AcPhe labeled with 1 mM biotin hydrazide, pH = 5.8. Lane 8, $\alpha_{NHA}70UAG + TQAS-p$ -AcPhe labeled with 1 mM biotin hydrazide, pH = 6.3. Lane 9, $\alpha_{NHA}70UAG + TQAS-p$ -AcPhe labeled with 1 mM biotin hydrazide, pH = 6.6. Lane 10, $\alpha_{NHA}70UAG + TQAS-p$ -AcPhe labeled with 1 mM biotin hydrazide, pH = 7.5. Each lane contains four whole oocytes. Numbers on the left are molecular weight markers (KD).

Densitometric analysis of $\alpha 70p$ -AcPhe labeled with biotin hydrazide at different pH is shown in Figure 6.6. Significant labeling is seen from pH = 4–6.3 (Figure 6.6, A).

Labeling at pH = 4.6 is expected to be greater than pH = 5.3 and pH = 5.8 is expected to be greater than pH = 6.3. Labeling may be decreased by variability of labeling, protein expression, or oocytes (Figure 6.6, A). α -subunit expression at different pH shows a gradual decrease as acidity increases (Figure 6.6, B). Even though the α -subunit is severely diminished at pH = 4, the greatest labeling is seen at pH = 4 (Figure 6.6, A & B). Streptavidin-680 labeling was then normalized by the amount of protein detected by the HA antibody to allow for comparison of biotin hydrazide labeling as a function of pH alone (Figure 6.6, C). pH = 7.5 shows virtually no labeling, which is expected of an acid catalyzed reaction (Figure 6.6, C). pH = 4 is the optimum labeling condition, even though protein production is decreased significantly (Figure 6.6, C). All subsequent hydrazide labeling experiments were performed at pH = 4.

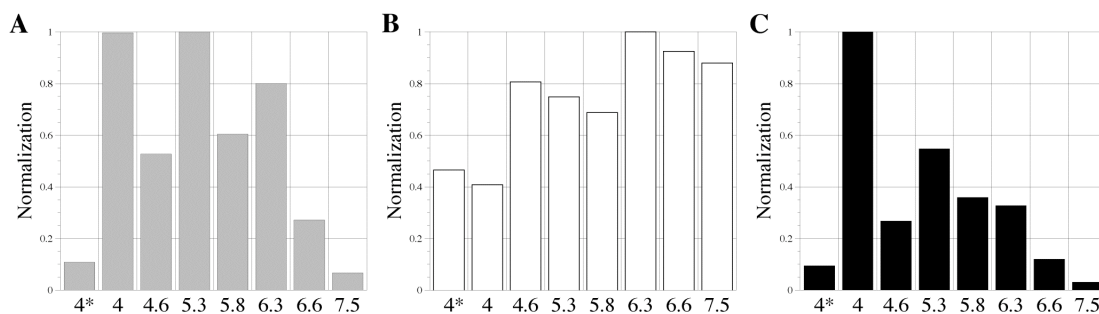


Figure 6.6: Analysis of *p*-AcPhe labeled with biotin hydrazide. Analysis performed on Western blots in Figure 6.5, C and D. (A) Densitometric analysis of biotin hydrazide labeling at different pH. Signals were normalized to the highest labeling (Figure 6.5, C, Lanes 2–10). (B) Densitometric analysis of protein expression as a function of pH. Signals were normalized to the highest expression (Figure 6.5, D, Lanes 2–10). (C) Normalization of biotin hydrazide labeling with the amount of protein expressed (value from A / value from B and renormalized to the highest value). Biotin hydrazide labeling is optimal at pH = 4, but protein translation is decreased. Numbers below each graph are pH. 4* was not labeled with biotin hydrazide.

6.2.5 Attempts to Block Nonspecific Biotin Hydrazide Labeling of Uninjected

Oocytes

The labeling of three bands in Figure 6.5 is undesired because the reaction of biotin hydrazide is expected to be specific for the $\alpha 70p$ -AcPhe. Therefore, carbohydrazide was added to uninjected oocytes to try and block proteins that are reacting with the biotin hydrazide (Figure 6.7, A). Treatment of uninjected oocytes with 1 mM or 10 mM carbohydrazide for 1 day (Figure 6.7, A, Lanes 5–10) shows no reduction in biotin hydrazide labeling when compared to untreated, uninjected oocytes labeled with biotin hydrazide (Figure 6.7, A, Lanes 3–4). Another possibility is that ketones or aldehydes exist on the cell surface by protein modification or glycosylation of proteins and these are reacting with the biotin hydrazide. NaBH_4 reduces ketones and aldehydes into alcohols, which would not react with biotin hydrazide. Treatment of uninjected oocytes with 1 mM or 10 mM NaBH_4 showed no significant reduction in biotin hydrazide labeling (Figure 6.7, B Lanes 5–10) when compared to the untreated, uninjected oocytes labeled with biotin hydrazide (Figure 6.7, B, Lanes 3–4). Treatment of oocytes with carbohydrazide or NaBH_4 showed no reduction in biotin hydrazide labeling on uninjected oocytes (Figure 6.7, A & B) and surprisingly showed little effect on oocyte health and survival.

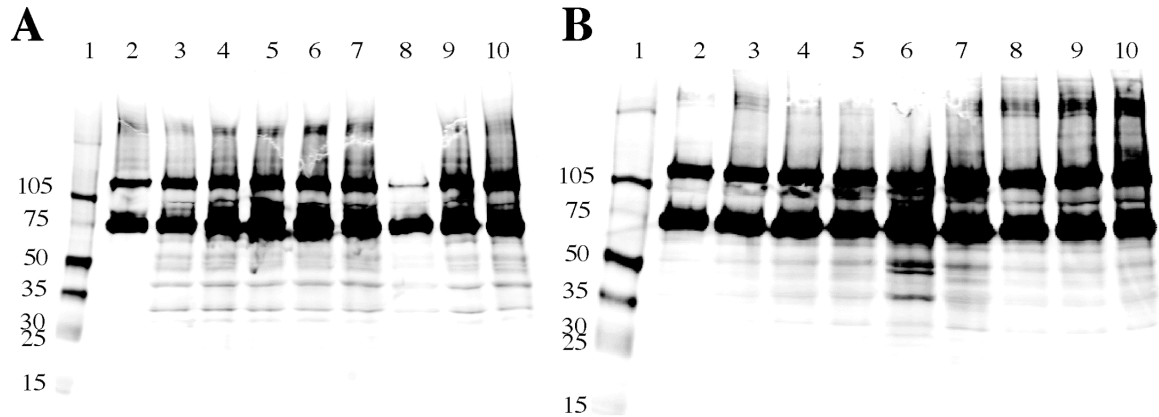


Figure 6.7: Uninjected oocytes labeled with biotin hydrazide after treatment with carbohydrazide or NaBH_4 . (A) Carbohydrazide treatment prior to biotin hydrazide labeling. Lane 1 is molecular weight marker. Lane 2 is uninjected oocytes. Lanes 3 and 4 are uninjected oocytes labeled with 1 mM biotin hydrazide. Lanes 5–7, uninjected oocytes treated with 1 mM carbohydrazide, followed by labeling with 1 mM biotin hydrazide. Lanes 8–10, uninjected oocytes treated with 10 mM carbohydrazide, followed by labeling with 1 mM biotin hydrazide. (B) NaBH_4 treatment prior to biotin hydrazide labeling. Lane 1 is molecular weight marker. Lane 2 is uninjected oocytes. Lanes 3 and 4 are uninjected oocytes labeled with 1 mM biotin hydrazide. Lanes 5–7, uninjected oocytes treated with 1 mM NaBH_4 , followed by labeling with 1 mM biotin hydrazide. Lanes 8–10, uninjected oocytes treated with 10 mM NaBH_4 , followed by labeling with 1 mM biotin hydrazide. Each lane contains four oocytes and all labeling was performed at pH = 4. Numbers on the left are molecular weight markers (KD).

6.2.6 Bioorthogonal Labeling of $\alpha 70p$ -AcPhe with Cy5.5 Hydrazide

Previous labeling experiments used biotin hydrazide, which contains the biotin moiety and could possibly be recognized by endogenous proteins and attached to proteins in order to sequester free biotin. Removing biotin from the environment is thought to be an antimicrobial mechanism used by avidin in egg whites and streptavidin in *S. avidinii* to inhibit microorganism growth (55). Therefore, it is possible that the *Xenopus* oocytes are removing the biotin hydrazide in a similar manner to inhibit microorganism growth. We then choose to label $\alpha 70p$ -AcPhe with Cy5.5 hydrazide (structure shown in Figure 6.8, A) because the molecule doesn't resemble biologically active molecules and the infrared fluorophore would allow for direct detection by the Li-Cor Odyssey.

Labeling of uninjected oocytes, wild-type nAChR, and $\alpha 70p$ -AcPhe with Cy5.5 hydrazide is shown in Figure 6.8, B. Permeabilized $\alpha 70p$ -AcPhe labeled with Cy5.5 hydrazide show intense signals from many proteins (Figure 6.8, B, Lane 6), illustrating that many proteins within the cell can react with the Cy5.5 hydrazide and similar to biotin hydrazide (Figure 6.5, A, Lanes 4 & 7). Uninjected oocytes and oocytes expressing wild-type nAChR show three protein bands labeled by Cy5.5 hydrazide (Figure 6.8, B, Lanes 3 & 5). Three bands are also seen when labeling $\alpha 70p$ -AcPhe (Figure 6.8, B, Lanes 7–8), which is similar to the labeling with biotin hydrazide (Figure 6.5, C, Lanes 4–9). Wild-type nAChR shows no reduction in protein when labeled with Cy5.5 hydrazide (Figure 6.8, C, Lanes 4–5). Labeling of $\alpha 70p$ -AcPhe shows greatly diminished protein (Figure 6.8, C, Lanes 7–8) when compared to the untreated $\alpha 70p$ -AcPhe (Figure 6.8, C, Lanes 9–10). This suggests covalent attachment of Cy5.5 hydrazide to $\alpha 70p$ -AcPhe may be occurring and attachment of the large fluorophore is decreasing recognition by the HA antibody. However, there is still labeling of three protein bands and bioorthogonal labeling of the ketone doesn't appear to be a specific reaction on the surface of *Xenopus* oocytes.

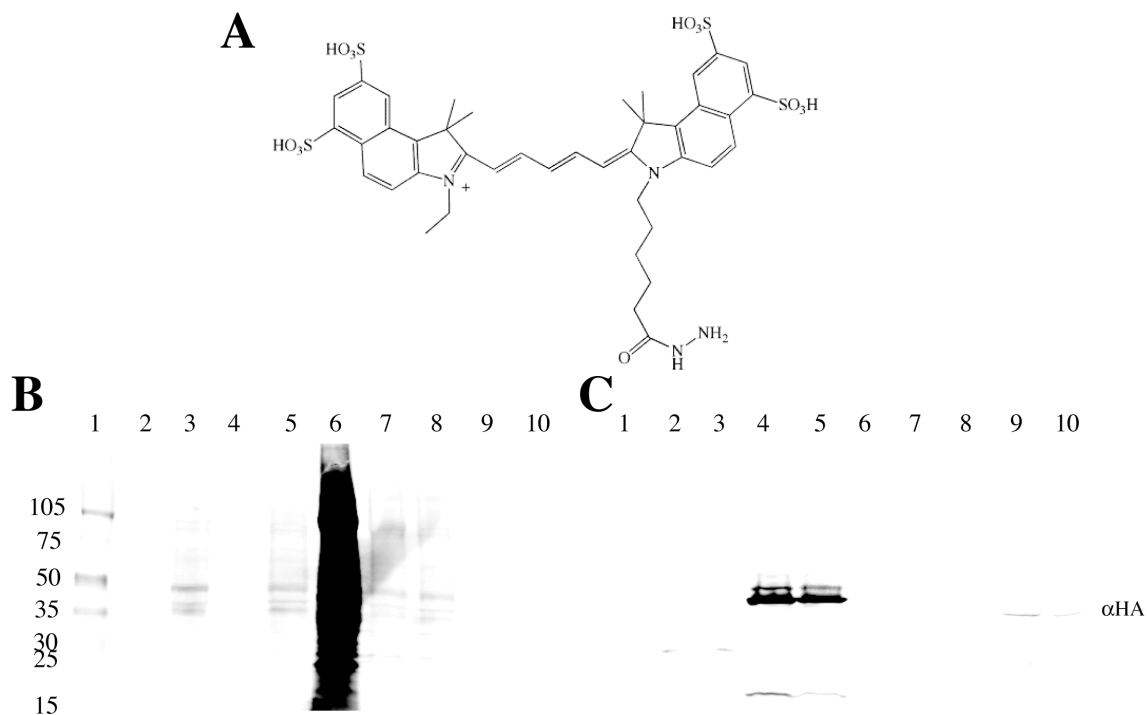


Figure 6.8: Bioorthogonal labeling of $\alpha 70p$ -AcPhe with Cy5.5 hydrazide. (A) Chemical structure of Cy5.5 hydrazide. Maximal absorbance is 675 nm, maximal emission is 694 nm, and maximal extinction is $250,000 \text{ M}^{-1} \text{ cm}^{-1}$ (Amersham Biosciences product manual). Cy5.5 hydrazide allows for direct detection of labeled proteins. (B) Detection of Cy5.5 hydrazide labeled proteins. (C) Detection of the HA tag. (B & C) Lane 1 is molecular weight marker. Lane 2 is uninjected oocytes. Lane 3 is uninjected oocytes labeled with 1 mM Cy5.5 hydrazide. Lane 4 is α_{HA} and β_{HA} . Lane 5 is α_{HA} and β_{HA} labeled with 1 mM Cy5.5 hydrazide. Lane 6 is $\alpha_{\text{NHA}} 70\text{UAG} + \text{TQAS-}p\text{-AcPhe}$ permeabilized with detergent and labeled with 1 mM Cy5.5. Lanes 7 and 8 are $\alpha_{\text{NHA}} 70\text{UAG} + \text{TQAS-}p\text{-AcPhe}$ labeled with 1 mM Cy5.5 hydrazide. Lanes 9 and 10 are $\alpha_{\text{NHA}} 70\text{UAG} + \text{TQAS-}p\text{-AcPhe}$. Each lane contains four oocytes and all labeling and incubations were performed at $\text{pH} = 4$. Numbers on the left are molecular weight markers (KD).

6.2.7 Analysis of ^{125}I -Streptavidin Binding to *Xenopus* Oocytes Labeled with Biotin Hydrazide

Using Dr. Gallivan's lab notebook, I reanalyzed all experiments involving biotin hydrazide labeling (unpublished data). All experiments were performed previously by Dr. Gallivan using published methods (39). Oocytes expressing $\alpha 70\text{Biocytin}$ show significant radioactive signal when labeled with ^{125}I -Streptavidin (Figure 6.9, black bar).

However, oocytes labeled with ≥ 0.5 mM biotin hydrazide (Figure 6.9, pink bar, light blue bars, & light green bars) show a similar radioactive signal to $\alpha 70$ Biocytin (Figure 6.9, black bar). The labeling with biotin hydrazide is concentration dependent and 10 mM labeling of $\alpha 70$ UAG + THG73-dCA or THG73-*p*-AcPhe/KetoTyr (Figure 6.9) shows comparable radioactive signal to nAChRs labeled with ^{125}I - α -Bungarotoxin (Figure 6.3). Therefore, the nonspecific labeling of biotin hydrazide is seen by Western blot (Figure 6.5 & 6.7) and also by ^{125}I -Streptavidin labeling of the oocyte surface (Figure 6.9).

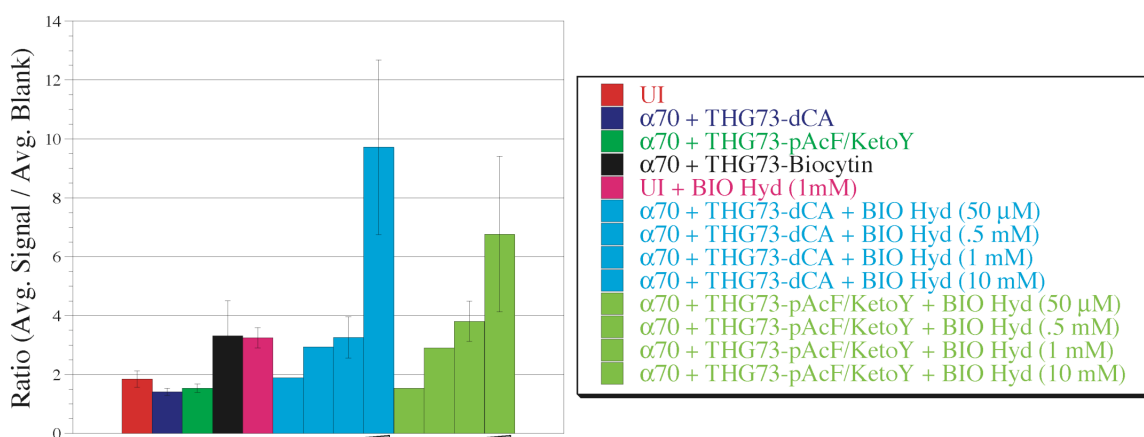


Figure 6.9: Analysis of ^{125}I -Streptavidin binding to *Xenopus* oocytes treated with biotin hydrazide. Abbreviations: UI is uninjected oocytes, $\alpha 70$ is $\alpha 70$ UAG, THG73-dCA is the 76mer tRNA, THG73-dCA-pAcF/KetoY is THG73-*p*-AcPhe or THG73-KetoTyr, and BIO Hyd is biotin hydrazide, concentration shown in parentheses. Biotin hydrazide labeling is nonspecific and amplified with increasing concentrations.

6.2.8 α -, β -, γ -, and δ -Subunit Detection By Western Blot

Previously, Dr. Gabriel Brandt prepared the α -, β -, γ -, and δ -subunits containing the HA tag in the M3-M4 loop (denoted x_{HA} in contrast to the N-terminal HA tag, α_{NHA}). The M3-M4 loop is an intracellular loop that is highly flexible, can tolerate insertion of GFP (56), and can tolerate deletion of 108 amino acids in the 5-HT_{3A} receptor and 75

amino acids in the GABA ρ 1 receptor (57). All subunits showed \approx 100% expression, except the δ -subunit (\approx 90%), as determined by electrophysiology in *Xenopus* oocytes (58). We hoped that by using these constructs and the sensitivity of the Li-Cor Odyssey, we would be able to determine the subunit stoichiometry of the nAChR on whole oocytes. The subunit stoichiometry of the mouse muscle nAChR is known to be $2\alpha:\beta:\gamma:\delta$ (Figure 6.1) and this would allow for us to assay the feasibility of determining an ion channel stoichiometry on whole *Xenopus* oocytes by Western blot.

Figure 6.10 shows the expression of the α_{HA} , β_{HA} , γ_{HA} , and δ_{HA} constructs. The α_{HA} -subunit is clearly visible in all lanes (Figure 6.10, A & B). The β_{HA} -subunit is clearly visible on the 4–15% linear gradient gel (Figure 6.10, A, Lanes 4, 5, & 10), but is slightly obscured by the α_{HA} band on the 15% gel (Figure 6.10, B, Lanes 4–5). The γ_{HA} - and δ_{HA} -subunits are only slightly visible and smeared (Figure 6.10, A, Lanes 6–10 and Figure 6.10, B, Lanes 6–8 & 10). The δ_{HA} -subunit is only clearly visible in one lane (Figure 6.10, B, Lane 9). Western blot analysis of these constructs previously showed severely decreased signal for the non- α subunits (58), but the β_{HA} -subunit is clearly visible when the oocytes are expressing large amounts of protein (Figure 6.10, A, Lanes 4, 5, & 10).

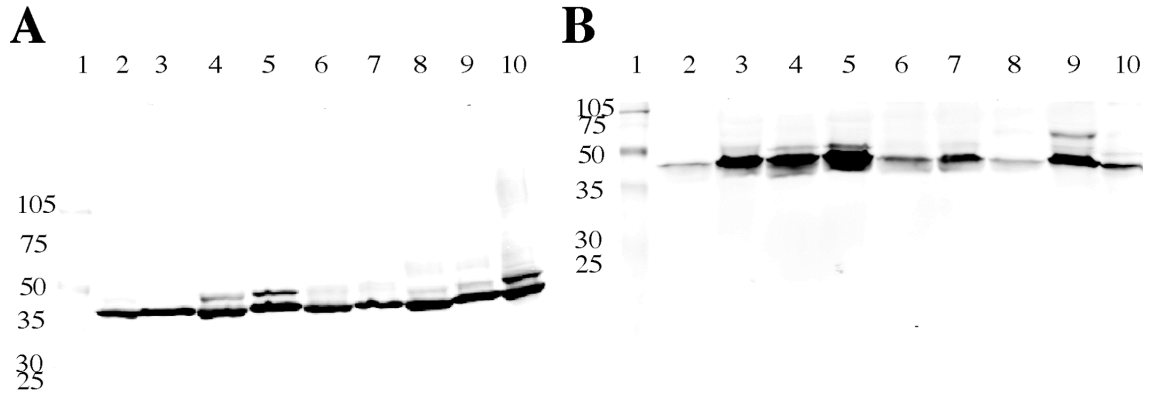


Figure 6.10: Detection of the α_{HA} , β_{HA} , γ_{HA} , and δ_{HA} subunits of the nAChR. (A) Subunit detection on a 4–15% linear gradient polyacrylamide gel. (B) Subunit detection on a 15% polyacrylamide gel. (A & B) Lane 1 is molecular weight marker. Lanes 2 and 3 are α_{HA} . Lanes 4 and 5 are α_{HA} and β_{HA} . Lanes 6 and 7 are α_{HA} and γ_{HA} . Lanes 8 and 9 are α_{HA} and δ_{HA} . Lane 10 is α_{HA} , β_{HA} , γ_{HA} , and δ_{HA} . Each lane contains four oocytes. Numbers on the left are molecular weight markers (KD).

6.2.9 α_{HA} and β_{HA} Detection After Various Incubation Times

In order to gain temporal information on protein translation of the α_{HA} and β_{HA} in *Xenopus* oocytes, the α_{HA} and β_{HA} were injected into oocytes and the whole-cell oocytes were homogenized at different time intervals after injection. Figure 6.11 shows the Western blot of different incubation times. Three hours after injection, only extremely little α_{HA} -subunit is seen (Figure 6.11, Lane 2). Six hours after injection, a slightly increased amount of α_{HA} -subunit is seen (Figure 6.11, Lanes 3–4). Twelve hours after injection, the α_{HA} -subunit is clearly visible (Figure 6.11, Lanes 5–6) and the β_{HA} -subunit is visible in only one lane (Figure 6.11, Lane 6). A day after injection, which is the typical minimum incubation time before electrophysiology, both the α_{HA} and β_{HA} subunits are clearly visible (Figure 6.11, Lanes 7–8). Two days after injection, there is increased amounts of both the α_{HA} and β_{HA} , clearly illustrating that protein translation has not saturated after two days.

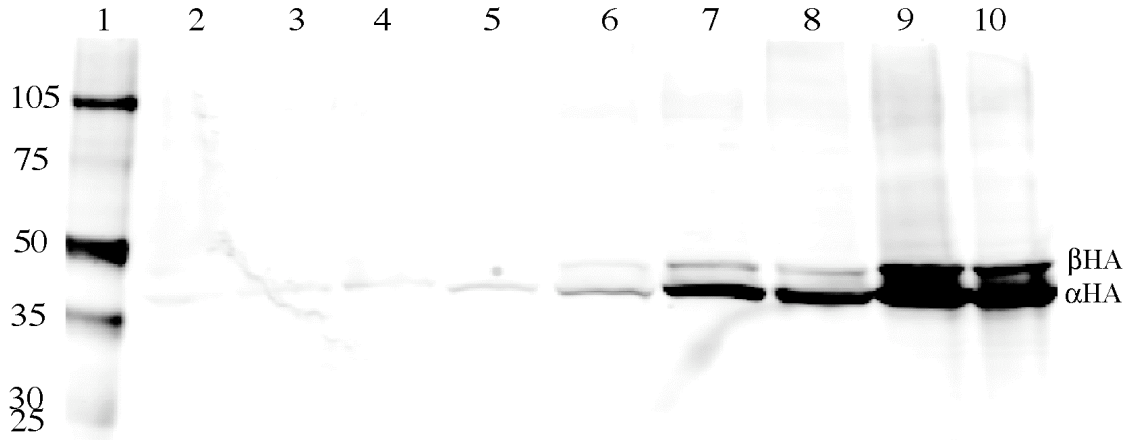


Figure 6.11: Detection of the α_{HA} and β_{HA} subunits at different incubation times. Lane 1 is molecular weight marker. Lane 2 is α_{HA} and β_{HA} 3 h after injection. Lanes 3 and 4 are α_{HA} and β_{HA} 6 h after injection. Lanes 5 and 6 are α_{HA} and β_{HA} 12 h after injection. Lanes 7 and 8 are α_{HA} and β_{HA} 24 h after injection. Lanes 9 and 10 are α_{HA} and β_{HA} 48 h after injection. Protein translation shows no saturation after 48 h. Each lane contains four oocytes. Numbers on the left are molecular weight markers (KD).

6.2.10 α_{HA} and β_{HA} Solubilization of Whole Cells or Insoluble Fraction

The nAChR is a membrane-associated ion channel and therefore may be difficult to solubilize in the presence of cytoplasmic proteins. In previous Western blots, whole cells were homogenized, all protein was solubilized, and samples were centrifuged to remove insoluble proteins, lipids, membrane, genomic DNA, etc. Cytoplasmic proteins were removed by homogenizing oocytes in ND96 buffer containing protease inhibitors, but no detergent. The samples were then centrifuged and the insoluble fraction was solubilized as done for the whole oocytes. Solubilization of the insoluble fraction greatly increases the yield of the α_{HA} and β_{HA} subunits (Figure 6.12, Lanes 6–9) when compared to the whole-cell homogenization (Figure 6.12, Lanes 2–5). The yield of the α_{HA} is increased 142%, while the β_{HA} is increased 108%. Therefore, homogenization of the insoluble fraction is useful for increased solubilization of the nAChR subunits and increased signal-to-noise when performing Western blots.

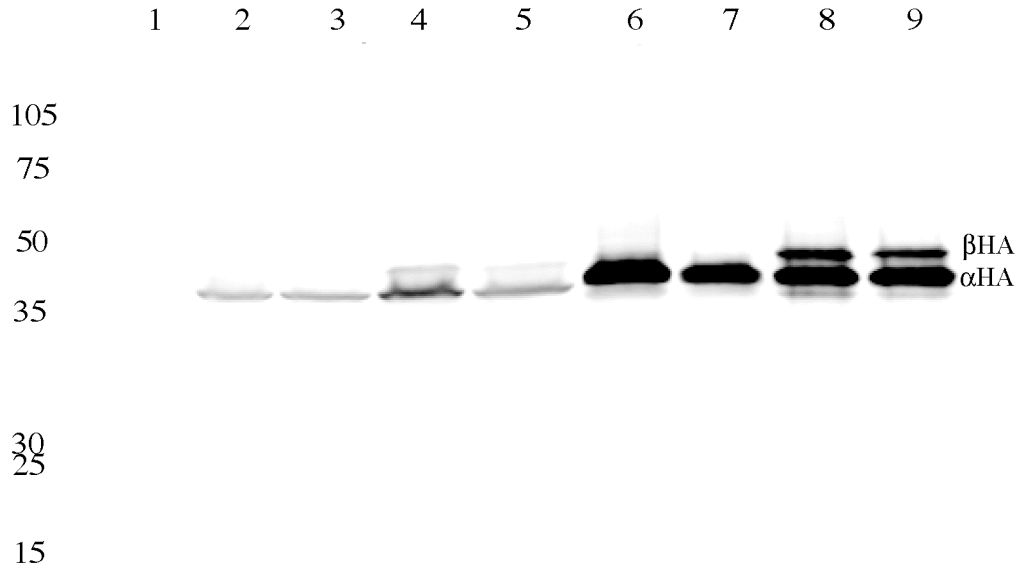


Figure 6.12: Increasing the yield of the α_{HA} and β_{HA} subunits. Lane 1 is molecular weight marker. Lanes 2 and 3 are α_{HA} . Lanes 4 and 5 are α_{HA} and β_{HA} . Lanes 6 and 7 are α_{HA} solubilized after cytoplasmic protein removal. Lanes 8 and 9 are α_{HA} and β_{HA} solubilized after cytoplasmic protein removal. Each lane contains four oocytes. Numbers on the left are molecular weight markers (KD).

6.2.11 α -, β -, γ -, and δ -Subunit Stoichiometry Determined By Densiometric Analysis

The densiometric analysis of all experiments is shown in Figure 6.13. The ratios were calculated by dividing the α_{HA} intensity by the intensity of the subunit expressed in the same lane. The expected ratio is 2 for all ratios in Figure 6.13 because the stoichiometry of the nAChR is $2\alpha:\beta:\gamma:\delta$. The α/β average ratio is 2.9 ± 0.13 (Figure 6.13) and is the best ratio because the β_{HA} is clearly visible and is the average of 30 Western blot lanes or 120 oocytes. The α/γ average ratio is 2.9 ± 0.24 (Figure 6.13), which is similar to the α/β ratio even though the γ_{HA} band has decreased intensity compared to β_{HA} . The α/δ average ratio is 3.5 ± 0.51 (Figure 6.13) and is higher than the α/β or α/γ ratio. All ratios appear to indicate that there are ≈ 3 α -subunits for every β -, γ -

, and δ -subunit, which is in disagreement with the expected nAChR subunit stoichiometry.

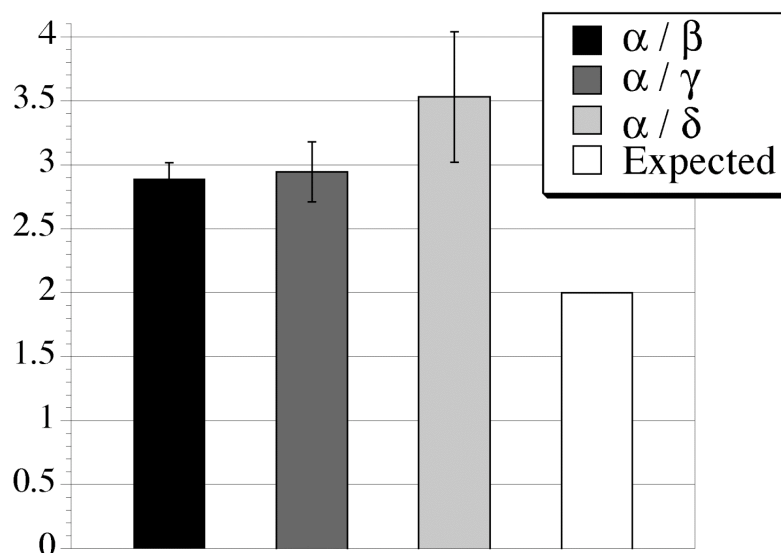


Figure 6.13: Average ratio of the β -, γ -, and δ -subunits relative to the α -subunit. The α/β ratio is an average of 30 lanes or 120 oocytes. The α/γ ratio is an average of 3 lanes or 12 oocytes. The α/δ ratio is an average of 3 lanes or 12 oocytes. The expected ratio is 2 by the nAChR stoichiometry being $2\alpha:\beta:\gamma:\delta$.

6.3 Discussion

UAA incorporation is a useful technique for the introduction of novel chemical moieties, biophysical probes, and altered amino acid structures. However, efficient incorporation of large, bulky UAAs requires a suppression site that is tolerant, able to express well without altering protein folding and function, and doesn't have large amounts of read-through of the suppression site. Table 6.1 illustrates the differences between multiple suppression sites on different subunits of the nAChR. $\alpha 70\text{UAG}$ incorporates Gln well with THG73 aminoacylated *in vivo* and shows little read-through of the stop codon (Table 6.1). $\beta 70\text{UAG}$ and $\beta 70\text{GGGU}$ both show large amounts of read-through (Table 6.1), even though a -1 frameshift at the GGGU quadruplet codon

presents multiple stop codons. TQAS'-WF1 shows a 180% increase in current when compared to THG73 not chemically aminoacylated (Table 6.1) and clearly illustrates that nonsense suppression with an UAA is more efficient than aminoacylation of THG73 *in vivo*. β 19'UAG and β 19'GGGU show increased amounts of read-through with large amounts of mRNA and less aminoacylation product than both α 70UAG and β 70UAG (Table 6.1). The β 19' site is suboptimal for UAA incorporation and requires less mRNA to avoid read-through. δ 69UAG, δ 69GGGU, and δ 70UGA all have very little read-through, but the aminoacylation of the suppressor tRNA doesn't significantly increase current (Table 6.1). δ 70UGA + TQOpS'-WF1 has lower expression than mRNA alone or the aminoacylation product, clearly showing that the UAA is not tolerated at this site. Overall, the only optimum site is α 70UAG for significant UAA incorporation without large amounts of read-through.

Western blot detection of UAAs has been exceedingly difficult because of the need for large amounts of protein on the oocyte surface, multiple injections of large quantities of tRNA-UAA, and manual removal of 10–25 oocyte membranes (51,52). Whole-cell homogenization of oocytes is a preferable alternative because the lack of manual membrane removal, decreased variability, and the need for only four oocytes. A single injection of large quantities of α 70UAG + TQAS-Biocytin allowed for significant expression for Western blot detection (Figure 6.2, A & C). Figure 6.2 shows direct detection of the UAA biocytin incorporated at α 70. Whole-cell homogenization shows increased intensity with four oocytes (Figure 6.2, A, Lanes 5–7) when compared to the traditional, manual membrane removal with twenty oocytes (Figure 6.2, C, Lane 7). Manual membrane removal requires a small amount of detergent in the hypotonic

solution, which causes loss of the α_{HA} -subunit in the supernatant (Figure 6.2, D Lanes 8–9). Whole-cell homogenization allows for increased intensity and fewer oocytes for each lane, so multiple experiments can be performed in a shorter amount of time. Solubilization of the insoluble fraction after removal of cytoplasmic proteins also increases the yield of the α_{HA} and β_{HA} subunits (Figure 6.12) and should further increase the signal-to-noise ratio in Western blot experiments.

Previous work has explicitly shown that there is protein translation saturation for luciferase after 3 h (59) or 12 h (60) with mRNA injection in *Xenopus* oocytes. However, Figure 6.11 clearly shows that protein expression is increasing for both the α_{HA} and β_{HA} subunits in the *Xenopus* oocytes, and no saturation is seen after 48 h. The experiment was performed using whole cell homogenization, which would solubilize α_{HA} and β_{HA} on the membrane surface, in vesicles, in the golgi, and in the endoplasmic reticulum. The increase in current with extended incubation time has been seen consistently within our lab, but it was unknown whether this was due to increased protein production or whether transport of ion channels from the endoplasmic reticulum to the cell surface was causing an increase in overall current. Figure 6.11 clearly shows that the α and β subunits are being expressed for at least 48 h from a single injection of wild-type mRNA.

$\alpha 70\text{UAG} + \text{THG73}$ shows large amount of current (Table 6.1) because THG73 is aminoacylated *in vivo* with Gln (48). TQAS is aminoacylated significantly less than THG73 in Nasco oocytes (Table 6.1 & (48)) and is useful for the incorporation of large amounts of biocytin and *p*-AcPhe. The incorporation of *p*-AcPhe is $\approx 200\%$ more efficient than the incorporation of biocytin, which is most likely due to the large side chain of biocytin. Electrophysiology allows for detection of functional ion channels on

the surface of the oocyte membrane, which can often be produced by the desired UAA incorporation, or the undesired read-through of the suppression site or aminoacylation of the suppressor tRNA *in vivo* (Table 6.1). α -bungarotoxin is a snake venom toxin that irreversibly and competitively binds to the α -subunit of the nAChR in a region distinct from $\alpha 70$ (54,61), and the first 210 amino acids of the α -subunit (with no other subunits) is sufficient for α -bungarotoxin binding in *Xenopus* oocytes (62). Binding of ^{125}I - α -Bungarotoxin to oocytes is significant when incorporating biocytin, *p*-AcPhe, ketoTyr, and Tyr, but significant signal is also seen with mRNA only and with mRNA + THG73, which is not chemically aminoacylated (Figure 6.3). The significant radioactive signal agrees with large current seen with tRNA that are not chemically aminoacylated (Table 6.1). THG73, not chemically aminoacylated, with $\beta 9'$ UAG also produces large current (48,49,58) and the $\beta 9'$ Gln (aminoacylation product) has been detected by Western blot on the surface of *Xenopus* oocytes (58). Therefore, caution should be observed when labeling oocytes with α -bungarotoxin, because binding may not be limited to functional nAChRs, but also mutants, single α -subunits, and/or aminoacylation by products of UAA incorporation that may not be detected by electrophysiology.

Labeling of uninjected oocytes, wild-type nAChR, and $\alpha 70$ UAG + TQAS-*p*-AcPhe with biotin hydrazide (Figure 6.5, C & Figure 6.7) or Cy5.5 hydrazide (Figure 6.8) show labeling of at least three protein bands that migrate near the α -subunit. Direct labeling of $\alpha 70$ *p*-AcPhe with Cy5.5 hydrazide was not directly observed, but may be occurring due to the loss of α_{NHA} signal after labeling (Figure 6.8, C, Lanes 7–8), which was not seen in the unlabeled samples (Figure 6.8, C, Lanes 9–10). The nonspecific labeling with biotin hydrazide couldn't be prevented by treating uninjected oocytes with

carbohydrazide or NaBH_4 (Figure 6.7) and suggests that the labeled proteins contain an amino acid arrangement and/or glycosylation that is favorable for the reaction with the hydrazide chemical moiety. Previous work has labeled proteins containing the UAAs *p*-AcPhe and *m*-AcPhe with fluorescent hydrazides and biotin hydrazide *in vitro* and expressed in *E. coli* (13,19,20). Labeling of *E. coli* may not have nonspecific covalent attachment of hydrazides and/or the quantities of protein produced with UAAs is greater and gives a significant signal over background. In *Xenopus* oocytes, the ketone moiety does not appear to show site-specific labeling of $\alpha 70p$ -AcPhe with biotin or Cy5.5 hydrazide and may only be useful for single ion channels studies involving FRET pairs.

Analyzing the subunit stoichiometry of the nAChR from whole oocytes shows ≈ 3 α -subunits for each non- α -subunit (Figure 6.13). Intriguingly, solubilizing the insoluble fraction gives an α/β ratio of 3.6 compared to whole-cell homogenization having an α/β ratio of 2.6 (data from analysis of Figure 6.12). The α/β ratio is 3.0 after 24 h incubation and the α/β ratio is 3.0 after 48 h incubation (data from analysis of Figure 6.11), which shows no variability in these two time points (the α/β ratio could not be calculated for 3, 6, and 12 h incubation because the signal was not above background). After injection of oocytes with α -subunit mRNA only, the α -subunit is expressed on the surface of *Xenopus* oocyte and can be detected by Western blot (58). Therefore, the oocytes can transport single α -subunits to the surface of the *Xenopus* oocyte that aren't in fully formed ion channels. The mouse α -subunit of the nAChR can also properly fold and have a high affinity α -bungarotoxin binding site when expressed alone in quail fibroblast cells (63). Notably, the α -subunit also has the slowest rate of degradation of all the subunits (38,63,64). The increased α_{HA} signal may also be caused by the injection of

mRNA in the subunit ratio of $2\alpha:\beta:\gamma:\delta$, but this has been an established technique for many heteromeric ion channels expressed in *Xenopus* oocytes. Overall, subunit stoichiometry of the mouse muscle nAChR appears inaccurate using whole *Xenopus* oocytes and densitometric analysis of Western blots.

6.4 Experimental Methods

6.4.1 Materials

All oligonucleotides were synthesized by Integrated DNA Technologies (Coralville, IA). NotI and complete, EDTA-free protease inhibitor cocktail was from Roche Applied Science (Indianapolis). T4 RNA ligase and FokI were from NEB (Beverly, MA). T7 MEGAscript and T7 mMessage mMachine kits were from Ambion (Austin, TX). ACh chloride, biotin hydrazide, carbohydrazide, NaBH_4 , and yeast inorganic pyrophosphatase were purchased from Sigma-Aldrich. HA.11 monoclonal antibody from mouse was from Covance (Berkeley, CA). Streptavidin conjugated to AlexaFluor680 and anti-mouse IgG from goat conjugated to AlexaFluor680 was from Molecular Probes (Eugene, OR). IRDyeTM800CW conjugated affinity purified anti-mouse IgG from goat was from Rockland (Gilbertsville, PA). Cy5.5 hydrazide was from Amersham Biosciences (Piscataway, NJ). dCA, 6-nitroveratryloxycarbonyl protected dCA-WF1, 6-nitroveratryloxycarbonyl protected dCA-Biocytin, and 6-nitroveratryloxycarbonyl protected dCA-*p*-AcPhe were prepared as reported (39,65–67).

6.4.2 tRNA Transcription and dCA or dCA-UAA Ligation

THG73, YFaFS_{ACCC}, TQAS, TQAS', and TQOpS' subcloned in the pUC19 vector were previously made (45,48–50). Template DNA for tRNA lacking the 3'CA

was prepared by FokI digestion and tRNA was transcribed using the T7 MEGAscript kit with 0.5 μ l of yeast inorganic pyrophosphatase (40 U/ml in 75 mM Tris, 10 mM MgCl₂, and pH 7). tRNA was desalted using CHROMA SPIN-30 DEPC-H₂O columns (BD Biosciences) and concentration was determined by absorption at 260 nm. 75 μ M of dCA (48,50) or 6-nitroveratryloxycarbonyl protected dCA-WF1/Biocytin/*p*-AcPhe were coupled to tRNA by using T4 RNA ligase for 30 min as previously reported (68,69), desalted using CHROMA SPIN-30 DEPC-H₂O columns, and quantified by absorption at 260 nm. tRNA ligation efficiency was qualitatively determined by MALDI mass spectrometry (69), and all tRNA ligations were > 90%.

6.4.3 nAChR Gene Preparation and mRNA Transcription

The masked $\alpha_{\text{NHA-}}$, β -, γ -, and δ -subunits (all ending with the ochre (UAA) stop codon) of the nAChR subcloned in the pAMV vector were previously prepared (48,50). α 70UAG, β 70UAG, β 70GGGU, β 19'UAG, β 19'GGGU, δ 69UAG, δ 69GGGU, and δ 70UGA were prepared by QuikChange mutagenesis. Mutations were verified by DNA sequencing (California Institute of Technology Sequencing / Structure Analysis Facility). The α_{HA} (347), β_{HA} (365), γ_{HA} (365), and δ_{HA} (367) subunits all contain the HA tag in the M3-M4 intracellular loop and were previously prepared by Dr. Gabriel Brandt (58). DNA was linearized with NotI and mRNA was prepared with the T7 mMessage mMachine kit with 0.5 μ l of yeast inorganic pyrophosphatase. mRNA was purified using the RNeasy Mini kit (Qiagen, Valencia, CA) and quantified by absorption at 260 nm.

6.4.4 *In Vivo* nAChR Expression Experiments

Prior to *in vivo* aminoacylation and suppression experiments, all tRNAs and mRNAs were simultaneously made and normalized by UV and densitometric analysis

using AlphaEaseFC Stand Alone (Alpha Innotech, San Leandro, CA). Stage VI oocytes of *Xenopus laevis* were prepared as described (70). All tRNAs were refolded at 65 °C for 2 min and 6-nitroveratryloxycarbonyl protected dCA-WF1/Biocytin/*p*-AcPhe was deprotected for 5 min by UV irradiation before injection (45). Oocytes were injected with 50 nl of mRNA alone or with tRNA and incubated at 18 °C for 44–52 h (unless otherwise stated in the Figure legends). 20 ng of mRNA in a subunit ratio of 10:1:1:1 for α :70UAG: β : γ : δ ; 2:5:1:1 for α : β :70UAG: γ : δ , α : β :70GGGU: γ : δ , α : β :19'UAG: γ : δ , α : β :19'GGGU: γ : δ ; and 2:1:1:5 for α : β : γ : δ :69UAG, α : β : γ : δ :69GGGU, and α : β : γ : δ :70UGA was injected in Table 6.1 with 10 ng of tRNA (when listed in Table 6.1). For TQAS-Biocytin and TQAS-*p*-AcPhe incorporation, 30 ng of mRNA (α :70UAG: β : γ : δ) in a subunit ratio of 10:1:1:1 was injected with 100 ng of tRNA-UAA. 15 ng of mRNA (α : β : γ : δ) in a subunit ratio of 2:1:1:1 was injected for the wild-type nAChR.

6.4.5 Electrophysiology

Recordings employed two-electrode voltage clamp on the OpusXpress 6000A (Molecular Devices). ACh was stored at -20 °C as a 1 M stock, diluted in Ca²⁺-free ND96, and delivered to oocytes by computer-controlled perfusion system. For all experiments, the holding potential was -60 mV. Suppression comparisons were tested with a single 1 mM ACh dose. Number of oocytes (*n*) is listed in Table 6.1.

6.4.6 Oocyte Labeling with Biotin Hydrazide and Cy5.5 Hydrazide

A 20 mM stock solution of biotin hydrazide was prepared in DMSO. 1 mM biotin hydrazide was prepared by adding 500 μ l of 20 mM biotin hydrazide in DMSO (5% DMSO in final volume) to 9.5 ml ND96 with Ca²⁺ with no antibiotics and no horse serum added to avoid reaction with biotin hydrazide. When varying pH, the final

solution was adjusted using a pH meter and the pH is listed with each figure legend. A single oocyte (uninjected, α 70UAG + TQAS-*p*-AcPhe, or α_{HA} and β_{HA}) was placed in a 1.5 ml eppendorf and labeled with 500 μ l of 1 mM biotin hydrazide for > 20 h.

1 mg of Cy5.5 hydrazide was dissolved in 500 μ l DMSO and added to 9.57 ml ND96 with Ca^{2+} (no antibiotics and no horse serum) pH = 4 to create 1 mM Cy5.5 hydrazide labeling solution. A single oocyte (uninjected, α 70UAG + TQAS-*p*-AcPhe, or α_{HA} and β_{HA}) was placed in a 1.5 ml eppendorf and 500 μ l of 1 mM Cy5.5 hydrazide solution was added. Oocytes were labeled for 22 h.

6.4.7 Oocyte Treatment with Carbohydrazide and NaBH_4

Carbohydrazide and NaBH_4 was dissolved in ND96 with Ca^{2+} (no antibiotics and no horse serum) pH = 4 to create 1 mM and 10 mM solutions immediately prior to treatment of cells. Single oocytes were placed in 1.5 ml eppendorfs and 500 μ l of 1 mM or 10 mM of carbohydrazide or NaBH_4 was added. Oocytes were treated with carbohydrazide for 45 h and NaBH_4 for 24 h. Oocytes were subsequently labeled with 1 mM biotin hydrazide (as described in Section 6.4.6).

6.4.8 Whole Oocyte Homogenization and Membrane Preparation

Whole-cell homogenization was preformed by placing four oocytes (either immediately from 18 °C incubator or after storage at -80 °C) in a 1.5 ml eppendorf and removing excess ND96. 10 μ l of homogenization buffer (100 mM NaCl, 50 mM Tris pH = 7.9, 0.6% SDS (w/v), 35 mM *n*-dodecyl β -D-maltoside (DDM) (Anatrace), and 1 protease inhibitor tablet) was added to the oocytes and oocytes were lysed manually with a pipette tip. The solution was sonicated for 10 min and centrifuged for 30 min to

remove insoluble debris. The supernatant was transferred to a new eppendorf and 10 μ l of 2X loading buffer was added. Samples were either stored at -80 °C or run on a gel.

Manual removal of membranes was performed as follows: oocytes were placed in hypotonic solution (5 mM NaCl, 5 mM HEPES pH = 7.5, 0.07% SDS (w/v)) and incubated for 10 min or until translucent oocyte membrane can be seen. The membrane was manually removed using forceps and placed in a 1.5 ml eppendorf kept on ice. 20 oocyte membranes were collected and then centrifuged for 10 min at 4 °C. The supernatant was removed and saved for Western blotting. 10 μ l of smashing buffer (100 mM NaPhosphate pH = 7.8, 0.5% (w/v) DDM, and 1 protease inhibitor tablet) was added to the membranes. The membranes were sonicated for 10 min and centrifuged for 10 min at 4 °C. The supernatant was removed from the insoluble fraction. 10 μ l of 2X loading buffer was added to 10 μ l of sample. Samples were either stored at -80 °C or run on a gel.

6.4.9 Western Blotting of Proteins Expressed in *Xenopus* Oocytes

Western blotting was performed as previously described (51). Briefly 20 μ l of samples were loaded on a 4–15% linear gradient, polyacrylamide-ready gel Tris-HCl (Bio-Rad) or 15% polyacrylamide-ready gel Tris-HCl (Bio-Rad) and run at 150 V for 1.25 h. Protein was transferred to nitrocellulose (Bio-Rad) at 30 V for 30 min and 100 V for 1.5 h. Nitrocellulose was blocked overnight using BSA (for biocytin detection) or non-fat dairy milk (NFDM) (for subunit stoichiometry determination) in 1X PBS / 0.1% Tween. 12.5 μ l of 1° Ab anti-HA from mouse and 5 μ l of Streptavidin-AlexaFluor680 in 15 ml BSA / 1X PBS / 0.1% Tween was for 1 h, washed 4X with 30 ml 1X PBS / 0.1% Tween for 5 min each, placed in 3 μ l 2° 800CW goat anti-mouse IgG in 15 mL BSA / 1X

PBS / 0.1% Tween was for 1 h, and washed 4X with 30 ml 1X PBS / 0.1% Tween for 5 min each. For subunit stoichiometry determination, the same procedure was used but NFDm replaced BSA and Streptavidin-680 was not used. Nitrocellulose was visualized using two-color infrared dye detection on the Odyssey (Li-Cor, Lincoln, NE) (Hsieh-Wilson lab). Densiometric analysis was performed using the Li-Cor Odyssey software package.

6.5 References

1. Prescher, J.A., and Bertozzi, C.R. (2005) Chemistry in living systems. *Nat. Chem. Biol.*, **1**, 13–21.
2. Griffin, B.A., Adams, S.R., and Tsien, R.Y. (1998) Specific covalent labeling of recombinant protein molecules inside live cells. *Science*, **281**, 269–272.
3. Adams, S.R., Campbell, R.E., Gross, L.A., Martin, B.R., Walkup, G.K., Yao, Y., Llopis, J., and Tsien, R.Y. (2002) New biarsenical ligands and tetracysteine motifs for protein labeling *in vitro* and *in vivo*: Synthesis and biological applications. *J. Am. Chem. Soc.*, **124**, 6063–6076.
4. Chen, I., Howarth, M., Lin, W., and Ting, A.Y. (2005) Site-specific labeling of cell surface proteins with biophysical probes using biotin ligase. *Nat. Methods*, **2**, 99–104.
5. Howarth, M., Takao, K., Hayashi, Y., and Ting, A.Y. (2005) Targeting quantum dots to surface proteins in living cells with biotin ligase. *Proc. Natl. Acad. Sci. USA*, **102**, 7583–7588.

6. Khidekel, N., Ficarro, S.B., Peters, E.C., and Hsieh-Wilson, L.C. (2004) Exploring the O-GlcNAc proteome: Direct identification of O-GlcNAc-modified proteins from the brain. *Proc. Natl. Acad. Sci. USA*, **101**, 13132–13137.
7. Laughlin, S.T., and Bertozzi, C.R. (2007) Metabolic labeling of glycans with azido sugars and subsequent glycan-profiling and visualization via Staudinger ligation. *Nat. Protoc.*, **2**, 2930–2944.
8. Chang, P.V., Prescher, J.A., Hangauer, M.J., and Bertozzi, C.R. (2007) Imaging cell surface glycans with bioorthogonal chemical reporters. *J. Am. Chem. Soc.*, **129**, 8400–8401.
9. Baskin, J.M., Prescher, J.A., Laughlin, S.T., Agard, N.J., Chang, P.V., Miller, I.A., Lo, A., Codelli, J.A., and Bertozzi, C.R. (2007) Copper-free click chemistry for dynamic *in vivo* imaging. *Proc. Natl. Acad. Sci. USA*, **104**, 16793–16797.
10. Yarema, K.J., Mahal, L.K., Bruehl, R.E., Rodriguez, E.C., and Bertozzi, C.R. (1998) Metabolic delivery of ketone groups to sialic acid residues. Application to cell surface glycoform engineering. *J. Biol. Chem.*, **273**, 31168–31179.
11. Saxon, E., and Bertozzi, C.R. (2000) Cell surface engineering by a modified Staudinger reaction. *Science*, **287**, 2007–2010.
12. Laughlin, S.T., Baskin, J.M., Amacher, S.L., and Bertozzi, C.R. (2008) *In vivo* imaging of membrane-associated glycans in developing zebrafish. *Science*, **320**, 664–667.
13. Datta, D., Wang, P., Carrico, I.S., Mayo, S.L., and Tirrell, D.A. (2002) A designed phenylalanyl-tRNA synthetase variant allows efficient *in vivo*

- incorporation of aryl ketone functionality into proteins. *J. Am. Chem. Soc.*, **124**, 5652–5653.
14. Kiick, K.L., Saxon, E., Tirrell, D.A., and Bertozzi, C.R. (2002) Incorporation of azides into recombinant proteins for chemoselective modification by the Staudinger ligation. *Proc. Natl. Acad. Sci. USA*, **99**, 19–24.
 15. Link, A.J., and Tirrell, D.A. (2003) Cell surface labeling of *Escherichia coli* via copper(I)-catalyzed [3+2] cycloaddition. *J. Am. Chem. Soc.*, **125**, 11164–11165.
 16. Beatty, K.E., Xie, F., Wang, Q., and Tirrell, D.A. (2005) Selective dye-labeling of newly synthesized proteins in bacterial cells. *J. Am. Chem. Soc.*, **127**, 14150–14151.
 17. Dieterich, D.C., Link, A.J., Graumann, J., Tirrell, D.A., and Schuman, E.M. (2006) Selective identification of newly synthesized proteins in mammalian cells using bioorthogonal noncanonical amino acid tagging (BONCAT). *Proc. Natl. Acad. Sci. USA*, **103**, 9482–9487.
 18. Chin, J.W., Santoro, S.W., Martin, A.B., King, D.S., Wang, L., and Schultz, P.G. (2002) Addition of *p*-azido-L-phenylalanine to the genetic code of *Escherichia coli*. *J. Am. Chem. Soc.*, **124**, 9026–9027.
 19. Wang, L., Zhang, Z., Brock, A., and Schultz, P.G. (2003) Addition of the keto functional group to the genetic code of *Escherichia coli*. *Proc. Natl. Acad. Sci. USA*, **100**, 56–61.
 20. Zhang, Z., Smith, B.A., Wang, L., Brock, A., Cho, C., and Schultz, P.G. (2003) A new strategy for the site-specific modification of proteins *in vivo*. *Biochemistry*, **42**, 6735–6746.

21. Deiters, A., and Schultz, P.G. (2005) *In vivo* incorporation of an alkyne into proteins in *Escherichia coli*. *Bioorg. Med. Chem. Lett.*, **15**, 1521–1524.
22. Zeng, H., Xie, J., and Schultz, P.G. (2006) Genetic introduction of a diketone-containing amino acid into proteins. *Bioorg. Med. Chem. Lett.*, **16**, 5356–5359.
23. Meddows, E., Le Bourdelles, B., Grimwood, S., Wafford, K., Sandhu, S., Whiting, P., and McIlhinney, R.A. (2001) Identification of molecular determinants that are important in the assembly of N-methyl-D-aspartate receptors. *J. Biol. Chem.*, **276**, 18795–18803.
24. Atlason, P.T., Garside, M.L., Meddows, E., Whiting, P., and McIlhinney, R.A. (2007) N-Methyl-D-aspartate (NMDA) receptor subunit NR1 forms the substrate for oligomeric assembly of the NMDA receptor. *J. Biol. Chem.*, **282**, 25299–25307.
25. Keller, S.H., and Taylor, P. (1999) Determinants responsible for assembly of the nicotinic acetylcholine receptor. *J. Gen. Physiol.*, **113**, 171–176.
26. Ben-Ami, H.C., Yassin, L., Farah, H., Michaeli, A., Eshel, M., and Treinin, M. (2005) RIC-3 affects properties and quantity of nicotinic acetylcholine receptors via a mechanism that does not require the coiled-coil domains. *J. Biol. Chem.*, **280**, 28053–28060.
27. Saedi, M.S., Conroy, W.G., and Lindstrom, J. (1991) Assembly of *Torpedo* acetylcholine receptors in *Xenopus* oocytes. *J. Cell Biol.*, **112**, 1007–1015.
28. Wanamaker, C.P., Christianson, J.C., and Green, W.N. (2003) Regulation of nicotinic acetylcholine receptor assembly. *Ann. N.Y. Acad. Sci.*, **998**, 66–80.

29. Green, W.N. (1999) Ion channel assembly: Creating structures that function. *J. Gen. Physiol.*, **113**, 163–170.
30. Le Novere, N., Corringer, P.J., and Changeux, J.P. (2002) The diversity of subunit composition in nAChRs: Evolutionary origins, physiologic and pharmacologic consequences. *J. Neurobiol.*, **53**, 447–456.
31. Cooper, E., Couturier, S., and Ballivet, M. (1991) Pentameric structure and subunit stoichiometry of a neuronal nicotinic acetylcholine receptor. *Nature*, **350**, 235–238.
32. MacKinnon, R., Aldrich, R.W., and Lee, A.W. (1993) Functional stoichiometry of Shaker potassium channel inactivation. *Science*, **262**, 757–759.
33. Liman, E.R., Tytgat, J., and Hess, P. (1992) Subunit stoichiometry of a mammalian K⁺ channel determined by construction of multimeric cDNAs. *Neuron*, **9**, 861–871.
34. He, Y., Ruiz, M., and Karpen, J.W. (2000) Constraining the subunit order of rod cyclic nucleotide-gated channels reveals a diagonal arrangement of like subunits. *Proc. Natl. Acad. Sci. USA*, **97**, 895–900.
35. Zheng, J., Trudeau, M.C., and Zagotta, W.N. (2002) Rod cyclic nucleotide-gated channels have a stoichiometry of three CNGA1 subunits and one CNGB1 subunit. *Neuron*, **36**, 891–896.
36. Zhong, H., Molday, L.L., Molday, R.S., and Yau, K.W. (2002) The heteromeric cyclic nucleotide-gated channel adopts a 3A:1B stoichiometry. *Nature*, **420**, 193–198.

37. Ulbrich, M.H., and Isacoff, E.Y. (2007) Subunit counting in membrane-bound proteins. *Nat. Methods*, **4**, 319–321.
38. Christianson, J.C., and Green, W.N. (2004) Regulation of nicotinic receptor expression by the ubiquitin-proteasome system. *EMBO J.*, **23**, 4156–4165.
39. Gallivan, J.P., Lester, H.A., and Dougherty, D.A. (1997) Site-specific incorporation of biotinylated amino acids to identify surface-exposed residues in integral membrane proteins. *Chem. Biol.*, **4**, 739–749.
40. Tzartos, S.J., Cung, M.T., Demange, P., Loutrari, H., Mamalaki, A., Marraud, M., Papadouli, I., Sakarellos, C., and Tsikaris, V. (1991) The main immunogenic region (MIR) of the nicotinic acetylcholine receptor and the anti-MIR antibodies. *Mol. Neurobiol.*, **5**, 1–29.
41. Mamalaki, A., and Tzartos, S.J. (1994) Nicotinic acetylcholine receptor: Structure, function and main immunogenic region. *Adv. Neuroimmunol.*, **4**, 339–354.
42. Miyazawa, A., Fujiyoshi, Y., and Unwin, N. (2003) Structure and gating mechanism of the acetylcholine receptor pore. *Nature*, **423**, 949–955.
43. Dahan, D.S., Dibas, M.I., Petersson, E.J., Auyeung, V.C., Chanda, B., Bezanilla, F., Dougherty, D.A., and Lester, H.A. (2004) A fluorophore attached to nicotinic acetylcholine receptor beta M2 detects productive binding of agonist to the alpha delta site. *Proc. Natl. Acad. Sci. USA*, **101**, 10195–10200.
44. Pantoja, R., Rodriguez, E.A., Dibas, M.I., Dougherty, D.A., and Lester, H.A. (2008) Single-molecule imaging of a fluorescent unnatural amino acid incorporated into functional nicotinic acetylcholine receptors. *Submitted*.

45. Saks, M.E., Sampson, J.R., Nowak, M.W., Kearney, P.C., Du, F.Y., Abelson, J.N., Lester, H.A., and Dougherty, D.A. (1996) An engineered *Tetrahymena* tRNA^{Gln} for *in vivo* incorporation of unnatural amino acids into proteins by nonsense suppression. *J. Biol. Chem.*, **271**, 23169–23175.
46. Beene, D.L., Dougherty, D.A., and Lester, H.A. (2003) Unnatural amino acid mutagenesis in mapping ion channel function. *Curr. Opin. Neurobiol.*, **13**, 264–270.
47. Dougherty, D.A. (2000) Unnatural amino acids as probes of protein structure and function. *Curr. Opin. Biotechnol.*, **4**, 645–652.
48. Rodriguez, E.A., Lester, H.A., and Dougherty, D.A. (2007) Improved amber and opal suppressor tRNAs for incorporation of unnatural amino acids *in vivo*. Part 1: Minimizing misacylation. *RNA*, **13**, 1703–1714.
49. Rodriguez, E.A., Lester, H.A., and Dougherty, D.A. (2006) *In vivo* incorporation of multiple unnatural amino acids through nonsense and frameshift suppression. *Proc. Natl. Acad. Sci. USA*, **103**, 8650–8655.
50. Rodriguez, E.A., Lester, H.A., and Dougherty, D.A. (2007) Improved amber and opal suppressor tRNAs for incorporation of unnatural amino acids *in vivo*. Part 2: Evaluating suppression efficiency. *RNA*, **13**, 1715–1722.
51. England, P.M., Zhang, Y.N., Dougherty, D.A., and Lester, H.A. (1999) Backbone mutations in transmembrane domains of a ligand-gated ion channel: Implications for the mechanism of gating. *Cell*, **96**, 89–98.
52. England, P.M., Lester, H.A., and Dougherty, D.A. (1999) Mapping disulfide connectivity using backbone ester hydrolysis. *Biochemistry*, **38**, 14409–14415.

53. Watanabe, T., Muranaka, N., Iijima, I., and Hohsaka, T. (2007) Position-specific incorporation of biotinylated non-natural amino acids into a protein in a cell-free translation system. *Biochem. Biophys. Res. Commun.*, **361**, 794–799.
54. Changeux, J.P., Kasai, M., and Lee, C.Y. (1970) Use of a snake venom toxin to characterize the cholinergic receptor protein. *Proc. Natl. Acad. Sci. USA*, **67**, 1241–1247.
55. Green, N.M. (1990) Avidin and streptavidin. *Methods Enzymol.*, **184**, 51–67.
56. Drenan, R.M., Nashmi, R., Imoukhuede, P., Just, H., McKinney, S., and Lester, H.A. (2008) Subcellular trafficking, pentameric assembly, and subunit stoichiometry of neuronal nicotinic acetylcholine receptors containing fluorescently labeled alpha6 and beta3 subunits. *Mol. Pharmacol.*, **73**, 27–41.
57. Jansen, M., Bali, M., and Akabas, M.H. (2008) Modular design of Cys-loop ligand-gated ion channels: Functional 5-HT₃ and GABA_A rho1 receptors lacking the large cytoplasmic M3M4 loop. *J. Gen. Physiol.*, **131**, 137–146.
58. Brandt, G.S. (2003) *Ph. D. Thesis*, California Institute of Technology, Pasadena, CA.
59. Shafer, A.M., Kalai, T., Bin Liu, S.Q., Hideg, K., and Voss, J.C. (2004) Site-specific insertion of spin-labeled L-amino acids in *Xenopus* oocytes. *Biochemistry*, **43**, 8470–8482.
60. Tokmakov, A.A., Matsumoto, E., Shirouzu, M., and Yokoyama, S. (2006) Coupled cytoplasmic transcription-and-translation—a method of choice for heterologous gene expression in *Xenopus* oocytes. *J. Biotechnol.*, **122**, 5–15.

61. Harel, M., Kasher, R., Nicolas, A., Guss, J.M., Balass, M., Fridkin, M., Smit, A.B., Brejc, K., Sixma, T.K., Katchalski-Katzir, E. *et al.* (2001) The binding site of acetylcholine receptor as visualized in the X-Ray structure of a complex between alpha-bungarotoxin and a mimotope peptide. *Neuron*, **32**, 265–275.
62. West, A.P., Jr., Bjorkman, P.J., Dougherty, D.A., and Lester, H.A. (1997) Expression and circular dichroism studies of the extracellular domain of the alpha subunit of the nicotinic acetylcholine receptor. *J. Biol. Chem.*, **272**, 25468–25473.
63. Blount, P., and Merlie, J.P. (1988) Native folding of an acetylcholine receptor alpha subunit expressed in the absence of other receptor subunits. *J. Biol. Chem.*, **263**, 1072–1080.
64. Claudio, T., Paulson, H.L., Green, W.N., Ross, A.F., Hartman, D.S., and Hayden, D. (1989) Fibroblasts transfected with Torpedo acetylcholine receptor beta-, gamma-, and delta-subunit cDNAs express functional receptors when infected with a retroviral alpha recombinant. *J. Cell Biol.*, **108**, 2277–2290.
65. Robertson, S.A., Noren, C.J., Anthony-Cahill, S.J., Griffith, M.C., and Schultz, P.G. (1989) The use of 5'-phospho-2 deoxyribocytidylylriboadenosine as a facile route to chemical aminoacylation of tRNA. *Nucleic Acids Res.*, **17**, 9649–9660.
66. Kearney, P.C., Nowak, M.W., Zhong, W., Silverman, S.K., Lester, H.A., and Dougherty, D.A. (1996) Dose-response relations for unnatural amino acids at the agonist binding site of the nicotinic acetylcholine receptor: Tests with novel side chains and with several agonists. *Mol. Pharmacol.*, **50**, 1401–1412.
67. Zhong, W., Gallivan, J.P., Zhang, Y., Li, L., Lester, H.A., and Dougherty, D.A. (1998) From ab initio quantum mechanics to molecular neurobiology: A cation- π

- binding site in the nicotinic receptor. *Proc. Natl. Acad. Sci. USA*, **95**, 12088–12093.
68. Nowak, M.W., Gallivan, J.P., Silverman, S.K., Labarca, C.G., Dougherty, D.A., and Lester, H.A. (1998) *In vivo* incorporation of unnatural amino acids into ion channels in *Xenopus* oocyte expression system. *Meth. Enzymol.*, **293**, 504–529.
69. Petersson, E.J., Shahgholi, M., Lester, H.A., and Dougherty, D.A. (2002) MALDI-TOF mass spectrometry methods for evaluation of *in vitro* aminoacyl tRNA production. *RNA*, **8**, 542–547.
70. Quick, M.W., and Lester, H.A. (1994) Methods for expression of excitability proteins in *Xenopus* oocytes. In Narahashi, T. (ed.), *Ion Channels of Excitable Cells*. Academic Press, San Diego, CA, Vol. 19, pp. 261–279.

Chapter 7

Unnatural Amino Acid Replacement Scanning
in *Xenopus* oocytes

7.1 Introduction

There are many methodologies for the incorporation of unnatural amino acids (UAAs) *in vivo* (1–7). UAA incorporation by the endogenous translational machinery is typically performed in *E. coli* or other prokaryotes using auxotrophs (reassignment of sense codons) or by removing natural amino acids (aas) from growth media (statistical UAA incorporation) (8–19). Recent *in vitro* techniques identified 90 UAAs (59 previously unknown) that are substrates of *E. coli* aaRSs and aminoacylated onto tRNA (20). Of these 90, 71 UAAs were tested and 41 UAAs were accepted by the *E. coli* translational machinery *in vitro*, allowing for the simultaneous incorporation of 13 UAAs (21). UAA incorporation by the endogenous translational machinery in eukaryotic cells hasn't been studied extensively and experiments cause heterogeneous incorporation of UAAs (statistical UAA incorporation) in all proteins translated (22–24). Site-specific UAA incorporation, reassignment of sense codons, or statistical UAA incorporation is known to alter the stability, spectral properties, substrate binding, folding, expression, pore gating, and function of proteins (2–8,14,16,17,19,25–35).

Recently, UAAs have become commercially available for use in eukaryotic cells. Azidohomoalanine has been used to identify newly translated proteins in HEK cells and neurons (23) and is commercially available from Molecular Probes. Photoleucine (PLeu) and Photomethionine (PMet) (shown in Figure 7.1) are used to identify protein-protein interactions in eukaryotic cells (22) and are commercially available from Pierce. These UAAs are heterogeneously incorporated in all translated proteins upon supplementation in the growth media, but little is known about the effect (if any) on protein stability, folding, expression, and function.

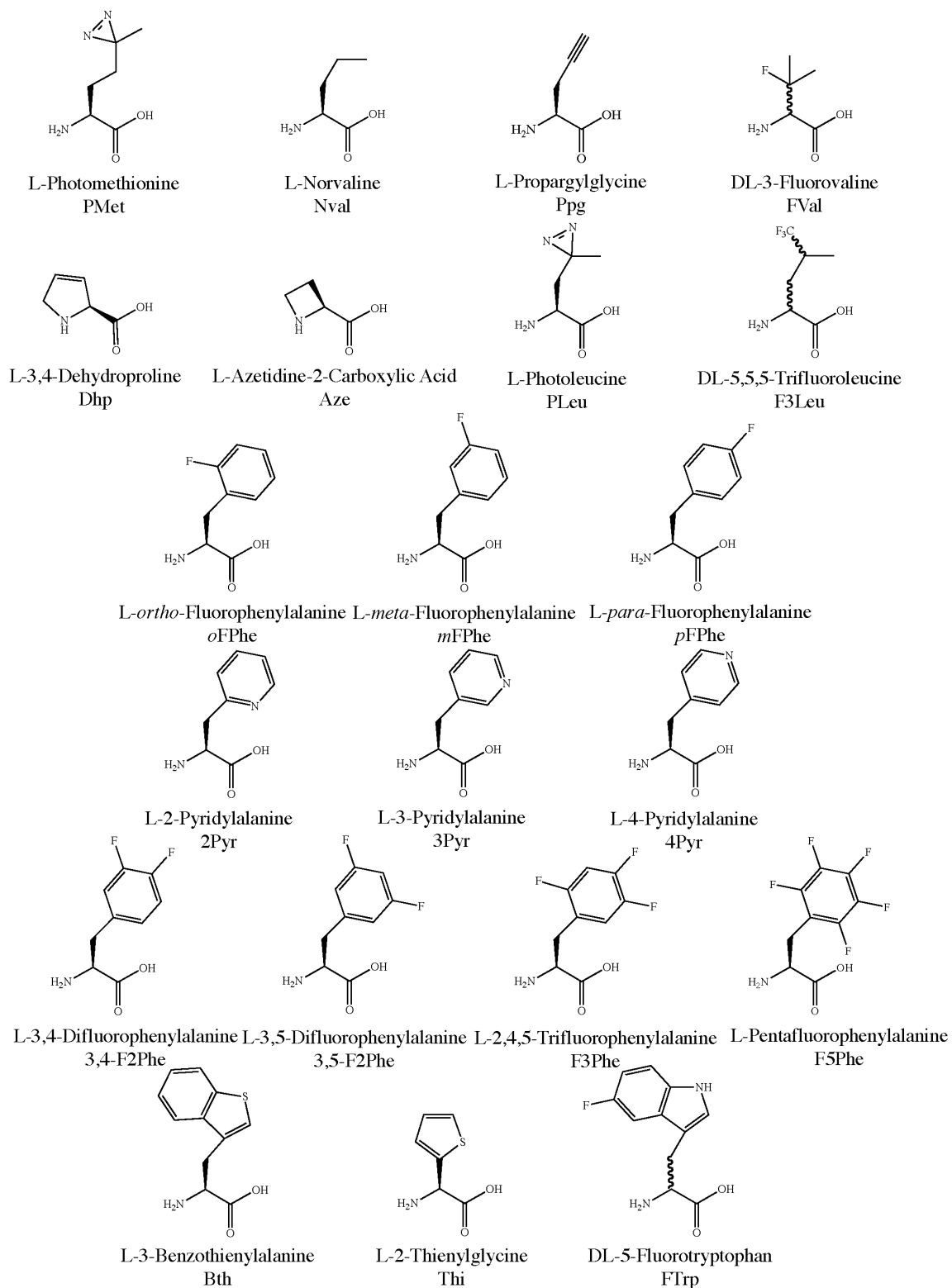


Figure 7.1: Unnatural amino acids used in this research.

In this research, we heterogeneously incorporated UAAs into the nicotinic acetylcholine receptor (nAChR) expressed in *Xenopus* oocytes. The heterogeneous incorporation of UAAs is termed unnatural amino acid replacement scanning (UAARS) because of the similarity to alanine scanning mutagenesis, where specific aas are mutated to Ala and the functions of proteins are examined. Because only UAAs that are similar to the cognate natural aa will be charged onto a tRNA, UAARS results in less side chain perturbation than most conventional mutagenesis. UAARS does not require DNA mutation and creates a large heterogeneous population of protein (discussed in detail below). The nAChR was expressed with UAAs in the incubation media, and changes in function were identified by shifts in EC_{50} . The incorporation of PLeu and PMet was also identified by inter-subunit cross-linking of the nAChR. The expression of functional ion channels on the surface of *Xenopus* oocytes was determined by electrophysiology and compared to total protein synthesized by Western blot analysis. UAARS should be useful for identifying UAAs that are recognized by the endogenous translational machinery, identifying changes in protein function without the need for DNA manipulation, and creation of extremely large populations of chemically unique proteins.

7.2 Results

7.2.1 Unnatural Amino Acid Replacement Scanning

In this research, the $\alpha_{\text{HA His}}$ (contains the HA tag in the M3-M4 loop and a 6-His tag on the C-terminus) construct was initially used, because it was hoped that the α -subunit could be purified using the 6-His tag as previously described (36). The EC_{50} of $\alpha_{\text{HA His}}$ nAChR was reported as 25.5 μM ACh (36), but references a paper that has a wild-

type nAChR $EC_{50} = 47 \mu\text{M}$ (37). During the course of this research, the $\alpha_{\text{HA His}}$ construct gave a variable EC_{50} ranging from 48–70 μM depending on the batch of oocytes. The α_{NHA} (contains the HA tag at the N-terminus) construct gave EC_{50} values ranging from 47–56 μM and is a better construct for reproducible wild-type nAChR values. Due to the variability of the $\alpha_{\text{HA His}}$ EC_{50} , the UAARS experiments are compared to the $\alpha_{\text{HA His}}$ wild-type EC_{50} recorded on the same batch of oocytes.

The *Xenopus* oocyte (stage VI) is a large cell measuring $\approx 1.2\text{--}1.3$ mm in diameter (38,39). The oocyte starts at stage I and is approximately 0.1 mm in diameter (38). Oogenesis is asynchronous, and oocytes of all stages are present in the ovary of a *Xenopus laevis* frog (38). Complete oogenesis takes ~ 8 months to reach stage VI, and oocytes remain in this stage until they are stimulated for maturation or the oocyte is absorbed by the ovary (38,39). During oogenesis, the oocyte accumulates ribosomes, yolk, glycogen, lipids, aas, and “maternal mRNA” (39). Oocytes contain a large pool of endogenous aas in preparation for protein synthesis (40). Heterologous expression of protein through injection of DNA or mRNA is an invaluable tool for studying ion channels, transporters, and receptors. Injected oocytes are typically incubated in saline solutions lacking any aas and still produce large amounts of protein (39,40).

Oocytes maintained in saline solution contain a large pool of aas that is greater than the concentration of aas found in *Xenopus laevis* plasma (40). The most abundant aas are Glu (3.6 mM) and Lys (1.1 mM), which are present in the plasma at concentrations of 0.11 mM and 0.29 mM, respectively (40). Oocytes maintained in saline solution have 0.20 mM Val, 0.19 mM Leu, and 0.13 mM Phe, but when incubated with saline solutions containing aas that mimic plasma concentrations, the oocytes uptake

aas to give 0.72 mM Val, 0.62 mM Leu, and 0.30 mM Phe (40). Therefore, oocytes rapidly import aas, and it was hoped that the same would occur for UAAs. The large endogenous pool of aas is a limiting factor for UAARS. Based on the determined concentration of aas in *Xenopus* oocytes kept in saline solution (40), Ile is the limiting aa, and yet there is enough Ile to make 2.4×10^{11} nAChRs (corresponding to $6.1 \times 10^5 \mu\text{A}$), which is at least three orders of magnitude greater expression than we ever see in a single oocyte. To incorporate UAAs by the endogenous translational machinery we must get a large amount of UAA inside the oocyte in order to compete with the endogenous aas.

Figure 7.2 schematically shows unnatural amino acid replacement scanning (UAARS) in *Xenopus* oocytes. Oocytes contain endogenous natural aas and are injected with mRNA for the nAChR. After injection, the oocytes are placed in media containing 0.5–4 mM UAA (Figure 7.2 A). The oocytes then begin to translate the nAChR, which depletes endogenous aas. Initially, all nAChRs are wild-type (containing no UAAs). Also during this time, UAAs are transported into the oocyte (Figure 7.2 B). Translation of the nAChR causes further depletion of the endogenous aas. As the concentration of UAA increases in the oocyte, an endogenous aminoacyl-tRNA synthetase (aaRS) recognizes the UAA and charges the cognate tRNA. The UAA is then heterogeneously incorporated into the nAChR at all positions recognized by the tRNA (Figure 7.2 C). Further incubation causes increased UAAs inside of the oocyte and further incorporation into the nAChR (Figure 7.2 D). During the incubation periods, the media is changed every 24 h to maintain excess UAA and to increase incorporation into the nAChR. After an incubation period, the oocytes are assayed by electrophysiology to determine shifts in EC_{50} and alterations in functional ion channel expression relative to oocytes not incubated

with UAAs. Electrophysiology only detects channels that are functional (gated by acetylcholine (ACh)) and on the oocyte membrane surface. For the UAAs PLeu and PMet (shown in Figure 7.1), oocytes were irradiated with UV to cross-link the subunits within an individual nAChR and analyzed by Western blot for increased molecular weight bands. Oocytes can also be analyzed by whole-cell Western blot to determine the total amount of protein translated (nAChR that is on the membrane surface, in the endoplasmic reticulum, in the golgi apparatus, and in vesicles) relative to oocytes not incubated with UAAs.

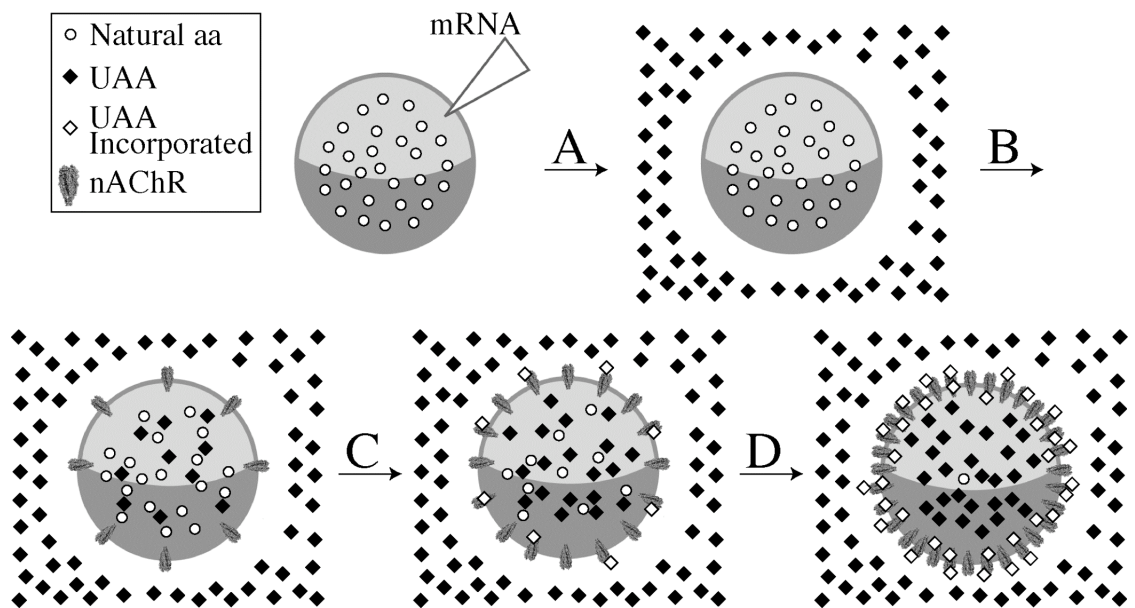


Figure 7.2: Unnatural amino acid replacement scanning (UAARS). A) Oocytes are injected with wild-type nAChR mRNA, which have endogenous, natural aas. The oocytes are placed in media containing UAAs and lacking the natural aa. B) After incubation; mRNA is translated, endogenous aas are depleted, and UAAs are transported inside the oocyte. C) With further incubation; more mRNA is translated, endogenous aas are further depleted, more UAAs are transported inside the oocyte, and UAAs are heterogeneously incorporated into the nAChR. D) Increased incubation time causes further mRNA translation, depletion of endogenous aas, increased UAAs inside the oocyte, and increased heterogeneous incorporation of UAAs into the nAChR. Figure adapted from (4) and nAChR created from 2BG9.pdb (41).

UAARS creates a large population of nAChRs, which is unprecedented without mutating DNA. For example, there are 251 Leu residues in the mouse muscle nAChR, and this is the most abundant aa (Figure 7.3). There are 37 Leu in the α -subunit, 57 Leu in the β -subunit, 65 Leu in the γ -subunit, and 55 Leu in the δ -subunit. The subunit stoichiometry of the nAChR is $2\alpha:\beta:\gamma:\delta$ (Figure 6.1). Treating each of the five subunits as chemically distinct, there are 251 possible nAChRs when only a single UAA is incorporated. If a single UAA is incorporated in three of the subunits, there are 1.2×10^6 possible nAChRs. A single UAA incorporated in each of the five subunits results in 2.8×10^8 possible nAChRs. If all of the 251 sites can contain either Leu or an UAA, there are 7.8×10^{16} possible nAChRs, which is 7.8×10^5 times greater than the $\sim 1 \times 10^{11}$ neurons in an adult human brain. This example only includes UAARS at Leu but in theory incorporation at multiple UAAs is possible and can create increased populations of nAChRs.

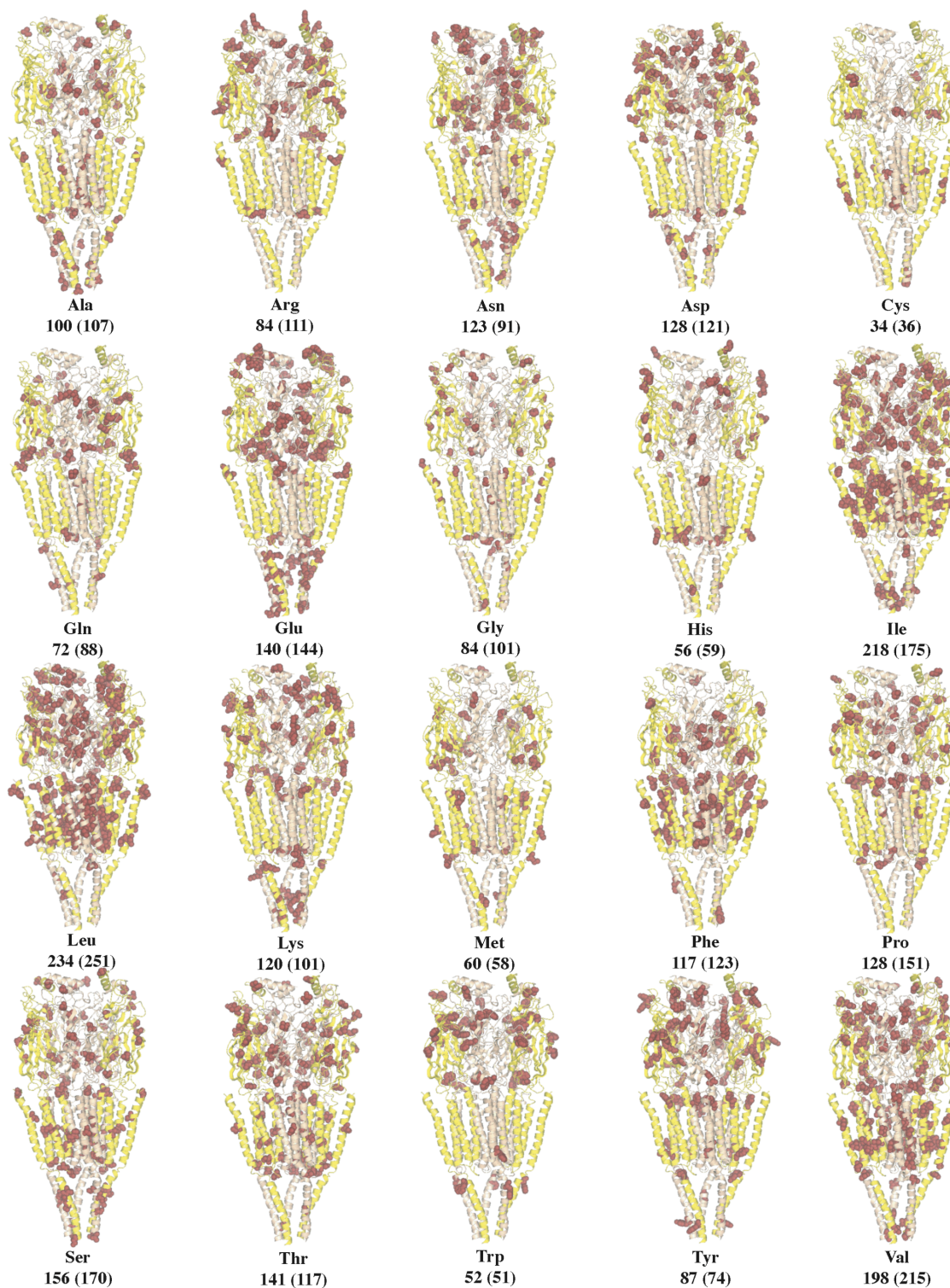


Figure 7.3: Amino acid composition of the nAChR. Number on left is the number of aas in the *Torpedo* nAChR (shown in red) and (number) is the number of aas in the mouse muscle nAChR. The α -subunit is shown in yellow and all other subunits are beige. Images created from 2BG9.pdb (41).

7.2.2 Met Derivatives

There are 58 Met aas in the nAChR (Figure 7.3). PMet (shown in Figure 7.1) is accepted by the translational machinery and incorporated into proteins in COS7 (monkey kidney) and HeLa (human cervical cancer) cells (22). UAARS with PMet showed no significant shift in EC_{50} (Table 7.1). Nval (shown in Figure 7.1) is accepted by the *E. coli* methionyl-aminoacyl synthetase (MetRS) and aminoacylated on tRNA^{Met} *in vitro* (20), and Nval is also accepted by the *E. coli* translational machinery *in vitro* (21). Nval incorporation was also detected in *E. coli* Met auxotrophs *in vivo* (13). UAARS with Nval showed no significant shift in EC_{50} (Table 7.1). Ppg has been shown to be accepted by the *E. coli* MetRS and aminoacylated on tRNA^{Met} *in vitro* (20), but was not accepted by the *E. coli* translational machinery *in vitro* and *in vivo* (13,21). UAARS with Ppg showed no shift in EC_{50} (Table 7.1). While no significant shift was seen in the EC_{50} for these three Met derivatives, UAA incorporation into the nAChR may occur and cause no change in function. Other methods may be necessary for detection or UAARS into other ion channels.

Table 7.1: UAARS EC₅₀ determination

	UAA	EC ₅₀	Shift ^a	n _H	n ^b	Incubation	
						Time	[UAA] ^c
Met Derivatives	PMet	64 ± 1	1.05	1.5 ± .04	8	48 h	0.5 mM
	Nval	49 ± 1	1.02	1.5 ± 1	7	48 h	1 mM
	Ppg	72 ± 4	1.07	1.5 ± .09	8	48 h	2 mM
Pro Derivatives	Dhp	58 ± 3	1.16	1.4 ± .08	6	48 h	1 mM
	Dhp	39 ± 2	1.33	1.5 ± .07	5	120 h	4 mM
	Aze	48 ± 1	1.04	1.4 ± .05	8	48 h	1 mM
	Aze	38 ± 1	1.37	1.4 ± .08	7	120 h	4 mM
Val Derivative	FVal	81 ± 3	1.65	1.7 ± .09	7	48 h	2 mM
Leu Derivatives	PLeu	18 ± 2	3.72	.93 ± .07	6	48 h	0.5 mM
	PLeu	17 ± 2	3.94	.99 ± .1	4	48 h	1 mM
	PLeu	2.5 ± .3	21.2	1.1 ± .1	6	120 h	1 mM
	F3Leu	25 ± 1	2.12	1.1 ± .05	6	48 h	2 mM
	F3Leu	11 ± 1	4.82	1.2 ± .1	7	120 h	2 mM
Phe Derivatives	<i>o</i> FPhE	82 ± 3	1.57	1.4 ± .06	6	48 h	1 mM
	<i>m</i> FPhE	32 ± 1	1.66	1.1 ± .06	7	48 h	1 mM
	<i>p</i> FPhE	8.2 ± .4	6.46	0.89 ± .03	6	48 h	1 mM
	3,4-F2PhE	53 ± 0.8	1.26	1.2 ± .01	8	48 h	2 mM
	3,5-F2PhE	69 ± 1	1.03	1.4 ± .03	8	48 h	2 mM
	F3PhE	60 ± 2	1.12	1.5 ± .05	8	48 h	2 mM
	F5PhE	63 ± 0.9	1.06	1.6 ± .03	8	48 h	2 mM
	2Pyr	74 ± 1	1.35	1.3 ± .02	6	48 h	2 mM
	3Pyr	41 ± .9	1.22	1.5 ± .04	5	48 h	2 mM
	4Pyr	51 ± 1	1.08	1.4 ± .05	5	48 h	2 mM
Trp Derivatives	Bth	49 ± 1	1.1	1.4 ± .05	6	48 h	2 mM
	Thi	52 ± 2	1.06	1.2 ± .05	6	48 h	2 mM
	FTrp	144 ± 9	2.88	1.4 ± .09	7	48 h	2 mM
Multiple UAAs	PMet + PLeu	13 ± 2	5.08	1.4 ± .2	6	48 h	0.5 mM PMet 1 mM PLeu

^a Shift in EC₅₀ relative to wild-type nAChR EC₅₀ recorded on the same day.

^b Number of oocytes.

^c Concentration of UAA in media.

7.2.3 Pro Derivatives

There are 151 Pro aas in the nAChR (Figure 7.3). Dhp (shown in Figure 7.1) is recognized by the *E. coli* prolyl-aminoacyl tRNA synthetase (ProRS) *in vitro* (20) and accepted by the *E. coli* translational machinery *in vitro* (21). Dhp has also been

incorporated into protein expressed in *E. coli* (10). UAARS with Dhp shows only a slight shift in EC_{50} with a 2 d incubation (Table 7.1). UAARS with Dhp shows a meaningfully increased shift in EC_{50} with a 5 d incubation (Table 7.1). Aze (shown in Figure 7.1) is recognized by the *E. coli* ProRS *in vitro* (20) and accepted by the *E. coli* translational machinery *in vitro* (21). Aze has also been incorporated into protein expressed in *E. coli* (9). UAARS with Aze shows no shift in EC_{50} with a 2 d incubation (Table 7.1). With a 5 d incubation, Aze shows a significant shift in EC_{50} (Table 7.1). Both Dhp and Aze show significant shifts in EC_{50} that are gain of function (GOF) phenotypes with 5 d incubations, but are insignificant with 2 d incubations. Further incubation time may be necessary to obtain more efficient incorporation of these Pro derivatives.

7.2.4 Val Derivative

There are 215 Val aas in the nAChR (Figure 7.3). FVal (shown in Figure 7.1) is recognized by the *E. coli* valyl-aminoacyl tRNA synthetase *in vitro* (20) and accepted by the *E. coli* translational machinery *in vitro* (21). UAARS with FVal shows a significant 1.7-fold shift in EC_{50} (Table 7.1) and causes a loss of function (LOF) phenotype.

7.2.5 Leu Derivatives

There are 251 Leu aas in the nAChR, which is the most abundant aa (Figure 7.3). PLeu is accepted by the translational machinery and incorporated into proteins in COS7 and HeLa cells (22). UAARS shows a 3.7- and 3.9-fold shift in EC_{50} with 0.5 mM and 1 mM PLeu, respectively (Figure 7.4 A). This experiment clearly illustrates that 0.5 mM PLeu in the media is sufficient and gives approximately the same EC_{50} as 1 mM PLeu. UAARS shows no shift in EC_{50} with 0.5 mM and 1 mM PMet (Figure 7.4 A). *In vivo*

cross-linking experiments typically use both PLeu and PMet (22). UAARS with PLeu and PMet show 5.1-fold shift in EC_{50} (Figure 7.4 A). This EC_{50} is approximately the same for PLeu incorporation alone (Figure 7.4 A), showing that changes in nAChR function is primarily, if not exclusively, due to PLeu incorporation alone.

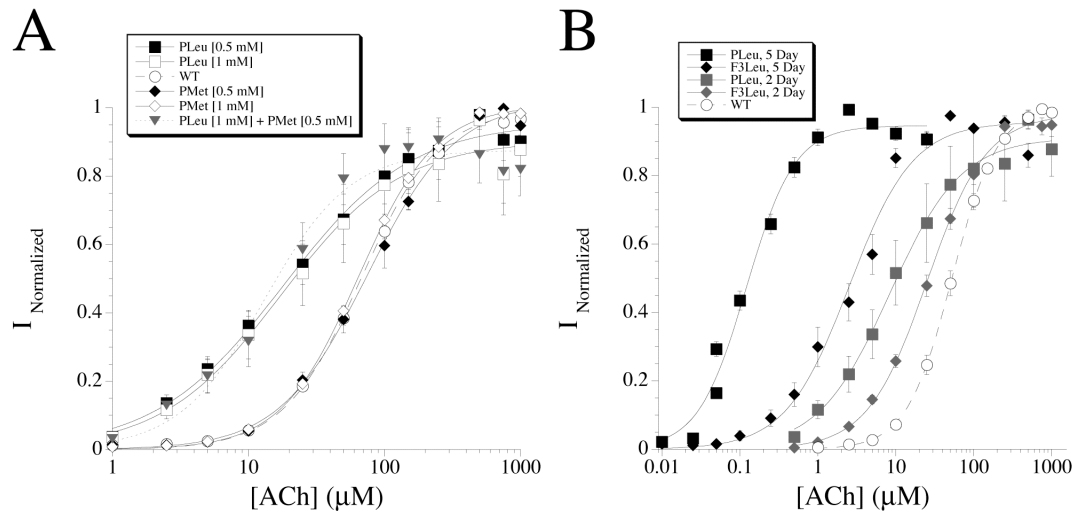


Figure 7.4: Fits to the Hill equation for UAARS with PLeu, PMet, and F3Leu. A) UAARS with PLeu, PMet, and PLeu + PMet. PLeu [0.5 mM] $EC_{50} = 18 \pm 2$ and $n_H = 0.93 \pm 0.07$. PLeu [1 mM] $EC_{50} = 17 \pm 2$ and $n_H = 0.99 \pm 0.1$. Wild-type $\alpha_{HA His}$ nAChR $EC_{50} = 67 \pm 2$ and $n_H = 1.5 \pm 0.06$. PMet [0.5 mM] $EC_{50} = 75 \pm 4$ and $n_H = 1.4 \pm 0.09$. PMet [1 mM] $EC_{50} = 64 \pm 1$ and $n_H = 1.5 \pm 0.04$. PLeu [1 mM] + PMet [0.5 mM] $EC_{50} = 13 \pm 2$ and $n_H = 1.4 \pm 0.2$. In each experiment $n > 4$ oocytes. B) UAARS with PLeu and F3Leu with 2 and 5 d incubations. PLeu (5 d incubation) $EC_{50} = 2.5 \pm 0.3$ and $n_H = 1.1 \pm 0.1$. F3Leu (5 d incubation) $EC_{50} = 11 \pm 1$ and $n_H = 1.2 \pm 0.1$. PLeu (2 d incubation) $EC_{50} = 17 \pm 2$ and $n_H = 0.99 \pm 0.1$. F3Leu (2 d incubation) $EC_{50} = 25 \pm 1$ and $n_H = 1.1 \pm 0.05$. Wild-type $\alpha_{HA His}$ nAChR $EC_{50} = 53 \pm 0.7$ and $n_H = 1.5 \pm 0.02$. In each experiment $n > 3$ oocytes.

F3Leu (shown in Figure 7.1) is recognized by the *E. coli* leucyl-aminoacyl tRNA synthetase *in vitro* (20) and accepted by the *E. coli* translational machinery *in vitro* (21). F3Leu has also been incorporated in proteins expressed in *E. coli* auxotrophs *in vivo* (17). UAARS with F3Leu shows a 2.1- and 4.8-fold shift in EC_{50} with 2 and 5 d incubation, respectively (Figure 7.4 B). UAARS with PLeu shows a 3.9- and 21-fold shift in EC_{50}

with 2 and 5 d incubation, respectively (Figure 7.4 B). Both F3Leu and PLeu show increased UAA incorporation with increased time, but the shift in F3Leu (2.3 from 5 d to 2 d) is not as strong as PLeu (5.4 from 5 d to 2 d) even though these UAAs are both replacing Leu.

7.2.6 Phe Derivatives

There are 123 Phe aas in the nAChR (Figure 7.3). *o*FPhe is recognized by the *E. coli* phenylalanyl-aminoacyl tRNA synthetase (PheRS) *in vitro* (20) and accepted by the *E. coli* translational machinery *in vitro* (21). *o*FPhe, *m*FPhe, and *p*FPhe have been incorporated into proteins expressed in *P. aeruginosa* (16). *p*FPhe has also been incorporated in proteins expressed in *E. coli* auxotrophs *in vivo* (8). UAARS with *o*FPhe shows a 1.6-fold shift in EC₅₀ and causes a LOF phenotype (Figure 7.5 A). UAARS with *m*FPhe shows a 1.7-fold shift in EC₅₀ and causes a GOF phenotype (Figure 7.5 A). UAARS with *p*FPhe shows a 6.5-fold shift in EC₅₀, causes a GOF phenotype, and causes the largest shift with a 2 d incubation of all the UAAs shown in Figure 7.1. The shifts for *o*FPhe, *m*FPhe, and *p*FPhe were observed for two different batches of oocytes. UAARS with *o*FPhe, *m*FPhe, and *p*FPhe shows that the nAChR functions differently when the fluorine substituent is moved around the phenyl ring.

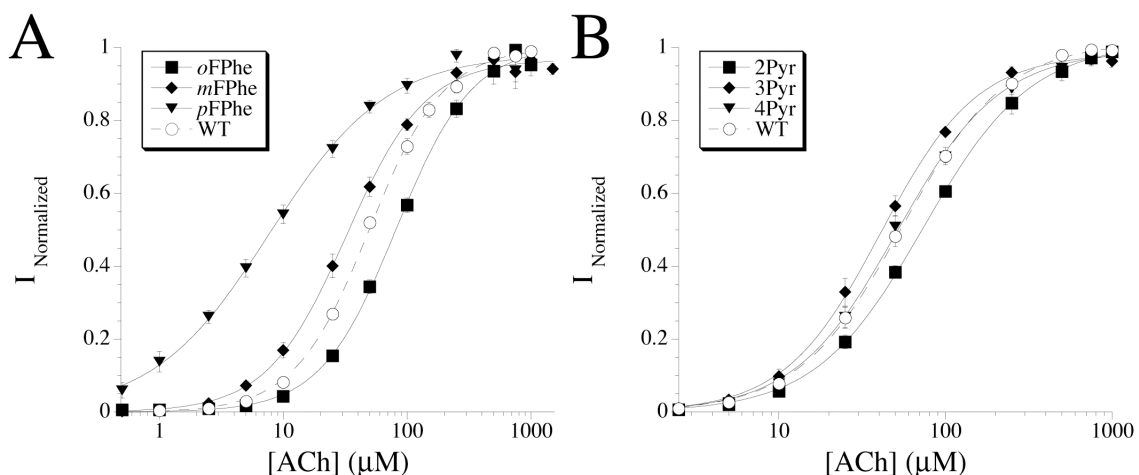


Figure 7.5: Fits to the Hill equation for UAARS with *o*FPhe, *m*FPhe, *p*FPhe, 2Pyr, 3Pyr, and 4Pyr. A) UAARS with *o*FPhe, *m*FPhe, and *p*FPhe. *o*FPhe $EC_{50} = 82 \pm 3$ and $n_H = 1.4 \pm 0.06$. *m*FPhe $EC_{50} = 32 \pm 1$ and $n_H = 1.1 \pm 0.06$. *p*FPhe $EC_{50} = 8.2 \pm 0.4$ and $n_H = 0.89 \pm 0.03$. Wild-type $\alpha_{HA} His$ nAChR $EC_{50} = 49 \pm 1$ and $n_H = 1.4 \pm 0.04$. In each experiment $n > 5$ oocytes. A) UAARS with 2Pyr, 3Pyr, and 4Pyr. 2Pyr $EC_{50} = 74 \pm 1$ and $n_H = 1.3 \pm 0.02$. 3Pyr $EC_{50} = 41 \pm 0.9$ and $n_H = 1.5 \pm 0.04$. 4Pyr $EC_{50} = 51 \pm 1$ and $n_H = 1.4 \pm 0.05$. Wild-type α_{NHA} nAChR $EC_{50} = 55 \pm 0.9$ and $n_H = 1.4 \pm 0.03$. In each experiment $n > 4$ oocytes.

2Pyr, 3Pyr, and 4Pyr (shown in Figure 7.1) have been incorporated in proteins expressed in *E. coli* auxotrophs *in vivo* (15,18). UAARS with 2Pyr shows a 1.4-fold shift in EC_{50} and causes a LOF phenotype (Figure 7.5 B). UAARS with 3Pyr shows a 1.2-fold shift in EC_{50} and causes a GOF phenotype (Figure 7.5 B). Both 2Pyr and 3Pyr show a similar phenotypical shift in EC_{50} to *o*FPhe and *m*FPhe, respectively (Figure 7.5 A & B). UAARS with 4Pyr shows no shift in EC_{50} (Figure 7.5). The lack of EC_{50} shift for 4Pyr suggests that or the loss of hydrogen at the *para* position has no affect on nAChR function. Overall, the pyridylalanine UAAs show smaller shifts in EC_{50} when compared to the fluorinated Phe UAAs.

UAARS with 3,4-F2Phe (shown in Figure 7.1) showed only a slight 1.3-fold shift in EC_{50} (Table 7.1) and further incubation time may be necessary to get increased UAA incorporation. UAARS with 3,5-F2Phe, F3Phe, and F5Phe (shown in Figure 7.1) all

showed slight shifts in EC_{50} (Table 7.1). F5Phe has been shown not to be accepted by the *E. coli* PheRS and a mutant *E. coli* PheRS *in vivo* (15). It appears that the addition of further fluorine substituents on the phenyl ring appears to block recognition by the *Xenopus* PheRS.

7.2.7 Trp Derivatives

There are 51 Trp aas in the nAChR (Figure 7.3). Bth and Thi (shown in Figure 7.1) are recognized by the *E. coli* tryptophanyl-aminoacyl tRNA synthetase (TrpRS) *in vitro* (20) and accepted by the *E. coli* translational machinery *in vitro* (21). Bth and Thi are both thought to be non-coding or not accepted *in vivo* (6). UAARS with Bth and Thi show no shift in EC_{50} (Table 7.1). Bth and Thi may be incorporated in the nAChR, but other methodologies for detection may be necessary.

FTrp is recognized by the *E. coli* TrpRS *in vitro* (20) and accepted by the *E. coli* translational machinery *in vitro* (21). FTrp is incorporated into proteins in *E. coli* (19). UAARS with FTrp results in a 2.9-fold shift in EC_{50} (Figure 7.6 A), and FTrp shows the greatest LOF phenotype of the UAAs tested in Figure 7.1. The UAARS with FTrp EC_{50} is close to the EC_{50} of the site-specific incorporation of FTrp at $\alpha 149$ (Figure 7.6 A), which makes a cation- π interaction with ACh (30).

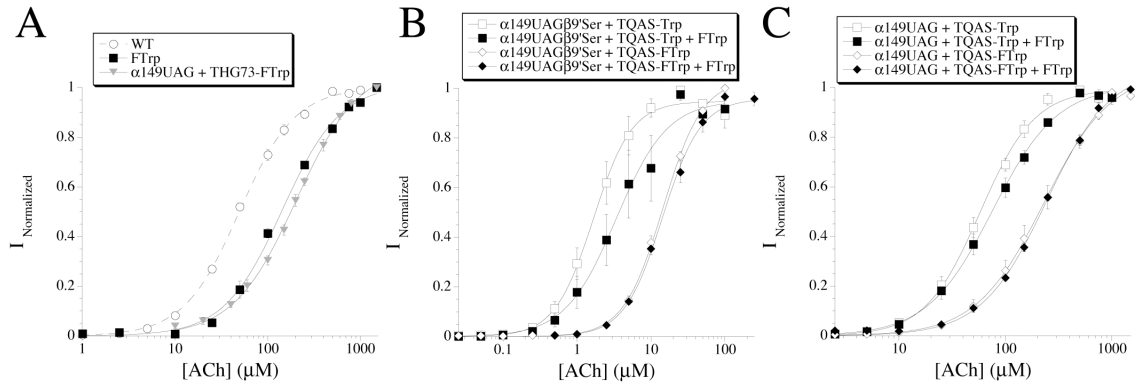


Figure 7.6: Fits to the Hill equation for UAARS with FTrp and nonsense suppression experiments. A) UAARS with FTrp. Wild-type α_{NHA} nAChR $EC_{50} = 48 \pm 2$ and $n_H = 1.5 \pm 0.03$. FTrp $EC_{50} = 140 \pm 9$ and $n_H = 1.4 \pm 0.09$. $\alpha 149\text{UAG} + \text{THG73-FTrp}$ $EC_{50} = 200 \pm 7$ and $n_H = 1.3 \pm 0.04$. In each experiment $n > 5$ oocytes. B) $\alpha 149\text{UAG}\beta 9'\text{Ser}$ nonsense suppression and UAARS with FTrp. $\alpha 149\text{UAG}\beta 9'\text{Ser} + \text{TQAS-Trp}$ $EC_{50} = 1.7 \pm 0.1$ and $n_H = 1.7 \pm 0.1$. $\alpha 149\text{UAG}\beta 9'\text{Ser} + \text{TQAS-Trp} + 2 \text{ mM FTrp}$ $EC_{50} = 3.4 \pm 0.4$ and $n_H = 1.3 \pm 0.2$. $\alpha 149\text{UAG}\beta 9'\text{Ser} + \text{TQAS-FTrp}$ $EC_{50} = 14 \pm 0.4$ and $n_H = 1.7 \pm 0.07$. $\alpha 149\text{UAG}\beta 9'\text{Ser} + \text{TQAS-FTrp} + 2 \text{ mM FTrp}$ $EC_{50} = 14 \pm 0.7$ and $n_H = 1.7 \pm 0.1$. In each experiment $n > 4$ oocytes. C) $\alpha 149\text{UAG}$ nonsense suppression and UAARS with FTrp. $\alpha 149\text{UAG} + \text{TQAS-Trp}$ $EC_{50} = 58 \pm 2$ and $n_H = 1.7 \pm 0.09$. $\alpha 149\text{UAG} + \text{TQAS-Trp} + 2 \text{ mM FTrp}$ $EC_{50} = 76 \pm 7$ and $n_H = 1.4 \pm 0.06$. $\alpha 149\text{UAG} + \text{TQAS-FTrp}$ $EC_{50} = 230 \pm 10$ and $n_H = 1.4 \pm 0.07$. $\alpha 149\text{UAG} + \text{TQAS-FTrp} + 2 \text{ mM FTrp}$ $EC_{50} = 240 \pm 10$ and $n_H = 1.4 \pm 0.06$. In each experiment $n > 3$ oocytes.

To determine whether the placement of FTrp at $\alpha 149$ was dominating the EC_{50} shift in UAARS experiments, we chose to combine site-specific incorporation of Trp or FTrp with UAARS with FTrp. Using nonsense suppression at $\alpha 149\text{UAG}$ results in either 0% FTrp when suppressing with TQAS-W or 100% FTrp when suppressing with TQAS-FTrp. Initially, the $\beta 9'\text{Ser}$ mutation was utilized to lower the EC_{50} by a factor of ≈ 33 , and the mutation doesn't alter the effect of UAAs incorporated at $\alpha 149$ (30,31). Suppression of $\alpha 149\text{UAG}\beta 9'\text{Ser}$ with TQAS-Trp results in an $EC_{50} = 1.7 \mu\text{M}$ ACh, but suppression of $\alpha 149\text{UAG}\beta 9'\text{Ser}$ with TQAS-Trp and UAARS with FTrp results in a 2-fold shift in EC_{50} (Figure 7.6 B). Suppression of $\alpha 149\text{UAG}\beta 9'\text{Ser}$ with TQAS-FTrp results in an $EC_{50} = 14 \mu\text{M}$ ACh, but suppression of $\alpha 149\text{UAG}\beta 9'\text{Ser}$ with TQAS-FTrp

and UAARS with FTrp causes no shift in EC_{50} (Figure 7.6 B). The EC_{50} for $\alpha 149FTrp\beta 9'Ser$ is expected to be $\approx 6 \mu M$ and it is unclear why the EC_{50} was higher for these experiments.

We then chose to use the wild-type, $\beta 9'Leu$ nAChR, which had been used in previous UAARS experiments. Suppression of $\alpha 149UAG$ with TQAS-Trp results in an $EC_{50} = 58 \mu M$ ACh, but suppression of $\alpha 149UAG$ with TQAS-Trp and UAARS with FTrp results in a 1.3-fold shift in EC_{50} (Figure 7.6 C). Suppression of $\alpha 149UAG$ with TQAS-FTrp results in an $EC_{50} = 230 \mu M$ ACh, but suppression of $\alpha 149UAG$ with TQAS-FTrp and UAARS with FTrp causes no shift in EC_{50} (Figure 7.6 C). If $\alpha 149FTrp$ was causing the entire shift in EC_{50} , then both of the suppression experiments (TQAS-Trp or TQAS-FTrp) would be expected to show no shift in EC_{50} from UAARS.

7.2.8 Cross-Linking the nAChR with PLeu and PMet

The UAAs PLeu and PMet are used to detect protein-protein interactions *in vivo* (22). These UAAs are heterogeneously incorporated into all translated proteins and UV irradiation is used to convert the diazirine to a reactive carbene intermediate that irreversibly cross-links either within a protein or to another protein if the UAA is in close proximity. Cross-linked protein complexes are typically detected by Western blotting as an increased molecular weight relative to non-cross-linked protein. We chose to perform Western blots of the $\alpha_{HA His}$ (contains the HA tag in the M3-M4 loop and a 6-His tag at the C-terminus) or α_{NHA} (contains the HA at the N-terminus). By only detecting the α -subunit, we would expect to obtain four possible dimers $\alpha^1\beta$, $\alpha^1\gamma$, $\alpha^2\gamma$ or $\alpha^2\delta$; five possible trimers $\alpha^1\beta\delta$, $\alpha^1\gamma\alpha^2$, $\gamma\alpha^1\beta$, $\alpha^2\delta\beta$, $\delta\alpha^2\gamma$; five possible tetramers $\alpha^1\gamma\alpha^2\delta$, $\gamma\alpha^1\beta\delta$, $\beta\alpha^1\gamma\alpha^2$, $\alpha^2\beta\delta\alpha^1$, and $\beta\delta\alpha^2\gamma$; and one pentamer $\alpha^1\gamma\alpha^2\delta\beta$ (note: α^1 and α^2 are used to show

the uniqueness of the different subunit interfaces of the two α -subunits). Each subunit of the nAChR runs at a distinct molecular weight (see Figure 6.10), and therefore different subunit combinations may run at different masses. Also, trimers and tetramers with two α -subunits may be detected more readily because there are two HA tags and should bind two antibodies (Abs).

Oocytes that are supplemented with Leu and Met show no increased molecular weight bands with or without the exposure to UV light (Figure 7.7 A & B, Lanes 2, 3, 6, and 7). Oocytes that were supplemented with PLeu and PMet showed higher molecular weight bands when not irradiated with UV light (Figure 7.7 A & B, Lanes 4 and 8). These higher molecular weight bands are most likely caused by ambient light in the lab. Oocytes that were supplemented with PLeu and PMet and irradiated with UV light for 40 min at room temperature show no high molecular weight bands, but there is a loss of the α -subunit intensity (Figure 7.7 A & B, Lanes 5 and 9). A similar reduction in α -subunit intensity is seen for oocytes supplemented with Leu and Met (Figure 7.7 A & B, Lanes 3 and 7). Ponceau staining of the nitrocellulose membrane shows a loss in total protein for oocytes supplemented with PLeu and PMet (Figure 7.7 C & D, Lanes 5 and 9), but there is little loss with oocytes supplemented with Leu and Met (Figure 7.7 C & D, Lanes 3 and 7). Therefore UV irradiation at room temperature may be resulting in α -subunit and total protein loss by heat with 40 min. Irradiating whole oocytes on the arc lamp (3 min on each sides) shows only faint higher molecular weight bands (Figure 7.7 B, Lane 10) or nothing (Figure 7.7 A, Lane 10), but there appears to be no loss of α -subunit intensity with fewer UV irradiation periods.

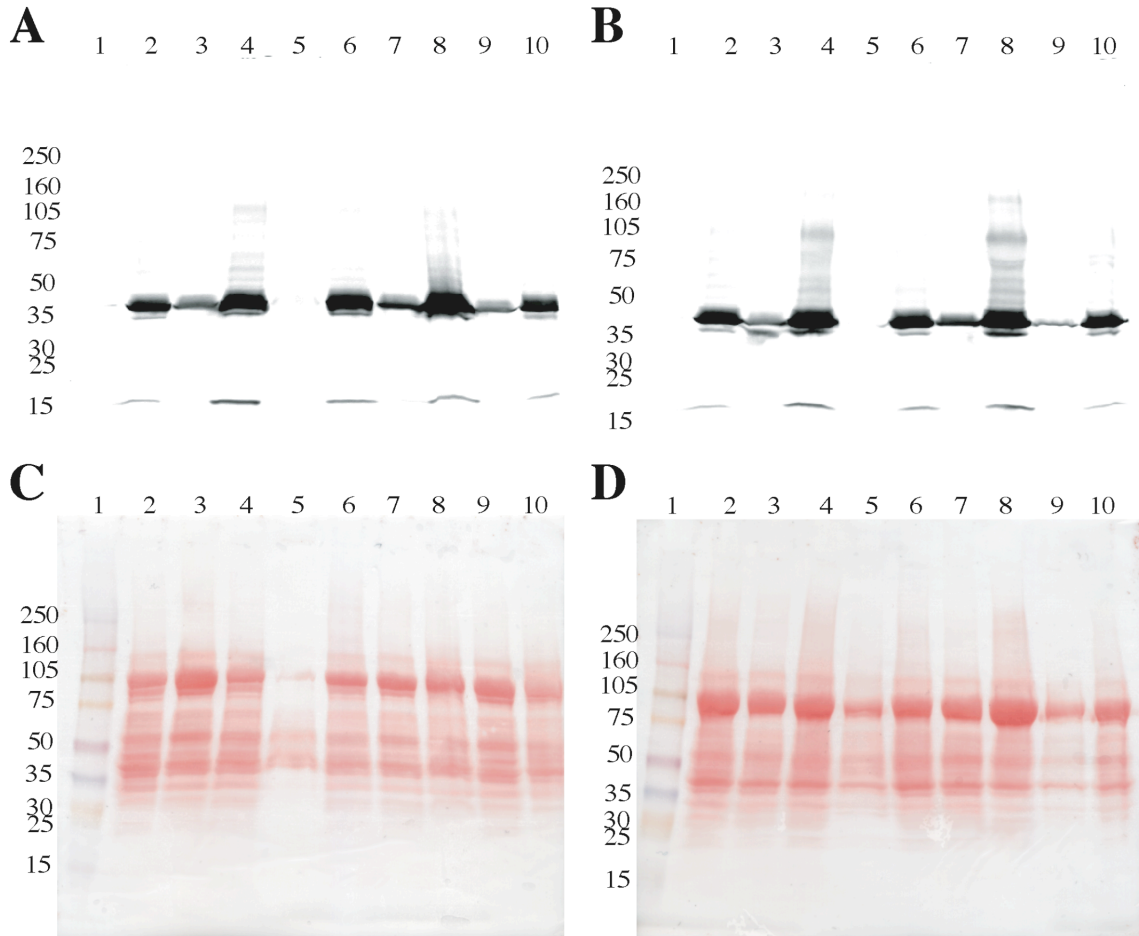


Figure 7.7: Detecting cross-linking of $\alpha_{\text{HA His}}$ with the HA Ab. (A & B) Gels are the same, but with different oocytes. Lane 1 is molecular weight marker. Lane 2 is $\alpha_{\text{HA His}}$ with 1 mM Leu and 0.5 mM Met. Lane 3 is $\alpha_{\text{HA His}}$ with 1 mM Leu and 0.5 mM Met irradiated with UV light. Lane 4 is $\alpha_{\text{HA His}}$ with 1 mM PLeu and 0.5 mM PMet. Lane 5 is $\alpha_{\text{HA His}}$ with 1 mM PLeu and 0.5 mM PMet irradiated with UV light. Lane 6 is $\alpha_{\text{HA His}}$ with 1 mM Leu, 0.5 mM Met, and 0.17 mM 18 other aas. Lane 7 is $\alpha_{\text{HA His}}$ with 1 mM Leu, 0.5 mM Met, and 0.17 mM 18 other aas irradiated with UV light. Lane 8 is $\alpha_{\text{HA His}}$ with 1 mM PLeu, 0.5 mM PMet, and 0.17 mM 18 other aas. Lane 9 is $\alpha_{\text{HA His}}$ with 1 mM PLeu, 0.5 mM PMet, and 0.17 mM 18 other aas irradiated with UV light. Lane 10 is $\alpha_{\text{HA His}}$ with 1 mM PLeu, 0.5 mM PMet, and 0.17 mM 18 other aas irradiated with UV light on the arc lamp (3 min on each side of the oocyte). (C & D) Ponceau staining of Western blots in (A & B). Staining shows loss of total protein after irradiation with UV light. UV irradiation was done 40 min at room temperature (unless otherwise noted). Each lane contains four whole oocytes. Numbers on the left are molecular weight markers (KD).

Cross-linking may hinder detection of the α -subunit because the HA tag is in the M3-M4 loop and may form secondary structure during cross-linking, such as a loop. The

HA Ab detects a linear sequence of aas and any structure may not allow for detection. We choose to detect the α -subunit with the His Ab because the 6-His tag is at the C-terminus and is unlikely to cross-link. The α_{NHA} was also used because the HA tag is in the N-terminus and is also unlikely to cross-link. Using the same amount of His Ab as the HA antibody, no α -subunit could be detected (Figure 7.8 A). After stripping the membrane, the membrane was reprobed with the HA, Ab and the α -subunit is clearly visible (Figure 7.8 B). Oocytes injected with $\alpha_{\text{HA His}}$ and supplemented with PLeu and PMet show faint higher molecular weight bands without UV irradiation (Figure 7.8 B, Lanes 3 and 9). Intriguingly, no higher molecular weight bands are visualized for oocytes injected with $\alpha_{\text{HA His}}$ and supplemented with only PLeu (Figure 7.8 B, Lane 5 and 6). The α_{NHA} didn't express as well as $\alpha_{\text{HA His}}$, and no higher molecular weight bands are seen with or without UV irradiation (Figure 7.8 B, Lanes 7 and 8). Less UV irradiation time (10 min, instead of 40 min as in Figure 7.7) was used to avoid loss of α -subunit and total protein. Oocytes expressing $\alpha_{\text{HA His}}$ supplemented with PLeu and PMet only show higher molecular weight bands in Figure 7.8 B, Lane 4. Other oocytes expressing $\alpha_{\text{HA His}}$ supplemented with PLeu and PMet or only PLeu show no increased molecular weight bands, and there is still a slight reduction in the α -subunit intensity (Figure 7.8 B, Lanes 6 and 10).

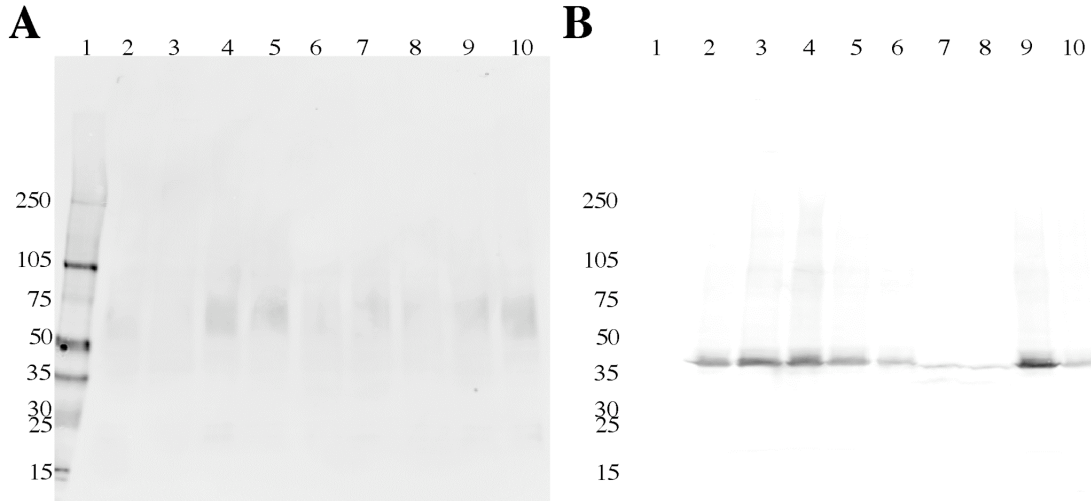


Figure 7.8: Detecting cross-linking of $\alpha_{\text{HA His}}$ with the His Ab and HA Ab. A) Detection of $\alpha_{\text{HA His}}$ with the His Ab. B) Is the same gel as in A, but detected with the HA Ab after stripping the membrane. (A & B) Lane 1 molecular weight marker. Lane 2 is $\alpha_{\text{HA His}}$ with 1 mM Leu and 0.5 mM Met. Lane 3 is $\alpha_{\text{HA His}}$ with 1 mM PLeu and 0.5 mM PMet. Lane 4 is $\alpha_{\text{HA His}}$ with 1 mM PLeu and 0.5 mM PMet irradiated with UV light. Lane 5 is $\alpha_{\text{HA His}}$ with 1 mM PLeu. Lane 6 is $\alpha_{\text{HA His}}$ with 1 mM PLeu irradiated with UV light. Lane 7 is α_{NHA} with 1 mM PLeu and 0.5 mM PMet. Lane 8 is α_{NHA} with 1 mM PLeu and 0.5 mM PMet irradiated with UV light. Lane 9 is $\alpha_{\text{HA His}}$ with 1 mM PLeu and 0.5 mM PMet. Lane 10 is $\alpha_{\text{HA His}}$ with 1 mM PLeu and 0.5 mM PMet irradiated with UV light. UV irradiation was done for 10 min at room temperature. Each lane contains four whole oocytes. Numbers on the left are molecular weight markers (KD).

The loss of α -subunit intensity with increased molecular weight bands is concerning, and therefore UV irradiation was performed for 2 h at 4 °C. The lack of high molecular weight bands may be due to the minimal amount of nAChR produced in an oocyte (pico-femto grams) and therefore oocytes were homogenized and solubilized for 2 d at 18 °C. Oocytes that were supplemented with Leu and Met show no high molecular weight bands (Figure 7.9 A & B, Lane 2). The large smear running between 75 KD and 105 KD is an abundant protein in the *Xenopus* oocyte (see Figure 7.7 C & D), which is more abundant in this gel because of the 2 d solubilization and is detected because of non-specific HA and/or 2° Ab binding. Oocytes that were supplemented with PLeu and PMet either show higher molecular weight bands (Figure 7.9 A, Lane 3) or no higher

molecular weight bands (Figure 7.9 B, Lane 3) without UV irradiation, the latter is most likely due to minimal protein expression. Oocytes supplemented with PLeu and PMet show higher molecular weight bands with 2 h of UV irradiation (Figure 7.9 A, Lanes 4, 5, 8, and 9, and Figure 7.9 B, Lanes 4–8), but these are not seen in some lanes with lower protein loading (Figure 7.9 A, Lanes 6, 7, and 10, and Figure 7.9 B, 9 and 10). Some lanes also show higher molecular weight bands than a pentamer expected for the nAChR (Figure 7.9 B, Lanes 4–7). Therefore cross-linking of the α -subunit appears to be minimal in the *Xenopus* oocytes and longer UV irradiation at 4 °C and solubilization is necessary to obtain higher yields of the cross-linked subunits.

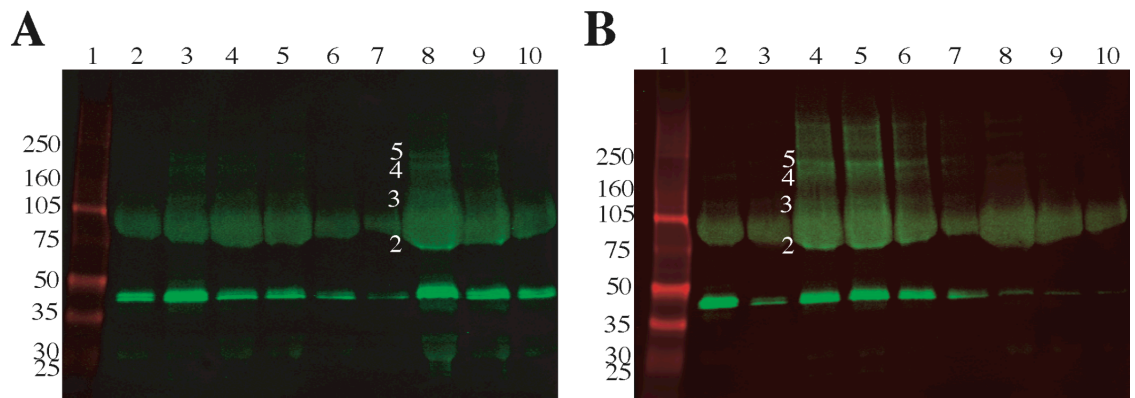


Figure 7.9: Detecting cross-linking of $\alpha_{\text{HA His}}$ with the HA Ab after extended UV irradiation. (A & B) Gels are the same, but with different oocytes. Lane 1 molecular weight marker. Lane 2 is $\alpha_{\text{HA His}}$ with 1 mM Leu and 0.5 mM Met, half oocyte. Lane 3 is $\alpha_{\text{HA His}}$ with 1 mM PLeu and 0.5 mM PMet, half oocyte. Lane 4 is $\alpha_{\text{HA His}}$ with 1 mM PLeu and 0.5 mM PMet irradiated with UV light, one oocyte. Lane 5 is $\alpha_{\text{HA His}}$ with 1 mM PLeu and 0.5 mM PMet irradiated with UV light, half oocyte. Lane 6 is $\alpha_{\text{HA His}}$ with 1 mM PLeu and 0.5 mM PMet irradiated with UV light, quarter oocyte. Lane 7 is $\alpha_{\text{HA His}}$ with 1 mM PLeu and 0.5 mM PMet irradiated with UV light, eighth oocyte. Lane 8 is $\alpha_{\text{HA His}}$ with 1 mM PLeu and 0.5 mM PMet irradiated with UV light, one oocyte. Lane 9 is $\alpha_{\text{HA His}}$ with 1 mM PLeu and 0.5 mM PMet irradiated with UV light, half oocyte. Lane 10 is $\alpha_{\text{HA His}}$ with 1 mM PLeu and 0.5 mM PMet irradiated with UV light, quarter oocyte. UV irradiation was done for 2 h at 4 °C. Numbers on the left are molecular weight markers (KD). Numbers in white are the number of subunits cross-linked.

7.2.9 Unnatural Amino Acid Replacement Scanning Expression Determined by Electrophysiology and Western Blot

During the course of the UAARS experiments done in Sections 7.2.2 through 7.2.7, many UAAs showed unusually low current when compared to wild-type nAChR not supplemented with UAAs. To analyze this phenomenon among different batches of oocytes, the average maximal current (I_{\max}) from UAARS experiments were normalized to wild-type nAChR I_{\max} , not supplemented with UAAs. Figure 7.10 shows the variable effect that natural aas and UAAs in the incubation media have on functional expression of ion channels on the membrane of *Xenopus* oocytes. Met, Pro, and Leu are all natural aas and when they are supplemented at 1 mM in the media there is $\approx 40\%$ reduction in I_{\max} (Figure 7.10). PMet, Nval, 2Pyr, 3Pyr, 4Pyr, Bth, and Thi all show increased I_{\max} (Figure 7.10), but PMet, Nval, 4Pyr, Bth, and Thi show no change in EC_{50} (Table 7.1 and Figure 7.5). Of the Met derivatives, Ppg shows a decrease in I_{\max} , and PMet and Nval show an increase in I_{\max} (Figure 7.10). Both Pro derivatives, Aze and Dhp, show a decrease in I_{\max} equal to the addition of Pro (Figure 7.10). PLeu shows I_{\max} equivalent to oocytes not supplemented with UAAs, but F3Leu shows a severe reduction in I_{\max} (Figure 7.10). Intriguingly, *o*FPhe, *m*FPhe, and *p*FPhe all show different I_{\max} profiles (Figure 7.10). *p*FPhe reduces I_{\max} by 94%, while *m*FPhe is comparable to Met, Leu, and Pro (Figure 7.10). 3,4-F2Phe shows only a slight reduction in EC_{50} (Table 7.1), but shows I_{\max} reduction (57%) that is close to the average reduction of I_{\max} for *m*FPhe and *p*FPhe (62%) (Figure 7.10). 3,5-F2Phe, F3Phe, and F5Phe showed no change in EC_{50} (Table 7.1) and the reduction in I_{\max} is similar to Met, Leu, and Pro (Figure 7.10). FVal and

FTrp also cause a reduction in I_{\max} (Figure 7.10). Overall, fluorinated UAAs appear to reduce the functional nAChR on the surface of the oocyte membrane (Figure 7.10).

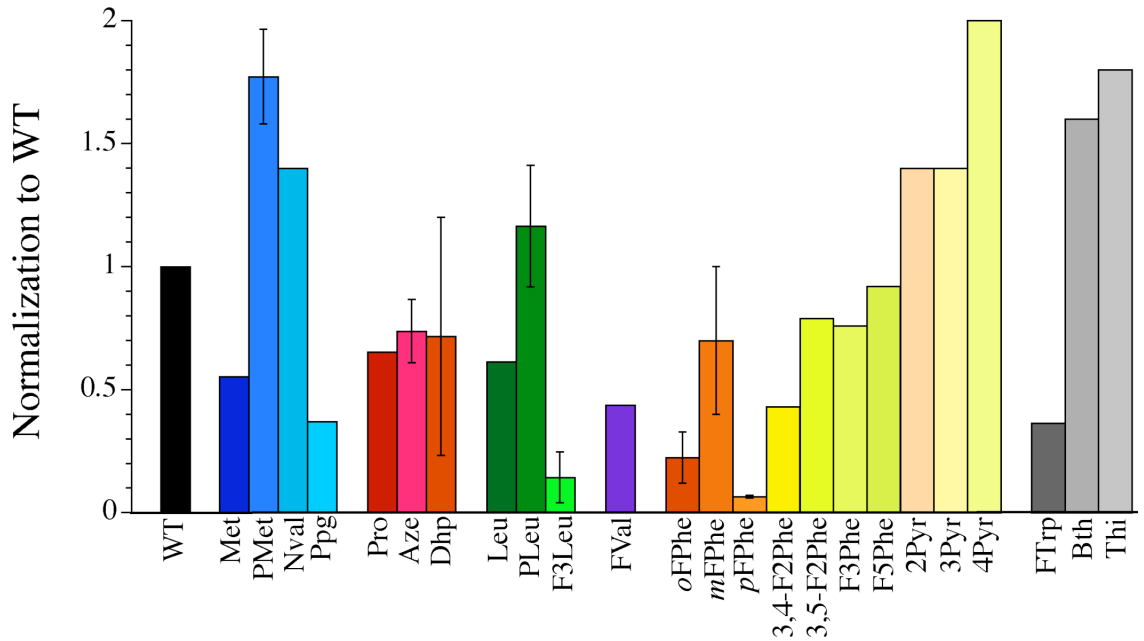


Figure 7.10: UAARS effect on functional nAChR expression detected by electrophysiology. I_{\max} for UAARS experiments was normalized to I_{\max} for nAChR without UAAs. WT is wild-type nAChR and natural aas or UAAs (chemical structure shown in Figure 7.1) are listed below each bar. Error bars are standard error.

To determine whether UAARS causes decreased nAChR translation or increased protein degradation, whole cell homogenization and Western blot were utilized to look at α -subunit protein. Figure 7.11 A shows that the α -subunit is translated and present in oocytes equally without UAAs in the media (Figure 7.11 A, Lane 2) and in the presence of UAAs (Figure 7.11 A, Lanes 3–10). Densitometric analysis of Figure 7.11 A confirms that *o*FPhe, *m*FPhe, *p*FPhe, FTrp, and FVal all have the same amount of α -subunit as oocytes not supplemented with UAAs (Figure 7.11 B). Therefore reduction of I_{\max} for these UAAs (Figure 7.10) is not due to decreased translation or protein degradation, but rather another mechanism.

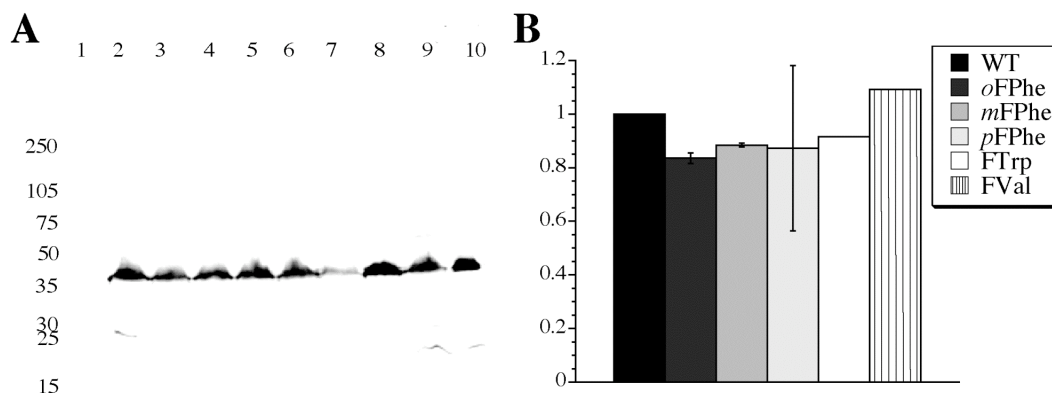


Figure 7.11: UAARS effect on nAChR expression detected by Western blot. A) UAARS with *o*FPhe, *m*FPhe, *p*FPhe, FTrp, and FVal. Lane 1 molecular weight marker. Lane 2 is $\alpha_{\text{HA His}}$. Lanes 3 and 4 are $\alpha_{\text{HA His}}$ with 1 mM *o*FPhe. Lanes 5 and 6 are $\alpha_{\text{HA His}}$ with 1 mM *m*FPhe. Lanes 7 and 8 are α_{NHA} with 1 mM *p*FPhe. Lane 9 is $\alpha_{\text{HA His}}$ with 2 mM FTrp. Lane 10 is $\alpha_{\text{HA His}}$ with 2 mM FVal. Each lane contains four whole oocytes. Numbers on the left are molecular weight markers (KD). B) Densitometric analysis of Western blot in part A. Signal intensity was normalized to $\alpha_{\text{HA His}}$ not supplemented with UAAs (Lane 2). Error bars are standard error.

7.3 Discussion

UAARS requires depletion of the endogenous aas for efficient incorporation of UAAs (shown schematically in Figure 7.2). This is experimentally shown by the increased shift in EC_{50} for PLeu and F3Leu from 2 to 5 d incubations (Figure 7.4 B). Injection of PLeu and PMet (final concentration in an oocyte 1 mM and 0.5 mM, respectively) caused no shift in EC_{50} of the nAChR and resulted in $\approx 50\%$ reduction in nAChR expression when determined by electrophysiology (data not shown). Therefore the use of excess UAAs in the media is needed for increased UAA concentration in the oocyte and for efficient UAARS.

Many UAAs showed no shift in EC_{50} , which may be due to lack of efficient UAA incorporation by the translational machinery, lack of UAA recognition by aaRSs, or no change in nAChR function. Increased incubation times are required to get significant

shifts for Aze, which may be required for 3,4-F2Phe (Table 7.1). F5Phe was not recognized in *E. coli* (15) and therefore may also not be in *Xenopus* oocytes. The Met derivatives (PMet, Nval, and Ppg) all showed no shift in EC₅₀ (Table 7.1) and other ion channels (5HT_{3A}, GABA_A, MOD-1, etc.) may be useful to screen for these Met derivatives. With increased research on other ion channels, hopefully UAARS EC₅₀ shifts can be determined for all 20 canonical aas (or 19 if Gly is omitted) to allow efficient screening of all UAA derivatives. Other methods of detection will also be useful, including bioorthogonal labeling of UAAs with fluorophores (23,24,42) and detection by total internal reflectance microscopy (TIRF) (43). TIRF will not only show the presence of UAAs, but can also be used to count the number of accessible UAAs of a single nAChR and can be used to determine the distribution of UAAs incorporated into nAChRs.

The commercially available PLeu causes a change in the function of the nAChR, but no shift is seen with PMet (Figure 7.4 A). PLeu is hydrophilic compared to F3Leu, but both UAAs cause a GOF phenotype in the nAChR (Figure 7.4 B). This is intriguing, because Leu is the most abundant UAA in the nAChR and Leu is a hydrophobic aa thought to stabilize the interior of proteins and to interact with the lipid bilayer (Figure 7.3). The two UAAs—PLeu and F3Leu—are distinguishable by the number of functional ion channels present on the surface. The hydrophilic PLeu results in comparable expression to wild-type nAChR not supplemented with UAAs, but the hydrophobic F3Leu results in a 86% reduction in current (Figure 7.10). This may result from differential interactions with chaperones, interactions with lipid bilayers in the endoplasmic reticulum and/or golgi, folding by the translocon, change in conductance, or

differences in the amount of functional receptors for each UAA. Val is another hydrophobic aa and is present comparably to Leu in the nAChR (Figure 7.3). The incorporation of the more hydrophobic FVal results in a LOF phenotype (Table 7.1), which contrasts to the GOF phenotype of PLeu and F3Leu. Expression of functional ion channels is decreased by 56% with FVal and is similar to F3Leu (Figure 7.10). Further research on hydrophobic residues will be intriguing on the nAChR because they are so abundant, contact subunit interfaces, and interact with the lipid bilayer (Figure 7.3).

Phe is the most abundant aromatic aa in the nAChR and forms extensive interactions with the lipid bilayer (Figure 7.3). Fluorination of Phe decreases the cation- π binding ability of the phenyl ring (44), but also places a highly electronegative substituent and increases the hydrophobicity of the side chain. Intriguingly, fluorination of the *ortho*, *meta*, and *para* positions of Phe have different effects on the function of the nAChR. *o*FPhe causes a LOF phenotype, *m*FPhe causes a slight GOF phenotype, and *p*FPhe causes the greatest GOF phenotype of UAAs screened (Figure 7.5 A). The pyridylalanine derivatives have decreased cation- π binding ability as well (44), but also remove a H atom and increase hydrophilicity of the side chain. 2Pyr results in a LOF phenotype similar to *o*FPhe (Figure 7.5 A & B). 3Pyr results in a GOF phenotype similar to *m*FPhe (Figure 7.5 A & B). 4Pyr shows no shift in EC_{50} (Figure 7.5 B), which is either due to possible protonation of 4Pyr or evidence that the loss of a H atom doesn't influence the function of the nAChR. Fluorination of the *para* position on *p*FPhe causes a significant shift in EC_{50} , which greatly alters nAChR function. These UAAs show distinct interactions of the Phe side chain and clearly illustrate that the *ortho*, *meta*, and *para* positions have differential interactions within the nAChR and/or the lipid bilayer.

Trp is the least used aromatic aa in the nAChR (Figure 7.3), and in proteins in general. UAARS with FTrp results in a LOF phenotype similar to the site-specific incorporation of FTrp at $\alpha 149$ (Figure 7.6 A). 4-FTrp and 6-FTrp are accepted by *E. coli* (19) and these derivatives should be intriguing to see if there is a functional difference on the nAChR similar to the Phe derivatives. Differences in EC_{50} shift have been seen at $\alpha 149$ in the nAChR, where site-specific incorporation of 4-FTrp and 6-FTrp cause no shift in EC_{50} , but 5-FTrp (FTrp) cause a 4-fold shift in EC_{50} (30). Combining site-specific UAA incorporation with UAARS allows for a novel experimental technique to remove one position from UAARS. Using $\alpha 149$ UAG and suppressing with TQAS-W, 0% of the ion channels will contain FTrp at this position and there is still a LOF phenotype seen with UAARS with FTrp (Figure 7.6 B & C), although significantly smaller than that from simple UAARS. Intriguingly, suppressing $\alpha 149$ UAG with TQAS-FTrp (100% of the ion channels will have FTrp at $\alpha 149$) shows no shift in EC_{50} (Figure 7.6 B & C). Both experiments should show a shift in EC_{50} if there is a global change in function with UAARS with FTrp or no shift if the $\alpha 149$ FTrp position is dominating the shift in EC_{50} . This difference may be explained by a positional affect near the ACh binding site, known as the aromatic box. $\alpha 149$ Trp may show a shift because FTrp at the only other Trp in the aromatic box may alter ACh binding, but $\alpha 149$ FTrp may dominate the reduction in ACh binding and FTrp at the other site has no effect. Further research is needed to explain this phenomenon, but clearly illustrates the utility of combining site-specific UAA incorporation with UAARS.

PLeu and PMet allow for detection of UAA incorporation by cross-linking subunits within the nAChR upon UV irradiation and detection of higher molecular weight

bands on a Western blot. Detection of $\alpha_{\text{HA His}}$ was not possible with the His Ab (Figure 7.8 A) and clearly illustrates the difficulty in detecting a low abundance ion channel with Abs other than the HA Ab from Covance. Wild-type nAChR supplemented with Leu and Met show no higher molecular weight bands with and without UV irradiation (Figure 7.7 A & B, Lanes 2, 3, 6, and 7, Figure 7.8 B, Lane 2, and Figure 7.9 A & B, Lane 2). nAChR supplemented with PLeu and PMet show higher molecular weight bands without UV irradiation, even though the oocytes are kept in an opaque box and only exposed to light during media exchange and homogenization (Figure 7.7 A & B, Lanes 4 and 8, Figure 7.8 B, Lanes 3 and 9, and Figure 7.9 A, Lane 3). This suggests that many Leu and/or Met positions of the nAChR are in close contact with other subunits. nAChR supplemented with PLeu and PMet sometimes show higher molecular weight bands with UV irradiation (Figure 7.8 B, Lane 4, Figure 7.9 A, Lanes 4, 5, 8, and 9, and Figure 7.9 B, Lanes 4–8). The detection of higher molecular weight bands is highly variable, but is seen more readily with UV irradiation for 2 h at 4 °C and solubilization of whole oocytes for 2 d at 18 °C (Figure 7.9 A, Lanes 4, 5, 8, and 9, and Figure 7.9 B, Lanes 4–8). When the nAChR is supplemented with PLeu only, no higher molecular weight bands are seen with or without UV irradiation (Figure 7.9 B, Lanes 5 and 6). This suggests that PMet is critical for cross-linking of the nAChR. The nAChR is a pentamer, but occasionally higher molecular weight bands were seen (Figure 7.9 B, Lanes 4–7). Cross-linking of the nAChR requires highly specialized conditions in order to maximize the yield of the cross-linked subunits, which are present in extremely low yield and/or difficult to solubilize. UAARS with PLeu and PMet can be detected by Western blot, but cross-linking is inefficient and highly variable.

The supplementation of natural aas and UAAs (0.5–4 mM) effects the functional expression of the nAChR. 1 mM of Leu, Met, and Pro all decrease expression by $\approx 40\%$ relative to oocytes not supplemented with natural aas (Figure 7.10). The decrease in channel expression may be caused by overwhelming the translation machinery through increased concentration of natural aas, which increases aminoacylated tRNAs, imbalances the aminoacylated tRNA pool and portion bound to EF-1 α , and could cause ribosomal stalling, increased frameshifting, and protein truncation. P_{Met} and N_{val} both *increase* expression by 77% and 40%, respectively (Figure 7.10). This suggests that the Met concentration in *Xenopus* oocytes is not optimal for nAChR expression and the increase of P_{Met} and N_{val} may also increase translation and/or initiation of translation. This may be useful for increasing nAChR translation and/or site-specific UAA incorporation experiments by supplementation of Met (< 1 mM) or Met derivatives. D_{hp} and A_{ze} result in $\approx 40\%$ decrease in functional channel expression, which is similar to Pro (Figure 7.10). *o*FPhe and *p*FPhe show 88% and 93%, respectively, reduction in expression, while *m*FPhe shows 30% reduction (Figure 7.10). 3,5-F₂Phe, F₃Phe, and F₅Phe (no shift in EC₅₀ Table 7.1) all show $\approx 20\%$ reduction in functional channel expression, while 3,4-F₂Phe shows a 57% reduction and suggests incorporation (Figure 7.10). 2Pyr and 3Pyr show 50% increase in expression, while 4Pyr shows a 100% increase in expression (Figure 7.10). B_{th} and T_{hi} show an 60% and 80% increase in expression (Figure 7.10) even though there is no shift in EC₅₀ (Table 7.1). Of the UAAs that caused a shift in EC₅₀, UAARS with fluorinated UAAs (F₃Leu, F_{Val}, F_{Trp}, *o*FPhe, *m*FPhe, and *p*FPhe) appears to decrease functional ion channel expression relative to non-fluorinated UAAs (P_{Leu}, 2Pyr, and 3Pyr) (Figure 7.10). Intriguingly, there is no change

in the total α -subunit when detected by Western blot for *o*FPhe, *m*FPhe, *p*FPhe, FTrp, and FVal (Figure 7.11). Therefore the UAA incorporation doesn't cause decreased translation or increased protein degradation, but most likely the channels are not functional, have altered conductance, or are not present on the cell surface (remain sequestered in the endoplasmic reticulum, golgi, or vesicles). Western blots of the membrane only can further elucidate where the nAChR is located. Natural aas and UAAs supplemented in the media effect functional nAChR expression, but appear not to diminish protein translation for tested fluorinated UAAs.

UAARS is a useful method for analyzing the global effect of UAA incorporation. The commercially available UAA PLeu alters nAChR function and caution should be observed when heterogeneously incorporating UAAs. Further research is necessary to extend UAARS to other ion channels to try and attain shifts for the 20 natural aas (or 19 if Gly is omitted). UAARS with UAAs not used in this research will further extend trends discussed and gain further insight into aa function in the nAChR. Extension of UAARS to charged and polar aas will also be interesting to see the effect on the function of the nAChR. UAARS is a useful technique for evaluating whether the translational machinery of the *Xenopus* oocyte accepts an UAA. UAAs that are accepted by the translational machinery require site-specific incorporation by chemically aminoacylated tRNAs, but UAAs that are not accepted can be incorporated by evolved aminoacyl synthetase/tRNA pairs for site-specific UAA incorporation. The use of *E. coli* mutant aaRS can be useful to incorporate UAAs that are not recognized by the endogenous aaRS (site-specific or statistical incorporation) and can also be utilized with a specific isoacceptor *E. coli* tRNA to only incorporate UAAs at a subset of triplet codons.

UAARS with multiple UAAs will lead to diverse populations of nAChR and can be used to look at specific interactions between classes of aas, such as salt bridges (Lys/Arg and Glu/Asp). UAARS combined with site-specific UAA incorporation should be a useful technique for analyzing whether specific sites dominate functional changes. The UAARS method is an intriguing technique that should have many applications in *Xenopus* oocytes for many different proteins.

7.4 Experimental Methods

7.4.1 Materials

T7 mMessage mMachine kits were from Ambion (Austin, TX). ACh chloride and yeast inorganic pyrophosphatase were purchased from Sigma-Aldrich. HA.11 monoclonal antibody from mouse was from Covance (Berkeley, CA). IRDyeTM800CW conjugated affinity purified anti-mouse IgG from goat was from Rockland (Gilbertsville, PA). Mouse anti-His antibody was from Amersham Biosciences (Piscataway, NJ). 5-Fluoro-DL-Tryptophan (FTrp) was from Acros (Geel, Belgium). 5,5,5-Trifluoro-DL-leucine (F3Leu) was from Alfa Aesar (Ward Hill, MA). H-3,4-Dehydro-L-Proline (Dhp) and L-Azetidine-2-Carboxylic Acid (Aze) were from Chem-Impex Int (Wood Dale, IL). 3-Fluoro-DL-Valine (FVal) was from Fluka (Seelze, Germany). L-2-Fluorophe (*o*FPhe), L-3-Fluorophe (*m*FPhe), L-4-Fluorophe (*p*FPhe), L-3,4-Difluorophe (3,4-F2Phe), L-3,5-Difluorophe (3,5-F2Phe), L-2,4,5-Trifluorophe (F3Phe), L-Pentafluorophe (F5Phe), L-2-Pyridylalanine (2Pyr), L-3-Pyridylalanine (3Pyr), L-4-Pyridylalanine (4Pyr), L-Propargylglycine (Ppg), (R)-2-Thienylglycine (Thi), and L-3-Benzothienylalanine (Bth)

were from Peptech (Burlington, MA). L-Photo-Leucine (PLeu), L-Photo-Methionine (PMet), and dialyzed FBS were from Pierce (Rockford, IL).

7.4.2 nAChR Gene Preparation and mRNA Transcription

The masked α_{NHA} -, β -, γ -, and δ -subunits (all ending with the ochre (UAA) stop codon) of the nAChR subcloned in the pAMV vector were previously prepared (45,46). The $\alpha_{\text{HA His}}$ in the pAMV vector was previously prepared (36). DNA was linearized with NotI (New England Biolabs) and mRNA was prepared with the T7 mMessage mMachine kit with 0.5 μl of yeast inorganic pyrophosphatase. mRNA was purified using the RNeasy Mini kit (Qiagen, Valencia, CA) and quantified by absorption at 260 nm.

7.4.3 *In Vivo* nAChR Expression, UAARS, and Site-Specific UAA Incorporation

Stage VI oocytes of *Xenopus laevis* were prepared as described (47). Oocytes were incubated at 18 °C for 41–56 h (unless otherwise stated in the figure legends). 2 ng of mRNA in a subunit ratio of 2:1:1:1 for $\alpha_{\text{HA His}}$ or $\alpha_{\text{NHA}}:\beta:\gamma:\delta$ was injected for 2 d incubations, and 1 ng of mRNA in the same subunit ratio was injected for 5 d incubations. UAAs were added to ND96 with Ca^{2+} and 5% FBS immediately prior to injection. After injection, oocytes were divided equally among all dishes containing exactly 4 mL of solution. Media was changed every 24 h after injection. For α 149UAG (β 9'Ser) nonsense suppression, 40 ng of mRNA in a subunit ratio of 10:1:1:1 α 149UAG: β (or β 9'Ser): γ : δ was injected with 7.5 ng of deprotected TQAS-Trp or TQAS-FTrp (as described in Chapter 5 and (46)). Prior to nonsense suppression the oocytes were incubated in 2 mM FTrp for 24 h and after injection oocytes were incubated for 2 d. For PLeu and PMet experiments, oocytes were kept in an opaque box and exposed to ambient light only during media exchange and homogenization.

7.4.4 Electrophysiology

Recordings employed two-electrode voltage clamp on the OpusXpress 6000A (Molecular Devices). ACh was stored at -20 °C as a 1 M stock, diluted in Ca²⁺-free ND96, and delivered to oocytes by computer-controlled perfusion system. For all experiments, the holding potential was -60 mV. Dose-response data were obtained from at least 12 ACh concentrations. Dose-response relations were fit to the Hill equation to determine EC₅₀ and the Hill coefficient (η_H). All reported values are represented as a mean \pm SE of the tested oocytes (number (n) listed with each table).

7.4.5 UV Irradiation

Oocytes were placed in a dish containing ND96 (no FBS or UAAs) and placed on an orbital shaker. Oocytes were UV irradiated with a 100 W Blak-Ray Lamp (UVP Inc.) with conditions listed with each figure. For arc lamp UV irradiation, oocytes were placed in a 1.5 ml eppendorf and were irradiated through the open end of the eppendorf.

7.4.6 Whole Oocyte Homogenization

Whole oocyte homogenization was performed by placing four oocytes (either immediately from 18 °C incubator or after storage at -80 °C) in a 1.5 ml eppendorf and removing excess ND96. 10 μ l of homogenization buffer (100 mM NaCl, 50 mM Tris pH = 7.9, 0.6% SDS (w/v), 35 mM *n*-dodecyl β -D-maltoside (DDM) (Anatrace), and 1 protease inhibitor tablet (Roche)) were added to the oocytes, and oocytes were lysed manually with a pipette tip. The solution was sonicated for 10 min and centrifuged for 30 min to remove insoluble debris. The supernatant was transferred to a new eppendorf and 10 μ l of 2X loading buffer was added. Samples were either stored at -80 °C or run on a gel. For PL_{eu} and PM_{et} 2 d solubilization, the oocytes were homogenized manually

as described above, placed in an eppendorf rack covered in aluminum foil, and placed in 18 °C incubator for 2 d.

7.4.6 Western Blotting of Proteins Expressed in *Xenopus* Oocytes

Western blotting was performed as previously described (37). Briefly 20 µl of samples were loaded on a 4–15% linear gradient, polyacrylamide ready gel Tris-HCl (Bio-Rad) and run at 150 V for 1.25 h. Protein was transferred to nitrocellulose (Bio-Rad) at 30 V for 30 min and 100 V for 1.5 h. Nitrocellulose was blocked overnight using non-fat dairy milk (NFDM) in 1X PBS / 0.1% Tween. 12.5 µl of 1° Ab anti-HA from mouse (or 14.9 µl, for same µg as HA Ab, of 1° Ab anti-His from mouse) was placed in 15 ml NFDM / 1X PBS / 0.1% Tween for 1h, washed 4X with 30 ml 1X PBS / 0.1% Tween for 5 min each, placed in 3 µl 2° 800CW goat anti-mouse IgG in 15 mL NFDM / 1X PBS / 0.1% Tween for 1 h, and washed 4X with 30 ml 1X PBS / 0.1% Tween for 5 min each. Nitrocellulose was visualized using two-color infrared dye detection on the Odyssey (Li-Cor, Lincoln, NE) (Hsieh-Wilson lab). Densitometric analysis was performed using the Li-Cor Odyssey software package.

7.5 References

1. Montclare, J.K., and Tirrell, D.A. (2006) Evolving proteins of novel composition. *Angew. Chem. Int. Ed. Engl.*, **45**, 4518–4521.
2. Link, A.J., and Tirrell, D.A. (2005) Reassignment of sense codons *in vivo*. *Methods*, **36**, 291–298.
3. Link, A.J., Mock, M.L., and Tirrell, D.A. (2003) Non-canonical amino acids in protein engineering. *Curr. Opin. Biotechnol.*, **14**, 603–609.

4. Beene, D.L., Dougherty, D.A., and Lester, H.A. (2003) Unnatural amino acid mutagenesis in mapping ion channel function. *Curr. Opin. Neurobiol.*, **13**, 264–270.
5. Dougherty, D.A. (2000) Unnatural amino acids as probes of protein structure and function. *Curr. Opin. Biotechnol.*, **4**, 645–652.
6. Budisa, N. (2004) Prolegomena to future experimental efforts on genetic code engineering by expanding its amino acid repertoire. *Angew. Chem. Int. Ed. Engl.*, **43**, 6426–6463.
7. Wang, L., Xie, J., and Schultz, P.G. (2006) Expanding the genetic code. *Annu. Rev. Biophys. Biomol. Struct.*, **35**, 225–249.
8. Yoshikawa, E., Fournier, M.J., Mason, T.L., and Tirrell, D.A. (1994) Genetically engineered fluoropolymers. Synthesis of repetitive polypeptides containing *p*-fluorophenylalanine residues. *Macromolecules*, **27**, 5471–5475.
9. Deming, T.J., Fournier, M.J., Mason, T.L., and Tirrell, D.A. (1996) Structural modification of a periodic polypeptide through biosynthetic replacement of proline with azetidine-2-carboxylic acid. *Macromolecules*, **29**, 1442–1444.
10. Deming, T.J., Fournier, M.J., Mason, T.L., and Tirrell, D.A. (1997) Biosynthetic incorporation and chemical modification of alkene functionality in genetically engineered polymers. *J. Macromol. Sci. Pure Appl. Chem.*, **34**, 2143–2150.
11. van Hest, J.C., and Tirrell, D.A. (1998) Efficient introduction of alkene functionality into proteins *in vivo*. *FEBS Lett.*, **428**, 68–70.

12. van Hest, J.C.M., Kiick, K.L., and Tirrell, D.A. (2000) Efficient incorporation of unsaturated methionine analogues into proteins *in vivo*. *J. Am. Chem. Soc.*, **122**, 1282–1288.
13. Kiick, K.L., Weberskirch, R., and Tirrell, D.A. (2001) Identification of an expanded set of translationally active methionine analogues in *Escherichia coli*. *FEBS Lett.*, **502**, 25–30.
14. Niemz, A., and Tirrell, D.A. (2001) Self-association and membrane-binding behavior of melittins containing trifluoroleucine. *J. Am. Chem. Soc.*, **123**, 7407–7413.
15. Kirshenbaum, K., Carrico, I.S., and Tirrell, D.A. (2002) Biosynthesis of proteins incorporating a versatile set of phenylalanine analogues. *Chembiochem.*, **3**, 235–377.
16. Minks, C., Huber, R., Moroder, L., and Budisa, N. (2000) Noninvasive tracing of recombinant proteins with "fluorophenylalanine-fingers". *Anal. Biochem.*, **284**, 29–34.
17. Tang, Y., Ghirlanda, G., Petka, W.A., Nakajima, T., DeGrado, W.F., and Tirrell, D.A. (2001) Fluorinated coiled-coil proteins prepared *in vivo* display enhanced thermal and chemical stability. *Angew. Chem. Int. Ed. Engl.*, **40**, 1494–1496.
18. Koide, H., Yokoyama, S., Katayama, Y., Muto, Y., Kigawa, T., Kohno, T., Takusari, H., Oishi, M., Takahashi, S., Tsukumo, K. *et al.* (1994) Receptor-binding affinities of human epidermal growth factor variants having unnatural amino acid residues in position 23. *Biochemistry*, **33**, 7470–7476.

19. Pratt, E.A., and Ho, C. (1975) Incorporation of fluorotryptophans into proteins of *Escherichia coli*. *Biochemistry*, **14**, 3035–3040.
20. Hartman, M.C., Josephson, K., and Szostak, J.W. (2006) Enzymatic aminoacylation of tRNA with unnatural amino acids. *Proc. Natl. Acad. Sci. USA*, **103**, 4356–4361.
21. Hartman, M.C., Josephson, K., Lin, C.W., and Szostak, J.W. (2007) An expanded set of amino acid analogs for the ribosomal translation of unnatural peptides. *PLoS ONE*, **2**, e972.
22. Suchanek, M., Radzikowska, A., and Thiele, C. (2005) Photo-leucine and photo-methionine allow identification of protein-protein interactions in living cells. *Nat. Methods*, **2**, 261–267.
23. Dieterich, D.C., Link, A.J., Graumann, J., Tirrell, D.A., and Schuman, E.M. (2006) Selective identification of newly synthesized proteins in mammalian cells using bioorthogonal noncanonical amino acid tagging (BONCAT). *Proc. Natl. Acad. Sci. USA*, **103**, 9482–9487.
24. Beatty, K.E., Liu, J.C., Xie, F., Dieterich, D.C., Schuman, E.M., Wang, Q., and Tirrell, D.A. (2006) Fluorescence visualization of newly synthesized proteins in mammalian cells. *Angew. Chem. Int. Ed. Engl.*, **45**, 7364–7367.
25. Son, S., Tanrikulu, I.C., and Tirrell, D.A. (2006) Stabilization of bzip peptides through incorporation of fluorinated aliphatic residues. *ChemBiochem.*, **7**, 1251–1257.

26. Tang, Y., Ghirlanda, G., Vaidehi, N., Kua, J., Mainz, D.T., Goddard, I.W., DeGrado, W.F., and Tirrell, D.A. (2001) Stabilization of coiled-coil peptide domains by introduction of trifluoroleucine. *Biochemistry*, **40**, 2790–2796.
27. Tang, Y., and Tirrell, D.A. (2001) Biosynthesis of a highly stable coiled-coil protein containing hexafluoroleucine in an engineered bacterial host. *J. Am. Chem. Soc.*, **123**, 11089–11090.
28. Cirino, P.C., Tang, Y., Takahashi, K., Tirrell, D.A., and Arnold, F.H. (2003) Global incorporation of norleucine in place of methionine in cytochrome P450 BM-3 heme domain increases peroxygenase activity. *Biotechnol. Bioeng.*, **83**, 729–734.
29. Lummis, S.C., Beene, D.L., Lee, L.W., Lester, H.A., Broadhurst, R.W., and Dougherty, D.A. (2005) *Cis-trans* isomerization at a proline opens the pore of a neurotransmitter-gated ion channel. *Nature*, **438**, 248–252.
30. Zhong, W., Gallivan, J.P., Zhang, Y., Li, L., Lester, H.A., and Dougherty, D.A. (1998) From ab initio quantum mechanics to molecular neurobiology: A cation- π binding site in the nicotinic receptor. *Proc. Natl. Acad. Sci. USA*, **95**, 12088–12093.
31. Kearney, P.C., Zhang, H., Zhong, W., Dougherty, D.A., and Lester, H.A. (1996) Determinants of nicotinic receptor gating in natural and unnatural side chain structures at the M2 9' position. *Neuron*, **17**, 1221–1229.
32. Chung, H.H., Benson, D.R., Cornish, V.W., and Schultz, P.G. (1993) Probing the role of loop 2 in Ras function with unnatural amino acids. *Proc. Natl. Acad. Sci. USA*, **90**, 10145–10149.

33. Cornish, V.W., Kaplan, M.I., Veenstra, D.L., Kollman, P.A., and Schultz, P.G. (1994) Stabilizing and destabilizing effects of placing beta-branched amino acids in protein alpha-helices. *Biochemistry*, **33**, 12022–12031.
34. Koh, J.T., Cornish, V.W., and Schultz, P.G. (1997) An experimental approach to evaluating the role of backbone interactions in proteins using unnatural amino acid mutagenesis. *Biochemistry*, **36**, 11314–11322.
35. Steiner, T., Hess, P., Bae, J.H., Wiltschi, B., Moroder, L., and Budisa, N. (2008) Synthetic biology of proteins: Tuning GFPs folding and stability with fluoroproline. *PLoS ONE*, **3**, e1680.
36. Leite, J.F., Blanton, M.P., Shahgholi, M., Dougherty, D.A., and Lester, H.A. (2003) Conformation-dependent hydrophobic photolabeling of the nicotinic receptor: Electrophysiology-coordinated photochemistry and mass spectrometry. *Proc. Natl. Acad. Sci. USA*, **100**, 13054–13059.
37. England, P.M., Zhang, Y.N., Dougherty, D.A., and Lester, H.A. (1999) Backbone mutations in transmembrane domains of a ligand-gated ion channel: Implications for the mechanism of gating. *Cell*, **96**, 89–98.
38. Dumont, J.N. (1972) Oogenesis in *Xenopus laevis* (Daudin). I. Stages of oocyte development in laboratory maintained animals. *J. Morphol.*, **136**, 153–179.
39. Weber, W. (1999) Ion currents of *Xenopus laevis* oocytes: State of the art. *Biochim. Biophys. Acta.*, **1421**, 213–233.
40. Taylor, P.M., Kaur, S., Mackenzie, B., and Peter, G.J. (1996) Amino-acid-dependent modulation of amino acid transport in *Xenopus laevis* oocytes. *J. Exp. Biol.*, **199**, 923–931.

41. Miyazawa, A., Fujiyoshi, Y., and Unwin, N. (2003) Structure and gating mechanism of the acetylcholine receptor pore. *Nature*, **423**, 949–955.
42. Beatty, K.E., Xie, F., Wang, Q., and Tirrell, D.A. (2005) Selective dye-labeling of newly synthesized proteins in bacterial cells. *J. Am. Chem. Soc.*, **127**, 14150–14151.
43. Ulbrich, M.H., and Isacoff, E.Y. (2007) Subunit counting in membrane-bound proteins. *Nat. Methods*, **4**, 319–321.
44. Mecozzi, S., West, A.P., Jr., and Dougherty, D.A. (1996) Cation- π interactions in aromatics of biological and medicinal interest: Electrostatic potential surfaces as a useful qualitative guide. *Proc. Natl. Acad. Sci. USA*, **93**, 10566–10571.
45. Rodriguez, E.A., Lester, H.A., and Dougherty, D.A. (2007) Improved amber and opal suppressor tRNAs for incorporation of unnatural amino acids *in vivo*. Part 1: Minimizing misacylation. *RNA*, **13**, 1703–1714.
46. Rodriguez, E.A., Lester, H.A., and Dougherty, D.A. (2007) Improved amber and opal suppressor tRNAs for incorporation of unnatural amino acids *in vivo*. Part 2: Evaluating suppression efficiency. *RNA*, **13**, 1715–1722.
47. Quick, M.W., and Lester, H.A. (1994) Methods for expression of excitability proteins in *Xenopus* oocytes. In Narahashi, T. (ed.), *Ion Channels of Excitable Cells*. Academic Press, San Diego, CA, Vol. 19, pp. 261–279.